

**Investigating the Impact of Aquifer Long Term Replenishment
on the Potomac Aquifer System in Virginia**

Meredith Grace Martinez

Dissertation submitted to the faculty of the Virginia Polytechnic Institute and State
University in partial fulfillment of the requirements for the degree of

Doctor of Philosophy

In

Civil Engineering

Mark A. Widdowson, Chair

Charles B. Bott, Co-Chair

Amy J. Pruden-Bagchi

Thomas J. Burbey

Kyle B. Strom

March 23, 2022

Blacksburg, VA

Keywords: groundwater, multi-aquifer, flowmeter, tracer test, indirect potable reuse

Investigating the Impact of Aquifer Long Term Replenishment on the Potomac Aquifer System in Virginia

Meredith Grace Martinez

ABSTRACT

Groundwater plays a fundamental role in water resource sustainability in Virginia (USA), but overpumping has caused significant declines in the potentiometric surface in the Potomac Aquifer System (PAS). With water levels falling, communities are at risk of wells running dry, saltwater intrusion, and land subsidence. The Sustainable Water Initiative for Tomorrow (SWIFT) project is an aquifer long-term replenishment (ALTR) project that uses continuous recharge into the multi-layered confined aquifer system to restore the potentiometric surface over space and time and increase storage in the system. The SWIFT Research Center (SWIFT-RC) is a 1 million gallon per day (MGD) demonstration facility in Suffolk, Virginia that recharges the PAS through a multi-screen well.

Addressing research questions about the impact of continuous, sustained recharge on aquifer systems is crucial to the long-term sustainability of an ALTR project. Quantifying how flow moves through the multi-layered system is necessary to communicate travel times and water quality impacts on the aquifer system. This work uses injectate as an intrinsic tracer, an in-situ flowmeter, and a bromide tracer test to evaluate how flow is distributed through the eleven screens in the recharge well and to assess how flow distribution changes over time. Typically, flow distribution in multi-screen wells is estimated only once over the length of a project and assumed to remain constant for modeling purposes; by measuring flow distribution using multiple methods over the course of the project, this work shows that flow distribution is not constant. In

future ALTR projects, developing a consistent and robust monitoring plan to use injectate as an indicator of movement through the aquifer system, paired with other methods to monitor changes in flow distribution, will be a critical part of effectively evaluating how flow moves through the groundwater system.

Investigating the Impact of Aquifer Long Term Replenishment on the Potomac Aquifer System in Virginia

Meredith Grace Martinez

GENERAL AUDIENCE ABSTRACT

Groundwater plays a fundamental role in water resource sustainability in Virginia (USA), but overpumping has left the Potomac Aquifer System (PAS) depleted. With water levels falling, communities are at risk of wells running dry, adverse water quality changes, and even changes to the land surface due to subsurface settling. The Sustainable Water Initiative for Tomorrow (SWIFT) project is an aquifer long-term replenishment (ALTR) project that uses continuous recharge into the deep aquifer system to restore water levels and increase storage in the system. The SWIFT Research Center (SWIFT-RC) is a 1 million gallon per day (MGD) demonstration facility in Suffolk, Virginia that recharges the PAS through a multi-screen well.

Addressing research questions about the impact of continuous, sustained recharge on aquifer systems is crucial to the long-term sustainability of an ALTR project. Quantifying how flow moves through the multi-layered system is necessary to communicate travel times and water quality impacts on the aquifer system. This work uses multiple methods to evaluate how flow is distributed through the eleven screens in the recharge well and to assess how flow distribution changes over time. Typically, flow distribution in multi-screen wells is estimated only once over the length of a project and is assumed to remain constant for modeling purposes; by measuring flow distribution using multiple methods over the course of the project, this work shows that flow distribution is not constant. In future ALTR projects, developing a consistent and robust monitoring plan to use recharge water itself as an indicator of movement through the

aquifer system, paired with other methods to monitor changes in flow distribution, will be a critical part of effectively evaluating how flow moves through the groundwater system.

Dedication

*It may be that when we no longer know what to do,
we have come to our real work.*

*And that when we no longer know which way to go,
we have come to our real journey.*

*The mind that is not baffled is not employed.
The impeded stream is the one that sings.*

*"The Real Work" by Wendell Berry,
from Standing by Words. © 1983*

To all the educators who nourished my love of learning: Wini Boswell, Jon Sherwin, Joel Ducoste, Tarek Aziz, and many more.

And to my first and favorite teacher, my mentor, and my mom: Dr. Lisa Gardner Bullard.

Acknowledgments

“In ordinary life we hardly realize that we receive a great deal more than we give, and that it is only with gratitude that life becomes rich. It is very easy to overestimate the importance of our own achievements in comparison with what we owe others.”

– Dietrich Bonhoeffer, *Letters and Papers from Prison (1943-45)*

Thank you to my advisor, Dr. Mark Widdowson, for encouraging me to grow in my skills as a researcher, for your thoughtful feedback that has improved everything I’ve written, and for your interest in my success. Your influence on me as an engineer and scholar cannot be understated. Thank you to my co-advisor, Dr. Charles Bott, whom I can only hope to emulate in his love of learning, attention to detail, and simply superhuman time-management skills. Additional thanks are due to my committee members, Dr. Tom Burbey, Dr. Amy Pruden, and Dr. Kyle Strom for their insightful and thought-provoking comments every time we meet.

Thank you to my teammates and VT lab cohort, specifically Thomas Dziura (double thanks to Thomas for being a reliable sounding board as well as a chemistry and crossword whiz), Kayla Shirley, Eric Matynowski, and Andrew Frazier. Thank you also to my colleagues at HRSD, who were my eyes and hands when I wasn’t there in person and are the source of much of the data in this dissertation – including (but not limited to) Germano Salazar-Benites, Samantha Hogard, Savannah Moretz, Dan Holloway, Li Zhang, Jennifer Reitz, and the rest of the team at the CEL.

There are too many friends to name who have walked with me through this five-year journey who have, at times, acted as encouragers, listeners, sources of much-needed distraction, book recommenders, anti-imposter syndrome co-warriors, and who have always graciously smiled and nodded as I talk about my research, even if they had no clue what I was talking about. Thank you specifically to Elizabeth, Cassidy, Rachel, and the Hunnies (Kallie, Neelam, Nicola, and Savannah). You are each a perfect example of what it means to be a badass woman!

To the many artists whose soundtracks took me through all of my writing sessions – including Concerned Ape (Stardew Valley), Joe Hisaishi (of more Studio Ghibli movies than I can name), Yuki Hayashi (Haikyū! and My Hero Academia composer), and Kato (Anime Lofi Playlist) – thank you for sharing your art with the world and with me.

To my parents, Michael and Lisa Bullard, who have acted as proofreaders, constant encouragers, prayer warriors, problem solvers, and who have always made time for a call, a Zoom, or a visit. I am better because of you. Thank you for always believing in me. I am who I am, in so many ways, because you are who you are.

Finally, to my wonderful husband, Jake, I’m so glad that you became my life partner in 2019 and my coworker in 2020. I love sharing an office with you (even if you don’t). You have supported me in so many ways, big and small, throughout this journey. Your patience, strength, kindness, and cooking skills have carried me through. Without you, this wouldn’t have been possible. I love you – today and every day, but especially today.

Table of Contents

1. Introduction.....	1
1.1 Managed Aquifer Recharge	2
1.2 Research Question Development.....	9
References.....	12
2. Literature Review.....	16
2.1. Flow Behavior and Transport in a High-Capacity Recharge Well	16
2.2. Modeling of ASR/ASTR Projects.....	24
2.3. Operational Effects on Aquifer Behavior and Breakthrough	27
References.....	31
3. Demonstration of Managed Aquifer Recharge in a Coastal Plain Aquifer: Lessons Learned	42
Title.....	42
Abstract.....	42
3.1 Introduction.....	43
3.2 SWIFT Research Center (SWIFT-RC) Overview	45
3.2.1 Project Status	45
3.2.2 Source Water.....	46
3.2.3 Regulatory Considerations for the SWIFT Project.....	46
3.2.4 Project Costs	47
3.3 Project Infrastructure	48
3.3.1 Advanced Treatment Process.....	48
3.3.2 Multiscreen, Multi-Aquifer Recharge Well and Sampling System.....	48
3.4 Lessons Learned.....	51
3.4.1 Aquifer Compatibility.....	51
3.4.2 Monitoring Network	54

3.4.3 Dynamic Well Performance.....	55
3.4.4 Benefits of a Demonstration Facility	58
3.5 Future Prospects.....	58
Acknowledgements.....	59
References.....	60
4. Managed Aquifer Recharge: Transport and Attenuation in a Coastal Plain Aquifer ...	62
Title.....	62
Abstract.....	62
4.1 Introduction.....	63
4.2 Data Collection and Analysis.....	64
4.2.1 Monitoring System and Sample Collection	64
4.2.2 Tracer Selection	67
4.2.3 Analysis of Breakthrough Curves	69
4.3 Results and Discussion	72
4.4 Conclusion and Implications.....	80
Acknowledgements.....	81
Supplemental Information	82
References.....	82
5. Evaluating Flow Distribution in a Multiaquifer Recharge Well Using an In-Situ Flowmeter	83
Title.....	83
Abstract.....	83
5.1 Introduction.....	84
5.2 Study Area and Methods.....	88
5.2.1 Project Background.....	88
5.2.2 Site Description.....	89

5.2.3. Instrument and Data Collection	90
5.3 Results.....	94
5.3.1 Flow Distribution Within the Well	94
5.3.2. Flow Distribution at Well Screens.....	98
5.3.3. Hydraulic Conductivity Distribution	99
5.3.4. Consideration of Turbulence Flow Within the Well.....	104
5.4 Discussion.....	106
5.5 Conclusions.....	108
Acknowledgments.....	109
Supplemental Information	109
References.....	110
6. Multiple Tracers to Evaluate Flow Through a Multi-Layered Aquifer Using a Novel Transport Approximation.....	115
Title.....	115
Abstract.....	115
6.1 Introduction.....	116
6.2 Methods.....	120
6.2.1 Site and Project Description.....	120
6.2.2 Tracer Selection	124
6.2.3. Tracer Monitoring.....	126
6.2.4. Radial Breakthrough Model Development	127
6.3 Results.....	133
6.4 Discussion.....	137
6.4.1. Sulfate	138
6.4.2. TOC.....	138
6.4.3. Chloride.....	138

6.4.4. Fluoride	140
6.4.5. 1,4-Dioxane and NDMA.....	143
6.5 Conclusions.....	143
Acknowledgments.....	144
Supplemental Information	144
References.....	145
7. Forced Gradient Tracer Test in a Multiscreen, Multi-Aquifer Recharge Well.....	150
Title.....	150
Abstract.....	150
7.1 Introduction.....	151
7.2 Methods.....	154
7.2.1. Site Description.....	154
7.2.2. Experimental Setup and Field Sampling Procedures.....	156
7.2.3. Modeling.....	158
7.3. Results and Discussion	162
7.3.1. Tracer Test Operational Conditions.....	162
7.3.2. Single-Zone and Two-Zone Models	164
7.4. Conclusions.....	174
Acknowledgments.....	175
Supplemental Information	175
References.....	175
8. Conclusions.....	180
8.1. Objectives and Findings.....	180
8.2. Major Themes and Engineering Significance.....	182
8.3. Future Research Directions.....	184

References.....	186
Appendices.....	187
Appendix A: SWIFT Research Center Site Description and Initial Aquifer Characterization	188
Appendix B: Initial Conductivity Work Results.....	223
Appendix C: Flowmeter Supplemental Information.....	237
Flowmeter Calibration	239
Static Testing	241
Dynamic Testing Results	242
Reynolds Number	253
Appendix D: Multi Tracer Supplemental Information	256
Upper Potomac Aquifer (UPA)	257
Middle Potomac Aquifer (MPA)	268
Appendix E: Bromide Tracer Supplemental Information.....	274
Sampling Schedule.....	275
Experimental Data	276
Initial Breakthrough Model.....	279
Variable Flow Optimization	286
Single Zone Optimization.....	286
References.....	299

List of Figures

Figure 1-1. Eastern Virginia Groundwater Management Area (EVGWMA) and Eastern Shore Groundwater Management Area as of August 2017 (Rubin 2017)..... 2

Figure 1-2. Conceptual diagram of aquifer storage and recovery (ASR) operations. Recharge water is injected during periods of low demand and removed at the same well for use during high demand periods. During the injection cycle, a mixing zone is created, which essentially creates a buffer between recoverable water and native groundwater. Upon pumping, the buffer zone is usually left in place (e.g., the recovered volume is similar but slightly lower than the injected volume). 5

Figure 1-3. Conceptual diagram of aquifer storage transfer and recovery (ASTR) operations. During operations, water is injected at one well and removed at one or more nearby wells. ASTR includes the concept of soil aquifer treatment (SAT), in which contaminants are removed during advective transport. 6

Figure 1-4. Conceptual diagram of aquifer long term replenishment (ALTR) operations. While pumping does occur at the recharge well, pumping is primarily for well maintenance and not for recovery, leading the recharge volume to steadily increase over time. 8

Figure 3-1. Location of the HRSD service area (blue), future full-scale SWIFT locations, and the SWIFT demonstration facility site (SWIFT-RC) in southeast Virginia, USA. ... 45

Figure 3-2. Well locations at the SWIFT-RC. Figure adapted from (Bullard et al. 2019). 50

Figure 3-3. Variability of flow distribution over time at multiscreen recharge well TW-1 based on three different measurement methods..... 57

Figure 4-1. Schematic of the recharge well (TW-1) showing the distribution of flow through 11 well screens in the Upper, Middle, and Lower Potomac Aquifer and position of monitoring well MW-SAT. 66

Figure 4-2. Sampling taps for FLUTe screens 1-11. Taps 1-4 are screened in the Upper Potomac Aquifer, taps 5-9 are screened in the Middle Potomac Aquifer, and taps 10-11 are screened in the Lower Potomac Aquifer. Each tap is connected to the respective FLUTe sample tube..... 67

Figure 4-3. Correlation developed between specific conductivity and chloride concentrations in groundwater samples collected at MW-SAT. 68

Figure 4-4. Recharge flow rate at recharge well TW-1 (gpm). Extended backflushing period is noted in August 2018. No recharge is observed from late November 2018 onward..... 73

Figure 4-5. Comparison of fit between screen 1 breakthrough curves from fluoride relative concentrations (upper) and relative conductivity data (lower). 77

Figure 4-6. Screen 7 shows the improvement between the initial and stoppage breakthrough curves at predicting relative concentration based on incremental flow..... 78

Figure 4-7. While the stoppage breakthrough curve is more accurate than the initial breakthrough curve for screen 5, it fails to explain the major spike that occurred between days 80-100. This period was during the 18-day backflush. 79

Figure 4-8. Breakthrough in the LPA has not yet occurred..... 80

Figure 5-1. HRSD Service Area in eastern Virginia, USA. The existing demonstration facility (SWIFT-RC) in Suffolk is the study site, while future full-scale sites are marked by blue stars (Martinez et al. 2022). 89

Figure 5-2. Flowmeter profile during Test R2 in well TW-1. Results are shown with 1-foot precision. Screen depths relative to land surface are shown on the right..... 96

Figure 5-3. Mean flow distribution to each well screen (%) under recharge and pumping testing conditions in well TW-1..... 97

Figure 5-4. Flow distribution across (a) Screen 2 and (b) Screen 9 during recharge and pumping. Normalized screen length indicates bottom of screen at 0.0 and top of screen at 1.0. For recharge conditions (open markers), flow is normalized based on the difference between flow between the top of screen (TOS) and bottom of screen (BOS); because flow starts entering the screen at TOS, normalized flow reaches 100% at BOS. During pumping conditions (closed markers), flow enters the screen starting at BOS and reaches 100% at TOS..... 99

Figure 5-5. Hydraulic conductivity (ft/day) at each screen in the Upper Potomac Aquifer (Screens 1-4) and in the Middle Potomac Aquifer (Screens 5-9)..... 101

Figure 5-6. Conductivity distribution measured over five-foot intervals in screen 2..... 104

Figure 6-1. Site map of the SWIFT Research Center. TW-1 is the injection well location, MW-SAT is the depth discrete sampling system, and MW-UPA, MW-MPA, and MW-LPA are the Upper, Middle, and Lower Potomac conventional wells, respectively..... 121

Figure 6-2. SWIFT Water concentrations of the constituents of interest. 130

Figure 6-3. Modeled constituent concentrations. Four models are compared: (1) Model 1, which assumes a constant flow and constant concentration; (2) Model 2, which assumes a constant influent concentration but transient flow and variable flow distribution; (3) Model 3, which varies influent concentration and transient flow but maintains a constant flow distribution; and (4) Model 4, which varies influent concentration and flow distribution with time and accounts for transient flow. 136

Figure 6-4. Coefficient of determination for each constituent under Condition (4) – variable concentration, variable flow, and variable flow distribution conditions..... 137

Figure 6-5. Chloride concentrations in SWIFT Water and MW-SAT Screen 1. In the initial breakthrough period (June 2018), observed concentrations at Screen 1 were higher than influent SWIFT Water concentrations. 139

Figure 6-6. Preliminary chloride breakthrough at MW-MPA. This breakthrough is based on Model 4. 140

Figure 6-7. Generalized fluoride distribution in the Virginia Coastal Plain (McFarland 2010). 142

Figure 7-1. HRSD Service Area in eastern Virginia, USA. The existing demonstration facility (SWIFT-RC) in Suffolk is the study site, while future full-scale sites are marked by blue stars (Martinez et al. 2022). 155

Figure 7-2. Bromide transport in Screen 1 [(a) and (b)] and Screen 2 [(c) and (d)] for the Single-Zone model [(a) and(c)] and the Two-Zone model [(b) and (d)]. The Two-Zone model increases the capability to fit both the initial peak and the steep drop in concentration after initial breakthrough. 165

Figure 7-3. Bromide transport in Screen 3 [(a) and (b)] and Screen 4 [(c) and (d)] for the Single-Zone model [(a) and(c)] and the Two-Zone model [(b) and (d)]. The Two-Zone model increases the capability to fit both the steep initial peak and the tailing effect after initial breakthrough. 166

Figure 7-4. Bromide transport in Screen 5 [(a) and (b)] and Screen 6 [(c) and (d)] for the Single-Zone model [(a) and(c)] and the Two-Zone model [(b) and (d)]. The Two-Zone model increases the capability to fit both the initial peak and the steep drop in concentration after initial breakthrough at Screen 5 and is able to accurately capture the entire breakthrough in Screen 6. 167

Figure 7-5. Bromide transport in Screen 7 [(a) and (b)] and Screen 8 [(c) and (d)] for the Single-Zone model [(a) and(c)] and the Two-Zone model [(b) and (d)]. The Two-Zone model is able to accurately capture the entire breakthrough in Screen 7 and captures the narrow initial breakthrough and the tailing effect in Screen 8 following breakthrough. 168

Figure 7-6. Bromide transport in Screen 10 [(a) and (b)] and Screen 11 [(c) and (d)] for the Single-Zone model [(a) and(c)] and the Two-Zone model [(b) and (d)]. The Two-Zone model increases the capability to fit both the initial peak breakthrough and the tailing effect following breakthrough. 169

Figure 7-7. Bromide transport in Screen 9 for (a) Single-Zone model and (b) Two-Zone model. The Single-Zone model better captures peak breakthrough. 169

Figure A-1. Screen Depths at TW-1, MW-SAT, and Conventional Wells 189

Figure A-2. TW-1 Well Completion Report. This includes well location information, screen depths, well diameter, and soil type with depth. (Includes the next 6 pages.) 191

Figure A-3. MW-SAT Well Completion Report. This includes well location information, screen depths, well diameter, and soil type with depth. (Includes the next 6 pages.) 197

Figure A-4. MW-UPA Well Completion Report. This includes well location information, screen depths, well diameter, and soil type with depth. (Includes the next 4 pages.) 203

Figure A-5. MW-MPA Well Completion Report. This includes well location information, screen depths, well diameter, and soil type with depth. (Includes the next 4 pages.) 207

Figure A-6. MW-LPA Well Completion Report. This includes well location information, screen depths, well diameter, and soil type with depth. (Includes the next 5 pages.) 211

Figure A-7. NP-MAR-1 Well Completion Report. This includes well location information, screen depths, well diameter, and soil type with depth. (Includes the next 7 pages.) 216

Figure B-1. Conductivity breakthrough in the first 250 days at Screen 1. 224

Figure B-2. Fluoride breakthrough in the first 250 days at Screen 1..... 225

Figure B-3. Comparison of conductivity and fluoride measurements at Screen 1. 226

Figure B-4. Conductivity breakthrough in the first 250 days at Screen 2. 227

Figure B-5. Conductivity breakthrough in the first 250 days at Screen 3. 228

Figure B-6. Conductivity breakthrough in the first 250 days at Screen 4. 229

Figure B-7. Conductivity breakthrough in the first 250 days at Screen 5. 230

Figure B-8. Conductivity breakthrough in the first 250 days at Screen 6. 231

Figure B-9. Conductivity breakthrough in the first 250 days at Screen 7. 232

Figure B-10. Conductivity breakthrough in the first 250 days at Screen 8. 233

Figure B-11. Conductivity breakthrough in the first 250 days at Screen 9. 234

Figure B-12. Conductivity breakthrough in the first 800 days at Screen 10. 235

Figure B-13. Conductivity breakthrough in the first 800 days at Screen 11. 236

Figure C-1. Schematic of the recharge well (TW-1) and monitoring well (MW-SAT) 50 feet away showing the screen depths and hydrostratigraphy at the SWIFT Research Center site surrounding TW-1 and MW-SAT. This figure is vertically to scale, but not horizontally to scale. 238

Figure C-2. Flowmeter response to step backflush calibration..... 239

Figure C-3. Backflush calibration. The data used for calibration is in orange. 240

Figure C-4. Recharge calibration..... 240

Figure C-5. Flow distribution to screens during recharge tests using multiple calculation methods. 243

Figure C-6. Flow distribution to screens during backflush tests using multiple calculation methods. 243

Figure C-7. Comparison of TFAS/BOS and TOS/BOS measurements at capturing the total pump flow at TW-1..... 244

Figure C-8. Comparison of flow distribution calculation methods for tests R1 and R2 under recharge conditions. TOS/BOS in red, TFAS/BOS in yellow, BOSa/BOS in green for each screen. 245

Figure C-9. Comparison of flow distribution calculation methods for tests R3 and R4 under recharge conditions. TOS/BOS in red, TFAS/BOS in yellow, BOSa/BOS in green for each screen. 246

Figure C-10. Comparison of flow distribution calculation methods under backflush conditions. TOS/BOS in red, TFAS/BOS in yellow, BOSa/BOS in green for each screen. 247

Figure C-11. Flow profile for Test R1. Results are shown with 1-foot precision. 248

Figure C-12. Flow profile for Test R3. Results are shown with 1-foot precision. 249

Figure C-13. Flow profile for Test R4. Results are shown with 1-foot precision. 250

Figure C-14. Flow profile for Test B1. Results are shown with 1-foot precision. 251

Figure C-15. Flow profile for Test B2. Results are shown with 1-foot precision. 252

Figure C-16. Reynold's Number at the top of each screen. 255

Figure D-17. Well locations and screen depths of wells at the SWIFT Research Center. Screen depths range from 500 to 1400 feet (152 to 427 m) below grade, but this study focuses on the UPA, which contains screens 1-4. Horizontal distance between wells is not shown to scale. 257

Figure D-18. Breakthrough calculated at each screen using aquifer characteristics (n and α) determined in Bullard et al. (2019). Coefficients of determination are shown for the constant concentration model (labeled Bullard et al. 2019) and the variable concentration model (labeled VF/VC/VFD). Both models account for variable flow and variable flow distribution. 258

Figure D-19. Flow- and length-weighted models using screens 1-4. Coefficients of determination are shown for the constant concentration model (labeled Bullard et al. 2019) and the variable concentration model (labeled VF/VC/VFD). Both models account for variable flow and variable flow distribution. 259

Figure D-20. Flow- and length-weighted models using screens 1 and 2 only. Coefficients of determination are shown for the constant concentration model (labeled Bullard et al. 2019) and the variable concentration model (labeled VF/VC/VFD). Both models account for variable flow and variable flow distribution. 260

Figure D-21. Coefficient of determination 261

Figure D-22. Length-weighted model using Screens 1 and 2..... 262

Figure D-23. Length-weighted model coefficients of determination. 263

Figure D-24. Pre-rehab flow weighted model using Screens 1 and 2. 264

Figure D-25. Pre-rehab flow-weighted model coefficients of determination..... 265

Figure D-26. Post-rehab flow weighted model using Screens 1 and 2..... 266

Figure D-27. Post-rehab flow-weighted model coefficients of determination. 267

Figure D-28. Breakthrough calculated at each individual screen (5-9) using aquifer characteristics (n and α) determined in Bullard et al. (2019). Coefficients of determination are shown for the constant concentration model (labeled Bullard et al. 2019) and the variable concentration model (labeled VF/VC/VFD). Both models account for variable flow and variable flow distribution. 269

Figure D-29. Flow- and length-weighted models using screens 5-9. Coefficients of determination are shown for the constant concentration model (labeled Bullard et al. 2019) and the variable concentration model (labeled VF/VC/VFD). Both models account for variable flow and variable flow distribution. 270

Figure D-30. Flow- and length-weighted models using screens 5-6. Coefficients of determination are shown for the constant concentration model (labeled Bullard et al. 2019) and the variable concentration model (labeled VF/VC/VFD). Both models account for variable flow and variable flow distribution. 271

Figure D-31. Flow- and length-weighted models using screens 5-7. Coefficients of determination are shown for the constant concentration model (labeled Bullard et al. 2019) and the variable concentration model (labeled VF/VC/VFD). Both models account for variable flow and variable flow distribution. 272

Figure D-32. Flow- and length-weighted models using screens 5-8. Coefficients of determination are shown for the constant concentration model (labeled Bullard et al.

2019) and the variable concentration model (labeled VF/VC/VFD). Both models account for variable flow and variable flow distribution.	273
Figure E-33. Bromide concentration (mg/L) during injection period.....	278
Figure E-34. Screen 1 initial bromide observations and breakthrough model.	280
Figure E-35. Screen 2 initial bromide observations and breakthrough model.	280
Figure E-36. Screen 3 initial bromide observations and breakthrough model.	281
Figure E-37. Screen 4 initial bromide observations and breakthrough model.	281
Figure E-38. Screen 5 initial bromide observations and breakthrough model.	282
Figure E-39. Screen 6 initial bromide observations and breakthrough model.	282
Figure E-40. Screen 7 initial bromide observations and breakthrough model.	283
Figure E-41. Screen 8 initial bromide observations and breakthrough model.	283
Figure E-42. Screen 9 initial bromide observations and breakthrough model.	284
Figure E-43. Screen 10 initial bromide observations and breakthrough model.	284
Figure E-44. Screen 11 initial bromide observations and breakthrough model.	285
Figure E-45. Single-zone breakthrough at Screen 1.	288
Figure E-46. Two-zone breakthrough at Screen 1.	288
Figure E-47. Single-zone breakthrough at Screen 2.	289
Figure E-48. Two-zone breakthrough at Screen 2.	289
Figure E-49. Single-zone breakthrough at Screen 3.	290
Figure E-50. Two-zone breakthrough at Screen 3.	290
Figure E-51. Single-zone breakthrough at Screen 4.	291
Figure E-52. Two-zone breakthrough at Screen 4.	291
Figure E-53. Single-zone breakthrough at Screen 5.	292
Figure E-54. Two-zone breakthrough at Screen 5.	292
Figure E-55. Single-zone breakthrough at Screen 6.	293
Figure E-56. Two-zone breakthrough at Screen 6.	293

Figure E-57. Single-zone breakthrough at Screen 7.	294
Figure E-58. Two-zone breakthrough at Screen 7.	294
Figure E-59. Single-zone breakthrough at Screen 8.	295
Figure E-60. Two-zone breakthrough at Screen 8.	295
Figure E-61. Single-zone breakthrough at Screen 9.	296
Figure E-62. Two-zone breakthrough at Screen 9.	296
Figure E-63. Single-zone breakthrough at Screen 10.	297
Figure E-64. Two-zone breakthrough at Screen 10.	297
Figure E-65. Single-zone breakthrough at Screen 11.	298
Figure E-66. Two-zone breakthrough at Screen 11.	298

List of Tables

Table 2-1. Injection Well MBI-1 Spinner Log Test Results (Burriss 2018). GPM indicates gallons per minute. BGS indicates below ground surface.	20
Table 3-1. Time-averaged concentration of SWIFT-RC influent before treatment (NTP 2°), after treatment (SWIFT), and time-averaged background concentrations in the Upper, Middle, and Lower Potomac Aquifer (UPA, MPA, and LPA, respectively).	51
Table 4-1. Well Screen Depth and Length of Screen in TW-1 and MW-SAT.....	65
Table 4-2. Calibrated model input parameter values and travel time results.....	74
Table 5-1. Well screen depth and length of screen in recharge well TW-1.....	90
Table 5-2. Flowmeter test conditions.....	94
Table 5-3. Flow distribution (%) results of static, dynamic recharge (tests denoted by R-), and dynamic pumping (tests denoted by B-) flowmeter testing.	95
Table 5-4. Comparison of hydraulic conductivity estimates. All estimates are in ft/day.	102
Table 5-5. Percent flow distribution (Q_i / total Q) during recharge and pumping conditions and percent transmissivity (T_i / total T).....	107
Table 6-1. Well Screen Depth and Length of Screen in TW-1 and MW-SAT.....	122
Table 6-2. Well Screen Depth and Length of Screen in the Conventional Wells	122
Table 6-3. General description of operating conditions for each phase of the SWIFT Project to date.	123
Table 6-4. Recharge and pumping volumes during the length of the tracer test. All volumes are given in gallons. Parentheses indicate negative flow or pumping from the well.....	124
Table 6-5. Time split during each phase of the bromide tracer test. All units are in days.	124
Table 6-6. Pre-recharge native groundwater concentrations of identified constituents of interest. Individual screens in MW-SAT are noted with S-[screen number] (e.g., MW-SAT S 1 for Screen 1). 1,4-Dioxane and NDMA are not included because both were below detection (0.06 $\mu\text{g/L}$ and 2 ng/L , respectively) in every screen in MW-SAT and the conventional wells. For the detected constituents, one standard deviation is listed in parentheses. Measured TOC in MW-SAT is likely higher than actual native groundwater concentrations due to interference during installation.	126

Table 6-7. Number of SWIFT Water influent and MW-UPA samples included in the breakthrough model. 127

Table 6-8. SWIFT Water characteristics for tracer constituents..... 131

Table 6-9. Pre- and post-rehab flow distributions and aquifer characteristics for MW-UPA..... 133

Table 7-1. Upper and lower parameter estimates for the two-zone model. The same boundaries for $\left(\frac{Q}{n}\right)_1$ and α_1 are applied to the single-zone model. 162

Table 7-2. Recharge and pumping volume during the length of the tracer test. All volumes are given in gallons. Parentheses indicate negative flow or pumping from the well..... 163

Table 7-3. Time split during each phase of the bromide tracer test. All units are in days. 163

Table 7-4. Background concentration, peak observed bromide concentration, and travel time measured at each screen..... 164

Table 7-5. Two-Zone solution parameters and total flow estimates. The variable b_1 indicates the percentage of the total thickness that makes up the high permeability/flow zone, Zone 1. Screen 9 is a single-zone solution, denoted by $b_1 = 100\%$. For the total flow estimate, the low estimate assumes porosity in both zones is 0.20, and the high estimate assumes porosity in both zones is 0.45..... 170

Table 7-6. Comparison of Q/n values between original estimate in 2018 (Bullard et al. 2019), extrapolated values from an in-situ flowmeter test in 2019 (Chapter 5), and Single-Zone and Two-Zone results. Flowmeter values are extrapolated based on the estimated porosity from the original work. 171

Table 7-7. Longitudinal dispersivity comparison between the original estimate (Bullard et al. 2019) and the bromide tracer analysis. The thickness-averaged value of longitudinal dispersivity in the Two-Zone model is also included with the individual zone values. . 172

Table 7-8. Mass discharge at MW-SAT. Original indicates the flow distribution based on porosities estimated by Bullard et al. (2019), Low Estimate assumes porosity in both zones is 0.20, and High Estimate assumes porosity in both zones is 0.45..... 173

Table 8-1. Estimated travel time (days) for individual screens at MW-SAT (50-ft radial distance) assuming constant recharge flow (700 gpm) at the recharge well (TW-1). Actual travel times will be longer, and in some cases may be significantly longer depending on operating conditions on site..... 184

Table A-1. Well Screen Depth and Length of Screen in TW-1 and MW-SAT..... 190

Table A-2. Well Screen Depth and Length of Screen in the Conventional Wells.....	190
Table C-1. Static flowmeter testing results.....	241
Table C-2. Review of relevant field studies.....	253
Table C-3. Reynold’s Number at the top of each screen during recharge.....	254
Table C-4. Reynold’s Number at the top of each screen during backflush.	254
Table D-1. Pre- and post-rehab flow distributions and aquifer characteristics for MW-MPA.....	268
Table E-1. Bromide Tracer initial sampling frequency chart. Frequencies were adjusted over time based on screen-specific responses.....	275
Table E-2. Calculation of influent concentration using drawdown measured in the totes.	276
Table E-3. Summary of results from initial constant flow model.....	279
Table E-4. Range of Q/n values.	286
Table E-5. Optimized Q/n and dispersivity (α) values for the Single-Zone optimization. Ranges of potential flow distribution are included based on estimated porosities.	287

List of Abbreviations

ACH	Aluminum chlorohydrate
ALTR	Aquifer long-term replenishment
AR	Aquifer Recharge
ASR	Aquifer storage and recovery
ASTR	Aquifer storage, transfer, and recovery
BGD	Brackish groundwater development
bgs	Below ground surface
CEL	Central Environmental Lab
DBP	Diffusion byproduct
EM	Electromagnetic
EPA	Environmental Protection Agency
EVGWMA	Eastern Virginia Ground Water Management Area
FGTT	Forced gradient tracer test
FLUTe	Flexible Liner Underground Technology
FSO	Full-Scale Output
GAC	Granular activated carbon
gpm	Gallons per minute
GWMA	Groundwater management area
GWRS	Groundwater Replenishment System
HDPE	High density polyethylene
HRSD	Hampton Roads Sanitation District
HTO	Tritiated water
IAH	International Association of Hydrogeologists
LPA	Lower Potomac Aquifer
MAR	Managed aquifer recharge
MCL	Maximum contaminant level
MGD	Million gallons per day
MPA	Middle Potomac Aquifer
MW	Monitoring well
ND	Not detected
NDMA	N-Nitrosodimethylamine
OCWD	Orange County Water District
ODE	Ordinary differential equation

PAS	Potomac Aquifer System
PFP	Preferential flow path
PPA	Portable parallel analyzer
RO	Reverse osmosis
RSS	Residual sum of squares
SAT	Soil aquifer treatment
SCADA	Supervisory control and data acquisition
SWIFT	Sustainable Water Initiative for Tomorrow
SWIFT-RC	Sustainable Water Initiative for Tomorrow Research Center
TDS	Total dissolved solids
TMDL	Total Maximum Daily Load
TOC	Total organic carbon
UPA	Upper Potomac Aquifer
USGS	United States Geological Survey
UV	Ultraviolet
VDEQ	Virginia Department of Environmental Quality
WRF	Water reclamation facility

Preface/Attribution

Several colleagues provided feedback and aided with the development of the published manuscripts presented within this dissertation. A brief description of co-authors and their contributions is included below:

Chapter 3: Demonstration of Managed Aquifer Recharge in a Coastal Plain Aquifer: Lessons Learned

Mark A. Widdowson, Ph.D., P.E., is a Professor and Department Head of the Via Department of Civil and Environmental Engineering at Virginia Tech. He served as a co-author on the manuscript and provided feedback and additional language.

Charles Bott, Ph.D., P.E., is the Director of Water Technology and Research (Chief Technical Officer) for Hampton Roads Sanitation District (HRSD). Charles served as a co-author and provided feedback and data regarding economic analysis of the project and future directions for the project.

Dan Holloway, M.S., is a hydrogeologist at HRSD. Dan served as a co-author on the paper and provided language regarding the pretreatment of the aquifer

Jamie Heisig-Mitchell, M.S., is the Chief of Technical Services for HRSD. Jamie served as a co-author on the paper and provided language regarding permit negotiations and regulatory compliance for the SWIFT Project.

Christopher Wilson, Ph.D., P.E., is the Chief of Process Engineering and Research at HRSD. Chris served as a co-author and provided feedback and made suggestions on the draft of the case study

Chapter 4: Managed Aquifer Recharge: Transport and Attenuation in a Coastal Plain Aquifer

Mark A. Widdowson, Ph.D., P.E., is a Professor and Department Head of the Via Department of Civil and Environmental Engineering at Virginia Tech. He aided with model development and provided feedback on data analysis and manuscript writing.

Germano Salazar-Benites, M.S., is the SWIFT Project Manager for HRSD. He coordinated data collection for the project at the SWIFT Research Center and provided feedback on the manuscript.

Jamie Heisig-Mitchell, M.S., is the Chief of Technical Services for HRSD. Jamie served as a co-author on the paper and provided feedback on the manuscript.

Andy Nelson is a Project Manager for Nansemond Treatment Plant at HRSD. Andy is a co-author on the paper and helped with sample collection and maintenance on the FLUTe system during the duration of the project.

Charles Bott, Ph.D., P.E., is the Director of Water Technology and Research (Chief Technical Officer) for Hampton Roads Sanitation District (HRSD). Charles served as a co-author and provided general feedback on the manuscript.

1. Introduction

With 41% of the population of the United States depending on groundwater as its primary source of drinking water, groundwater is a vitally important resource for a significant fraction of the country (NGWA 2020). Moreover, groundwater plays a fundamental role in non-drinking water uses like agricultural production, and groundwater utilization and stewardship transcend direct use to impact those who do not use it directly as a drinking water source in the area of food security. According to United States Geological Survey (USGS) estimates in 2015, groundwater made up approximately 29.3% of the total freshwater supply (gallons per day) for the United States, an 8% increase in groundwater withdrawals since 2010. Nationally, fresh and saline groundwater use as a fraction of total water use has increased from 18.5% in 1950 to 26.3% in 2015 – a 42.2% increase.

In the state of Virginia, approximately 298 million gallons per day (MGD) are withdrawn from the state's groundwater resources. Groundwater in Virginia is primarily drawn from domestic wells (125 MGD), public supply wells (83 MGD), and industrial wells (66 MGD) (Dieter et al. 2018). In 1992, the General Assembly of Virginia authorized the State Water Control Board to form the Eastern Virginia Groundwater Management Area (EVGWMA) (Figure 1-1. Groundwater management areas (GWMAs) are designated where an area is experiencing declining groundwater levels or is at risk of groundwater pollution; as a result, GWMAs are subject to stringent withdrawal permitting to address groundwater management concerns (Rubin 2017). In the EVGWMA, groundwater is derived from the Virginia Coastal Plain Aquifer System; approximately 74% of groundwater withdrawals from this system come from the Potomac Aquifer System (PAS) (McFarland and Bruce 2006). Heywood and Pope employed numerical modeling of the EVGWMA to demonstrate substantial groundwater level

declines in the PAS as a result of industrial groundwater use over the last century, which puts the area at risk for saltwater intrusion (Heywood and Pope 2009). As groundwater becomes a more important water source, considerations must be taken to implement effective groundwater monitoring systems to ensure sustainable use for the long-term viability of the resource (Dennehy et al. 2015).

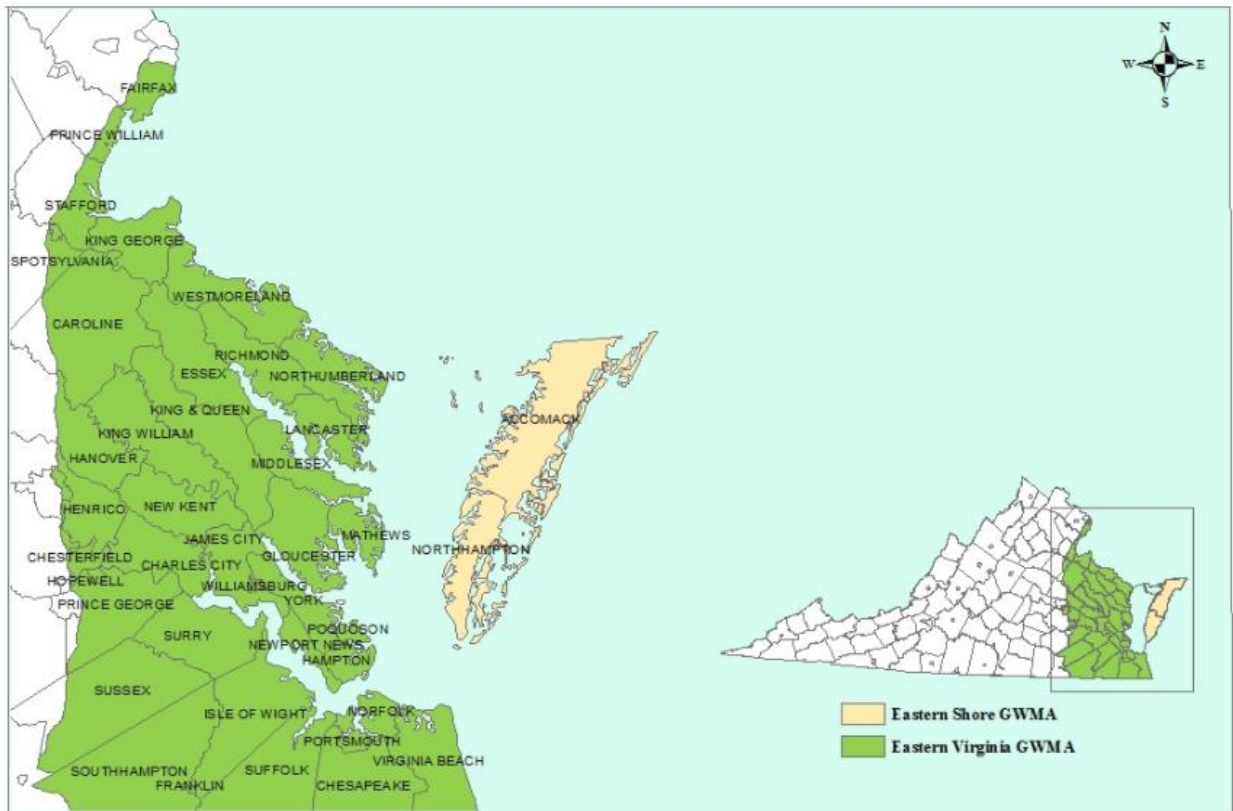


Figure 1-1. Eastern Virginia Groundwater Management Area (EVGWMA) and Eastern Shore Groundwater Management Area as of August 2017 (Rubin 2017).

1.1 Managed Aquifer Recharge

Managed aquifer recharge (MAR) is an important component of safeguarding groundwater resources and is well established, with more than 1,200 projects documented globally in over fifty countries (Pyne 2004; Stefan and Ansems 2018; IGRAC 2019). MAR serves as an umbrella term to describe all methods of artificial recharge of groundwater resources. The term “managed aquifer recharge” was coined by Ian Gale, a British

hydrogeologist and founding co-chair of the International Association of Hydrogeologists (IAH) Commission on Managed Aquifer Recharge (Dillon et al. 2019). While the term was adopted within the last two decades, the concept of artificially increasing recharge rates has existed for centuries (Maliva 2015; Dillon et al. 2019). MAR takes “artificial recharge” a step further by adding an aspect of intentionality and considering the impacts not only of quantity of recharge, but also of quality (NRMMC, EPHC, and NHMRC 2009). Examples of MAR include, but are not limited to, induced riverbank filtration, spreading methods (such as infiltration basins, excess irrigation, or flooding); in-channel modification (such as dams and channel spreading); and well, shaft, and borehole recharge (Ringleb et al. 2016; Stefan and Ansems 2018; Dillon et al. 2019; IGRAC 2019). The approach implemented at a site depends on the goal of the project and the available footprint for operation (i.e., a large footprint could sustain spreading methods while smaller footprints would necessitate well recharge).

The use of injection wells for aquifer storage and recovery (ASR) or aquifer storage, transfer, and recovery (ASTR) has become more common because of the maturing of recharge technologies, the reduced land footprint required for implementation relative to land surface strategies like spreading methods, the elimination of dependence on surface characteristics, and the ability to recharge into deep, confined aquifers. ASR involves injecting potable water into a storage aquifer during periods of low demand and recovering it from the same well during periods of high demand (Figure 1-2). The goal of ASR is indirect potable reuse in the near term with an emphasis on the recovery aspect of the project (Pyne 2005). ASTR is a recharge method that builds on the concept of ASR in which water is injected at one well and recovered at one or more nearby wells (Figure 1-3); this method includes the additional aspect of groundwater transport as a method of soil aquifer treatment (SAT) (Harpaz and Bear 1964; Miotliński et al.

2014). SAT is the process of contaminant removal from source water for an MAR project by straining, attenuation via adsorption, or chemical or biological degradation during advective transport through an aquifer system (Idelovitch and Michail 1984; Grinshpan et al. 2021).

ASR/ASTR projects are currently implemented on every continent except Antarctica, with the majority of projects located in the United States, Europe, Australia, and China (Stefan and Ansems 2018; IGRAC 2019). Influent sources for ASR projects vary based on available water sources, regulations, and project purpose. In the United States, most projects use either treated groundwater or surface water (lake or river water) as an influent source; however, this is often region dependent due to source water availability. States including California, Arizona, Texas, Florida, and Virginia have implemented ASR and ASTR projects using reclaimed wastewater facility effluent as an influent source to maximize natural storage, prevent saltwater intrusion, or limit nutrient discharge into local water bodies (IGRAC 2019).

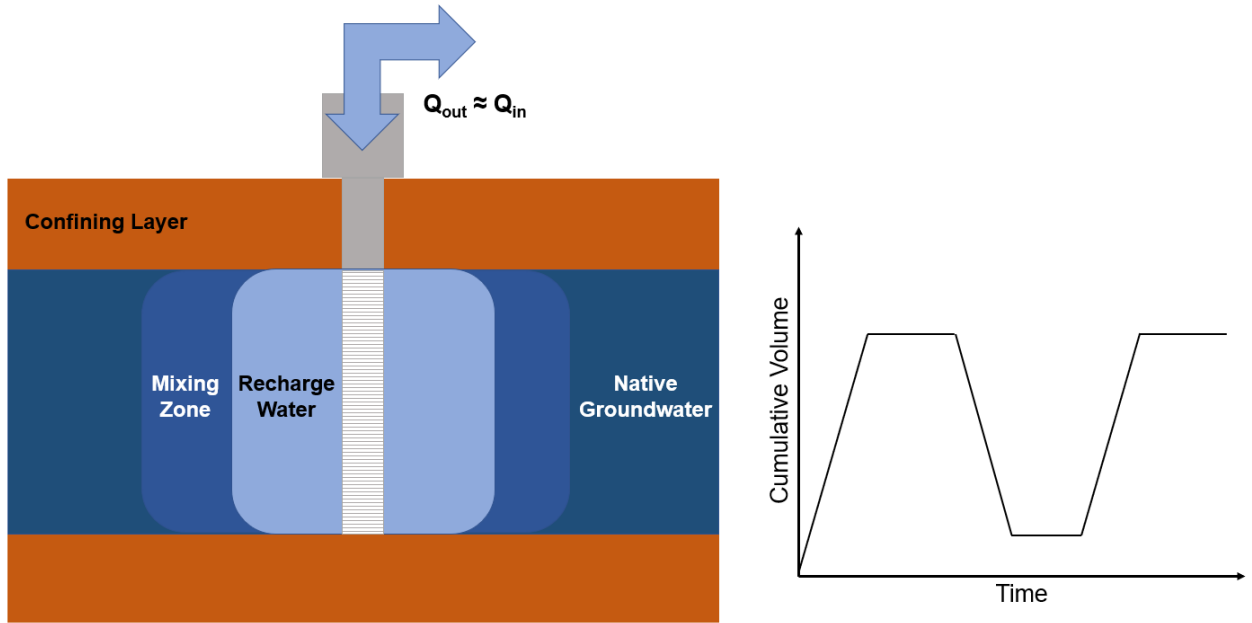


Figure 1-2. Conceptual diagram of aquifer storage and recovery (ASR) operations. Recharge water is injected during periods of low demand and removed at the same well for use during high demand periods. During the injection cycle, a mixing zone is created, which essentially creates a buffer between recoverable water and native groundwater. Upon pumping, the buffer zone is usually left in place (i.e., the recovered volume is similar but slightly lower than the injected volume).

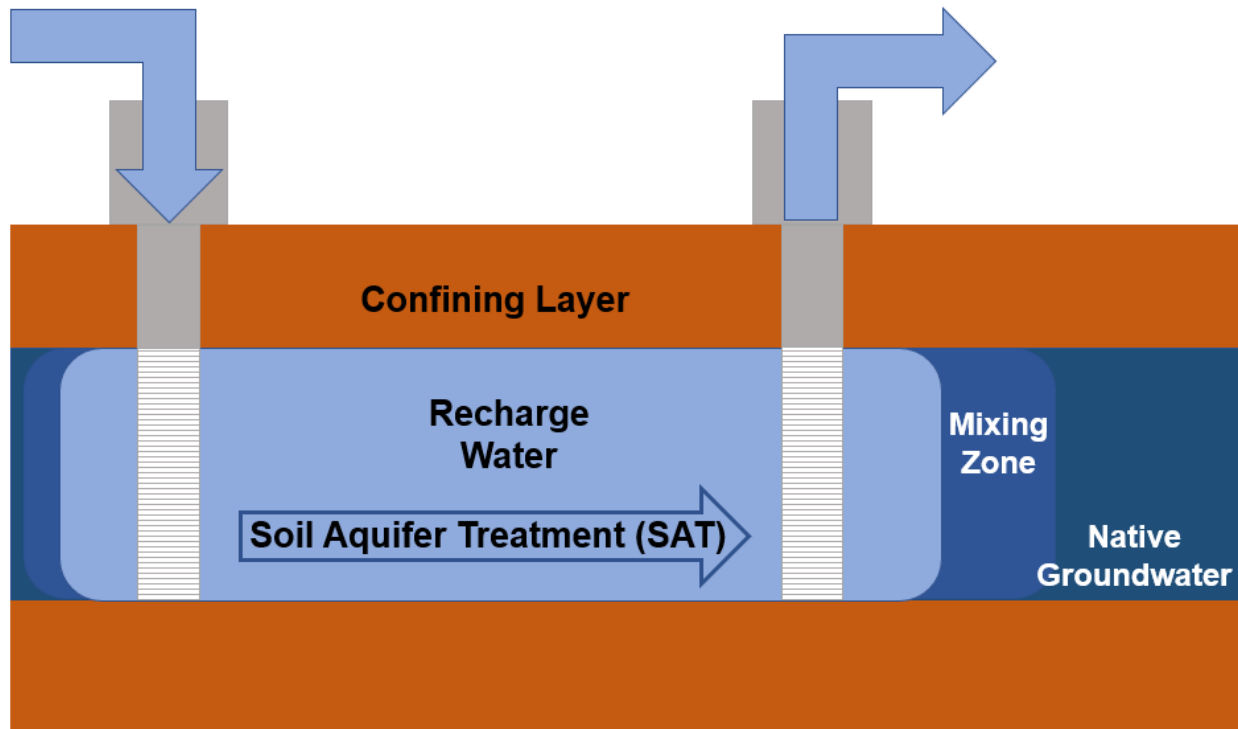


Figure 1-3. Conceptual diagram of aquifer storage transfer and recovery (ASTR) operations. During operations, water is injected at one well and removed at one or more nearby wells. ASTR includes the concept of soil aquifer treatment (SAT), in which contaminants are removed during advective transport.

Because source water for recharge projects is injected directly into the aquifer instead of entering the aquifer via infiltration methods, questions of source water quality and geochemical compatibility are paramount to the feasibility of any project. To prevent injection well clogging, injectate should be from a source already compatible with the aquifer or pre-treated to meet the geochemical characteristics of the aquifer. Hydrogeological compatibility has been a significant area of ASR/ASTR research (Mirecki et al. 1998; Herczeg et al. 2004; Lowry and Anderson 2006; Vanderzalm et al. 2010; Guo et al. 2015). Case studies highlight the importance of maintaining a “recharge bubble” to improve recovery efficiency (e.g., Vacher et al. 2006), and studies suggest that ASR recovery efficiency can be influenced by multiple factors, including aquifer heterogeneity, density differences between injectate and native groundwater, and the length of the storage period (Missimer et al. 2002; Fram et al. 2003; Pyne 2005; 2006; Vacher et

al. 2006; Maliva, et al. 2006; Reese and Alvarez-Zarikian 2007). In the future, however, recharge technology will also be implemented to achieve other goals beyond storage and recovery, including aquifer replenishment and rehabilitation.

Continuous artificial recharge to deep aquifers using injection wells conceptually aligns with MAR. Unlike ASR or ASTR, the goal of a third MAR strategy, aquifer long-term replenishment (ALTR), is to replenish and rehabilitate confined aquifer systems where groundwater storage has been depleted and the potentiometric surface has declined over space and time. ALTR is becoming increasingly necessary where local or regional groundwater usage exceeds natural recharge rates, resulting in groundwater depletion and reduction of available groundwater storage (Wada et al. 2010; Wada et al. 2012; Konikow 2013; Dennehy et al. 2015; Hartmann et al. 2017; Moeck et al. 2020). Aquifer Recharge (AR) is the conventional term to describe the practice of recharging an aquifer without the goal of recovery of the recharged water, but this term is simplistic and can complicate the discussion since it could refer to multiple methods of recharge (e.g., injection wells, paleochannels) or recharge goals (increasing long term storage, dewatering to prevent subsidence in deep excavation projects) (Sheng 2005; Bouri and Dhia 2010; Hernández et al. 2011; Samadder et al. 2011; Zhang et al. 2015; Zhang et al. 2017a, 2017b). A review of the literature suggests the terms “aquifer rehabilitation” or “aquifer restoration” involve removing or treating groundwater contaminants (Lehr and Nielsen 1982; Josephson 1983; Chen et al. 2019). In the present discussion, ALTR does not refer to remediation of contaminants, but rather rehabilitation of depleted aquifers by increasing storage and raising the potentiometric surface specifically through the use of injection wells (Figure 1-4). ALTR is conceptually focused on confined aquifers since long term injection into an unconfined aquifer could result in water levels increasing above the land surface. In a confined aquifer,

ALTR is more likely to have regional effects compared to an unconfined aquifer. ALTR injects geochemically compatible water into an aquifer with the goal of increasing storage and returning the aquifer to pre-development conditions. Moreover, land subsidence and saltwater intrusion are both issues that threaten aquifers. By injecting freshwater into an aquifer system, saltwater intrusion can be prevented, and the effects of increased land subsidence can be slowed or halted.

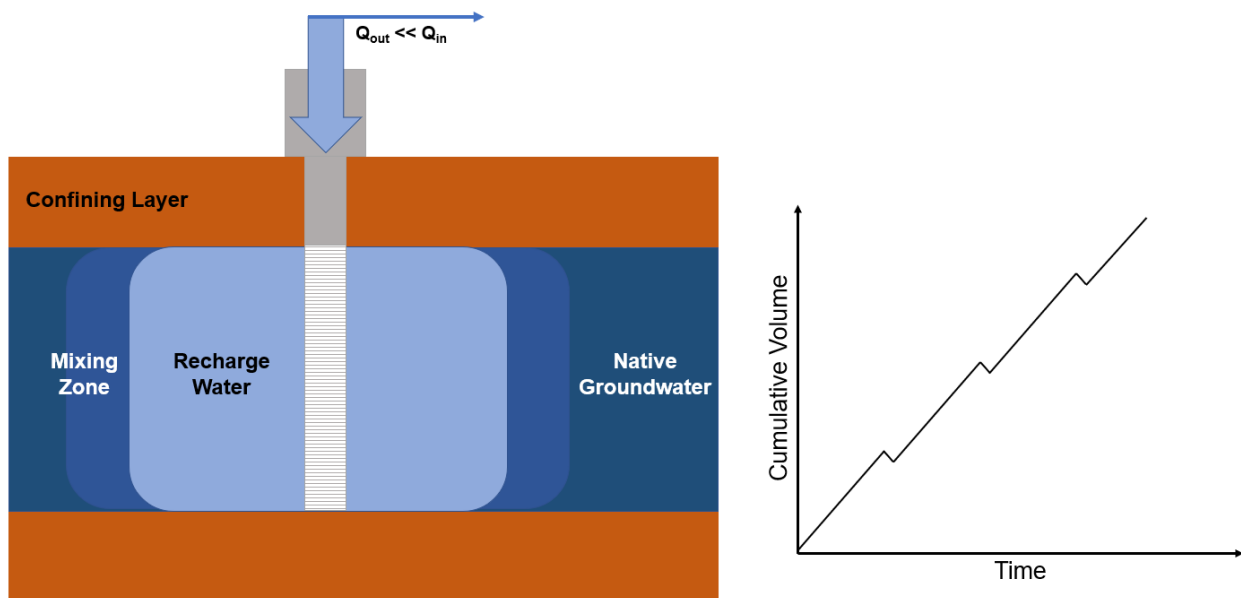


Figure 1-4. Conceptual diagram of aquifer long term replenishment (ALTR) operations. While pumping does occur at the recharge well, pumping is primarily for well maintenance and not for recovery, leading the recharge volume to steadily increase over time.

While the implementation of ALTR is similar to ASR and ASTR, the goals are different. On the one hand, ASR is like putting money into a savings account; you deposit extra money when you can and withdraw it when you are running low on funds. ASTR is like putting money into a “certificate of deposit”; you invest money and are interested in short term growth (i.e., additional treatment). Both financial management approaches are short-term solutions, and it is important that managers keep the assets liquid and easily available. ALTR, on the other hand, is like placing your money in a trust – while there is not an expectation that the assets will be used

immediately or even within a reasonable timeframe, the goal is to achieve significant long-term benefits over generations. ALTR presents similar research questions to ASR and ASTR, including the extent of SAT through the confined aquifer over the course of the recharge period and the impacts of aquifer heterogeneity on transport. However, because the water management goals are different, ALTR also increases the scale of long-term transport and provides new avenues for research questions not previously considered.

1.2 Research Question Development

Addressing research questions about the impact of continuous, sustained recharge on aquifer systems is crucial to the long-term sustainability of an ALTR project. The literature review discusses existing research regarding physiochemical transport during MAR operations in unconfined aquifer systems and fractured rock aquifers during ASR/ASTR; however, questions remain about recharge behavior in deep, confined multi-layered aquifers. If the goal is to inject large volumes (~10-15 MGD at a site) continuously, the spatial and temporal distribution of recharge flow over multiple screens or aquifers becomes a critical question in relation to solute transport and potential water quality impacts. Understanding what controls water quality outcomes in the subsurface depends on the success of modeling solute transport related to flow distribution, recharge operations, and hydrogeological processes.

To effectively investigate the issues surrounding the impact of MAR on an aquifer system that is multi-layered and multi-screened, the existing relevant literature is discussed in detail in Chapter 2 based on its applicability to the following questions:

1. How is flow distributed in a high-capacity, multi-screen recharge well in a confined multi-layered aquifer? Quantifying the flow distribution within a multi-screen recharge

well may significantly impact aquifer replenishment and solute transport through an aquifer system, especially if distribution is non-constant.

2. What transport mechanisms control solute transport and water quality at the scale associated with ALTR operations? Monitoring the impacts of ALTR on an aquifer system and identifying relevant transport mechanisms are key parts of understanding flow and transport, as well as water quality impacts on the aquifer system.
3. How can ALTR through a multi-layered aquifer be modeled to interpret existing data? Creating a model of chemical constituents relevant to an ALTR project supports the identification of known transport mechanisms and provides guidance as to where understanding is lacking in terms of describing solute transport and where unconsidered processes may be affecting water quality. A calibrated model leads to analysis of breakthrough data at nearby monitoring wells and an improved understanding of transport coupled to attenuation mechanisms at the ALTR scale.
4. What are the effects of recharge operations on aquifer parameters, flow distribution, and recharge breakthrough? Though the goal is to recharge continuously, stoppage and backflush (pumping) are inevitable on a long-term project. Identifying the impacts of stoppage and pumping on breakthrough behavior at monitoring wells is an important step to understand mechanisms that impact water quality in the aquifer system.

Multiple methods are used in this dissertation to characterize flow behavior in a multi-screen, multi-aquifer well and address the research questions posed above. Chapter 3 provides an overview of the research location and project: Hampton Roads Sanitation District's (HRSD) Sustainable Water Initiative for Tomorrow (SWIFT) Project – a large-scale aquifer

replenishment project using injection wells in the Tidewater area of Virginia, USA. Chapters 4 and 6 describe the use of injectate (SWIFT Water) as an intrinsic tracer to characterize flow at nearby monitoring wells at the SWIFT Research Center, a 1 million gallon per day (MGD) demonstration facility in Suffolk, VA, USA. Chapter 4 primarily focuses on the use of injectate to characterize flow distribution based on breakthrough at a nearby (50 foot) monitoring well in 2018 and the initial development of an analytical model to describe transport under non-constant recharge flow conditions. Chapter 5 describes the use of an in-situ flowmeter to measure flow distribution during recharge operations under a range of flow conditions. Chapter 6 builds on Chapters 4-5 by analyzing transient chemical concentration data of multiple intrinsic tracers and previously estimated flow distributions to describe breakthrough at a distant (340 feet) monitoring well on site. Chapter 6 further develops the model created in Chapter 4 to account for variable influent concentration and dynamic flow distribution. Chapter 7 explores the use of sodium bromide solution as an artificial tracer to measure flow distribution at the nearby (50 foot) monitoring well, addresses model updates from Chapter 6 to consider the dual-domain nature of the aquifer, and provides a comparison of the efficacy of intrinsic to artificial tracers at the SWIFT Research Center.

References

- Bouri, S., and H.B. Dhia. 2010. "A Thirty-Year Artificial Recharge Experiment in a Coastal Aquifer in an Arid Zone: The Teboulba Aquifer System (Tunisian Sahel)." *Comptes Rendus Geoscience* 342 (1): 60–74. <https://doi.org/10.1016/j.crte.2009.10.008>.
- Chen, Q., G. Fan, W. Na, J. Liu, J. Cui, and H. Li. 2019. "Past, Present, and Future of Groundwater Remediation Research: A Scientometric Analysis." *International Journal of Environmental Research and Public Health* 16 (20): 3975. <https://doi.org/10.3390/ijerph16203975>.
- Dennehy, K.F., T.E. Reilly, and W.L. Cunningham. 2015. "Groundwater Availability in the United States: The Value of Quantitative Regional Assessments." *Hydrogeology Journal* 23 (8): 1629–32. <https://doi.org/10.1007/s10040-015-1307-5>.
- Dieter, C.A., M.A. Maupin, R.R. Caldwell, M.A. Harris, T.I. Ivahnenko, J.K. Lovelace, N.L. Barber, and K.S. Linsey. 2018. "Estimated Use of Water in the United States in 2015." U.S. Geological Survey Circular 1441, 65. <https://doi.org/10.3133/cir1441>.
- Dillon, P., P. Stuyfzand, T. Grischek, M. Lluria, R.D.G. Pyne, R.C. Jain, J. Bear, et al. 2019. "Sixty Years of Global Progress in Managed Aquifer Recharge." *Hydrogeology Journal* 27: 1–30. <https://doi.org/10.1007/s10040-018-1841-z>.
- Fram, M.S., B.A. Bergamaschi, K.D. Goodwin, R. Fujii, and J.F. Clark. 2003. "Processes Affecting the Trihalomethane Concentrations Associated with the Third Injection, Storage, and Recovery Test at Lancaster, Antelope Valley, California, March 1998 through April 1999." U.S. Geological Survey Water-Resources Investigations Report 2003-4062, 72. <https://doi.org/10.3133/wri034062>
- Grinshpan, M., A. Furman, H.E. Dahlke, E. Raveh, and N. Weisbrod. 2021. "From Managed Aquifer Recharge to Soil Aquifer Treatment on Agricultural Soils: Concepts and Challenges." *Agricultural Water Management* 255 (May): 106991. <https://doi.org/10.1016/j.agwat.2021.106991>.
- Guo, W., K. Coulibaly, and R.G. Maliva. 2015. "Simulated Effects of Aquifer Heterogeneity on ASR System Performance." *Environmental Earth Sciences* 73 (12): 7803–9. <https://doi.org/10.1007/s12665-014-3822-4>.
- Harpaz, Y., and J. Bear. 1964. "Investigations on Mixing of Waters in Underground Storage Operations." In *XIII Assembly of the IUGG*, Vol. 64. Berkeley, California: IAHS-Red Books.
- Hartmann, A., T. Gleeson, Y. Wada, and T. Wagener. 2017. "Enhanced Groundwater Recharge Rates and Altered Recharge Sensitivity to Climate Variability through Subsurface Heterogeneity." *Proceedings of the National Academy of Sciences* 114 (11): 2842–47. <https://doi.org/10.1073/pnas.1614941114>.

- Herczeg, A.L., K.J. Rattray, P.J. Dillon, P. Pavelic, and K.E. Barry. 2004. "Geochemical Processes During Five Years of Aquifer Storage Recovery." *Ground Water* 42 (3): 438–45. <https://doi.org/10.1111/j.1745-6584.2004.tb02691.x>.
- Hernández, M., J. Tobella, F. Ortuño, and J. Ll. Armenter. 2011. "Aquifer Recharge for Securing Water Resources: The Experience in Llobregat River." *Water Science and Technology* 63 (2): 220–26. <https://doi.org/10.2166/wst.2011.036>.
- Heywood, C.E., and J.P. Pope. 2009. "Simulation of Groundwater Flow in the Coastal Plain Aquifer System of Virginia: Scientific Investigations Report 2009 – 5039." Reston, VA. <https://doi.org/10.3133/sir20095039>.
- Idelovitch, E., and M. Michail. 1984. "Soil-Aquifer Treatment: A New Approach to an Old Method of Wastewater Reuse." *Journal (Water Pollution Control Federation)* 56 (8): 936–43. <http://www.jstor.org/stable/25042398>.
- IGRAC. 2019. "MAR Portal." International Groundwater Resources Assessment Centre. 2019. <https://www.un-igrac.org/special-project/mar-portal>.
- Josephson, J. 1983. "Restoration of Aquifers." *Environmental Science & Technology* 17 (8): 347–50. <https://doi.org/10.1021/es00114a604>.
- Konikow, L.F. 2013. "Groundwater Depletion in the United States (1900–2008): U.S. Geological Survey Scientific Investigations Report 2013–5079." <http://pubs.usgs.gov/sir/2013/5079>.
- Lehr, J.H., and D.M. Nielsen. 1982. "Aquifer Restoration and Ground-Water Rehabilitation-A Light at The End of The Tunnel." *Ground Water* 20 (6): 650–56. <https://doi.org/10.1111/j.1745-6584.1982.tb01382.x>.
- Lowry, C.S., and M.P. Anderson. 2006. "An Assessment of Aquifer Storage Recovery Using Ground Water Flow Models." *Ground Water* 44 (5): 661–67. <https://doi.org/10.1111/j.1745-6584.2006.00237.x>.
- Maliva, R.G. 2015. "Managed Aquifer Recharge: State-of-the-Art and Opportunities." *Water Science and Technology: Water Supply* 15 (3): 578–88. <https://doi.org/10.2166/ws.2015.009>.
- Maliva, R.G., W. Guo, and T.M. Missimer. 2006. "Aquifer Storage and Recovery: Recent Hydrogeological Advances and System Performance." *Water Environment Research* 78 (13): 2428–35. <https://doi.org/10.2175/106143006X123102>.
- McFarland, E.R., and T.S. Bruce. 2006. "The Virginia Coastal Plain Hydrogeologic Framework." Professional Paper 1731, 118. <https://doi.org/10.3133/pp1731>
- Miotliński, K., P.J. Dillon, P. Pavelic, K. Barry, and S. Kremer. 2014. "Recovery of Injected Freshwater from a Brackish Aquifer with a Multiwell System." *Groundwater* 52 (4): 495–502. <https://doi.org/10.1111/gwat.12089>.

- Mirecki, J.E., B.G. Campbell, K.J. Conlon, and M.D. Petkewich. 1998. "Solute Changes During Aquifer Storage Recovery Testing in a Limestone/Clastic Aquifer." *Ground Water* 36 (3): 394–403. <https://doi.org/10.1111/j.1745-6584.1998.tb02809.x>.
- Missimer, T.M., W. Guo, C.W. Walker, and R.G. Maliva. 2002. "Hydraulic and Density Considerations in the Design of Aquifer Storage and Recovery Systems." *Florida Water Resources Journal* February: 30–36.
- Moeck, C., N. Grech-Cumbo, J. Podgorski, A. Bretzler, J.J. Gurdak, M. Berg, and M. Schirmer. 2020. "A Global-Scale Dataset of Direct Natural Groundwater Recharge Rates: A Review of Variables, Processes and Relationships." *Science of The Total Environment* 717 (May): 137042. <https://doi.org/10.1016/j.scitotenv.2020.137042>.
- NGWA. 2020. "Groundwater Use in the United States of America."
- NRMCC, EPHC, and NHMRC. 2009. "Australian Guidelines for Water Recycling, Managing Health and Environmental Risks, Vol 2C: Managed Aquifer Recharge."
- Pyne, R.D.G. 2004. "Known Operating ASR Systems in the United States (as of May 2004)." ASR Systems LLC. 2004. <http://www.asrforum.com/picturepages/OperASRUS052404.pdf>.
- . 2005. *Aquifer Storage Recovery: A Guide to Groundwater Recharge Through Wells*. Gainesville, FL: ASR Press.
- . 2006. *Groundwater Recharge and Wells: A Guide to Aquifer Storage Recovery*. 2nd ed. CRC Press, Inc.
- Reese, R.S., and C.A. Alvarez-Zarikian. 2007. "Hydrogeology and Aquifer Storage and Recovery Performance in the Upper Floridan Aquifer, Southern Florida: U.S. Geological Survey Scientific Investigations Report 2006-5239," 117.
- Ringleb, J., J. Sallwey, and C. Stefan. 2016. "Assessment of Managed Aquifer Recharge through Modeling-A Review." *Water (Switzerland)* 8 (12): 1–32. <https://doi.org/10.3390/w8120579>.
- Rubin, M.E. 2017. "Eastern Virginia Groundwater Management Advisory Committee Report to the Virginia Department of Environmental Quality and Virginia General Assembly." Richmond.
- Samadder, R.K., S. Kumar, and R.P. Gupta. 2011. "Paleochannels and Their Potential for Artificial Groundwater Recharge in the Western Ganga Plains." *Journal of Hydrology* 400 (1–2): 154–64. <https://doi.org/10.1016/j.jhydrol.2011.01.039>.
- Sheng, Z. 2005. "An Aquifer Storage and Recovery System with Reclaimed Wastewater to Preserve Native Groundwater Resources in El Paso, Texas." *Journal of Environmental Management* 75 (4): 367–77. <https://doi.org/10.1016/j.jenvman.2004.10.007>.

- Stefan, C., and N. Ansems. 2018. "Web-Based Global Inventory of Managed Aquifer Recharge Applications." *Sustainable Water Resources Management* 4 (2): 153–62. <https://doi.org/10.1007/s40899-017-0212-6>.
- Vacher, H.L., W.C. Hutchings, and D.A. Budd. 2006. "Metaphors and Models: The ASR Bubble in the Floridan Aquifer." *Ground Water* 44 (2): 144–54. <https://doi.org/10.1111/j.1745-6584.2005.00114.x>.
- Vanderzalm, J.L., D.W. Page, K.E. Barry, and P.J. Dillon. 2010. "A Comparison of the Geochemical Response to Different Managed Aquifer Recharge Operations for Injection of Urban Stormwater in a Carbonate Aquifer." *Applied Geochemistry* 25 (9): 1350–60. <https://doi.org/10.1016/j.apgeochem.2010.06.005>.
- Wada, Y., L.P.H. Van Beek, and M.F.P. Bierkens. 2012. "Nonsustainable Groundwater Sustaining Irrigation: A Global Assessment." *Water Resources Research* 48: 0–06. <https://doi.org/10.1029/2011WR010562>.
- Wada, Y., L.P.H. van Beek, C.M. van Kempen, J.W.T.M. Reckman, S. Vasak, and M.F.P. Bierkens. 2010. "Global Depletion of Groundwater Resources." *Geophysical Research Letters* 37 (20): n/a-n/a. <https://doi.org/10.1029/2010GL044571>.
- Zhang, Y.-Q., M.-G. Li, J.-H. Wang, J.-J. Chen, and Y.-F. Zhu. 2017a. "Field Tests of Pumping-Recharge Technology for Deep Confined Aquifers and Its Application to a Deep Excavation." *Engineering Geology* 228 (October): 249–59. <https://doi.org/10.1016/j.enggeo.2017.08.019>.
- Zhang, Y.-Q., J.-H. Wang, J.-J. Chen, and M.-G. Li. 2017b. "Numerical Study on the Responses of Groundwater and Strata to Pumping and Recharge in a Deep Confined Aquifer." *Journal of Hydrology* 548 (May): 342–52. <https://doi.org/10.1016/j.jhydrol.2017.03.018>.
- Zhang, Y., J. Wu, Y. Xue, Z. Wang, Y. Yao, X. Yan, and H. Wang. 2015. "Land Subsidence and Uplift Due to Long-Term Groundwater Extraction and Artificial Recharge in Shanghai, China." *Hydrogeology Journal* 23 (8): 1851–66. <https://doi.org/10.1007/s10040-015-1302-x>.

2. Literature Review

While each upcoming chapter includes a review of the literature relevant to the experiment or model that is the chapter focus, this chapter aims to broadly address the research questions posed in Chapter 1 by giving a general overview. More specifically, this chapter reviews the currently available experimental tools used to describe flow and transport in aquifer systems; describes how results of those methods have been used to model aquifer systems both analytically and computationally; and discusses investigations done into the effects of recharge operations on aquifer parameters, flow distribution, and recharge breakthrough. It also aims to identify gaps in the literature where further work is needed to better understand flow through complex groundwater systems during large-scale aquifer recharge projects.

2.1. Flow Behavior and Transport in a High-Capacity Recharge Well

Geophysical logging is an often used as an initial method to predict or measure well flow distribution, both through the well screen during pumping or recharge or vertical flow within the well under static conditions. Depending on the tool used, borehole logging can delineate hydrogeologic units, measure groundwater quality, and assess well condition. One commonly used type of geophysical logging is the flowmeter, which uses a range of methods to measure flow within the borehole. While initially used to measure horizontal flow, borehole flowmeters have also been used to investigate vertical flow within the borehole, which can affect water quality within the well (Collar and Mock 1997; Mayo 2010; Basiricò et al. 2015).

Initial work by Molz et al. (1989) at the Mobile test site defined hydraulic conductivity as a function of depth $K(z)$ by demonstrating a directly proportional relationship between transmissivity and flow measured along the depth of a pumping well. Others have since built on this work by:

- Comparing the Molz method to other direct and indirect methods (Rehfeldt et al. 1992; Zlotnik and Zurbuchen 2003a; Li et al. 2008)
- Evaluating conductivity and permeability distributions with newer, more precise flowmeter tools like the electromagnetic borehole flowmeter (Young et al. 1998; Zlotnik and Zurbuchen 2003b)
- Testing key assumptions of the approach of Molz et al. including that of a perfectly stratified aquifer and a steady flow regime (Riva, Ackerer, and Guadagnini 2012; Bianchi 2017)
- Using Molz et al. method to demonstrate the existence of preferential flow pathways, which develop when flow through high-transmissivity zones is preferential to low-transmissivity zones (Young 1995; Le Borgne et al. 2006; Le Borgne et al. 2007; Alazard et al. 2016)
- Improving flowmeter logging and data interpretation techniques (Oberlander and Russell 2006; A.H. Parker et al. 2010)

More recent papers suggest that flowmeter data can also be impacted by the following factors, which must be accounted for in data analysis:

- Head loss inducing non-uniform flow behavior across the flowmeter (Ruud et al. 1999; Zlotnik and Zurbuchen 2003b)
- Skin effect, or the effect of the difference in permeability in the gravel pack immediately surrounding a well, which can cause flow variations across the well screen (Ruud and Kabala 1997; Chen and Chang 2006; Chen et al. 2012; Riva et al. 2012; Cheng 2015)

- Nature of testing – whether static or dynamic tests (F. Paillet 2004; Oberlander and Russell 2006)

The use of flowmeters to investigate recharge behavior during MAR is often only a supplemental part of any experiment, though flow distribution is of critical importance. Alazard et al. (2016) also used borehole logging (heat pulse flowmeter and conductivity logging) to examine recharge flow paths and the implications for MAR; however, their study examined recharge via a “percolation tank,” which is essentially a water retention basin that infiltrates through the base to recharge the underlying aquifer. Paillet (1998) mentions that some tests included injection wells to measure hydraulic conductivity by logging flow at measured intervals within a well.

Few experiments measure well flow rate distribution during the operations of an ASR/ASTR project. Mukhopadhyay et al. (1995) mention the use a flowmeter in conjunction with a tracer test to measure flow distribution in a limestone aquifer during a feasibility study for artificial recharge in Kuwait, but data from that experiment are not included in the paper beyond the identification of the most transmissible depths. Pavelic et al. (2006) employed an electromagnetic (EM) flowmeter to measure flow in monitoring wells around an ASR recharge well to characterize heterogeneity in an aquifer but did not measure flow in the recharge well itself. Following the method of Molz et al. (F.J. Molz et al. 1994), flows were measured at set intervals, and dynamic testing did not occur.

Izbicki et al. (2010) describe the use of the tracer pulse method to determine flow distribution in a single-screen ASR well using chlorinated municipal drinking water coupled with EM flowmeter measurements at nearby monitoring wells. However, flow logs were not collected

from the ASR well during the injection phase of the project, and flow measurements in the ASR well were incremental due to the nature of the tracer pulse method, which essentially involves injecting a rhodamine dye at known depths and recording time taken to reach the surface discharge (Izbicki et al. 2010). Using this method during pumping, average flowrate was calculated at specific depth intervals to create a profile of borehole flow within the recharge well (Izbicki et al. 1999).

Much remains unknown about variability between pumping and recharge in an ASR well as well as variability within the well during full-scale operation. An impeller flowmeter was a supplemental part of an evaluation of arsenic mobilization during recharge via deep well injection in a multi-screen aquifer in the Orange County Groundwater Basin (Fakhreddine et al. 2020). While the study primarily focused on the development of a model to assess arsenic mobilization, the receiving aquifer consisted of eleven distinct units separated by low-conductivity silt and clay layers, and the injection volume fraction was estimated using a downhole impeller flowmeter survey (Fakhreddine et al. 2020). While the results of the survey were not published in the paper, they are available in the *Groundwater Replenishment System (GWRS) 2018 Annual Report* published by Orange County Water District (Burris 2018). The spinner log tests were completed under pumping and recharge conditions, and results are listed in Table 2-1. Results indicate that there is a difference in flow distribution between recharge and pumping conditions. However, the choice of distribution used in Fakhreddine's groundwater flow model is unclear. Additionally, no further research has been done to evaluate whether flow distribution at the site changed over time or how a dynamic flow distribution may have impacted the model results.

Table 2-1. Injection Well MBI-1 Spinner Log Test Results (Burris 2018). GPM indicates gallons per minute. BGS indicates below ground surface.

MBI-1 Screen No.	MBI-1 Screened Interval (ft bgs)	MBI-1 Screen Length (ft)	Flow contribution from each screened interval (%) ¹			
			Backwash Pumping 3,000 gpm	Pre-Backwash Injection 1,000 gpm	Post-Backwash Injection 1,100 gpm	Static ² 0 gpm
1	530-540	10	20	6	11	71
2	595-605	10	6	-6	-4	29
3	660-710	50	20	52	24	-29
4	770-780	10	13	16	17	-14
5	800-830 ³	30	0	0	0	0
6	970-980	10	7	16	18	-14
7	990-1,000	10	9	6	14	-14
8	1,100-1,120	20	14	3	17	-14
9	1,175-1,190	15	11	7	3	-14
Totals:		165	100	100	100	0

¹ Spinner log tests conducted on August 4, 2015.

² For the static case, a negative sign indicates flow out of the well screen; for the injection case, a negative sign indicates flow into the well.

³ Liner installed in 2012 due to excessive sand production during well development.

The use of borehole flowmeters allows for direct characterization of flow distribution within a well or along a well screen as well as the extrapolation of hydraulic conductivity using the relationship developed by Molz et al. (1989). However, flow logging does not allow for the characterization of aquifer parameters such as porosity or longitudinal dispersivity, nor does it allow for the determination of controlling transport mechanisms within the aquifer system. The use of flowmeters in conjunction with tracer tests allows for a more robust characterization of advective-dispersive transport through an aquifer system. Tracer tests are a commonly used tool for measuring groundwater velocity, hydrogeologic parameters (such as hydraulic conductivity, porosity, and dispersivity), and travel time in aquifer systems. Because an ideal tracer does not exist, Davis et al. (1985) posit that tracer selection should be well considered and account for multiple factors, including ease of detection, interaction potential with the aquifer, conservative nature of the tracer within the specific aquifer system, and native groundwater characteristics

(i.e., the tracer should be significantly higher or lower than the native groundwater). A wide range of both natural and artificial tracers is available, including temperature, ions, dyes, dissolved gases, stable isotopes, and radionuclides, and the choice of tracer depends on the goal of the project as well as cost and experimental design considerations.

The scope of this literature review will primarily cover the use of tracers introduced to a system via an injection well, although tracers can also be introduced through an aboveground source like an infiltration pond, especially when the goal of the experiment is to characterize groundwater/surface water interactions or groundwater behavior in unconfined aquifers (e.g., Moeck et al. 2017). In a confined aquifer, tracers are often introduced under forced gradient tracer test (FGTT) conditions (Fred J. Molz et al. 1988). FGTTs can use either one or two wells and a combination of recharge and pumping to create a forced hydraulic gradient between the tracer-introducing well and nearby monitoring wells (Güven et al. 1985; Molz et al. 1985; Güven et al. 1986; Molz et al. 1986). Monitoring wells nearby are also used to evaluate changes in water level and water quality for the duration of the experiment.

Artificial tracers are added to injectate to differentiate between native groundwater and the movement of the recharge front. Ionized substances, particularly salt-based tracers like chloride (NaCl) and bromide (NaBr), are commonly used as conservative tracers (Ptak et al. 2004; Zakhem and Hafez 2012; Mosthaf et al. 2018; Gerenday et al. 2020). While chloride and bromide are the most popular, other ions may be used depending on the situation, including Li^+ , NO_3^- , and SO_4^{2-} (Davis et al. 1980; Mosthaf et al. 2018). Fluorescent dyes (e.g., fluorescein, sulforhodamine B, rhodamine B, and rhodamine WT) have also been used as artificial tracers (Smart and Laidlaw 1977; Kasnavia et al. 1999; Hadi et al. 2016; Mosthaf et al. 2018). Dyes were originally thought to be particularly useful in karst aquifers (Smart and Laidlaw 1977),

though they have also been implemented in other systems in conjunction with additional tracers to characterize travel times (e.g., Hadi et al. 2016; Moeck et al. 2017). Dissolved gases (e.g., sulfur hexafluoride [SF₆], noble gases) allow large volumes of water to be tagged (Moran et al. 2007; Mayer et al. 2014; Moeck et al. 2017; Gerenday et al. 2020) and are often used in conjunction with other conservative tracers. Gerenday demonstrated the use of SF₆ in conjunction with bromide in a MAR infiltration basin to evaluate aquifer heterogeneity, subsurface residence time, and porous media saturation, since SF₆ exsolves from groundwater when it encounters trapped air (Gerenday et al. 2020).

While artificial tracers are added to injectate to add or increase the concentration of the tracer constituent, intrinsic tracers are tracers that are native to the system or injectate. Intrinsic tracers have been used to infer groundwater ages and residence times and have been reviewed in depth (Geyh 1957; Plummer 2005; Newman et al. 2010; Herczeg and Leaney 2011; Turnadge and Smerdon 2014). Isotopes are common intrinsic tracers, especially in aquifers where groundwater age is significantly older than recent recharge (Mayer et al. 2014; Moeck et al. 2017), and they have even been used to directly estimate the rate of saltwater intrusion in a deep, confined aquifer in Israel (Yechieli et al. 2019). Temperature has also been used as an intrinsic tracer (Becker et al. 2013; Irvine et al. 2016; Moeck et al. 2017). Becker et al. (2013) used fiber optic temperature sensing to assess recharge basin performance over seasonal variations. Anthropogenic tracers also fall under the category of intrinsic tracers and can include persistent organic and chemical pollutants (Hillebrand et al. 2015; Urresti-Estala et al. 2015).

Intrinsic tracers are especially valuable in the context of an ALTR project, where large-scale site characterization is a primary goal. In recharge wells where the injectate has a water quality with constituents that are significantly different than the native groundwater, indicators

within the injectate can be used as the primary marker of breakthrough at nearby monitoring wells. The use of injectate as an intrinsic tracer can be a more cost-effective way to characterize a site; as site scale increases, the volume of artificial tracer necessary to be above detection at distant wells increases concomitantly and can be cost-prohibitive. Williams (2000) demonstrated the effectiveness of ASR injectate as an intrinsic tracer over the course of over a year with multiple ASR cycles occurring. Pavelic (2006) also employed ASR injectate as a long-term tracer, using both chloride breakthrough and thermal profiling data to characterize recovery efficiency in a heterogeneous receiving aquifer over the course of multiple ASR cycles. Izbicki et al. (2010) also demonstrated the use of chloride in ASR injectate as a conservative tracer to evaluate transport during ASR operations, determine fate and transport of non-conservative disinfection byproducts (DBPs), and assess recovery efficiency in a heterogeneous aquifer in Roseville, California. Zakhem et al. (2012) also used chloride, nitrate, and conductivity to evaluate recovery efficiency for an ASR project in Syria.

To increase confidence in aquifer parameters and identify potential water quality mechanisms in an aquifer system, multi-tracer tests can use a combination of intrinsic and artificial tracers over the course of an entire project to characterize aquifer properties and evaluate flow between aquifer systems. Sanford et al. found that using multiple tracers (CFC-113, SF₆, ³H, and ³He) in a fractured-rock aquifer to calculate groundwater age was useful to identify and constrain transport parameters in a site model, as well as evaluate the effect of the dual-porosity nature of the system (Sanford et al. 2017). Hillebrand et al. (2015) also employed multiple reference tracers (uranine, acesulfame, and carbamazepine) and reactive compounds (including caffeine, ibuprofen, and paracetamol) to monitor contaminant transport between a sinkhole and a karst spring in southwest Germany. Multiple tracers have also been used to

characterize inter- and intra-aquifer connectivity; for example, Hadi et al. (2016) performed a FGTT using multiple tracers (rhodamine-WT, fluorescein, and sodium bromide) at multiple injection wells. Using multiple intrinsic tracers within the injectate has the potential to be particularly valuable in a multi-aquifer system where water quality characteristics vary by depth; a tracer that is suitable in one layer may be too similar to the water quality of another layer to show significant breakthrough, requiring multiple tracers for complete characterization.

While the use of tracer tests is a time-proven and useful tool to characterize groundwater flow and chemical transport through an aquifer system, tracer tests can also be cost prohibitive, especially as the scale of the test expands. Depending on the tracer, a high volume of solute may be needed for detection at distant monitoring wells. Furthermore, in an aquifer that spans a large range of depths, native groundwater characteristics may introduce uncertainty regarding how tracers interact with the native groundwater in a range of water quality characteristics that vary by screen depth. In conventional wells where there is one pump intake and either a long screen or multiple sample screens, monitoring wells may not fully capture a representative sample from the entire depth, which could lead to an underestimation of flow through the system (Reilly et al. 1989; Poulsen et al. 2019).

2.2. Modeling of ASR/ASTR Projects

Model development of an ALTR site to simulate physical transport is a tool for interpreting existing data and provides one step toward understanding the fate and transport of non-conservative constituents of interest and how they interact with the aquifer system. Ringleb et al. (2016) have previously discussed the breadth and importance of groundwater modeling of MAR projects in their review of the subject. In their review, the authors categorize ASR modeling studies by objective, with the most common objectives being geochemical processes

(i.e., clogging and water quality upon recovery), recovery efficiency, and groundwater management (Ringleb et al. 2016). Analytical models are useful to describe geochemical processes, calculate breakthrough of recharge water, and estimate water quality characteristics of recovered water. Herczeg et al. (2004) use analytical models to quantify the extent of interaction between recharge and native groundwater and the impact on water quality and aquifer stability. Pavelic et al. (2006) combine experimental methods with analytical and numerical models in their work to characterize a heterogeneous aquifer during ASR, but their work is screened over a single 60 m (164 feet) open borehole in a limestone formation and would not reflect aquifer conditions in a different geological setting.

Analytical solutions for transport in a radially divergent flow field have been developed to describe advective-dispersive transport under pumping or recharge conditions, though most solutions assume constant operating conditions (Hoopes and Harleman 1967; D.H. Tang and Babu 1979; C.S. Chen 1985; Hsieh 1986; Moench 1989; Goltz and Oxley 1991; Novakowski 1992; Moench 1995; J. Chen et al. 2012; Lai et al. 2016). Assuming constant operating conditions simplifies the approach by assuming that the velocity field is not a temporal function and that influent concentration at the recharge well is constant. Chen et al. (2012) present a semi-analytical approach that accounts for multi-step pumping and a variable influent concentration. To account for multiple pumping rates, the solution transforms the time domain into the cumulative injected flow domain, which transforms the temporally varying velocity field into a steady state flow problem, uses Laplace transforms to solve, and then maps the solution back into the time domain. Chen's solution is then tested with synthetic test cases and compared to numerical solutions from MATLAB's ODE solver (Chen et al. 2012). Chen's solution also assumes a single screen with known transient flow to the screen that can be described by

discretized functions. It does not account for a well with multiple screens where transient flow to the well can be quantified but distribution to a single screen is unknown and could also change over time; it is unclear whether Chen's solution could be used to inversely determine flow to a single screen.

Beyond the use of analytical models, numerical modeling is widely used to answer the research questions about ASR projects discussed earlier in this section. MODFLOW (McDonald and Harbaugh 1988) has been used in conjunction with other tools to estimate recovery efficiency on ASR projects and quantify hydrogeologic parameters on a project site (Sheng 2005; Lowry and Anderson 2006; Wang et al. 2012; Forghani and Peralta 2017). Lowry and Anderson (2006) use MODFLOW in conjunction with MODPATH and MT3DMS to simulate the mixing of native groundwater and recharge water. They also show that solute transport modeling is more effective than using particle tracking models to predict recovery rates when mixing is a factor (i.e., when water chemistry between native groundwater and injectate is significantly different) (Lowry and Anderson 2006). Modeling is also useful for assessing system performance and evaluating how injection has impacted local water levels (Sheng 2005). To describe variable density sites and preferential flow in dual-porosity conditions, SEAWAT, which is a combination of MODFLOW and MT3DMS, has been used effectively (Guo et al. 2015; Maliva et al. 2006).

In addition to physical transport, modeling has also been used to describe contaminant transport, including interactions with the aquifer during transport. PHREEQC/PHREEQC-2 (Parkhurst and Appelo 1999) has been utilized to identify and simulate geochemical reactions that impact water quality with the goal of optimizing recovered water quality and efficiency (Mirecki 2006; Vanderzalm et al. 2010). Gaus et al. (2002) use PHREEQC-2 and SWIFT (a 3D

dual porosity transport model) to model fluoride concentrations affected by dual porosity behavior and fluorite dissolution near an injection well during an ASR project. PHREEQC can also be used to optimize ASR operations based on injectate water quality by identifying hydrogeochemical processes that contribute to water quality degradation (Antoniou et al. 2013; 2015).

Regardless of the tools employed for modeling, using models that simulate interaction between recharge and native groundwater is important to reflect dispersion in the aquifer system (Lowry and Anderson 2006). Konikow (2011) notes that because no numerical method works for all conditions, solute transport models should be incorporated into models calibrated with other data and should be used for interpreting existing data rather than predictive modeling. Though most injection wells in existing studies are comprised of a single long screen or an open borehole, ASR modeling studies discussing density variations in native groundwater characteristics over long screens are uncommon (Ward et al. 2007; 2008). These variations could contribute to preferential flow pathways or affect flow distribution along a screen in an injection well.

2.3. Operational Effects on Aquifer Behavior and Breakthrough

Water quality of the recharge injectate at the wellhead and groundwater at nearby monitoring wells are typically assessed on a regular basis to comply with regulatory requirements and to monitor recharge operations. Aquifer geochemistry and well clogging are common issues with aquifer replenishment projects, and incompatibility between injectate and the native groundwater causes clogging and often leads to loss of specific capacity at the well and ultimately to failure of the project (Pyne 2005; Bloetscher et al. 2014). Jeong et al. (2018) outlined clogging mechanisms and categorized them into physical clogging caused by suspended

solids, fine particles, aquifer sediment perturbation, or dissolved gases; biological clogging, which can aggravate clogging already triggered by physical processes via biofilm formation and biomass accumulation; and chemical clogging, which results from precipitation of minerals due to changing redox conditions and change in pH between injectate and native groundwater.

In an aquifer recharge project, clogging over time can change the permeability coefficient, which can impact transport and water level analyses (Du et al. 2013; Li et al. 2019; Ye et al. 2019; Tang et al. 2020). Rinck-Pfeiffer et al. (2000) demonstrated that physical, biological, and chemical clogging processes occurred in tandem in laboratory column experiments that preceded field trials of an ASR project in South Australia. Suspended solids caused physical clogging, despite relatively low levels (3-4 mg/L) in the influent (Rinck-Pfeiffer et al. 2000). However, the concentration of suspended solids that produce clogging has been shown to be site specific (Okubo and Matsumoto 1983; P. Pavelic et al. 1998; Rinck-Pfeiffer et al. 2000). Clogging can also give rise to preferential flow through an aquifer system. In the context of a multi-screen well, preferential clogging can happen not only within a screen but also across well screens and would likely contribute to flow distribution being dynamic; as some screens clog, flow to that screen will decrease while flow to other, less clogged screens will increase with time.

In addition to the impacts of clogging on flow behavior of a recharge well, recharge operations (i.e., changes in operating conditions between recharge, pumping, and shut-down conditions) can also impact water quality measured by breakthrough indicators (Bullard et al. 2019). Together with the advective transport impacts occurring in a system experiencing both recharge (flow moving in an outward radial direction) and pumping (flow moving in an inward radial direction) conditions, back diffusion, or diffusive interaction between high- and low-

porosity domains in a heterogeneous aquifer system, is another potential cause of changes in water quality at a monitoring well. Multiple studies have attempted to numerically quantify this type of aquifer heterogeneity (van Genuchten and Wierenga 1976; Bibby 1981; Małoszewski and Zuber 1985; Gerke and van Genuchten 1993; Haggerty and Gorelick 1995; Cihan and Tyner 2011; Knorr et al. 2016). In the context of an ASR project, back diffusion would occur when recharge water flushes native groundwater from high-permeability media while native groundwater remains in low-permeability media around the screen. When advective transport stops, diffusion occurs between the two domains, and samples from a monitoring well show traces of native groundwater after breakthrough of recharge water has taken place. Aquifer heterogeneity is known to impact system performance and recovery efficiency in ASR projects (Guo et al. 2015). While this is certainly a concern when recovery is a major project goal, the impact of back diffusion should be considered when modeling an aquifer system to reconcile differences in breakthrough characteristics estimated by multiple tracer tests (Sanford et al. 2017). This persistence of native groundwater must be understood before impacts to water quality can be fully quantified.

In the existing literature, back diffusion is often used to describe plume persistence in an aquifer system even after rehabilitation of a contaminated region (Chapman et al. 2007; Parker et al. 2008; Rasa et al. 2011; Seyedabbasi et al. 2012; Parker and Kim 2015; Adamson et al. 2016; Wanner et al. 2018). While back diffusion has been employed to describe pollutant behavior, less research exists regarding the relationship between groundwater recharge, native groundwater, and back diffusion. The implementation of a dual-domain component to model breakthrough concentrations affected by back diffusion near an injection well has been documented by Gaus et al. (2002). Levy et al. (2016) conclude that in a peat bog, back diffusion into recharge water from

a peat matrix can alter the geochemical characteristics of discharge into adjacent bog sites. Libera et al. (2017) show that pumping schedule can influence solute concentrations at a pumping well in a heterogeneous aquifer, but this research is theoretical in nature. They examine a contaminant remediation condition with a known mass of contaminant, whereas the ratio of native groundwater to recharge water between a recharge well and monitoring well one screen of a multi-screen well is not easily determined (Libera et al. 2017). Previous research does not cover a large depth variation with a range of water quality characteristics at different screens, nor does it delve into whether a relationship between periods of no flow (i.e., significantly low advective transport) and changes in measured concentrations exists.

References

- Adamson, D.T., P.C. de Blanc, S.K. Farhat, and C.J. Newell. 2016. "Implications of Matrix Diffusion on 1,4-Dioxane Persistence at Contaminated Groundwater Sites." *Science of The Total Environment* 562 (August): 98–107. <https://doi.org/10.1016/j.scitotenv.2016.03.211>.
- Alazard, M., A. Boisson, J.-C. Maréchal, J. Perrin, B. Dewandel, T. Schwarz, M. Pettenati, G. Picot-Colbeaux, W. Kloppman, and S. Ahmed. 2016. "Investigation of Recharge Dynamics and Flow Paths in a Fractured Crystalline Aquifer in Semi-Arid India Using Borehole Logs: Implications for Managed Aquifer Recharge." *Hydrogeology Journal* 24: 35–57. <https://doi.org/10.1007/s10040-015-1323-5>.
- Antoniou, E.A., P.J. Stuyfzand, and B.M. van Breukelen. 2013. "Reactive Transport Modeling of an Aquifer Storage and Recovery (ASR) Pilot to Assess Long-Term Water Quality Improvements and Potential Solutions." *Applied Geochemistry* 35 (August): 173–86. <https://doi.org/10.1016/j.apgeochem.2013.04.009>.
- Antoniou, E.A., B.M. Van Breukelen, and P.J. Stuyfzand. 2015. "Optimizing Aquifer Storage and Recovery Performance through Reactive Transport Modeling." *Applied Geochemistry* 61: 29–40. <https://doi.org/10.1016/j.apgeochem.2015.05.009>.
- Basiricò, S., G.B. Crosta, P. Frattini, A. Villa, and A. Godio. 2015. "Borehole Flowmeter Logging for the Accurate Design and Analysis of Tracer Tests." *Groundwater* 53 (S1): 3–9. <https://doi.org/10.1111/gwat.12293>.
- Becker, M.W., B. Bauer, and A. Hutchinson. 2013. "Measuring Artificial Recharge with Fiber Optic Distributed Temperature Sensing." *Groundwater* 51 (5): 670–78. <https://doi.org/10.1111/j.1745-6584.2012.01006.x>.
- Bianchi, M. 2017. "Validity of Flowmeter Data in Heterogeneous Alluvial Aquifers." *Advances in Water Resources* 102: 29–44. <https://doi.org/10.1016/j.advwatres.2017.01.003>.
- Bibby, R. 1981. "Mass Transport of Solutes in Dual-Porosity Media." *Water Resources Research* 17 (4): 1075–81. <https://doi.org/10.1029/WR017i004p01075>.
- Bloetscher, F., C.H. Sham, J.J. Danko III, and S. Ratick. 2014. "Lessons Learned from Aquifer Storage and Recovery (ASR) Systems in the United States." *Journal of Water Resource and Protection* 06 (17): 1603–29. <https://doi.org/10.4236/jwarp.2014.617146>.
- Borgne, T. Le, O. Bour, F.L. Paillet, and J.P. Caudal. 2006. "Assessment of Preferential Flow Path Connectivity and Hydraulic Properties at Single-Borehole and Cross-Borehole Scales in a Fractured Aquifer." *Journal of Hydrology* 328 (1–2): 347–59. <https://doi.org/10.1016/j.jhydrol.2005.12.029>.
- Borgne, T Le, O. Bour, M.S. Riley, P. Gouze, P. Pezard, A. Belghoul, G. Lods, et al. 2007. "Comparison of Alternative Methodologies for Identifying and Characterizing

- Preferential Flow Paths in Heterogeneous Aquifers.” *Journal of Hydrology* 345 (3-4): 134–48. <https://doi.org/10.1016/j.jhydrol.2007.07.007>.
- Bullard, M.G., M. Widdowson, G. Salazar-Benites, J. Heisig-Mitchell, A. Nelson, and C. Bott. 2019. “Managed Aquifer Recharge: Transport and Attenuation in a Coastal Plain Aquifer.” In *Proceedings of the EWRI World Environmental and Water Resources Congress 2019: Groundwater, Sustainability, Hydro-Climate/Climate Change, and Environmental Engineering*, 1–14. Pittsburgh: EWRI. <https://doi.org/https://doi.org/10.1061/9780784482346.011>.
- Burris, D.L. 2018. “Groundwater Replenishment System 2018 Annual Report.” Irvine, CA. <https://www.ocwd.com/media/7933/2018-gwrs-annual-report.pdf>.
- Chapman, S.W., B.L. Parker, and J.A. Cherry. 2007. “Back Diffusion Effects on Performance of Source Zone Containment / Reduction Measures.” In *60th Canadian Geotechnical Conference & 8th Joint CGS/IAH-CNC Groundwater Conference*, 7.
- Chen, C.-S. 1985. “Analytical and Approximate Solutions to Radial Dispersion From an Injection Well to a Geological Unit With Simultaneous Diffusion Into Adjacent Strata.” *Water Resources Research* 21 (8): 1069–76. <https://doi.org/10.1029/WR021i008p01069>.
- Chen, C.-S., and C.-C. Chang. 2006. “Theoretical Evaluation of Non-Uniform Skin Effect on Aquifer Response under Constant Rate Pumping.” *Journal of Hydrology* 317 (3-4): 190–201. <https://doi.org/10.1016/j.jhydrol.2005.05.017>.
- Chen, J.-S., K.-H. Lai, C.-W. Liu, and C.-F. Ni. 2012. “A Novel Method for Analytically Solving Multi-Species Advective – Dispersive Transport Equations Sequentially Coupled with First-Order Decay Reactions.” *Journal of Hydrology* 420–421 (14 February 2012): 191–204. <https://doi.org/10.1016/j.jhydrol.2011.12.001>.
- Chen, Y.-J., H.-D. Yeh, and K.-J. Chang. 2012. “A Mathematical Solution and Analysis of Contaminant Transport in a Radial Two-Zone Confined Aquifer.” *Journal of Contaminant Hydrology* 138–139: 75–82. <https://doi.org/10.1016/j.jconhyd.2012.06.006>.
- Chen, Y., C. Lu, and J. Luo. 2012. “Solute Transport in Divergent Radial Flow with Multistep Pumping.” *Water Resources Research* 48 (2): 1–10. <https://doi.org/10.1029/2011WR010692>.
- Cheng, H. 2015. “Computing Flow through Well Screens Using an Embedded Well Technique.” <https://hdl.handle.net/11681/2082>
- Cihan, A., and J.S. Tyner. 2011. “2-D Radial Analytical Solutions for Solute Transport in a Dual-Porosity Medium.” *Water Resources Research* 47. <https://doi.org/10.1029/2009WR008969>.
- Collar, R.J., and P.A. Mock. 1997. “Using Water-Supply Wells to Investigate Vertical Ground-Water Quality.” *Ground Water* 35 (5): 743–50.

- Davis, S.N., G.M. Thompson, H.W. Bentley, and G. Stiles. 1980. "Ground-Water Tracers - A Short Review." *Ground Water* 18 (1): 14–23. <https://doi.org/10.1111/j.1745-6584.1980.tb03366.x>.
- Davis, S.N., D.J. Campbell, H.W. Bentley, and T.J. Flynn. 1985. "An Introduction to Ground-Water Tracers." Tuscon: EPA.
- Du, X., Z. Wang, and X. Ye. 2013. "Potential Clogging and Dissolution Effects During Artificial Recharge of Groundwater Using Potable Water." *Water Resources Management* 27 (10): 3573–83. <https://doi.org/10.1007/s11269-013-0365-5>.
- Fakhreddine, S., H. Prommer, S.M. Gorelick, J. Dadakis, and S. Fendorf. 2020. "Controlling Arsenic Mobilization during Managed Aquifer Recharge: The Role of Sediment Heterogeneity." *Environmental Science and Technology* 54 (14): 8728–38. <https://doi.org/10.1021/acs.est.0c00794>.
- Forghani, A., and R.C. Peralta. 2017. "Transport Modeling and Multivariate Adaptive Regression Splines for Evaluating Performance of ASR Systems in Freshwater Aquifers." *Journal of Hydrology* 553 (October): 540–48. <https://doi.org/10.1016/j.jhydrol.2017.08.012>.
- Gaus, I., P. Shand, I.N. Gale, A.T. Williams, and J.C. Eastwood. 2002. "Geochemical Modelling of Fluoride Concentration Changes during Aquifer Storage and Recovery (ASR) in the Chalk Aquifer in Wessex, England." *Quarterly Journal of Engineering Geology and Hydrogeology* 35 (2): 203–8. <https://doi.org/10.1144/1470-9236/2001-52>.
- Genuchten, M.T. van, and P.J. Wierenga. 1976. "Mass Transfer Studies in Sorbing Porous Media I. Analytical Solutions." *Soil Science Society of America Journal* 40 (4): 473–80. <https://doi.org/10.2136/sssaj1976.03615995004000040011x>.
- Gerenday, S.P., J.F. Clark, J. Hansen, I. Fischer, and J. Koreny. 2020. "Sulfur Hexafluoride and Potassium Bromide as Groundwater Tracers for Managed Aquifer Recharge." *Groundwater* 58 (5): 777–87. <https://doi.org/10.1111/gwat.12983>.
- Gerke, H.H., and M.T. van Genuchten. 1993. "A Dual-Porosity Model for Simulating the Preferential Movement of Water and Solutes in Structured Porous Media." *Water Resources Research* 29 (2): 305–19. <https://doi.org/10.1029/92WR02339>.
- Geyh, M.A. 1957. "Dating of Old Groundwater — History, Potential, Limits and Future." In *Isotopes in the Water Cycle*, 221–41. Berlin/Heidelberg: Springer-Verlag. https://doi.org/10.1007/1-4020-3023-1_15.
- Goltz, M.N., and M.E. Oxley. 1991. "Analytical Modeling of Aquifer Decontamination by Pumping When Transport Is Affected by Rate-Limited Sorption." *Water Resources Research* 27 (4): 547–56. <https://doi.org/10.1029/90WR02760>.

- Guo, W., K. Coulibaly, and R.G. Maliva. 2015. “Simulated Effects of Aquifer Heterogeneity on ASR System Performance.” *Environmental Earth Sciences* 73 (12): 7803–9. <https://doi.org/10.1007/s12665-014-3822-4>.
- Güven, O., R.W. Falta, F.J. Molz, and J.G. Melville. 1986. “A Simplified Analysis of Two-Well Tracer Tests in Stratified Aquifers.” *Ground Water* 24 (1): 63–71. <https://doi.org/10.1111/j.1745-6584.1986.tb01460.x>.
- Güven, O., R.W. Falta, F.J. Molz, and J.G. Melville. 1985. “Analysis and Interpretation of Single-Well Tracer Tests in Stratified Aquifers.” *Water Resources Research* 21 (5): 676–84. <https://doi.org/10.1029/WR021i005p00676>.
- Hadi, K., U. Saravana Kumar, M. Al-Senafy, A. Mukhopadhyay, A. Al-Khalid, K. Al-Fahad, and H. Bhandary. 2016. “Multi-Well and Multi-Tracer Tests to Characterize the Groundwater Aquifers in Southern Kuwait.” *Environmental Earth Sciences* 75 (20): 1340. <https://doi.org/10.1007/s12665-016-6143-y>.
- Haggerty, R., and S.M. Gorelick. 1995. “Multiple-Rate Mass Transfer for Modeling Diffusion and Surface Reactions in Media with Pore-Scale Heterogeneity.” *Water Resources Research* 31 (10): 2383–2400. <https://doi.org/10.1029/95WR10583>.
- Herczeg, A.L., and F.W. Leaney. 2011. “Review: Environmental Tracers in Arid-Zone Hydrology.” *Hydrogeology Journal* 19 (1): 17–29. <https://doi.org/10.1007/s10040-010-0652-7>.
- Herczeg, A.L., K.J. Rattray, P.J. Dillon, P. Pavelic, and K.E. Barry. 2004. “Geochemical Processes During Five Years of Aquifer Storage Recovery.” *Ground Water* 42 (3): 438–45. <https://doi.org/10.1111/j.1745-6584.2004.tb02691.x>.
- Hillebrand, O., K. Nödler, M. Sauter, and T. Licha. 2015. “Multitracer Experiment to Evaluate the Attenuation of Selected Organic Micropollutants in a Karst Aquifer.” *Science of The Total Environment* 506–507 (February): 338–43. <https://doi.org/10.1016/j.scitotenv.2014.10.102>.
- Hoopes, J.A., and D.R.F. Harleman. 1967. “Dispersion in Radial Flow from a Recharge Well.” *Journal of Geophysical Research* 72 (14): 3595–3607. <https://doi.org/10.1029/JZ072i014p03595>.
- Hsieh, P.A. 1986. “A New Formula for the Analytical Solution of the Radial Dispersion Problem.” *Water Resources Research* 22 (11): 1597–1605. <https://doi.org/10.1029/WR022i011p01597>.
- Irvine, D.J., I. Cartwright, V.E.A. Post, C.T. Simmons, and E.W. Banks. 2016. “Uncertainties in Vertical Groundwater Fluxes from 1-D Steady State Heat Transport Analyses Caused by Heterogeneity, Multidimensional Flow, and Climate Change.” *Water Resources Research* 52 (2): 813–26. <https://doi.org/10.1002/2015WR017702>.

- Izbicki, J.A., A.H. Christensen, R.T. Hanson, P. Martin, S.M. Crawford, and G.A. Smith. 1999. "U.S. Geological Survey Combined Well-Bore Flow and Depth-Dependent Water Sampler." <https://doi.org/10.3133/fs19699>.
- Izbicki, J.A., C.E. Petersen, K.J. Glotzbach, L.F. Metzger, A.H. Christensen, G.A. Smith, D. O'leary, M.S. Fram, T. Joseph, and H. Shannon. 2010. "Aquifer Storage Recovery (ASR) of Chlorinated Municipal Drinking Water in a Confined Aquifer." *Applied Geochemistry* 25: 1133–52. <https://doi.org/10.1016/j.apgeochem.2010.04.017>.
- Jeong, H.Y., S.-C. Jun, J.-Y. Cheon, and M. Park. 2018. "A Review on Clogging Mechanisms and Managements in Aquifer Storage and Recovery (ASR) Applications." *Geosciences Journal* 22 (4): 667–79. <https://doi.org/10.1007/s12303-017-0073-x>.
- Kasnavia, T., D. Vu, and D.A. Sabatini. 1999. "Fluorescent Dye and Media Properties Affecting Sorption and Tracer Selection." *Ground Water* 37 (3): 376–81. <https://doi.org/10.1111/j.1745-6584.1999.tb01114.x>.
- Knorr, B., P. Maloszewski, F. Krämer, and C. Stumpp. 2016. "Diffusive Mass Exchange of Non-Reactive Substances in Dual-Porosity Porous Systems - Column Experiments under Saturated Conditions." *Hydrological Processes* 30 (6): 914–26. <https://doi.org/10.1002/hyp.10620>.
- Konikow, L.F. 2011. "The Secret to Successful Solute-Transport Modeling." *Ground Water* 49 (2): 144–59. <https://doi.org/10.1111/j.1745-6584.2010.00764.x>.
- Lai, K.-H., C.-W. Liu, C.-P. Liang, J.-S. Chen, and B.-R. Sie. 2016. "A Novel Method for Analytically Solving a Radial Advection-Dispersion Equation." *Journal of Hydrology* 542: 532–40. <https://doi.org/10.1016/j.jhydrol.2016.09.027>.
- Levy, Z.F., D.I. Siegel, P.H. Glaser, S.D. Samson, and S.S. Dasgupta. 2016. "Peat Porewaters Have Contrasting Geochemical Fingerprints for Groundwater Recharge and Discharge Due to Matrix Diffusion in a Large, Northern Bog-Fen Complex." *Journal of Hydrology* 541 (October): 941–51. <https://doi.org/10.1016/j.jhydrol.2016.08.001>.
- Li, J., J.-J. Chen, and M.-G. Li. 2019. "Theoretical Study on the Groundwater Flow Induced by Artificial Recharge in Confined Aquifer Considering Permeability Degradation." In *Geo-Congress 2019*, 1–12. Reston, VA: American Society of Civil Engineers. <https://doi.org/10.1061/9780784482131.001>.
- Li, W., A. Englert, O.A. Cirpka, and H. Vereecken. 2008. "Three-Dimensional Geostatistical Inversion of Flowmeter and Pumping Test Data." *Ground Water* 46 (2): 193–201. <https://doi.org/10.1111/j.1745-6584.2007.00419.x>.
- Libera, A., F.P.J. de Barros, and A. Guadagnini. 2017. "Influence of Pumping Operational Schedule on Solute Concentrations at a Well in Randomly Heterogeneous Aquifers." *Journal of Hydrology* 546 (March): 490–502. <https://doi.org/10.1016/j.jhydrol.2016.12.022>.

- Lowry, C.S., and M.P. Anderson. 2006. "An Assessment of Aquifer Storage Recovery Using Ground Water Flow Models." *Ground Water* 44 (5): 661–67. <https://doi.org/10.1111/j.1745-6584.2006.00237.x>.
- Maliva, R.G., W. Guo, and T.M. Missimer. 2006. "Aquifer Storage and Recovery: Recent Hydrogeological Advances and System Performance." *Water Environment Research* 78 (13): 2428–35. <https://doi.org/10.2175/106143006X123102>.
- Małoszewski, P., and A. Zuber. 1985. "On the Theory of Tracer Experiments in Fissured Rocks with a Porous Matrix." *Journal of Hydrology* 79 (3–4): 333–58. [https://doi.org/10.1016/0022-1694\(85\)90064-2](https://doi.org/10.1016/0022-1694(85)90064-2).
- Mayer, A., J. Sültenfuß, Y. Travi, R. Rebeix, R. Purtschert, C. Claude, C. Le Gal La Salle, H. Miche, and E. Conchetto. 2014. "A Multi-Tracer Study of Groundwater Origin and Transit-Time in the Aquifers of the Venice Region (Italy)." *Applied Geochemistry* 50: 177–98. <https://doi.org/10.1016/j.apgeochem.2013.10.009>.
- Mayo, A.L. 2010. "Ambient Well-Bore Mixing, Aquifer Cross-Contamination, Pumping Stress, and Water Quality from Long-Screened Wells: What Is Sampled and What Is Not?" *Hydrogeology Journal* 18: 823–37. <https://doi.org/10.1007/s10040-009-0568-2>.
- McDonald, M.G., and A.W. Harbaugh. 1988. "A Modular Three-Dimensional Finite-Difference Ground-Water Flow Model." In *Techniques of Water-Resources Investigations*, Book 6, Chapter A1 (TWR16-A1). Washington, D.C., USA: USGS.
- Mirecki, J. 2006. "Geochemical Models of Water-Quality Changes During Aquifer Storage Recovery (ASR) Cycle Tests, Phase 1: Geochemical Models Using Existing Data." U.S. Army Corps of Engineers, Engineers Research and Development Center, Vicksburg, MS, USA.
- Moeck, C., D. Radny, A. Popp, M. Brennwald, S. Stoll, A. Auckenthaler, M. Berg, and M. Schirmer. 2017. "Characterization of a Managed Aquifer Recharge System Using Multiple Tracers." *Science of The Total Environment* 609 (December): 701–14. <https://doi.org/10.1016/j.scitotenv.2017.07.211>.
- Moench, A.F. 1989. "Convergent Radial Dispersion: A Laplace Transform Solution for Aquifer Tracer Testing." *Water Resources Research* 25 (3): 439–47. <https://doi.org/10.1029/WR025i003p00439>.
- . 1995. "Convergent Radial Dispersion in a Double-Porosity Aquifer with Fracture Skin: Analytical Solution and Application to a Field Experiment in Fractured Chalk." *Water Resources Research* 31 (8): 1823–35. <https://doi.org/10.1029/95WR01275>.
- Molz, F.J., G.K. Boman, S.C. Young, and W.R. Waldrop. 1994. "Borehole Flowmeters: Field Application and Data Analysis." *Journal of Hydrology* 163 (3–4): 347–71. [https://doi.org/10.1016/0022-1694\(94\)90148-1](https://doi.org/10.1016/0022-1694(94)90148-1).

- Molz, F.J., O. Güven, J.G. Melville, R.D. Crocker, and K.T. Matteson. 1986. "Performance, Analysis, and Simulation of a Two-Well Tracer Test at the Mobile Site." *Water Resources Research* 22 (7): 1031–37. <https://doi.org/10.1029/WR022i007p01031>.
- Molz, F.J., O. Güven, J.G. Melville, J.S. Nohrstedt, and J.K. Overholtzer. 1988. "Forced-Gradient Tracer Tests and Inferred Hydraulic Conductivity Distributions at the Mobile Site." *Ground Water* 26 (5): 570–79. <https://doi.org/10.1111/j.1745-6584.1988.tb00790.x>.
- Molz, F.J., J.G. Melville, O. Güven, R.D. Crocker, and K.T. Matteson. 1985. "Design and Performance of Single-Well Tracer Tests at the Mobile Site." *Water Resources Research* 21 (10): 1497–1502. <https://doi.org/10.1029/WR021i010p01497>.
- Molz, F.J., R.H. Morin, A.E. Hess, J.G. Melville, and O. Güven. 1989. "The Impeller Meter for Measuring Aquifer Permeability Variations: Evaluation and Comparison With Other Tests." *Water Resources Research* 25 (7): 1677–83. <https://doi.org/10.1029/WR025i007p01677>.
- Moran, J.E., M.J. Singleton, S.F. Carle, and B.K. Esser. 2007. "Intrinsic and Extrinsic Chemical and Isotopic Tracers for Characterization of Groundwater Systems." In *3D Geological Mapping for Groundwater Applications* (Denver, CO; October 28, 2007), 6 pp. <https://e-reports-ext.llnl.gov/pdf/352597.pdf>.
- Mosthaf, K., B. Brauns, A.S. Fjordbøge, M.M. Rohde, H. Kern-Jespersen, P.L. Bjerg, P.J. Binning, and M.M. Broholm. 2018. "Conceptualization of Flow and Transport in a Limestone Aquifer by Multiple Dedicated Hydraulic and Tracer Tests." *Journal of Hydrology* 561 (June): 532–46. <https://doi.org/10.1016/j.jhydrol.2018.04.011>.
- Mukhopadhyay, A., F. Székely, and Y. Senay. 1995. "Artificial Ground Water Recharge Experiments in Carbonate and Clastic Aquifers of Kuwait." *Water Resources Bulletin* 30 (6): 1091–1107.
- Newman, B.D., K. Osenbrück, W. Aeschbach-Hertig, D.K. Solomon, P. Cook, K. Rózański, and R. Kipfer. 2010. "Dating of 'Young' Groundwaters Using Environmental Tracers: Advantages, Applications, and Research Needs." *Isotopes in Environmental and Health Studies* 46 (3): 259–78. <https://doi.org/10.1080/10256016.2010.514339>.
- Novakowski, K.S. 1992. "The Analysis of Tracer Experiments Conducted in Divergent Radial Flow Fields." *Water Resources Research* 28 (12): 3215–25.
- Oberlander, P.L., and C.E. Russell. 2006. "Process Considerations for Trolling Borehole Flow Logs." *Ground Water Monitoring and Remediation* 26 (3): 60–67. <https://doi.org/10.1111/j.1745-6592.2006.00084.x>.
- Okubo, T., and J. Matsumoto. 1983. "Biological Clogging of Sand and Changes of Organic Constituents during Artificial Recharge." *Water Research* 17 (7): 813–21. [https://doi.org/10.1016/0043-1354\(83\)90077-5](https://doi.org/10.1016/0043-1354(83)90077-5).

- Paillet, F.L. 1998. "Flow Modeling and Permeability Estimation Using Borehole Flow Logs in Heterogeneous Fractured Formations." *Water Resources Research* 34 (5): 997–1010. <https://doi.org/10.1029/98WR00268>.
- Paillet, F.L. 2004. "Borehole Flowmeter Applications in Irregular and Large-Diameter Boreholes." *Journal of Applied Geophysics* 55: 39–59. <https://doi.org/10.1016/j.jappgeo.2003.06.004>.
- Parker, A.H., L.J. West, N.E. Odling, and R.T. Bown. 2010. "A Forward Modeling Approach for Interpreting Impeller Flow Logs." *Ground Water* 48 (1): 79–91. <https://doi.org/10.1111/j.1745-6584.2009.00600.x>.
- Parker, B.L., S.W. Chapman, and M.A. Guilbeault. 2008. "Plume Persistence Caused by Back Diffusion from Thin Clay Layers in a Sand Aquifer Following TCE Source-Zone Hydraulic Isolation." *Journal of Contaminant Hydrology* 102 (1–2): 86–104. <https://doi.org/10.1016/j.jconhyd.2008.07.003>.
- Parker, J.C., and U. Kim. 2015. "An Upscaled Approach for Transport in Media with Extended Tailing Due to Back-Diffusion Using Analytical and Numerical Solutions of the Advection Dispersion Equation." *Journal of Contaminant Hydrology* 182: 157–72. <https://doi.org/10.1016/j.jconhyd.2015.09.008>.
- Parkhurst, D.L., and C.A.J. Appelo. 1999. "PHREEQC (Version 2)—A Computer Program for Speciation, Batch-Reaction, One-Dimensional Transport, and Inverse Geochemical Calculations." Denver, CO, USA.
- Pavelic, P., P.J. Dillon, K.E. Barry, A.L. Herczeg, K.J. Rattray, P. Hekmeijer, and N.Z. Gerges. 1998. "Well Clogging Effects Determined from Mass Balances and Hydraulic Response at a Stormwater ASR Site." In *Third International Symposium on Artificial Recharge*. Amsterdam, Holland, 21-25 September.
- Pavelic, P., P.J. Dillon, and C.T. Simmons. 2006. "Multiscale Characterization of a Heterogeneous Aquifer Using an ASR Operation." *Ground Water* 44 (2): 155–64. <https://doi.org/10.1111/j.1745-6584.2005.00135.x>.
- Plummer, L.N. 2005. "Dating of Young Groundwater." In *Isotopes in the Water Cycle*, 193–218. Berlin/Heidelberg: Springer-Verlag. https://doi.org/10.1007/1-4020-3023-1_14.
- Poulsen, D.L., P.G. Cook, C.T. Simmons, J.L. McCallum, and S. Dogramaci. 2019. "Effects of Intraborehole Flow on Purging and Sampling Long-Screened or Open Wells." *Groundwater* 57 (2): 269–78. <https://doi.org/10.1111/gwat.12797>.
- Ptak, T., M. Piepenbrink, and E. Martac. 2004. "Tracer Tests for the Investigation of Heterogeneous Porous Media and Stochastic Modelling of Flow and Transport—a Review of Some Recent Developments." *Journal of Hydrology* 294 (1–3): 122–63. <https://doi.org/10.1016/j.jhydrol.2004.01.020>.

- Pyne, R.D.G. 2005. *Aquifer Storage Recovery: A Guide to Groundwater Recharge Through Wells*. Gainesville, FL: ASR Press.
- Rasa, E., S.W. Chapman, B.A. Bekins, G.E. Fogg, K.M. Scow, and D.M. Mackay. 2011. "Role of Back Diffusion and Biodegradation Reactions in Sustaining an MTBE/TBA Plume in Alluvial Media." *Journal of Contaminant Hydrology* 126 (3–4): 235–47. <https://doi.org/10.1016/j.jconhyd.2011.08.006>.
- Rehfeldt, K.R., J.M. Boggs, and L.W. Gelhar. 1992. "Field Study of Dispersion in a Heterogeneous Aquifer: 3. Geostatistical Analysis of Hydraulic Conductivity." *Water Resources Research* 28 (12): 3309–24. <https://doi.org/http://doi.org/10.1029/9zwr01758>.
- Reilly, E.T., O.L. Franke, G.D. Bennett. 1989. "Bias in Groundwater Samples Caused By Wellbore Flow." *J. Hydraul. Eng.* 115 (2): 270–76. [https://doi.org/10.1061/\(ASCE\)0733-9429\(1989\)115:2\(270\)](https://doi.org/10.1061/(ASCE)0733-9429(1989)115:2(270)).
- Rinck-Pfeiffer, S., S. Ragusa, P. Sztajn bok, and T. Vandev elde. 2000. "Interrelationships between Biological, Chemical, and Physical Processes as an Analog to Clogging in Aquifer Storage and Recovery (ASR) Wells." *Water Research* 34 (7): 2110–18. [https://doi.org/10.1016/S0043-1354\(99\)00356-5](https://doi.org/10.1016/S0043-1354(99)00356-5).
- Ringleb, J., J. Sallwey, and C. Stefan. 2016. "Assessment of Managed Aquifer Recharge through Modeling-A Review." *Water (Switzerland)* 8 (12): 1–32. <https://doi.org/10.3390/w8120579>.
- Riva, M., P. Ackerer, and A. Guadagnini. 2012. "Interpretation of Flowmeter Data in Heterogeneous Layered Aquifers." *Journal of Hydrology* 452–453 (July): 76–82. <https://doi.org/10.1016/j.jhydrol.2012.05.040>.
- Ruud, N.C., and Z.J. Kabala. 1997. "Numerical Evaluation of the Flowmeter Test in a Layered Aquifer with a Skin Zone." *Journal of Hydrology* 203: 101–8.
- Ruud, N.C., Z.J. Kabala, and F.J. Molz. 1999. "Evaluation of Flowmeter-Head Loss Effects in the Flowmeter Test." *Journal of Hydrology* 224: 55–63. www.elsevier.com/locate/jhydrol.
- Sanford, W.E., L.N. Plummer, G. Casile, E. Busenberg, D.L. Nelms, and P. Schlosser. 2017. "Using Dual-Domain Advective-Transport Simulation to Reconcile Multiple-Tracer Ages and Estimate Dual-Porosity Transport Parameters." *Water Resources Research* 53 (6): 5002–16. <https://doi.org/10.1002/2016WR019469>.
- Seyedabbasi, M.A., C.J. Newell, D.T. Adamson, and T.C. Sale. 2012. "Relative Contribution of DNAPL Dissolution and Matrix Diffusion to the Long-Term Persistence of Chlorinated Solvent Source Zones." *Journal of Contaminant Hydrology* 134–135 (June): 69–81. <https://doi.org/10.1016/j.jconhyd.2012.03.010>.

- Sheng, Z. 2005. “An Aquifer Storage and Recovery System with Reclaimed Wastewater to Preserve Native Groundwater Resources in El Paso, Texas.” *Journal of Environmental Management* 75 (4): 367–77. <https://doi.org/10.1016/j.jenvman.2004.10.007>.
- Smart, P.L., and I.M.S. Laidlaw. 1977. “An Evaluation of Some Fluorescent Dyes for Water Tracing.” *Water Resources Research* 13 (1): 15–33. <https://doi.org/10.1029/WR013i001p00015>.
- Tang, D.H., and D.K. Babu. 1979. “Analytical Solution of a Velocity Dependent Dispersion Problem.” *Water Resources Research* 15 (6): 1471–78. <https://doi.org/10.1029/WR015i006p01471>.
- Tang, Y., X. Yao, Y. Chen, Y. Zhou, D.Z. Zhu, Y. Zhang, T. Zhang, and Y. Peng. 2020. “Experiment Research on Physical Clogging Mechanism in the Porous Media and Its Impact on Permeability.” *Granular Matter* 22 (2): 37. <https://doi.org/10.1007/s10035-020-1001-8>.
- Turnadge, C., and B.D. Smerdon. 2014. “A Review of Methods for Modelling Environmental Tracers in Groundwater: Advantages of Tracer Concentration Simulation.” *Journal of Hydrology* 519 (PD): 3674–89. <https://doi.org/10.1016/j.jhydrol.2014.10.056>.
- Urresti-Estala, B., I. Vadillo-Pérez, P. Jiménez-Gavilán, A. Soler, D. Sánchez-García, and F. Carrasco-Cantos. 2015. “Application of Stable Isotopes ($\Delta^{34}\text{S-SO}_4$, $\Delta^{18}\text{O-SO}_4$, $\Delta^{15}\text{N-NO}_3$, $\Delta^{18}\text{O-NO}_3$) to Determine Natural Background and Contamination Sources in the Guadalhorce River Basin (Southern Spain).” *Science of The Total Environment* 506–507 (February): 46–57. <https://doi.org/10.1016/j.scitotenv.2014.10.090>.
- Vanderzalm, J.L., D.W. Page, K.E. Barry, and P.J. Dillon. 2010. “A Comparison of the Geochemical Response to Different Managed Aquifer Recharge Operations for Injection of Urban Stormwater in a Carbonate Aquifer.” *Applied Geochemistry* 25 (9): 1350–60. <https://doi.org/10.1016/j.apgeochem.2010.06.005>.
- Wang, J., Y. Wu, X. Zhang, Y. Liu, T. Yang, and B. Feng. 2012. “Field Experiments and Numerical Simulations of Confined Aquifer Response to Multi-Cycle Recharge–Recovery Process through a Well.” *Journal of Hydrology* 464–465 (September): 328–43. <https://doi.org/10.1016/j.jhydrol.2012.07.018>.
- Wanner, P., B.L. Parker, and D. Hunkeler. 2018. “Assessing the Effect of Chlorinated Hydrocarbon Degradation in Aquitards on Plume Persistence Due to Back-Diffusion.” *Science of The Total Environment* 633 (August): 1602–12. <https://doi.org/10.1016/j.scitotenv.2018.03.192>.
- Ward, J.D., C.T. Simmons, and P.J. Dillon. 2007. “A Theoretical Analysis of Mixed Convection in Aquifer Storage and Recovery: How Important Are Density Effects?” *Journal of Hydrology* 343 (3–4): 169–86. <https://doi.org/10.1016/j.jhydrol.2007.06.011>.

- . 2008. “Variable-Density Modelling of Multiple-Cycle Aquifer Storage and Recovery (ASR): Importance of Anisotropy and Layered Heterogeneity in Brackish Aquifers.” *Journal of Hydrology* 356 (1–2): 93–105. <https://doi.org/10.1016/j.jhydrol.2008.04.012>.
- Williams, A.T. 2000. “Using an Aquifer Storage and Recovery (ASR) Trial as a Large Scale Tracer Test.” In *Tracers and Modelling in Hydrogeology*, edited by A Dassargues, 195–99. Liege, Belgium: IAHS.
[https://books.google.com/books?hl=en&lr=&id=Uv439c4rqvsC&oi=fnd&pg=PA195&dq=Using+an+aquifer+storage+and+recovery+\(ASR\)+trial+as+a+large+scale+tracer+test&ots=iH1Ok5M2vb&sig=m2ZofzIHAWuCEL_8vGI52PCIVyE#v=twopage&q&f=false](https://books.google.com/books?hl=en&lr=&id=Uv439c4rqvsC&oi=fnd&pg=PA195&dq=Using+an+aquifer+storage+and+recovery+(ASR)+trial+as+a+large+scale+tracer+test&ots=iH1Ok5M2vb&sig=m2ZofzIHAWuCEL_8vGI52PCIVyE#v=twopage&q&f=false).
- Ye, X., R. Cui, X. Du, S. Ma, J. Zhao, Y. Lu, and Y. Wan. 2019. “Mechanism of Suspended Kaolinite Particle Clogging in Porous Media During Managed Aquifer Recharge.” *Groundwater* 57 (5): 764–71. <https://doi.org/10.1111/gwat.12872>.
- Yechieli, Y., R. Yokochi, M. Zilberbrand, Z.-T. Lu, R. Purtschert, J. Sueltenfuss, W. Jiang, et al. 2019. “Recent Seawater Intrusion into Deep Aquifer Determined by the Radioactive Noble-Gas Isotopes ⁸¹Kr and ³⁹Ar.” *Earth and Planetary Science Letters* 507 (February): 21–29. <https://doi.org/10.1016/j.epsl.2018.11.028>.
- Young, S.C. 1995. “Characterization of High-K Pathways by Borehole Flowmeter and Tracer Tests.” *Ground Water* 33 (2): 311–18. <https://doi.org/10.1111/j.1745-6584.1995.tb00286.x>.
- Young, S.C., H.K. Julian, H.S. Pearson, F.J. Molz, and G.K. Boman. 1998. “Application of the Electromagnetic Borehole Flowmeter.” USEPA Report. Vol. EPA/600/R-.
- Zakhem, B.A., and R. Hafez. 2012. “Chemical and Isotopic Methods for Management of Artificial Recharge in Mazraha Station (Damascus Basin, Syria).” *Hydrological Processes* 26 (24): 3712–24. <https://doi.org/10.1002/hyp.8446>.
- Zlotnik, V.A., and B.R. Zurbuchen. 2003a. “Estimation of Hydraulic Conductivity from Borehole Flowmeter Tests Considering Head Losses.” *Journal of Hydrology* 281 (1–2): 115–28. [https://doi.org/10.1016/S0022-1694\(03\)00204-X](https://doi.org/10.1016/S0022-1694(03)00204-X).
- Zlotnik, V.A., and B.R. Zurbuchen. 2003b. “Field Study of Hydraulic Conductivity in a Heterogeneous Aquifer: Comparison of Single-Borehole Measurements Using Different Instruments.” *Water Resources Research* 39 (4): 1101.
<https://doi.org/10.1029/2002WR001415>.

3. Demonstration of Managed Aquifer Recharge in a Coastal Plain Aquifer: Lessons Learned

Title

Demonstration of Managed Aquifer Recharge in a Coastal Plain Aquifer: Lessons Learned

Published in: *Groundwater*

Citation: Martinez, M.B., Widdowson, M.A., Bott, C., Holloway, D., Heisig-Mitchell, J. and Wilson, C. (2022), Demonstration of Managed Aquifer Recharge in a Coastal Plain Aquifer: Lessons Learned. Groundwater. Accepted Author Manuscript. <https://doi.org/10.1111/gwat.13197>

Link: <https://doi.org/10.1111/gwat.13197>

Abstract

The Sustainable Water Initiative for Tomorrow (SWIFT) is a 378,000 m³/day (100 MGD) managed aquifer recharge (MAR) program designed by the Hampton Roads Sanitation District (HRSD) to rehabilitate the Potomac Aquifer System (PAS) in the Coastal Plain of Eastern Virginia. Groundwater is a primary water source in Eastern Virginia with over 93% of reported use derived from the PAS. Starting in May 2018, HRSD has operated a 3,780 m³/day (1.0 MGD) MAR demonstration facility at the SWIFT Research Center (SWIFT-RC) in Suffolk, Virginia. The primary aim of the SWIFT-RC is to demonstrate, at a meaningful scale, the feasibility of MAR using deep well recharge into confined PAS hydrostratigraphic unit. The SWIFT-RC employs advanced water treatment technology to bring secondary effluent from an HRSD wastewater treatment plant to drinking water standards. Lessons learned include the evaluation and selection of a multiple barrier carbon-based treatment system to ensure water quality and maintain geochemical compatibility between MAR water and native groundwater, and the evaluation and selection of aluminum chlorohydrate for stabilizing aquifer clays immediately around the well to accept the fresher recharge water. The distribution of flow in the SWIFT-RC multiscreen recharge well and associated well injectivity were variable with time

resulting from changing conditions in the well. Dynamic recharge well performance was quantified through the combined analysis of intrinsic and artificial tracer transport, in-situ flowmeter testing, and water level analysis. Monitoring well nests and a depth-discrete sampling system supported a robust sampling plan to analyze chemical transport and attenuation in SWIFT-RC groundwater.

3.1 Introduction

Groundwater withdrawals from the Potomac Aquifer System (PAS) in the Coastal Plain of Virginia (USA) over decades has resulted in a decline of the potentiometric surface by nearly 71 m (232 feet) near centers of large, regulated usage (Heywood and Pope 2009). Of the total groundwater withdrawals in the state reported in 2019 (527,100 m³/day), approximately 47% was withdrawn from wells in the Virginia Coastal Plain Aquifer System (VDEQ 2020) located in the Eastern Virginia Ground Water Management Area (EVGWMA). The primary use of groundwater in the EVGWMA is public water supply and industrial use, 85,090 m³/day (22.48 MGD) and 132,600 m³/day (35.02 MGD), respectively (Lovelace et al. 2020). Estimates of unreported self-supplied domestic groundwater use in the EVGWMA range from 92,000 m³/day (24 MGD) in Lovelace et al. (2020) to 150,000 m³/day (40 MGD) in Virginia Department of Environmental Quality (VDEQ) (2018). The majority of groundwater withdrawals (74%) in the EVGWMA are derived from the PAS (McFarland and Bruce 2006) with 94% of permitted use in 2017 attributed to the PAS (VDEQ 2018).

The Sustainable Water Initiative for Tomorrow (SWIFT) is a managed aquifer recharge (MAR) program designed by the Hampton Roads Sanitation District (HRSD) to rehabilitate the PAS at a regional scale. A critical program driver was the Virginia Chesapeake Bay restoration

effort and HRSD's goal to reduce nutrient discharge to the Chesapeake Bay by 90% through advanced water treatment of HRSD wastewater effluent. With highly treated water available at multiple HRSD facilities, the SWIFT program has the potential to reverse groundwater declines through direct recharge of the PAS. Unlike other indirect potable reuse MAR projects including aquifer storage and recovery (e.g., Pyne 2005), SWIFT is designed for continuous recharge with no intentional reuse or recovery. Other potential benefits of the SWIFT Project include reducing pumping-induced land subsidence in the southeastern region of Virginia (Eggleston and Pope 2013) and inhibiting saltwater intrusion in the PAS (Nylen 2021).

The SWIFT Research Center (SWIFT-RC) is a 3,780 m³/day (1.0 MGD) MAR demonstration facility located at the HRSD Nansemond Treatment Plant in Suffolk, Virginia (Figure 3-1). The primary role of the SWIFT-RC is to demonstrate, at a meaningful scale, the feasibility of MAR via deep well recharge within the Coastal Plain. SWIFT-RC operational and monitoring findings are used to support requests for the necessary state and federal regulatory approvals and support of other key stakeholders for full-scale implementation. The SWIFT-RC also serves as a platform to conduct research for advanced water treatment processes and chemical transport and attenuation in groundwater. At full scale, design capacity will increase to 378,000 m³/day (100 MGD) distributed at five HRSD treatment facilities (Figure 3-1).

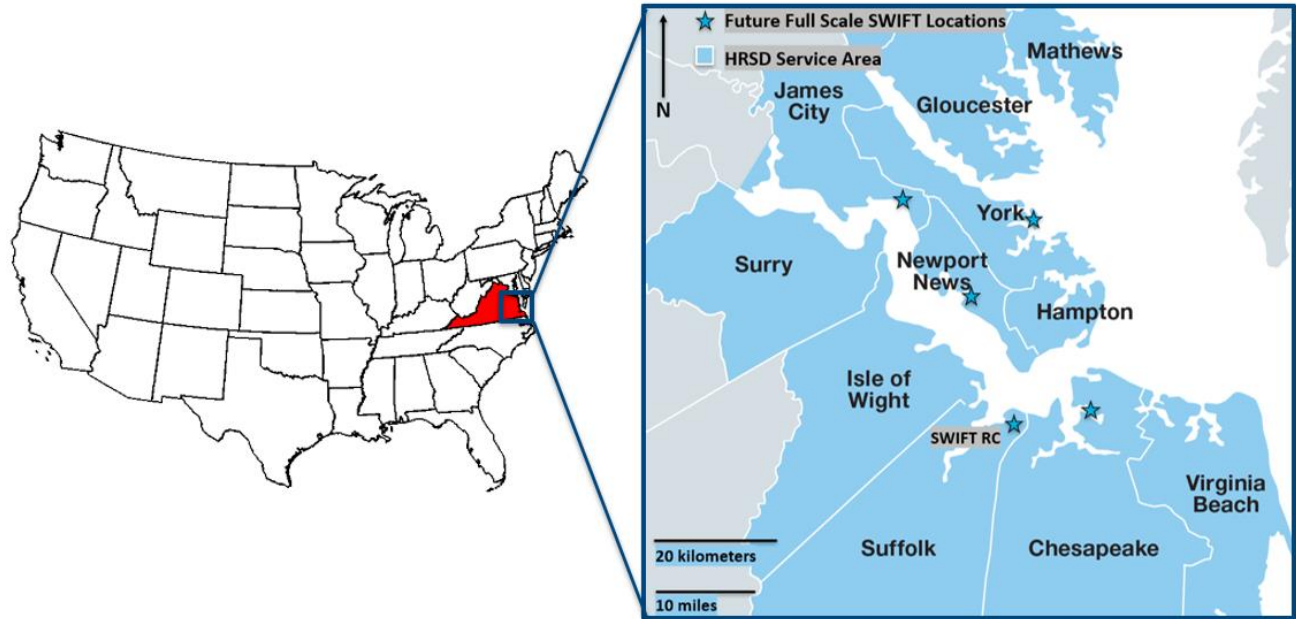


Figure 3-1. Location of the HRSD service area (blue), future full-scale SWIFT locations, and the SWIFT demonstration facility site (SWIFT-RC) in southeast Virginia, USA.

3.2 SWIFT Research Center (SWIFT-RC) Overview

3.2.1 Project Status

Recharge at the SWIFT-RC was initiated in May 2018 and has been continuous with several stoppages or withdrawal events of various durations. One extended withdrawal event occurred in August 2018 and lasted approximately 18 days. Two major stoppages enabled recharge well rehabilitation resulting from declining injectivity from November 2018 to April 2019 and from December 2020 to April 2021. Two shorter shutdowns of approximately one month occurred for treatment process maintenance during January and July 2020. During the first three years of operation, recharge to the PAS was supplied at the SWIFT-RC design capacity.

3.2.2 Source Water

Source water for the SWIFT Project is derived from secondary effluent from HRSD wastewater treatment plants, which already perform full nitrification and denitrification, as well as phosphorus removal. Prior to recharge at the SWIFT-RC, multiple pre-treatment steps are required to treat secondary effluent from the Nansemond Treatment Plant to drinking water standards. Following treatment, SWIFT-RC effluent or “SWIFT Water” is supplied to the PAS through a 30-cm diameter multi-screen recharge well located on site.

3.2.3 Regulatory Considerations for the SWIFT Project

As a potable water supply, native groundwater within the PAS generally meets The Environmental Protection Agency’s (EPA) Primary Safe Drinking Water Standards. Some exceptions include fluoride for certain locations within the upper zone of the PAS and radionuclides for the deeper zones of the PAS. However, total dissolved solids (TDS) in the PAS is at or above the secondary maximum contaminant level (MCL) of 500 mg/L, varying from 210 mg/L inland to 487,000 mg/L in wells adjacent to the coast (McFarland 2010). Unsustainable withdrawals from the PAS have reduced groundwater levels within the confined aquifer at rates from 0.4 to 0.6 m/yr over decades (Heywood and Pope 2009), reversing the natural gradient and making it susceptible to saltwater intrusion from brackish and saline portions of the aquifer (Smith 1999; McFarland 2010; 2015). At full scale the primary goal of the SWIFT program is to reverse PAS groundwater level declines and increase available groundwater storage. Although not a primary goal, the replenishment of the aquifer is anticipated to create a pressure barrier to prevent the lateral migration of saltwater onto the freshwater wellfields and reduce subsequent contamination of the potable aquifer supplies.

SWIFT Water and, subsequently, groundwater samples collected in SWIFT-RC monitoring wells, have consistently met U.S. drinking water quality standards, including MCLs as identified by the Safe Drinking Water Act. SWIFT-RC operations are permitted by rule, authorized by EPA Region 3's UIC program. Though Virginia does not have primary enforcement authority for the UIC program, a state oversight structure, the Potomac Aquifer Recharge Oversight Committee, was enabled through legislation to provide assurance that the SWIFT program, including its effect on the PAS, is monitored independently. The Potomac Aquifer Recharge Monitoring Laboratory, jointly led by Old Dominion University and Virginia Tech, provides the technical expertise necessary to accomplish this objective.

Pilot-scale column studies packed with aquifer sediment indicated that in-situ treatment occurs in the PAS and that chemical and biological contaminants, both regulated and unregulated, are removed during transport through the groundwater system (Dziura 2020). In-situ attenuation provides an additional post-treatment barrier against contaminants of concern and may inform the level of pre-recharge treatment required in future MAR projects.

3.2.4 Project Costs

The SWIFT program has been evaluated as part of an Integrated Plan designed to help communities prioritize capital investments in a manner that provides the maximum environmental and public health benefits. A cost evaluation was performed to evaluate various advanced treatment methods prior to MAR. This work suggested that a carbon-based advanced treatment scheme is approximately 25% and 50% less expensive on a capital and operational cost basis, respectively, as compared to a membrane-based approach that utilizes ultrafiltration, reverse osmosis, ultraviolet (UV) advanced oxidation, remineralization, and reverse osmosis

(RO) brine treatment (CH2M 2015). Full-scale buildout of SWIFT is estimated at a capital cost of approximately \$2.0B at five HRSD facilities with a final combined capacity of 378,000 m³/day (100 MGD). The capital and operating costs of the SWIFT-RC demonstration facility at 1% full capacity do not translate to the full-scale SWIFT as these costs are inflated due to the scale of the facility and the research capability and efforts ongoing there.

3.3 Project Infrastructure

3.3.1 Advanced Treatment Process

The activated carbon-based treatment train was determined to hold two significant advantages in comparison with membrane treatment: lower capital and annual operating and maintenance costs and the ability to produce water compatible with the geochemistry of the aquifer (CH2M 2015). The carbon-based train follows a state-of-the-art nutrient removal wastewater treatment facility and includes coagulation, flocculation, sedimentation, ozonation, biofiltration, granular activated carbon, UV disinfection, and pH adjustment before SWIFT Water is recharged to the PAS. SWIFT Water generated from this treatment approach has been shown to be protective of public health over the 38-month period of operation from the standpoint of organics, conventional and emerging contaminants, and pathogens by meeting the SWIFT-RC regulatory and monitoring limits and SWIFT-RC non-regulatory performance indicators established as part of its Underground Injection Control rule authorization.

3.3.2 Multiscreen, Multi-Aquifer Recharge Well and Sampling System

The PAS in the vicinity of the SWIFT-RC is primarily characterized by interbedded sands and clays segregated into three hydrostratigraphic units nearly 300 m in total thickness

(Bullard 2019). Recharge enters the PAS through 11 screens in recharge well TW-1 (Figure 3-2). To assess aquifer-scale transport with depth, several multiple-screen monitoring wells were constructed at varying depths in the PAS beneath the SWIFT-RC. A monitoring well (MW-SAT) located at a radial distance of 15.2 m from TW-1 and with 11 screens at depths consistent with TW-1 enabled evaluation of screen-specific transport and travel times. Samples were collected from each screen using a Flexible Liner Underground Technology (FLUTE) system, which has been documented previously in multiple groundwater monitoring projects (e.g., Keller 2017; Mosthaf et al. 2018; Ren et al. 2018). This system uses nitrogen purging to collect screen specific samples from the aquifer formation.

Three nested multiple-screen monitoring wells were installed in the Upper, Middle, and Lower PAS (MW-UPA, MW-MPA, and MW-LPA, respectively) to evaluate groundwater quality impacts at a larger transport scale. The three conventional wells are located between 104 m and 134 m from TW-1 and are spaced 15.2 m apart along a radial transect. Each well is screened in the most transmissive layers of the PAS within the three major units. Dedicated pumps in each of the conventional wells run continuously for groundwater sampling. Unlike the FLUTE liner at MW-SAT which produces discrete samples, each monitoring well produces a composite groundwater sample from multiple well screens.

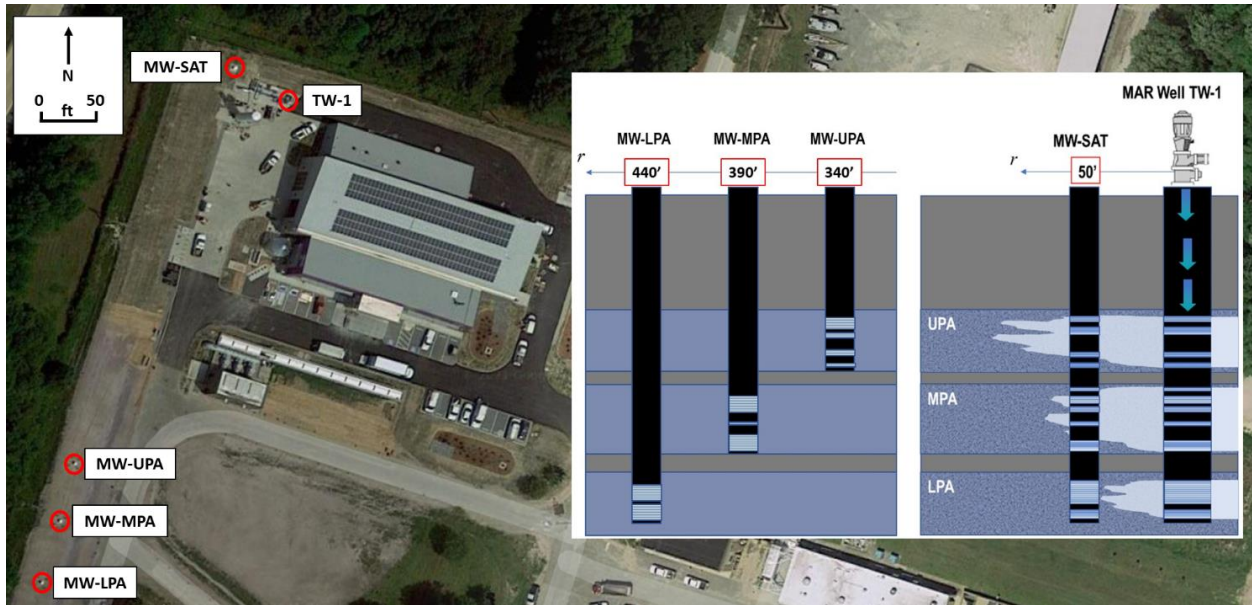


Figure 3-2. Well locations at the SWIFT-RC. Figure adapted from (Bullard et al. 2019).

SWIFT Water is of higher overall quality compared to the quality of the native groundwater of the PAS. With the exception of total organic carbon (TOC), concentrations of constituents of interest in SWIFT Water are lower than in the native groundwater. Representative values of water quality characteristics of SWIFT pre-treatment, SWIFT Water, and of PAS background concentrations are provided in Table 3-1 and demonstrate the variability within the PAS and the differences between SWIFT Water and the receiving aquifer.

Table 3-1. Time-averaged concentration of SWIFT-RC influent before treatment (NTP 2°), after treatment (SWIFT), and time-averaged background concentrations in the Upper, Middle, and Lower Potomac Aquifer (UPA, MPA, and LPA, respectively).

	Sample Location	Mean	Standard Deviation	Number of Samples
Chloride (mg/L)	NTP 2°	220	16.27	3
	SWIFT	186	40.71	34
	UPA	124	11.46	8
	MPA	1137	41.26	15
	LPA	4221	393.85	9
TOC (mg/L)	NTP 2°	10.80	2.36	256
	SWIFT	2.74	1.13	403
	UPA	0.36	0.31	23
	MPA	0.24	0.05	84
	LPA	0.92	0.51	86
TDS* (mg/L)	NTP 2°	644	0	1
	SWIFT	668	79.29	36
	UPA	714	31.57	8
	MPA	2500	127.98	9
	LPA	7437	782.15	9
Fluoride (mg/L)	NTP 2°	1.03	0.11	34
	SWIFT	0.89	0.13	687
	UPA	4.20	0.18	213
	MPA	0.61	0.09	129
	LPA	ND [†]	ND	122

* Total Dissolved Solids
[†] Detection Limit = 0.50 mg/L

3.4 Lessons Learned

3.4.1 Aquifer Compatibility

Sands of the PAS in Southeast Virginia contain a low percentage (2%-5%) of interstitial smectite clays, dominated by montmorillonite. The native groundwater at the SWIFT-RC is generally brackish, with TDS ranging from 738 mg/L to 7,437 mg/L. Flooding relatively fresh recharge water, an order of magnitude or lower ionic strength than the native groundwater,

reduces the surface charge on interstitial clay minerals residing in the sand matrix of the aquifer. Inter-particle attachments weaken due to the change in surface charge and diminish adhesive charges between individual clay layers causing clays to disperse. The fragmented clays collect in aquifer pore spaces, dramatically reducing aquifer permeability. Clogging due to migrating clay fragments is a special type of formation damage that can be catastrophic to recharge operations (Civan 2007).

Brown and Silvey (1977) described catastrophic loss in specific capacity and injectivity during pilot aquifer storage and recovery (ASR) test cycles in the PAS at a location 20 km from the SWIFT-RC. Fresh recharge water from the Moore's Bridges Water Treatment Plant in Norfolk, Virginia, exhibiting an ionic strength of 0.1 mM, was recharged into a test well screening the upper and middle portions of the PAS, where the ionic strength of the native groundwater was 10 mM. The specific capacity of the test well declined by nearly 80 percent over three ASR test cycles effectively ending the viability of the facility. The loss in permeability was attributed to destabilization of the interstitial clays. Attempts were made to recover the capacity however injectivity and injection capacity losses proved irreversible.

Selection of the advanced water treatment technology for SWIFT was driven in part by aquifer compatibility. Geochemical modeling of the expected effluent from the two pilot-tested treatment trains resulted in unacceptably low effluent concentrations of TDS for the membrane-based RO system and confirmed the incompatibility with the brackish native groundwater. The carbon-based pilot effluent maintained a TDS of approximately 673 mg/L, proving much more compatible with receiving aquifer.

Even with the carbon-based treatment process, SWIFT Water maintains a TDS with an ionic strength one order of magnitude less than the native groundwater depending on depth in the PAS, which can result in irreversible losses in aquifer permeability. To ensure viability of the recharge operation, HRSD decided to pre-condition the target recharge zones of the aquifer with an Aluminum salt (Al-salt).

Treating interstitial clay minerals in the aquifer surrounding the MAR well involves introducing an Al-salt solution to encourage exchange of the native sodium (Na⁺) ions, maintaining a +1 charge, with aluminum ions (Al³⁺) ions that maintain a +3 charge. The stronger charge protects the clay's structural integrity and adherence to the aquifer framework grains when more dilute recharge water enters the formation (Khilar and Fogler 1981).

HRSD conducted a pilot aquifer pre-conditioning, treating the SWIFT-RC monitoring well with the highest TDS and then recharging with potable water from the City of Suffolk, having lower TDS than SWIFT Water. The well was recharged for 124 hours with no signs of clay destabilization. Capacity testing results between pre-treating, post-treatment application and post injection testing revealed no significant changes in specific capacity (Jacobs Engineering Group, 2021).

Based on the pilot testing, HRSD applied similar pre-conditioning to the SWIFT-RC recharge well prior to start-up. The hydroxy-AlCl₃ proved difficult to mix in the field and produced a very turbid solution, therefore AlCl₃ was used. A conservative phased start-up approach was employed to avoid significant capacity losses if signs of clay dispersion were observed. Recharge started at 0.49 m³/min (130 gpm) and was stepped up to the target rate of 2.65 m³/min (700 gpm) over a month-long period, with specific capacity ranging from 35 to 25

gpm/ft, respectively. The aquifer pre-conditioning proved successful and clay destabilization was not observed. The SWIFT-RC has been operating since May 2018, with only a single pre-conditioning aquifer treatment, and continues to show no observable signs of clogging due to clay dispersion. Subsequent laboratory and field studies using test wells have proven aluminum chlorohydrate (ACH) to be very effective, maintaining a +6 charge density that adheres to the surface and the interlayers of the smectite clays (Jacobs Engineering Group, 2021).

3.4.2 Monitoring Network

Multiple monitoring wells and a robust sampling plan were essential to assessing chemical transport and attenuation in SWIFT-RC PAS groundwater. The proximity of MW-SAT to TW-1 and the depth discrete FLUTE sampling system allowed characterization of the flow distribution and solute transport through individual permeable units and provided valuable data for predictive modeling of breakthrough at the nested monitoring wells.

Before the initiation of recharge, multiple background samples were collected from each of the screens in MW-SAT and the monitoring well nest to characterize the native groundwater at various depths and each zone of the PAS. Initial breakthrough was measured at MW-SAT using specific conductivity as an indicator of SWIFT Water. Differences in the specific conductivity of SWIFT Water and native groundwater enabled the use of specific conductivity as a cost-effective intrinsic tracer during this initial period. When specific conductivity measurements crossed an initial threshold (decrease of 10% of background concentration) at specific screens at MW-SAT, sample frequency increased to capture breakthrough of other constituents of interest. The use of screen-specific sampling of specific conductivity prevented oversampling at screens where breakthrough of SWIFT Water had not been observed.

Breakthrough at MW-SAT varied by screen, with travel times ranging from three days to one month in screens associated with the UPA and MPA. Breakthrough in the LPA (Screens 10 and 11) was delayed the longest and was not observed until after the first well rehabilitation ending in April 2019.

Because of the variability of operating conditions at the SWIFT-RC (long periods of shutdown and occasional extended backflush periods), a simple radial transport model could not fully capture breakthrough at MW-SAT. A new model was developed to account for changing flow conditions using incremental volume by layer instead of assuming constant flow (Bullard et al. 2019). This model improved the ability to predict transport, but also indicated other transport mechanisms that impact flow through the PAS, including back diffusion.

Breakthrough was observed at well MW-UPA in April 2019 following the initial 5-month well rehabilitation. Multiple intrinsic tracers associated with SWIFT Water were used to determine breakthrough at MW-UPA, including sulfate, chloride, TOC, fluoride, 1,4-dioxane, and N-Nitrosodimethylamine (NDMA). Multiple tracer concentration data combined with flow distribution estimates at MW-SAT were useful in interpreting results at MW-UPA. Breakthrough concentrations showed that groundwater samples reflected a weighted average flow from Screens 1 and 2 instead of a weighted combination of all four screens in MW-UPA. This is most likely a result of the low flow from the sampling pump, which abstracted 7.6 L/min (2 gpm) from the well.

3.4.3 Dynamic Well Performance

The distribution of flow and associated injectivity in the multiscreen recharge well (TW-1) exhibited transient behavior during the course of operations. Injectivity declined from 23 to 12

gpm/ft in the preceding period starting in May 2018. This reduction was consistent with decreasing injectivity with time observed at an ASR facility in the PAS (Pyne 2005). Rehabilitation involved wire brushing, air lifting of debris from the well, chemical treatment with acid and dispersant, chlorine disinfection, and aggressive pumping of the well. These rehabilitation processes varied by well screen, which would explain the shift in flow distribution from Screen 9 to Screen 2. Similar processes were used for the second well rehabilitation, and changes in flow distribution were also observed. Post-rehabilitation camera surveys were completed and used in the second rehabilitation work to evaluate the degree to which well screens were clean and to target screens for additional cleaning. Following completion of well rehabilitation, a flow meter was installed inside TW-1.

Quantifying dynamic well performance was achieved using intrinsic and artificial tracers coupled with in-situ flowmeter testing and water level analysis (Figure 3-3). SWIFT Water was used as an intrinsic tracer to monitor breakthrough at MW-SAT and determine initial flow distribution at TW-1 (M. Bullard et al. 2019). An in-situ flowmeter test performed in May 2019 confirmed the dynamic nature of flow distribution within the aquifer. Significant changes in flow distribution were observed after the first well rehabilitation, which occurred between November 2018 and April 2019. A tracer test using sodium bromide was performed in late 2020, and preliminary results show reduced flow to the UPA and MPA screens and increasing flow to the LPA in the latter part of the 38-month period of performance. Dynamic flow distribution at the recharge well was attributed to: (1) step changes due to well rehabilitation or adjustments to treatment process and (2) gradual, continuous changes during recharge operations.

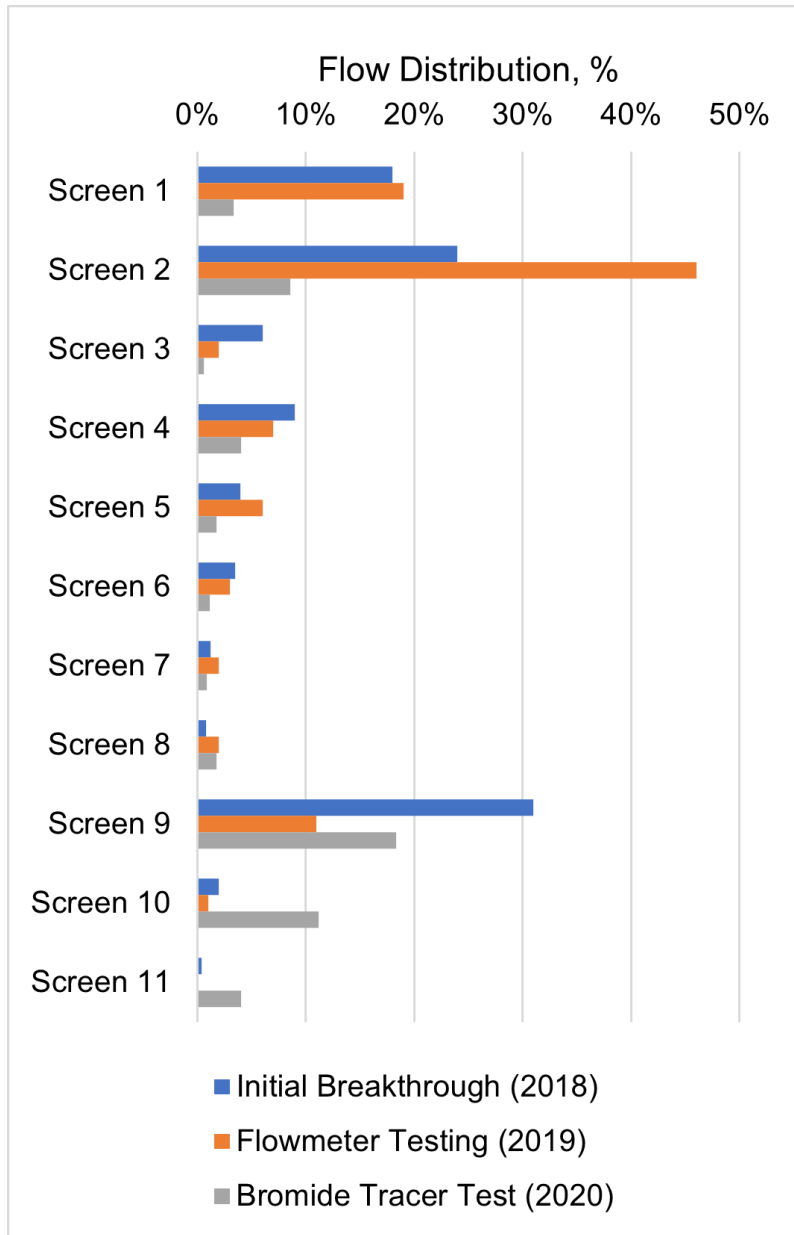


Figure 3-3. Variability of flow distribution over time at multiscreen recharge well TW-1 based on three different measurement methods.

While step changes in distribution are simpler to quantify by conducting flow distribution tests following major well rehabilitation events, gradual changes due to operational conditions and well clogging are a focus of future research at the SWIFT-RC. Changes in drawdown during extended pumping or recharge conditions at the conventional wells are a potential source for measuring response of the individual aquifer systems over time. Comparing drawdown under

similar conditions over time (e.g., drawdown after thirty minutes of pumping for pumping scenarios after SWIFT has been shut down for at least 24 hours) indicates shifts in response between aquifer layers; as the UPA becomes less responsive, both the MPA and LPA become more responsive. This can most likely be attributed to gradual clogging in the upper screens and the shift of flow distribution to the lower screens.

3.4.4 Benefits of a Demonstration Facility

The experience gained since 2018 at the SWIFT-RC has been valuable in confirming the appropriate regulatory targets for full-scale permitting and for optimizing treatment design and operation at full-scale facilities. HRSD also utilizes the SWIFT-RC as a training ground for operators assigned to future full-scale facilities, providing the opportunity for staff to learn the advanced treatment process at a smaller scale. Additionally, the SWIFT-RC was purpose-built with education and outreach in mind with the objective of actively engaging with the public, regulators, and other interested parties to highlight the multiple challenges facing our local waterways, the implications of depleting our groundwater supplies, and how the SWIFT program can provide benefits to address these key issues. The facility is designed so that visitors can connect visually with the treatment process and are offered an opportunity to taste the final treated product (following additional free chlorine disinfection), SWIFT Water. This has proven to be a successful approach to achieving local support and buy-in of the SWIFT program.

3.5 Future Prospects

At full scale, this \$2B infrastructure project will replenish the PAS at 378,000 m³/d (100 MGD) with wastewater treated to drinking water standards using a system of multiscreen recharge wells. Ultimately, HRSD plans to treat the secondary clarifier effluent from seven of

nine major HRSD wastewater treatment plants to drinking water standards and use recharge wells to replenish the PAS across the EVGWMA at five full-scale SWIFT treatment plants. This will significantly reduce nutrient loads to the Chesapeake Bay as well as rehabilitating the aquifer system. Two sites (Boat Harbor Treatment Plant and Army Base Treatment Plant) will not have SWIFT plants, but wastewater will be routed to a SWIFT treatment plant for treatment and recharge. The first of five full-scale SWIFT facilities will be constructed at the HRSD James River Treatment Plant, and that project is in the detailed design phase.

Acknowledgements

The authors would like to thank members of the SWIFT Research Center team, operators at Nansemond Treatment Plant, and members from the HRSD Technical Services Division for their help in collecting samples onsite at the SWIFT Research Center. This work was supported by HRSD and the Charles E. Via, Jr. Department of Civil and Environmental Engineering at Virginia Tech.

References

- Brown, D.L., and W.D. Silvey. 1977. Artificial Recharge to a Freshwater-Sensitive Brackish-Water Sand Aquifer, Norfolk, Virginia. *Geological Survey Professional Paper 939*. doi:10.3133/pp939.
- Bullard, M.G., M. Widdowson, G. Salazar-Benites, J. Heisig-Mitchell, A. Nelson, and C. Bott. 2019. Managed Aquifer Recharge: Transport and Attenuation in a Coastal Plain Aquifer. *Proceedings of the EWRI World Environmental and Water Resources Congress 2019: Groundwater, Sustainability, Hydro-Climate/Climate Change, and Environmental Engineering*, 1–14. Pittsburgh: EWRI. doi: 10.1061/9780784482346.011.
- CH2M. 2015. Aquifer Replenishment System Concept Cost Evaluation. Newport News, VA, USA.
- Civan, F. 2007. *Reservoir Formation Damage*, 2nd ed. Oxford: Elsevier. doi: 10.1016/B978-0-7506-7738-7.X5000-3.
- Dziura, T. 2020. Evaluation of Contaminant Removal Through Soil Aquifer Treatment by a Lab Scale Soil Column Experiment Including a Trace Contaminant Spike Test. Masters Thesis. Via Department of Civil and Environmental Engineering, Virginia Tech.
- Eggleston, J., and J. Pope. 2013. Land Subsidence and Relative Sea-Level Rise in the Southern Chesapeake Bay Region. US Geological Survey Circular 1392. doi:10.3133/cir1392.
- Heywood, C.E., and J.P. Pope. 2009. Simulation of Groundwater Flow in the Coastal Plain Aquifer System of Virginia. U.S. Geological Survey Scientific Investigations Report 2009 – 5039. doi:10.3133/sir20095039.
- Jacobs Engineering Group. 2021. Conditioning the Potomac Aquifer System Around Managed Recharge Test Wells at Sustained Water for Tomorrow Facilities at Nansemond, York River, James River, and the Virginia Initiative Plant: Methods and Baseline Results. Hampton, VA.
- Keller, C. 2017. A New Rapid Method for Measuring the Vertical Head Profile. *Groundwater* 55, no. 2: 244–254. doi:10.1111/gwat.12455.
- Khilar, K.C., and H.S. Fogler. 1981. Permeability Reduction in Water Sensitivity of Sandstones. *Surface Phenomena in Enhanced Oil Recovery*, 721–740. Boston, MA: Springer US. doi:10.1007/978-1-4757-0337-5_34.
- Lovelace, J.K., M.G. Nielsen, A.L. Read, C.J. Murphy, and M.A. Maupin. 2020. Estimated Groundwater Withdrawals from Principal Aquifers in the United States, 2015. U.S.

- Geological Survey Circular 1464. doi:10.3133/cir1464.
- McFarland, E.R., and T.S. Bruce. 2006. The Virginia Coastal Plain Hydrogeologic Framework. U.S. Geological Survey Professional Paper 1731. doi: 10.3133/pp1731.
- McFarland, E.R., 2010, Groundwater-quality data and regional trends in the Virginia Coastal Plain, 1906–2007: U.S. Geological Survey Professional Paper 1772, 86 p., 14 pls.. doi:10.3133/pp1772.
- McFarland, E.R., 2015, A conceptual framework and monitoring strategy for movement of saltwater in the Coastal Plain aquifer system of Virginia: U.S. Geological Survey Scientific Investigations Report 2015 – 5117, 30 p., 1 pl., doi:10.3133/sir20155117.
- Mosthaf, K., B. Brauns, A.S. Fjordbøge, M.M. Rohde, H. Kern-Jespersen, P.L. Bjerg, P.J. Binning, and M.M. Broholm. 2018. Conceptualization of Flow and Transport in a Limestone Aquifer by Multiple Dedicated Hydraulic and Tracer Tests. *Journal of Hydrology* 561, June: 532–546. doi: 10.1016/j.jhydrol.2018.04.011.
- Nylen, N.G. 2021. Surface Water Quality Regulation as a Driver for Groundwater Recharge. *Case Studies in the Environment* 5, no. 1: 1124592. doi: 10.1525/cse.2020.1124592.
- Pyne, R.D.G. 2005. *Aquifer Storage Recovery*, 2nd ed. (Gainesville: ASR Press).
- Ren, S., S. Gragg, Y. Zhang, B.J. Carr, and G. Yao. 2018. Borehole Characterization of Hydraulic Properties and Groundwater Flow in a Crystalline Fractured Aquifer of a Headwater Mountain Watershed, Laramie Range, Wyoming. *Journal of Hydrology* 561, June: 780–795. doi: 10.1016/j.jhydrol.2018.04.048.
- Smith, B.S. 1999. The Potential for Saltwater Intrusion in the Potomac Aquifers of the York-James Peninsula, Virginia. U.S. Geological Survey Water-Resources Investigations Report 98-4187. doi: 10.3133/wri984187
- Virginia Department of Environmental Quality. 2018. Status of Virginia’s Water Resources. <https://rga.lis.virginia.gov/Published/2018/RD347> (accessed October 22, 2021).
- Virginia Department of Environmental Quality. 2020. Status of Virginia’s Water Resources. <https://www.deq.virginia.gov/home/showpublisheddocument/2119/637432838113030000> (accessed October 22, 2021).

4. Managed Aquifer Recharge: Transport and Attenuation in a Coastal Plain Aquifer

Title

Managed Aquifer Recharge: Transport and Attenuation in a Coastal Plain Aquifer

Published in: Proceedings of the EWRI World Environmental and Water Resources Congress 2019: Groundwater, Sustainability, Hydro-Climate/Climate Change, and Environmental Engineering

Citation: **Bullard, M.G.**, M. Widdowson, G. Salazar-Benites, J. Heisig-Mitchell, A. Nelson, and C. Bott. 2019. Managed Aquifer Recharge: Transport and Attenuation in a Coastal Plain Aquifer. *Proceedings of the EWRI World Environmental and Water Resources Congress 2019: Groundwater, Sustainability, Hydro-Climate/Climate Change, and Environmental Engineering*, 1–14. Pittsburgh: EWRI. doi: 10.1061/9780784482346.011.

Link: <https://ascelibrary.org/doi/10.1061/9780784482346.011>

Abstract

The Sustainable Water Initiative for Tomorrow (SWIFT) program is an initiative to replenish the Potomac Aquifer System (PAS) using Managed Aquifer Recharge (MAR). The SWIFT Research Center is a 1 MGD advanced water treatment facility producing reuse water suitable for MAR. In order to characterize flow distribution through a multiscreen recharge well and solute travel time, we analyzed tracer breakthrough curves using solute transport models modified using the method of superposition. Distinct breakthrough was observed in the Upper and Middle Potomac Aquifers with travel time varying from approximately 2-37 days over a 50-ft radial distance. Approximately 73% of the recharge was delivered to 3 of the 11 well screens. Recharge flow to the Lower Potomac Aquifer was negligible as indicated by relatively slow breakthrough. Breakthrough curves were affected by recharge stoppages during the initial evaluation period with some screening locations exhibiting abrupt changes in specific conductivity during stoppages. Results of the initial groundwater recharge efforts are presented, including implications for full-scale implementation of SWIFT.

4.1 Introduction

The Potomac Aquifer System (PAS) extends from New Jersey to South Carolina and is the primary source of groundwater in Eastern Virginia. Sustained groundwater withdrawals by municipal and industrial entities since 1970 has resulted in declining potentiometric surface in the region. Due to nature of interbedded confining units, natural recharge of the PAS is insufficient to balance use of groundwater from the PAS. Groundwater withdrawals in Eastern Virginia have resulted in aquifer compaction and land subsidence (Eggleston et al. 2013). Increased withdrawal rates also increase the potential for saltwater intrusion, which could contaminate drinking water wells near coastlines. Furthermore, in 2010, the USEPA finalized the Chesapeake Bay Total Maximum Daily Load (TMDL), a restoration plan which established numerical limitations for nutrients entering the Chesapeake Bay, one of Virginia's prized landmarks. This TMDL includes accountability measures to ensure that the bay achieves the water quality standards intended to restore and protect aquatic life and habitat. As a result, reducing nutrient loads to the bay is also one of Hampton Roads Sanitation District's (HRSD's) top priorities.

The Sustainable Water Initiative for Tomorrow (SWIFT) project is an initiative of HRSD to address the aforementioned environmental challenges facing southeast Virginia. HRSD serves 1.7 million people across the eighteen cities and counties of southeast Virginia through 16 wastewater treatment plants which have a combined capacity of approximately 250 million gallons per day (MGD). At full-scale, HRSD intends to produce approximately 100 MGD of SWIFT Water to replenish the PAS through a program of Managed Aquifer Recharge (MAR). In May 2018 HRSD implemented MAR at the SWIFT Research Center (SWIFT-RC) located at the Nansemond Treatment Plant (NTP) in Suffolk, VA.

The SWIFT-RC operates an approximately 1 MGD advanced treatment facility to further treat secondary effluent from NTP to meet federal and state drinking water standards suitable for augmentation of a potable aquifer. The treatment train includes coagulation/flocculation/sedimentation, ozonation, biological filtration, granular activated carbon, and ultraviolet disinfection. Following advanced treatment, this “SWIFT Water” is then used to recharge the PAS at a rate of up to 1 MGD. The implementation of MAR with a recharge well fully screened at multiple intervals of a deep aquifer system is a novel approach and requires us to characterize flow distribution into the PAS.

Flow is distributed unevenly between 11 discrete screens in the Upper, Middle, and Lower Potomac Aquifer. Identifying breakthrough characteristics of recharge water at each screen level is a critical part of the implementation plan and design decision making process as the project progresses. Our objective was to analyze flow distribution through the multiscreen recharge well at the SWIFT-RC and determine solute travel times. To determine breakthrough characteristics, groundwater samples were collected from each discrete screen at an adjacent monitoring well and evaluated for conservative tracer transport. The observed concentrations of tracer were compared to two computational breakthrough models, where parameters were adjusted to fit the observed breakthrough. Using the adjusted parameters, breakthrough time for an ideal recharging situation was estimated.

4.2 Data Collection and Analysis

4.2.1 Monitoring System and Sample Collection

Recharge flow is distributed through 11 screens in a 1410-ft deep 12-in-diameter carbon steel casing test injection well (TW-1) into the upper, middle, and lower zones of the PAS (Table

4-1). This injection well is screened at eleven different levels of the PAS (Figure 4-1). All aquifer layers are confined. A monitoring well (MW-SAT) located at a radial distance of 50 ft from TW-1 enables collection of discrete samples from each of the 11 screens levels using a Flexible Liner Underground Technology (FLUTE) sampling system. Three conventional monitoring wells located 400-500 feet away are also screened in the Upper Potomac Aquifer (UPA), Middle Potomac Aquifer (MPA), and Lower Potomac Aquifer (LPA) for recharge monitoring.

Table 4-1. Well Screen Depth and Length of Screen in TW-1 and MW-SAT.

Aquifer Zone		Starting Depth (fbg)	Ending Depth (fbg)	Length of Screen (ft)
Upper Potomac Aquifer (UPA)				
	Screen 1	505	530	25
	Screen 2	550	595	45
	Screen 3	665	680	15
	Screen 4	720	755	35
Middle Potomac Aquifer (MPA)				
	Screen 5	820	835	15
	Screen 6	860	890	30
	Screen 7	905	920	15
	Screen 8	965	990	25
	Screen 9	1050	1090	40
Lower Potomac Aquifer (LPA)				
	Screen 10	1230	1335	105
	Screen 11	1370	1400	30
(fbg) – feet below grade				

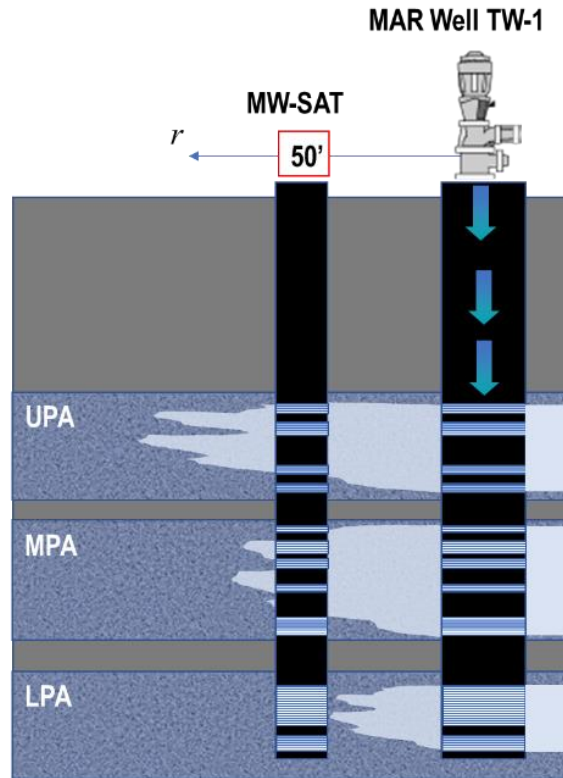


Figure 4-1. Schematic of the recharge well (TW-1) showing the distribution of flow through 11 well screens in the Upper, Middle, and Lower Potomac Aquifer and position of monitoring well MW-SAT.

Samples were collected from the monitoring well MW-SAT using the existing FLUTE system, which allows discrete samples to be taken from each of the 11 sample screens. The FLUTE system is comprised of a flexible liner with screen lengths and depths identical to the recharge well screens. The FLUTE liner seals the borehole from flow except for through sample tubes in each interval; this prevents contamination by allowing samples to flow directly from the aquifer without being mixed within the well borehole. More information about the operation of the FLUTE system can be found at <https://www.flut.com/water-flute>.

To take a sample, the sample tubes are flushed with nitrogen gas to remove standing water and allowed to refill for thirty minutes. Following a 30-minute wait period, gas pressure is applied through a pump tube at a pressure greater than the head of the formation. This pressure

pushes water through the sampling tube and allows for the collection of water samples from each interval from a sample tube that runs to sampling taps in the SWIFT Research Center (Figure 4-2).



Figure 4-2. Sampling taps for FLUTE screens 1-11. Taps 1-4 are screened in the Upper Potomac Aquifer, taps 5-9 are screened in the Middle Potomac Aquifer, and taps 10-11 are screened in the Lower Potomac Aquifer. Each tap is connected to the respective FLUTE sample tube.

4.2.2 Tracer Selection

During soil column testing performed by HRSD and Virginia Tech, we developed a strong, reproducible correlation between chloride concentrations and specific conductivity measurements in site groundwater (Figure 4-3). Triplicate samples were collected at each screen and were analyzed for both conductivity and chloride. On average, chloride accounted for 29%

of conductivity within the 11 screens, although this varied within each screen and generally increased according to screen depth. A similar correlation has also been noted by other researchers (Hem, 1985). Because specific conductivity involves other ions that will react with constituents in the aquifer, it does not qualify as an acceptable tracer. Specific conductivity can, however, be used as a screening indicator of chloride concentrations based on the correlation between the two measurements.

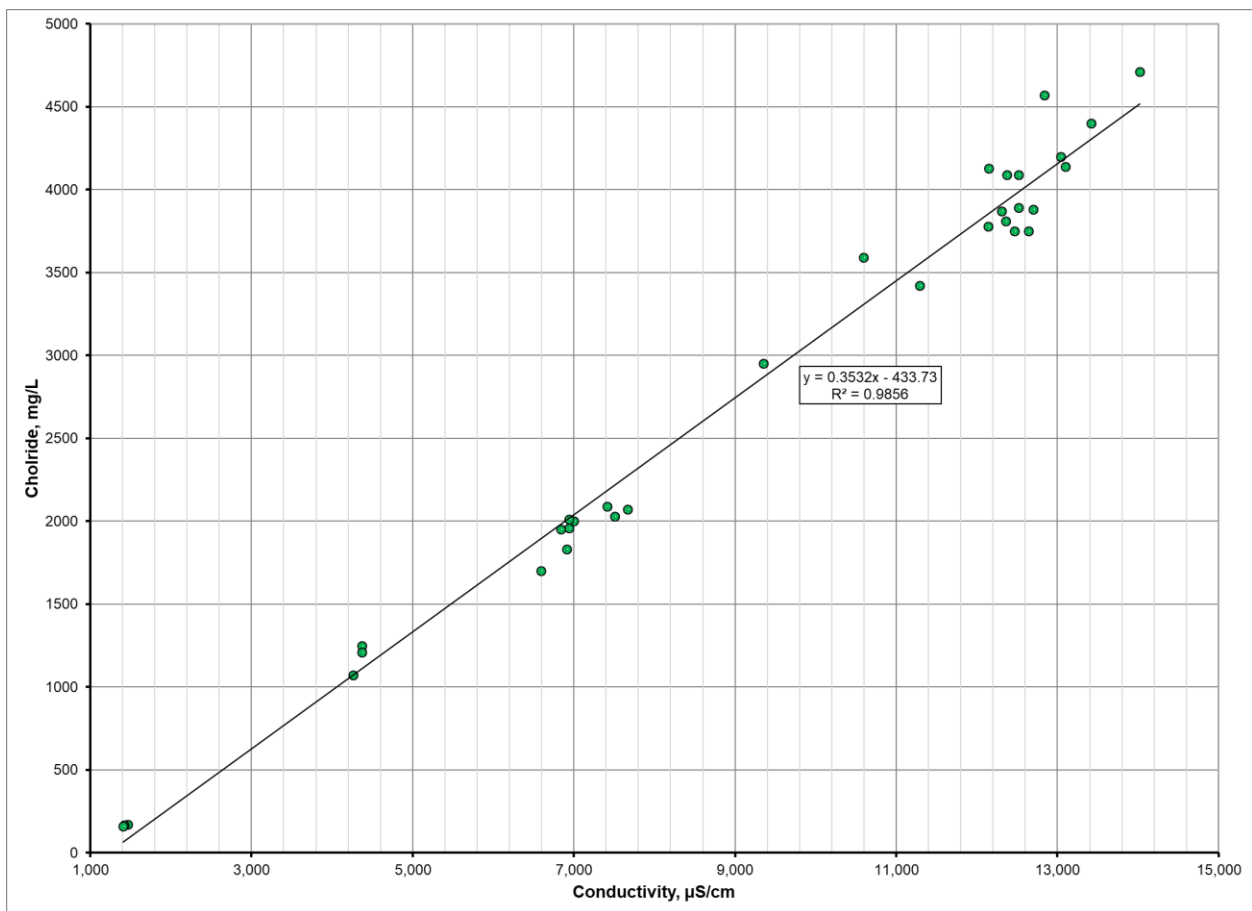


Figure 4-3. Correlation developed between specific conductivity and chloride concentrations in groundwater samples collected at MW-SAT.

Samples were collected and analyzed for specific conductivity approximately every four hours (~ six times per day) from the start of recharge (May 15, 2018) until December 2018. Because the specific conductivity of screen 1 was similar to the native groundwater conductivity,

the samples from screen 1 were measured for both specific conductivity and fluoride. Specific conductivity ($\mu\text{S}/\text{cm}$) was measured using a portable parallel analyzer (PPA) with a conductivity probe (Hach SL1000). Fluoride was tested using the SPADNS method using AccuVac® Ampules (Hach Method 8029). Conductivity of the SWIFT Water was measured using an online probe upstream of the recharge well with data extracted from the plant SCADA system as 15-minute average values. The PPA and online conductivity probe were calibrated to ensure that there was no bias between measurements. All measurements were recorded in a spreadsheet (EXCEL), and data were analyzed therein.

4.2.3 Analysis of Breakthrough Curves

Initial breakthrough sampling of a comprehensive suite of analytes was triggered when the conductivity of the native groundwater went below a threshold of 90% of the background conductivity. For example, if the background conductivity was 10,000 $\mu\text{S}/\text{cm}$, initial breakthrough sampling would be triggered when the conductivity was consistently below 9,000 $\mu\text{S}/\text{cm}$. Using 10% ensured that initial breakthrough was caused by conductivity values below three times the standard deviation of the background concentration values. Total breakthrough was determined in a specific screen when the conductivity of the screen was consistently within 25% of the SWIFT Water conductivity. Because the conductivity of SWIFT Water was variable, this threshold was determined by calculating the moving average of conductivity for 72 hours.

A breakthrough curve was created using relative concentration vs. time. Relative concentration is calculated using observed concentration (C_{obs}), background concentration of the native groundwater in the screen (C_b), and an average SWIFT Water (injection) concentration (C_{inj}):

$$C_{Rel} = \frac{C_b - C_{obs}}{C_b - C_{inj}} \quad (1)$$

The relative concentration at each well screen ($C_{Rel,i}$) was compared to a continuous flow model – an approximate solution of relative concentration based on the estimated flow to each screen at TW-1, the estimated porosity, vertical thickness of the screened interval, and the estimated longitudinal dispersivity at each screened interval at MW-SAT (Charbeneau, 2000).

$$C_{Rel,i}(r, t) = \frac{1}{2} * \operatorname{erfc} \left[\frac{r - R_i}{\sqrt{\frac{4}{3} \alpha_{L,i} R_i}} \right] \quad (2)$$

$$R_i(t) = \sqrt{\frac{Q_i t}{\pi n_i b_i}} \quad (3)$$

where r is the radial distance from the injection well (ft), t is the time since the start of injection (days), Q_i is the recharge flow rate to the individual well screen ($\text{ft}^3 \text{d}^{-1}$), $\alpha_{L,i}$ is the longitudinal dispersivity (ft), n_i is the effective porosity, and b_i is the screen length (ft). With this approach, we assume that the flow rate specified at each well screen at the recharge well coincides with the rate of transport at each well screen in the monitoring well.

To refine the initial calibration using the continuous flow model (Equations 2 and 3), a more advanced incremental flow model was developed that calculated breakthrough incrementally based on measured flow into the aquifer. Use of the superposition method enabled us to account for stoppage time (if the plant went off-spec and water was not used for recharge) and for well backflush (in which water was pumped out of the well in order to ensure that well injectivity was maintained). Backflush was considered a negative flow (flow out of the well) and

caused a decrease in the incremental volume calculation. Relative concentration was calculated in 15-minute intervals since the start of recharge using data for recharge flow in gallons per minute (gpm) from the SWIFT-RC SCADA system. Total flow was imported from SCADA, and the flow distribution (%) was estimated for each well screen based on the estimated flow distribution from the continuous flow model. At each time step, the flow to each screen was a fraction of the total flow into the recharge well (TW-1) at that time.

An incremental volume, V_i^* , was calculated for each well screen is a function of the time and flow distribution:

$$V_i^*(t) = [Q_i(t)\Delta t] + V_i^*(t - \Delta t) \quad (4)$$

where $Q_i(t)$ (ft^3d^{-1}) is the flow to the individual screen at a given time and Δt (d) is the time interval between measured Q_i values. Then, an incremental R value, R_i^* , was calculated for each screen based on Equation (4):

$$R_i^*(t) = \sqrt{\frac{V_i^*(t)}{\pi n_i b_i}} \quad (5)$$

This R_i^* value is substituted into the Equation (2) with the incremental value replacing the original R value in Equation (3):

$$C_{Rel,i}(r, t) = \frac{1}{2} \operatorname{erfc} \left[\frac{r - R_i^*(t)}{\sqrt{\frac{4}{3} \alpha_{L,i} R_i^*(t)}} \right] \quad (6)$$

The mean travel time at each well screen ($t_{m,i}$) was calculated for the incremental flow model using the following equation:

$$t_{m,i} = \frac{\pi r^2 n_i b_i}{A Q_i} \quad (7)$$

where $A = 192.5$ and converts the flow from gpm to cubic feet per day (cfd). In this calculation, the value of Q_i (gpm) is the fraction of the full recharge flow (700 gpm) allocated to the specific screen. Other variables are previously defined. This calculation of travel time is an approximate calculation, which assumes that the recharge rate is a constant 700 gpm and does not account for any periods of short-term backflush (pumping) or stoppages at TW-1.

4.3 Results and Discussion

Recharge into the PAS started May 15, 2018 at approximately 200 gpm and was increased incrementally by 100 gpm over time until a recharge rate of 700 gpm (1 MGD) was reached June 20, 2018. Backflushing occurred at rates between 1000-1200 gpm (1.4-1.7 MGD) every few days for approximately 15-45 minutes to maintain well injectivity. The recharge well was backflushed for a period of 18 days in August 2018 that removed approximately 21 million gallons of water from the aquifer following a period of high nitrite levels observed in the monitoring well, largely due to partial denitrification of SWIFT Water nitrate to nitrite in the PAS. Recharge was also stopped after November 21, 2018 in order to complete several warranty related repairs on the treatment equipment. Backflushing continued daily during the SWIFT-RC shutdown for approximately 15-30 minutes per day. Recharge trends are displayed in Figure 4-4.

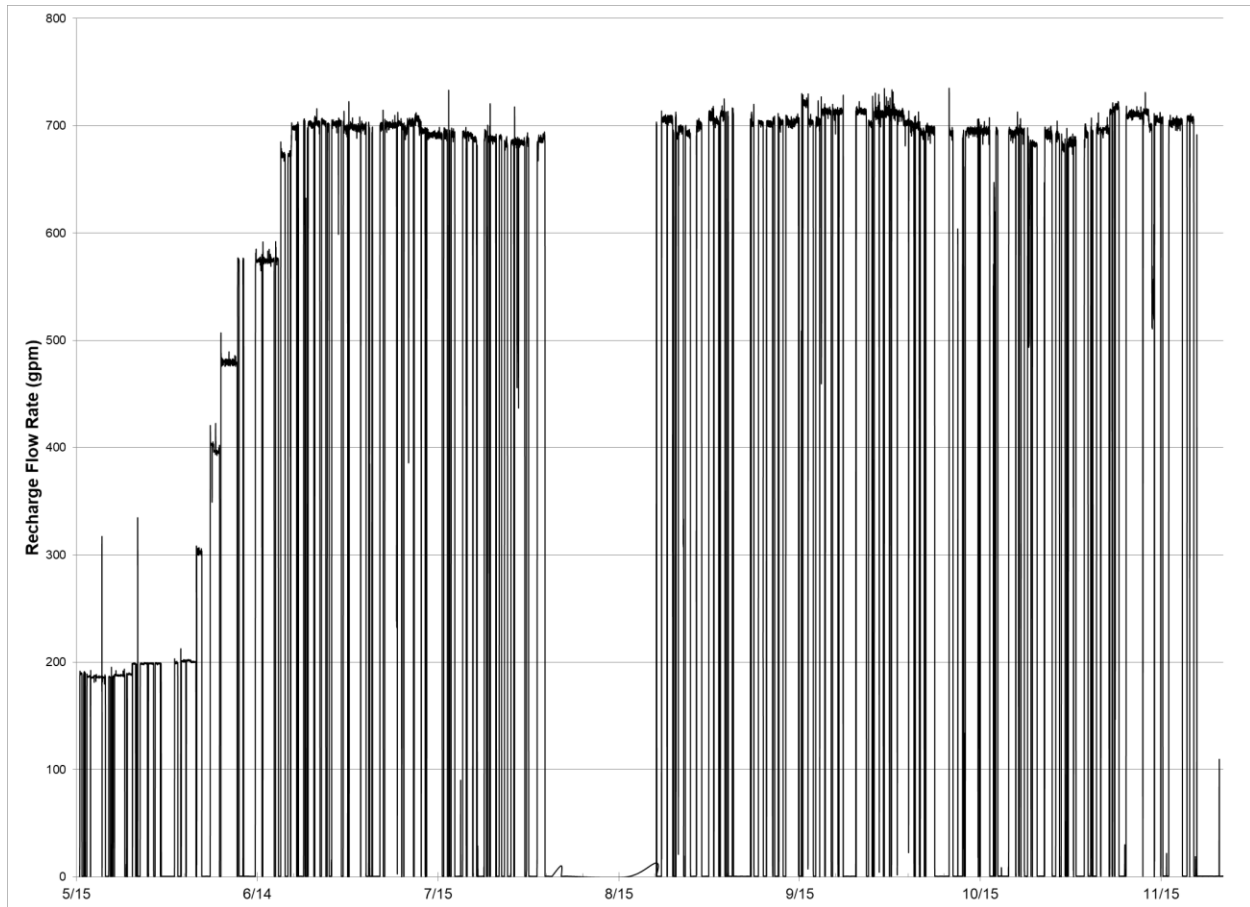


Figure 4-4. Recharge flow rate at recharge well TW-1 (gpm). Extended backflushing period is noted in August 2018. No recharge is observed from late November 2018 onward.

Model calibration was achieved by manually adjusting input parameters for porosity, flow rate, and longitudinal dispersivity to create breakthrough curves that best fit the observed data at each well screen (Table 4-2). For the initial calibration of input parameters using the continuous flow model, an estimated flow rate was used in Equation (3) to match conductivity measurements at MW-SAT. This estimated flow rate at each well screen was then calculated as a percent of the total recharge flow rate. Using these percentages as a starting point for the final calibration based on the incremental flow model, the estimated flow rates at each well screen were adjusted slightly to fit the observed data at MW-SAT. Consistent values of longitudinal dispersivity and porosity were employed for the two calibration steps and are only reported once

in Table 4-2. The final calibration flow rates were used to calculate the travel time in each screen.

Table 4-2. Calibrated model input parameter values and travel time results.

Screen	Initial Calibration – Continuous Flow Model		Final Calibration – Incremental Flow Model			
	Q _i (gpm)	Flow (%)	n _i	$\alpha_{L,i}$ (ft)	Flow (%)	Travel Time (days)
1	30	18%	0.20	5	18%	1.6
2	39	24%	0.25	10	24%	2.7
3	11.5	7.0%	0.27	10	6.0%	3.9
4	15	9.2%	0.35	20	9.0%	7.9
5	6.6	4.0%	0.25	8	4.0%	5.5
6	6.0	3.7%	0.30	20	3.5%	15
7	2.3	1.4%	0.28	30	1.2%	20
8	1.4	0.9%	0.32	10	0.8%	37
9	47	29%	0.23	10	31%	1.7
10	4.0	2.4%	0.25	10	2.0%	77
11	0.90	0.5%	0.27	10	0.4%	120

Average travel times in the UPA, MPA, and LPA were 4.1 days, 16 days, and 97 days, respectively. The lowest travel times were observed in screens 1 through 3 (UPA) and screen 9 (MPA), for an average travel time of 2.5 days. Effective porosity ranged from 0.20-0.35 with a mean value of 0.27. No correlation was found between calibrated effective porosity and mean travel time at the well screens. Consistent with the continuous and incremental flow models, a strong negative correlation was found between final calibrated flow rates and mean travel time at the well screens.

Estimations of flow rates using the incremental flow model was consistent with observed condition by accounting for periods when flow into the well is zero or negative (backflush conditions). At any point during the period represented in Figure 4-4, the exact total flow rate at TW-1 was incorporated into the calculations. Although the initial calibration flow and the final

calibration flow are quite similar based on percent of flow to each screen, the initial calibration of breakthrough curves using the continuous flow model resulted in a total combined rate of flow of approximately 160 gpm or 80% of the starting recharge flow rate. This discrepancy reflects the relatively slow breakthrough of conductivity at screens 4, 6-8, and 10-11, in which 17% of the flow rate was distributed. However, the distribution of flow rate to the well screens was consistent between the initial and final calibration, indicating the utility of the initial calibration in quantifying the magnitude of recharge flow into the aquifer at the maximum rate (700 gpm).

Based on our analysis, a substantial percentage of the recharge flow into the PAS passed through screens 1, 2, and 9, comprising an estimated 60-73% of recharge flow distribution. The range in this result was dependent on the constituent (fluoride – 60% or specific conductivity – 73%) used to determine the flow rate at screen 1. The breakthrough curves for screen 1 based on conductivity and fluoride are compared in Figure 4-5. Based on analysis of the conductivity-based breakthrough curve and the stoppage method, 57% of the total recharge flow was delivered to the UPA through the uppermost four well screens. Screens 1 through 4 comprise 120 ft of 380 ft of total well screen at TW-1 (only 32% of the total screened intervals). The MPA and the LPA received 40% and less than 3% of the total recharge flow, respectively. Approximately 72% of recharge to the MPA and LPA combined was delivered to the deepest well screen in the MPA (Screen 9), comprising 31% of the total recharge flow.

The model fit for the fluoride breakthrough curve was more sensitive to stoppages and backflush periods than the fit for conductivity, although the model results for conductivity yielded more accurate final calibration flow estimate sum totals than the estimated flow based on fluoride (100% vs. 87%, respectively). Because the difference between fluoride levels in screen 1 native groundwater and SWIFT Water were more statistically significant than the difference in

conductivity, fluoride is potentially a more accurate tracer to reflect the arrival of SWIFT Water in screen 1.

In some screens, the incremental flow model produced a more accurate representation of the observed data compared to the continuous flow model. The impact of flow stoppages on the breakthrough curve and improved model fit is notably observed in screens 4, 6, and 7. As shown in Figure 4-6, incremental flow model (final calibration) shows a better overall fit to the complete period of observed data at screen 7 compared to the continuous flow model (initial calibration) including the period of decreased relative concentration due to backflush.

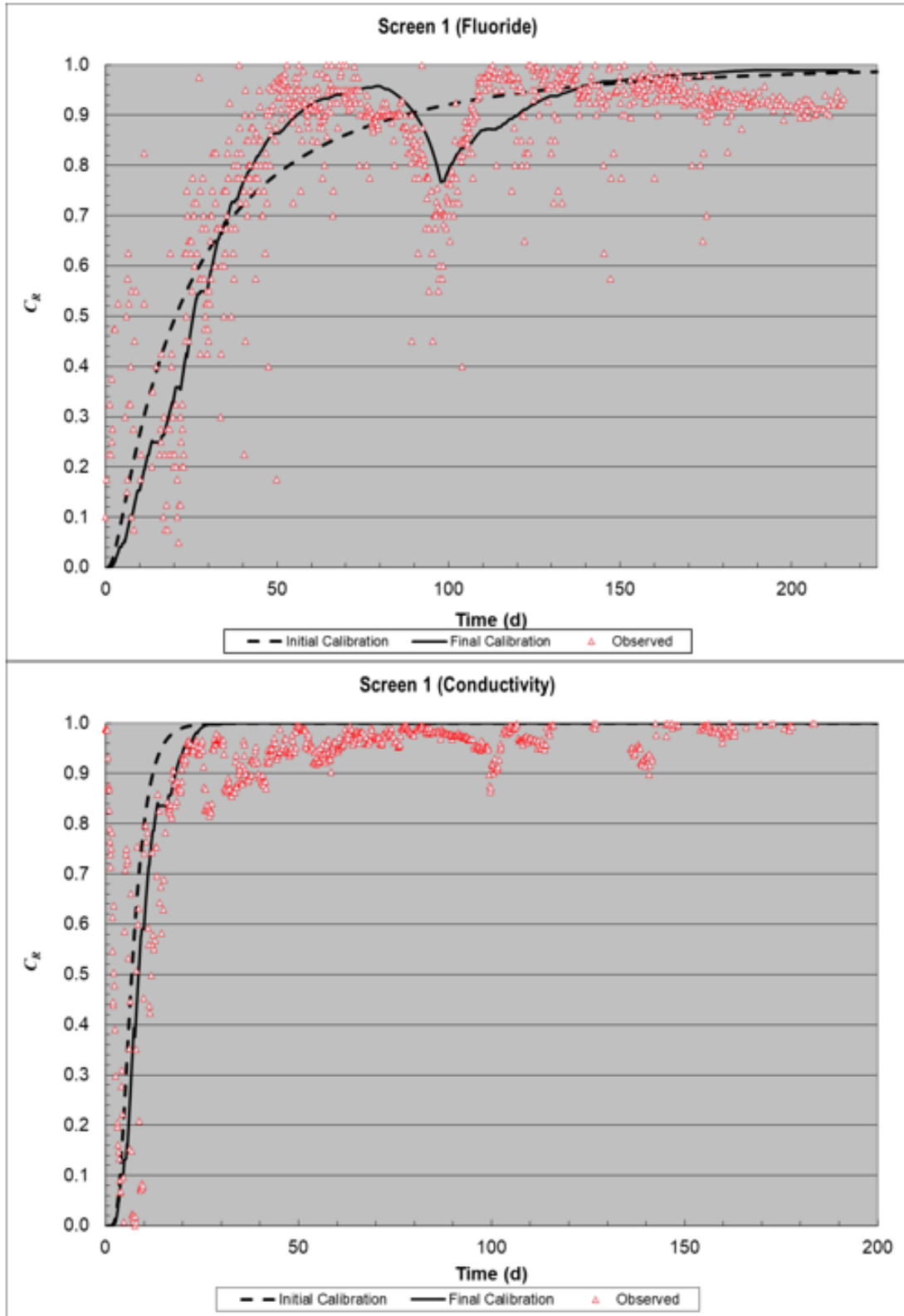


Figure 4-5. Comparison of fit between screen 1 breakthrough curves from fluoride relative concentrations (upper) and relative conductivity data (lower).

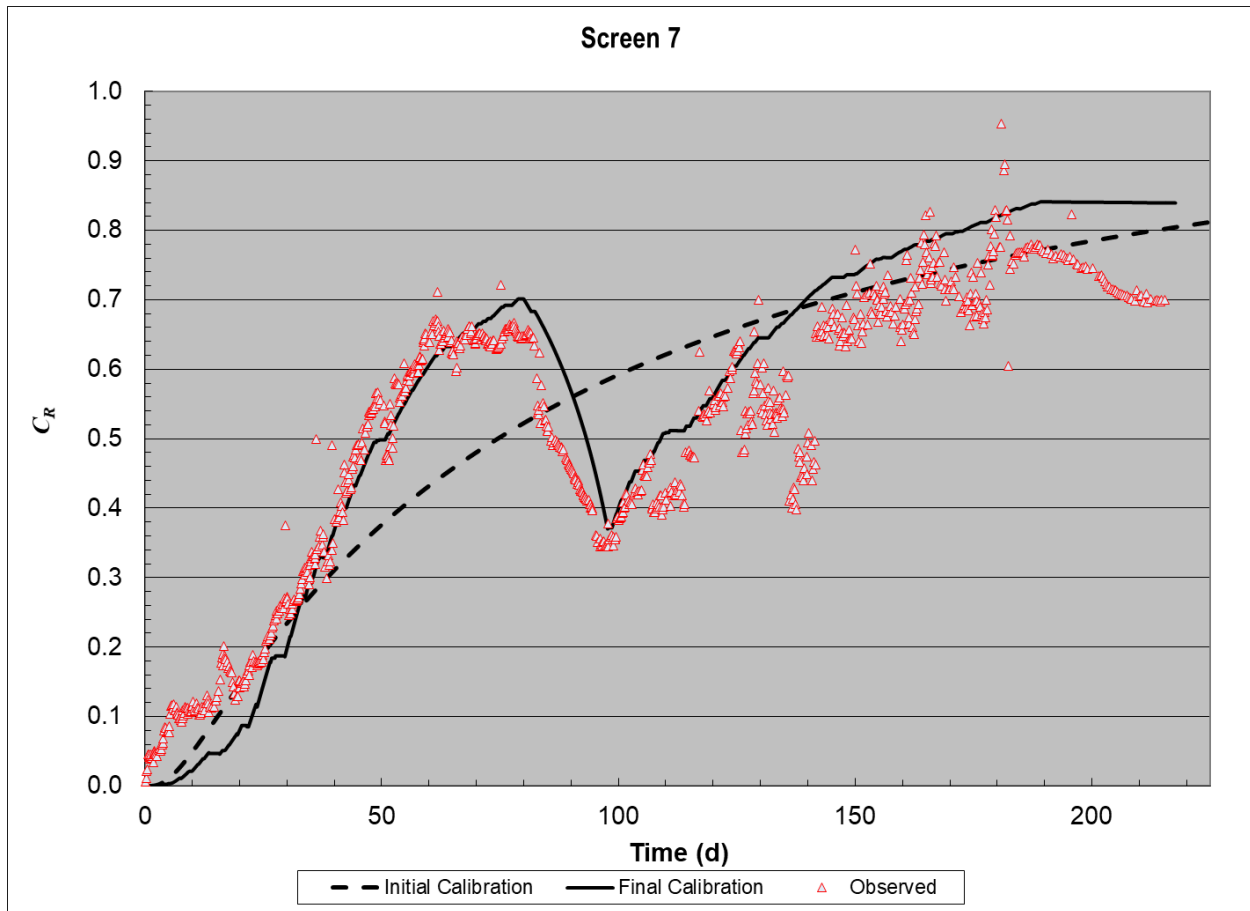


Figure 4-6. Screen 7 shows the improvement between the initial and stoppage breakthrough curves at predicting relative concentration based on incremental flow.

While the incremental flow model produced more accurate results on some well screens, the model failed to capture major downward spikes in the relative conductivity at other screens. This is most noticeable in screens 2, 3, 5, and 9. These observed drops reflect an increase in conductivity (Eq. 1) and may be due to the effects of back diffusion, where native groundwater (with high conductivity) remains in low permeability media around the more permeable aquifer materials. It is most often evident during periods of low to no flow when diffusion, not advection, is the primary transport mechanism. The increase in groundwater conductivity was particularly apparent during times of extended backflush at well screens (Figure 4-7).

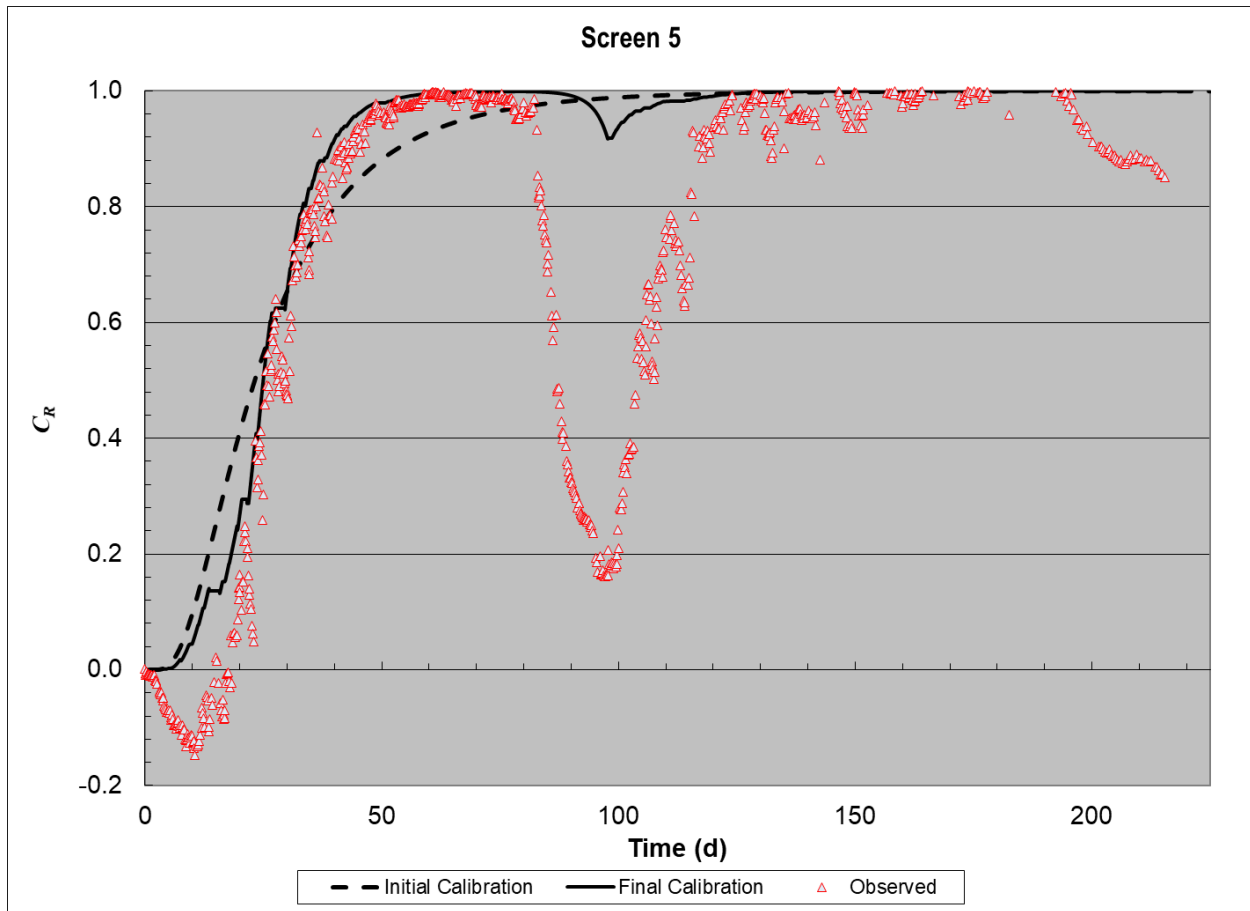


Figure 4-7. While the stoppage breakthrough curve is more accurate than the initial breakthrough curve for screen 5, it fails to explain the major spike that occurred between days 80-100. This period was during the 18-day backflush.

Flow in the LPA (screens 10-11) and in screen 8 was approximately 1% of the total recharge flow rate at TW-1. Screen 11 received the least percentage of the total recharge flow (0.4%) compared to the other ten well screens. As shown in Figure 4-8, conductivity breakthrough at screen 11 was gradual and did not reach a level consistent with SWIFT Water delivered through TW-1 (i.e., injection concentration, C_{inj}), resulting in a maximum observed relative concentration less than 1. The 18-day backflush starting at day 80 is not evident in the data. Some unexplained upward spikes in conductivity, which correspond with decreases in conductivity measurements from the native groundwater, were observed at screen 11 starting at day 100 and continuing through the period of observation.

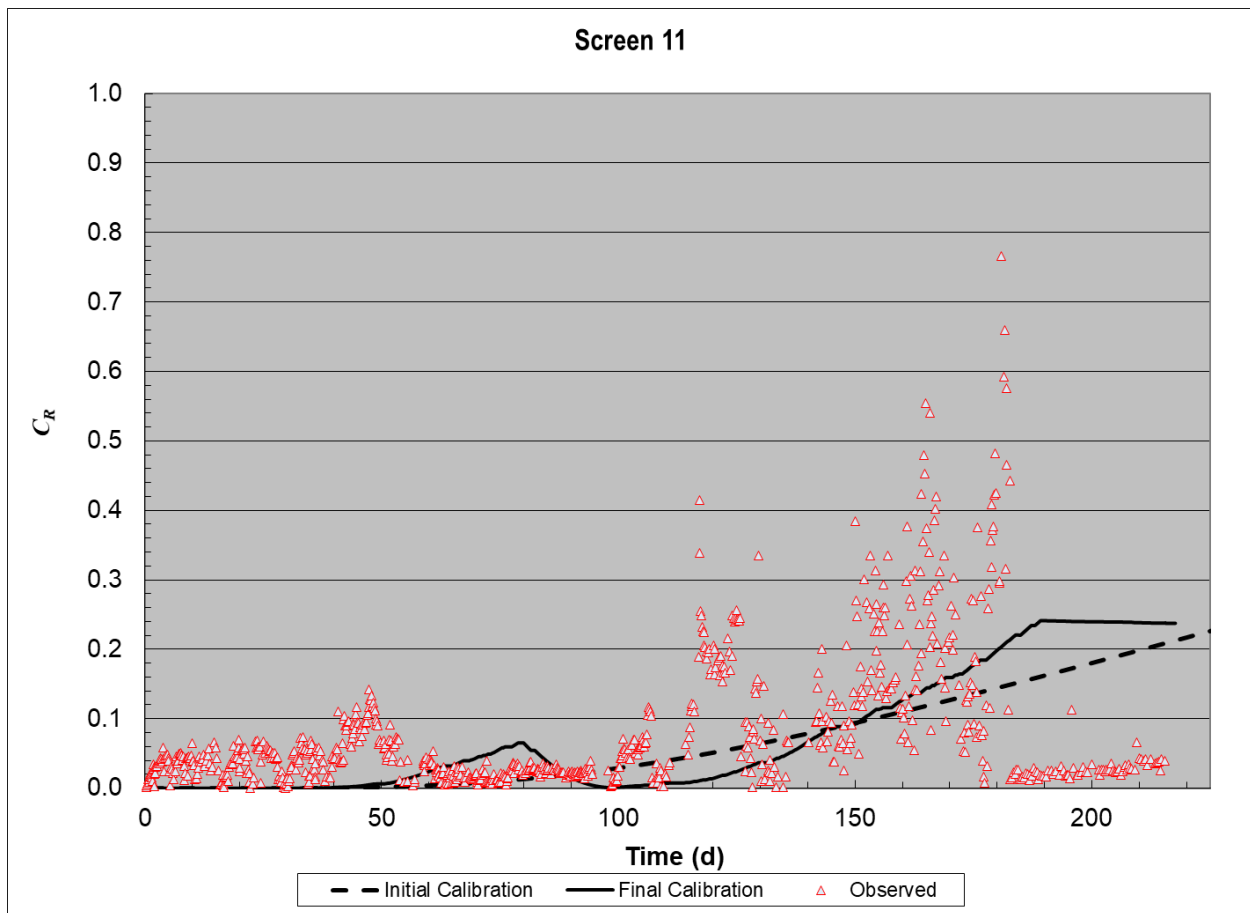


Figure 4-8. Breakthrough in the LPA has not yet occurred.

4.4 Conclusion and Implications

Use of the conventional breakthrough curve development method (continuous flow model) resulted in an approximate estimation of the distribution of flow in the multi-screen recharge well, but by not accounting for changes in recharge flow to the PAS during the MAR testing period, the match to the observed breakthrough curves was poor at some well screens. While the method was useful to estimate flow rate distribution and aquifer parameters (longitudinal dispersivity, and porosity), it was not suitable for predicting changes in tracer concentrations and travel times influenced by no flow or backflush flow conditions. The use of an incremental flow model developed using the method of superposition to simulate

breakthrough curves produced improved calibration to observed tracer concentrations and more accurate travel times. This approach was helpful for explaining downward spikes in relative conductivity during recharge operations restringing from prolonged backflush operations. This incremental flow model also aided in identifying unexplained decreases in relative conductivity that were not explained by changes in the recharge flow rate but potentially by another mechanism, including back diffusion.

Understanding the distribution of recharge flow at TW-1 will aid HRSD decision makers as they plan to scale up the SWIFT operation for full-scale implementation at up to five HRSD wastewater treatment facilities between now and 2030. The results of this study demonstrated that 73% of the recharge was delivered to 3 of the 11 well screens and that 57% was delivered to the UPA. While this finding has significance in the planning for new recharge wells (for example, limiting wells screens to the UPA and MPA), site specific conditions will govern well design. Future work on this topic will involve including effects of back diffusion into the computational model for breakthrough curves. This could be accomplished via the application of dual domain flow, where multiple porosities are used to simulate preferential pathways and pathways of low flow and storage.

Acknowledgements

The authors would like to thank members of the SWIFT Research Center team, operators at Nansemond Treatment Plant, and members from the HRSD Technical Services Division for their help in collecting samples onsite at the SWIFT Research Center. This work was supported by HRSD and the Charles E. Via, Jr. Department of Civil and Environmental Engineering at Virginia Tech.

Supplemental Information

Additional information and complete results from all screens can be found in Appendix B.

References

Charbeneau, R.J. (2000) *Groundwater Hydraulics and Pollutant Transport*. Upper Saddle River, Prentice-Hall, Inc.

Eggleston, J., and J. Pope. (2013) "Land subsidence and relative sea-level rise in the southern Chesapeake Bay region" U.S. Geological Survey Circular 1392, 30 p.

Hem, J.D. (1985) "Study and Interpretation of the Chemical Characteristics of Natural Water." U.S. Geological Survey Water-Supply Paper 2254 3, 225-249.

5. Evaluating Flow Distribution in a Multiaquifer Recharge Well Using an In-Situ Flowmeter

Title

Evaluating flow distribution in a multiaquifer recharge well using an in-situ flowmeter

Abstract

The distribution of flow is relevant to multiple-screen injection wells used in managed aquifer recharge (MAR) operations. To understand flow and transport behavior through a multi-layered aquifer, the distribution of flow to each screen within the recharge well must be quantitatively determined. In this study, an impeller flowmeter was deployed to measure flow rate distribution in a multiple-screen MAR well under both recharge and pumping conditions screened in multiple-strata of the Virginia Coastal Plain aquifer system. Flow distribution within the well moves preferentially through the uppermost screens during recharge while flow distribution is more distributed along all screens under pumping conditions. Analysis of flow along single screens also indicates preferential flow to the upper part of the screen during pumping and flow distribution distributed along the screen during pumping. Comparison of flowmeter results to previous site-specific measurements of flow distribution and transmissivity under both recharge and pumping conditions shows that flow distribution is dynamic and should be monitored over the course of an MAR project. These results have implications for transport modeling since flow distribution is typically considered to be largely constant over time and constant under a range of operational conditions.

5.1 Introduction

High-capacity pumping wells are routinely constructed with multiple screens to efficiently produce groundwater from the most permeable water-bearing strata of an aquifer (Konikow et al. 2009). Multiple-screen production wells are often constructed for groundwater withdrawals from two or more hydrostratigraphic units including openbore, multiaquifer wells in consolidated sediments (Neville and Tonkin 2004). Multiaquifer wells are a common feature in the layered semiconsolidated sediments of the Virginia Coastal Plain aquifer system (e.g., McFarland and Bruce 2006; Heywood and Pope 2009) and in similar hydrogeologic settings.

Typically, the distribution of the pumping flow rate among multiple screens is never directly measured, particularly once the production well is completed and put into operation. One common estimation technique is to apportion flow rates as a fraction of the total pumping rate where rates at individual screens are proportional to the ratio of the local transmissivity to the total transmissivity of all hydrostratigraphic units from which the well draws groundwater (Hanson et al. 2003). Here, local transmissivity is defined as the product of the individual well screen length and local hydraulic conductivity of the permeable strata adjacent to the well screen (Molz et al. 1994). This estimation technique applies to both pumping and injection wells and has been employed to assign flow to multiple-screen wells in multi-layer numerical groundwater flow models (Halford and Hanson 2002; Neville and Tonkin 2004).

The distribution of flow is particularly relevant to multiple-screen injection wells used in managed aquifer recharge (MAR) operations. MAR injection wells are used in aquifer storage and recovery (ASR) and aquifer storage transfer and recovery (ASTR) projects and for the replenishment of depleted groundwater systems (Pyne, 2006; Ringleb et al. 2016; Dillon et al. 2019; Martinez et al. 2022). Although the injection flow rate distribution was not directly

measured during the recharge phase of an ASR project, Izbicki et al. (2010) attributed differential flow and preferential transport of solutes in a single-screen well to aquifer heterogeneity with depth in alluvial deposits of the Sacramento Valley groundwater basin, California. Bullard et al. (2019) utilized intrinsic tracer concentration data to infer variable flow distribution in a multiple-screen MAR injection well penetrating multiple confined strata of the Potomac Aquifer System in eastern Virginia. Fakhreddine et al. (2020) observed variable flow distribution in an MAR injection well screened in four confined hydrostratigraphic units of the Orange County groundwater basin (California), resulting in depth-dependent solute travel times and differing geochemical concentration trends at an adjacent multiple-screen monitoring well. These studies indicate that quantifying the distribution of flow within the recharge well to each screen provides an improved understanding of flow and transport behavior through a multi-layered aquifer system.

Down-hole flowmeters provide for direct measurement of the flow distribution in pumping wells by obtaining a continuous profile of the cumulative inflow during pumping along the entire screened length of single-screened wells (Gossell et al. 1999; Newhouse et al. 2005) and multiple-screen wells (Hanson et al. 2003). Datel et al. (2009) describe geophysical logging as a useful practice to (1) identify crossflow and vertical flow in boreholes; (2) quantify permeability along an interval; and (3) identify leakage in test wells. Based on the study objective and flow sensitivity requirements, different types of borehole flowmeters are available for commercial use and research application, including impeller or spinner flowmeters, electromagnetic flowmeters, heat pulse flowmeters, acoustic Doppler flowmeters, and scanning colloidal borescope flowmeters (Hearst and Nelson 1985; Molz et al. 1994; Guerin 2005).

Spinner flowmeters, which work by measuring impeller rotation due to groundwater flow in a borehole, have been used since the 1950s to measure borehole flow (Newman et al. 1956; Rumble et al. 1959; Bryant 1960; Bullard et al. 1964). Impeller rotation is converted to velocity or flow measurements following calibration at known flow rates. Spinner flowmeters are ideal tools for situations with large ranges of flow magnitude while other flowmeters measurements are often limited to low-flow or ambient-flow applications (Boman et al. 1997; Young et al. 1998).

A number of researchers have employed borehole flowmeters to extrapolate depth-dependent hydraulic conductivity and permeability variations in a range of aquifer conditions (e.g., Molz et al. 1989; Rehfeldt et al. 1992; Hanson and Nishikawa 1996; Ruud et al. 1999; Zlotnik and Zurbuchen 2003; Basiricò et al. 2015; Ren et al. 2018). The theoretical relationships developed by Molz et al. (1989) which assumes that the transmissivity of the vertical interval of measurement is directly proportional to net flow entering the screen segment between flowmeter readings, $Q(z)$, have proven useful to quantify hydraulic conductivity independent of the type of flowmeter. Investigations of this nature typically employ low-flow, high-accuracy instruments to delineate $Q(z)$ at defined vertical intervals (Molz et al, 1989). However, more recent studies suggest that errors can be introduced into estimates of hydraulic conductivity based on measurements of $Q(z)$ following the Molz et al. (1989) method when head losses are not considered or the aquifer system does not reflect guiding assumptions, such as that of a perfectly stratified aquifer system (Xiang 1995; Ruud et al. 1999; Riva et al. 2012; Bianchi 2017).

Few studies have investigated flow distribution in high-capacity, multi-screen pumping or recharge wells because direct measurement using an impeller flowmeter requires access to the entire well column and an ability to pump or inject water at rates matching the well design.

Direct measurements often require removal of the pump column and installation of a supplemental pump, which may operate at a rate lower than the normal pumping rate. Alternatively, flow distribution may be inferred from data at nearby observation wells but with less certainty. In addition, little is known about differences in flow distribution behavior in MAR injection wells during sustained recharge operations as compared to backflush operations (i.e., short-term pumping for well maintenance). Orange County Water District tested a multi-screen well for flow distribution using an impeller flowmeter and the reported data revealed differences in the flow distribution under pumping conditions compared to recharge operations (Burriss 2018). Quantifying variations in flow distribution in a multi-screen well during regular operations and quantifying changes over time has the potential to provide valuable data to improve assessment of MAR design objectives and to reduce uncertainty on impacts to groundwater quality.

In this study, an impeller flowmeter was deployed to measure flow rate distribution in a multiple-screen MAR well under both recharge and pumping conditions. The primary objective seeks to quantify flow rates through well screens ranging in length from 15 to 105 ft (4.6 to 32 m) in an MAR well screened in eleven strata of the Virginia Coastal Plain aquifer system. A secondary objective seeks to compare percent flow distribution across single screens under both pumping and recharge flow conditions. To the best of our knowledge, previous investigations using flowmeters in well-capacity wells have not evaluated differences in the flow distribution between recharge and pumping conditions. Alternative lines of evidence include tracer data breakthrough data at a nearly multiple-screen depth discrete monitoring well and water level analysis at observation wells screened in the primary confined hydrostratigraphic units of the local aquifer.

5.2 Study Area and Methods

5.2.1 Project Background

Hampton Roads Sanitation District (HRSD) is a wastewater authority in eastern Virginia (USA) with a combined treatment capacity of 249 million gallons per day (942,000 m³/d) that serves 1.7 million people over an extensive service area (Figure 5-1). In 2018, HRSD initiated a large-scale MAR project known as SWIFT (Sustainable Water Initiative for Tomorrow) designed to recharge and increase storage in the Potomac Aquifer System (PAS) and reduce nutrient discharge to the Chesapeake Bay, with secondary goals to address coastal land subsidence and saltwater intrusion. SWIFT will utilize wastewater effluent treated to drinking water standards to recharge the PAS through injection wells at five HRSD water reclamation facilities. The study site is the HRSD SWIFT Research Center (SWIFT-RC), a 1.0-MGD (3,800 m³/d) aquifer recharge and advanced water treatment demonstration facility located in Suffolk, Virginia (Martinez et al. 2022).

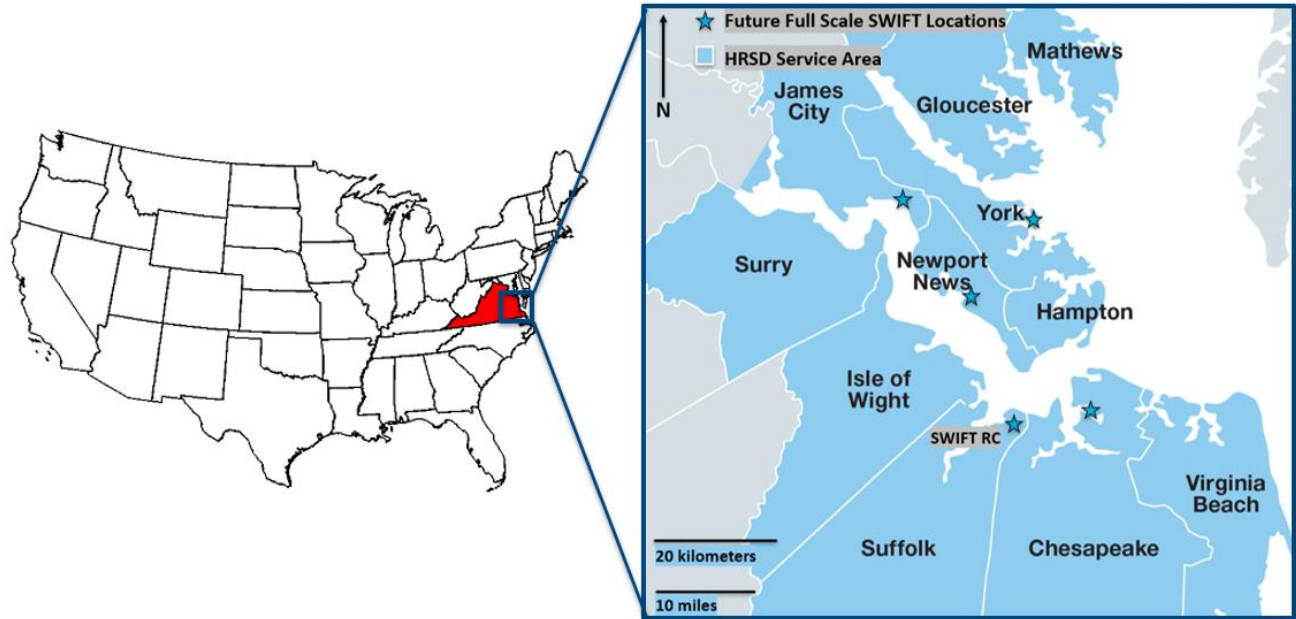


Figure 5-1. HRSD Service Area in eastern Virginia, USA. The existing demonstration facility (SWIFT-RC) in Suffolk is the study site, while future full-scale sites are marked by blue stars (Martinez et al. 2022).

5.2.2 Site Description

Flowmeter tests were conducted in a multiple-screen well (TW-1) designed for delivering 1.0 MGD (3,800 m³/d) of recharge to the PAS and for pumping at 1.4 MGD (5,300 m³/d) during backflushing operations. Regionally, the PAS is a heterogeneous semiconsolidated confined aquifer system that stretches from New Jersey to the coast of South Carolina and is the thickest aquifer in the Virginia Coastal Plain aquifer system (Trapp and Horn 1997). USGS reports describe the PAS as primarily fluvial-deltaic coarse-grained sands and gravels with interbedded clays of varying thicknesses (McFarland and Bruce 2006; Heywood and Pope 2009, McFarland 2013). The majority of groundwater withdrawals from the Virginia Coastal Plain aquifer system is derived from the PAS (McFarland and Bruce 2006). Because of the nature of the interbedded clays, confining units within the PAS function as local barriers but are not homogeneous and are often discontinuous across the extent of the PAS (Heywood and Pope 2009). Based on local PAS

hydrostratigraphy, TW-1 was constructed using 11 screens (Table 5-1) totaling 380 ft (115.8 m) screened across three distinct units of the PAS referred to as the Upper, Middle, and Lower Potomac Aquifer (UPA, MPA, LPA). Local hydrostratigraphy of the PAS based on well completion reports at TW-1 and MW-SAT is included in Appendix C (Figure C-1).

Table 5-1. Well screen depth and length of screen in recharge well TW-1.

Aquifer Zone	Starting Depth (fbg)	Ending Depth (fbg)	Length of Screen (ft)
Upper Potomac Aquifer (UPA)			
Screen 1	505	530	25
Screen 2	550	595	45
Screen 3	665	680	15
Screen 4	720	755	35
Middle Potomac Aquifer (MPA)			
Screen 5	820	835	15
Screen 6	860	890	30
Screen 7	905	920	15
Screen 8	965	990	25
Screen 9	1050	1090	40
Lower Potomac Aquifer (LPA)			
Screen 10	1230	1335	105
Screen 11	1370	1400	30

(fbg) – feet below grade

5.2.3. Instrument and Data Collection

Previous investigation at the SWIFT-RC determined flow distribution based on breakthrough of SWIFT Water at a nearby depth-discrete monitoring well (MW-SAT) located 50 feet (15.2 m) from TW-1 with screens matching the depths at TW-1 (Bullard et al. 2019). In May 2019, following a period of extended shutdown for well rehabilitation, the installation of an in-situ Mount Sopris QL40-SFM Spinner Flowmeter allowed for direct collection of data during operations to reduce uncertainty in flow distribution estimation. The flowmeter has a spinner

range of 0-3,000 rotations per minute (rpm) and an accuracy of better than 1%; it was also equipped with a centralizer to minimize the potential for error.

An impeller flowmeter was chosen for multiple reasons, first being the large range of flow conditions by depth during operations, ranging from 0 to 1,200 gallons per minute (0 to 75 L/s). Second, because the pump column would be installed after the flowmeter installation, rendering the flowmeter inaccessible during operations for any maintenance, a flowmeter equipped without flow diverters (e.g., inflatable packers) was chosen to minimize complexities and to reduce the potential of operational issues. Dinwiddie et al. (1999) have also shown that the use of a flow diverter in a well with a gravel pack can lead to bypass flow through the gravel pack instead of through the flowmeter, which could introduce error into the measurements. Finally, considering geochemical characteristics of the aquifer, which vary by depth and include high levels of total dissolved solids that would likely cause corrosion and a short lifespan of an in-situ test, the cost-effectiveness of an impeller flowmeter was a deciding factor. Because the tests were completed immediately following well rehabilitation, the potential of mechanical interference due to debris in the well was low and not considered something that would impact the effectiveness of an impeller flowmeter.

The flowmeter was calibrated 30 feet (9.1 m) above the uppermost screen during both recharge and pumping conditions before data collection with depth and was recalibrated following extended stoppage periods between tests. Details on the calibration process and the calibration curves can be found in Appendix C (Figure C-2 to C-4). During recharge operations, flow of SWIFT Water to the aquifer was measured with a Rosemount 8750W Magnetic Flowmeter System, which is commonly used in water and wastewater applications. Instantaneous flow rates were recorded using the SWIFT supervisory control and data

acquisition (SCADA) system. One-minute increment flows were accessed and averaged over the period of each recorded test.

Following the initial flowmeter calibration, static testing was completed during recharge operations. Static testing involved moving the flowmeter to the depth of the top and bottom of each screen (Table 1). After allowing for flow stabilization around the flowmeter (average time of 4.33 minutes), the flowmeter reading was logged for one minute and the average reading (counts per second) was recorded from the one-minute data. The calibration data were used to convert the average reading to flow in gallons per minute (gpm). Raw results for static testing are discussed in Appendix C (Table C-1).

Dynamic testing was completed during both recharge and pumping operations (Table 5-2). During the testing period, static and dynamic testing were completed under normal operating conditions to best reflect actual flow distribution. Comparison of results with varied flowmeter speeds (5 ft/min vs. 20 ft/min) showed that operating the dynamic tests at 20 ft/min produced similar results after data processing, and less influent flow rate variation was observed due to a shorter test period. Flowmeter speed was monitored during testing and was within 0.5 ft/min (0.15 m/min) of the target speed over the range of the testing period. Flow measurements were collected at an interval of 0.25 feet (7.6 cm). Data from the experiment runs were processed, and noise was removed using a log acquisition and processing software (WellCAD™, Advanced Logic Technology). To process the dynamic test data, background impeller rotation counts caused by the speed of the flowmeter were removed based on the average rotations measured in the lowermost region of the well (Screen 11), where a previous tracer study had established little to no flow (Bullard et al. 2019).

Flow distribution for the static test was calculated based on the difference between the flow measured at two locations: 1) above the screen of interest immediately below the adjacent screen and 2) at the bottom of the screen of interest. For tests conducted under dynamic conditions, total flow to each screen was measured by taking the difference between the flow measured 20 feet above the top of screen and flow measured at the bottom of screen. The location of flow measurements above the screen was based on the observation of unstable readings immediately at the top of each screen due to flow in the well casing. Further discussion of this reasoning is included in Appendix C (Figures C-5 to C-10). Flow distribution within the well was calculated by dividing the total flow to each screen by the total flow to the aquifer under recharge conditions or the total pumping rate. For both conditions, the total flow was determined by readings measured 20 feet above Screen 1 and verified using the SCADA readings. Flow distribution was compared to previously estimated flow and transmissivity distributions in the PAS during operations at the SWIFT-RC.

Table 5-2. Flowmeter test conditions.

Test	Average Flow Rate (gpm)*	Flowmeter Direction**	Flowmeter Speed (ft/min)
Static Testing			
S1	684	N/A	N/A
Pumping Testing			
B1	1122	Against	20
B2	1129	With	20
Recharge Testing			
R1	684	Against	5
R2	687	Against	20
R3	684	Against	20
R4	682	Against	20

* Time-averaged rates during test run

** Flowmeter direction indicates whether the flowmeter was moving with the direction of flow (i.e., up the well during pumping and vice versa during recharge) or against the direction of flow (i.e., down the well during pumping and vice versa during recharge)

5.3 Results

5.3.1 Flow Distribution Within the Well

Under static testing conditions, the time-averaged influent flow rate was 685 gpm (51.9 L/s) with slight variations in the recharge rate during the 158-minute test (standard deviation of 1.2 gallons per minute [0.09 L/s]). Comparison of the dynamic test results in TW-1 under both recharge and pumping conditions with the time-averaged SCADA flow rates show the flowmeter was able to account for 100% of the flow $\pm 1.5\%$ (Table 5-3). The flow rate variation over depth during Test R2 is shown in Figure 5-2. Similar flowmeter results for the other dynamic tests can be found in Appendix C (Figures C-11 to C-15). Screens 1, 2, and 9 were consistently the most productive zones under pumping conditions, accounting for 70% of the flow through 29% of the 380 ft of well screen. During recharge tests, the same three screens accepted 76% of SWIFT water.

Table 5-3. Flow distribution (%) results of static, dynamic recharge (tests denoted by R-), and dynamic pumping (tests denoted by B-) flowmeter testing.

Screen	Static Test	Dynamic Recharge Tests					Dynamic Pumping Tests		
	S1	R1	R2	R3	R4	Mean	B1	B2	Mean
1	19	17	22	15	22	19	17	17	17
2	52	49	44	48	41	46	38	41	39
3	1	2	1	0	5	2	1	2	1
4	8	8	9	9	4	7	7	7	7
5	6	6	5	8	6	6	8	8	8
6	3	3	2	2	4	3	2	3	2
7	2	2	1	3	3	2	5	3	4
8	2	2	3	1	2	2	2	2	2
9	8	9	11	13	12	11	16	13	14
10	0	1	0	2	1	1	5	4	4
11	0	0	0	0	0	0	0	0	0
SUM	100	99	98	101	100	99	99	98	99

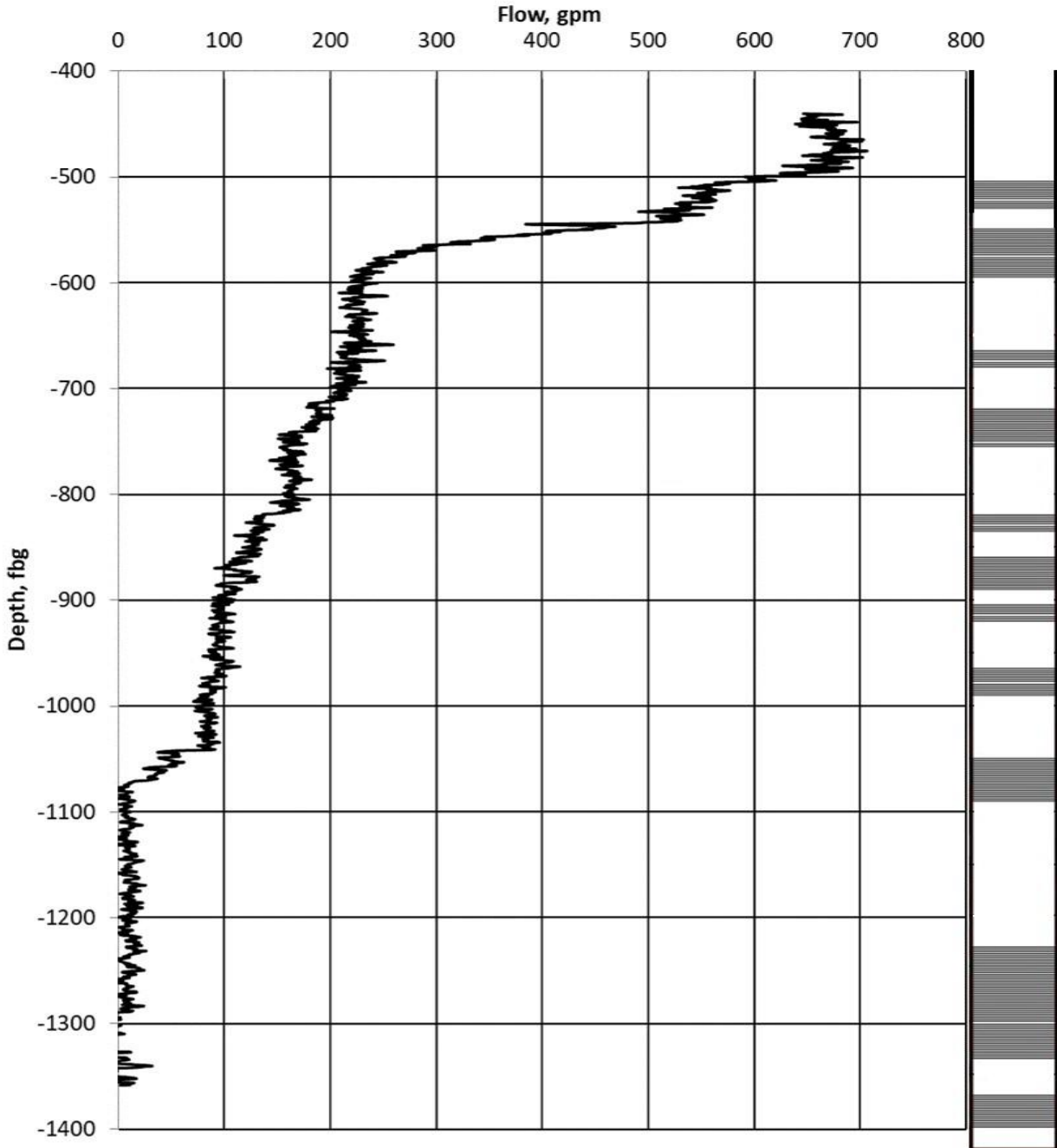


Figure 5-2. Flowmeter profile during Test R2 in well TW-1. Results are shown with 1-foot precision. Screen depths relative to land surface are shown on the right.

Mean flow distribution under recharge and pumping conditions is shown in Figure 5-3. The average difference between recharge and pumping flow distribution relative to the respective test flow rates is 1.7% for dynamic testing, with a 6.2% maximum difference at Screen 2 and a

minimum 0.2% difference at Screen 4. Recharge distribution is higher than pumping distribution at five of the six uppermost screens of TW-1 (Screens 1 through 4 and 6) while pumping distribution exceeds recharge distribution in the lowermost screens (Screens 5, 7 through 10). This suggests preferential recharge flow to the four uppermost screens connected to the UPA (74%) compared to pumping (64%). Flow derived from the MPA and LPA by pumping was 30% and 4%, respectively, reflecting a more uniformly distributed over the entire aquifer relative to recharge operations. This could also be a function of the difference in the mean flow rate magnitude between recharge and pumping (684 and 1126 gpm, respectively). Operational constraints of the SWIFT-RC limited recharge to a maximum of 700 gpm, which prevented a direct comparison of flow distribution in TW-1 under identical pumping conditions at the same flow rate.

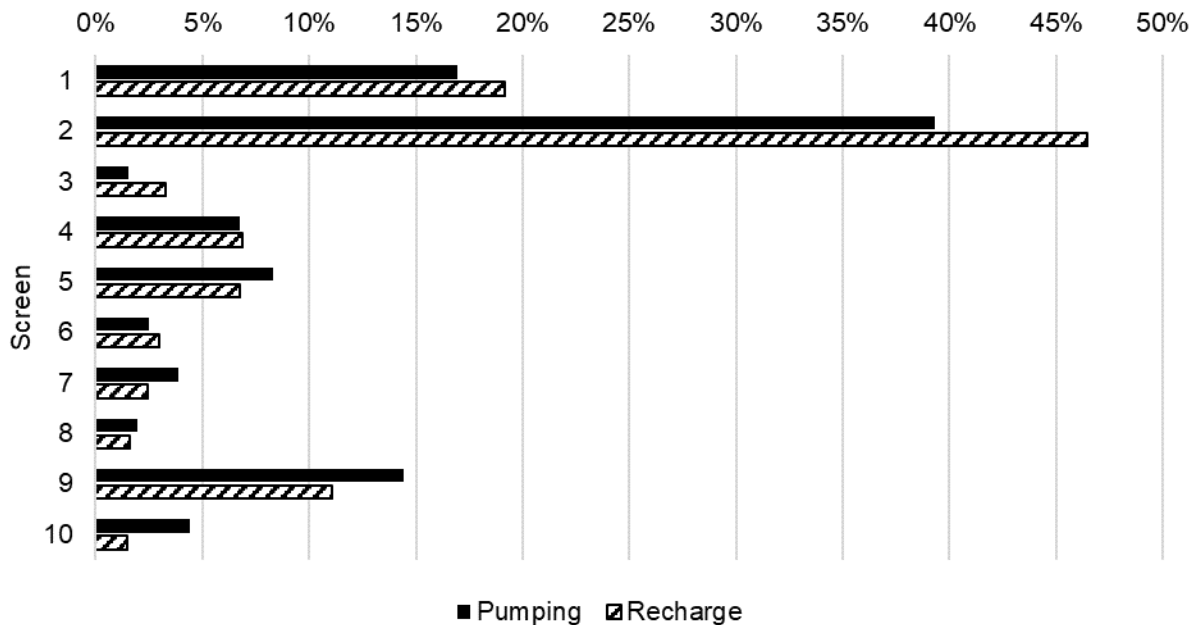


Figure 5-3. Mean flow distribution to each well screen (%) under recharge and pumping testing conditions in well TW-1.

5.3.2. Flow Distribution at Well Screens

Flow at Screens 2 and 9 was analyzed at 1-foot (0.3 m) intervals to determine trends in recharge and pumping behavior within the screen. Screens 2 and 9 were chosen because of their comparable screen lengths (45 feet and 40 feet [13.7 and 12.2 m], respectively) and the screen flow rates were large enough to show significant differences across each screen (i.e., differential flow rate between the bottom and top of the screens). Flow rates were normalized for each operational condition by subtracting the flow rate at the bottom of the screen and divided by the total screen flow rate at each screen. Results are plotted as a function of normalized screen length to allow comparison between screens (Figure 5-4).

During recharge, flow moved preferentially through the upper section of each screen relative to observations during pumping in which flow rates were more evenly distributed along the entire screens (Figure 5-4). Results in both Screens 2 and 9 showed that the bottom 10% of screen produced minimal contribution to flow during pumping and nearly 100% of flow was transmitted to the aquifer is the upper 90% of the well screens under recharge conditions. During recharge at Screen 2 and 9, 50% of the flow occurs in the upper 23% and 35% of the screen, respectively, and 80% of recharge is delivered to the upper 50% of each screen. During pumping at Screens 2 and 9, 50% of the flow occurs in the upper 40% and 53% of the screen, respectively, and 80% of flow was derived from the upper 64-66% of each screen. Normalized values from Screen 9 are more variable because of the lower absolute values of measured flowmeter readings, which resulted in larger absolute differences between measurements, but the data reflect the same general behavior as Screen 2.

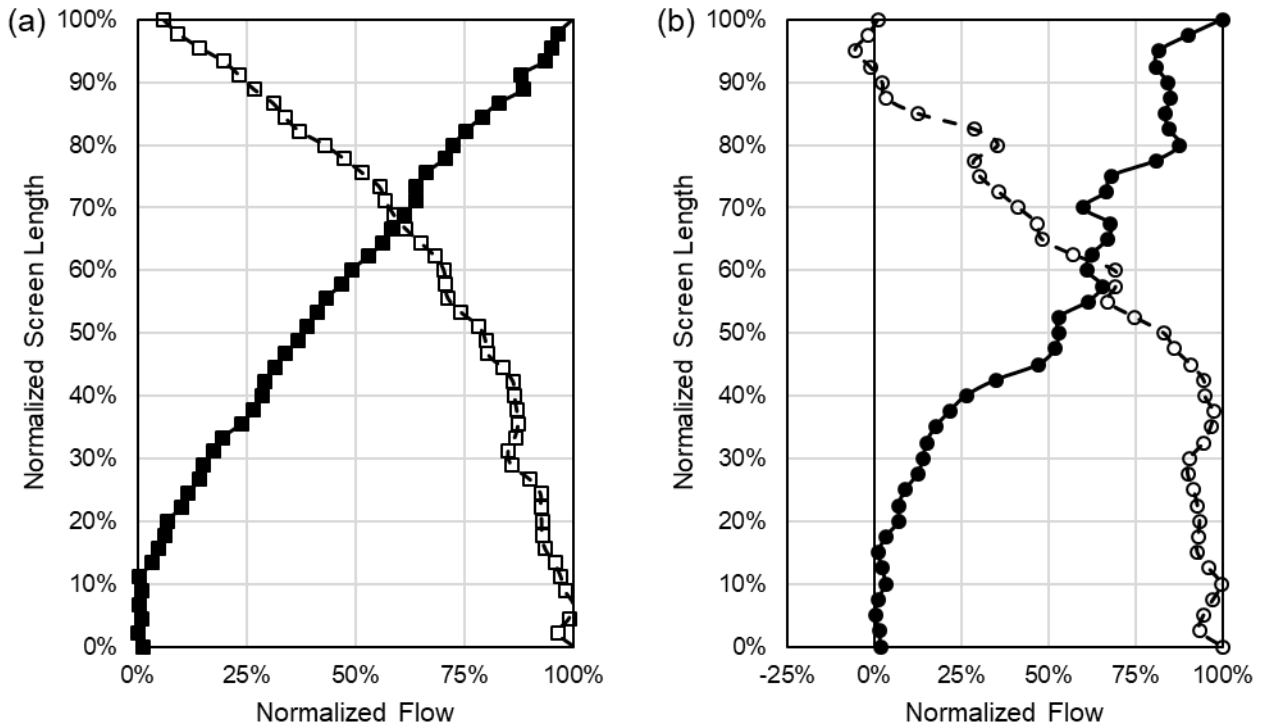


Figure 5-4. Flow distribution across (a) Screen 2 and (b) Screen 9 during recharge and pumping. Normalized screen length indicates bottom of screen at 0.0 and top of screen at 1.0. For recharge conditions (open markers), flow is normalized based on the difference between flow between the top of screen (TOS) and bottom of screen (BOS); because flow starts entering the screen at TOS, normalized flow reaches 100% at BOS. During pumping conditions (closed markers), flow enters the screen starting at BOS and reaches 100% at TOS.

5.3.3. Hydraulic Conductivity Distribution

Hydraulic conductivity was calculated at each well screen associated with the UPA (Screens 1-4) and at each well screen associated with the MPA (Screens 5-9) based on an adaption of the method used by Molz et al. (1989), which can be simplified to:

$$\frac{T_i}{T_T} = \frac{Q_i}{Q_T} \quad (1)$$

where T_i is the transmissivity in the strata of interest, T_T is the transmissivity over the total aquifer strata, Q_i is the flow rate at the well screen of interest, and Q_T is the total flow rate

entering or leaving the well. In a multi-screen, multi-aquifer well with known transmissivity for each aquifer, Equation 1 can be modified to find the screen-specific hydraulic conductivity:

$$K_i = \frac{T_A}{L_i} * \frac{Q_i}{Q_A} \quad (2)$$

where T_A is the aquifer transmissivity of either the UPA or MPA, L_s is the screen length, Q_i is the flow rate measured at the screen of interest, and Q_A is the sum of flow rates at well screens hydraulically connected with either the UPA or the MPA. Mean hydraulic conductivity in the UPA and MPA (K_A) were also calculated using Equation 3.

$$K_A = \frac{1}{\sum_1^N L_i} \sum_1^N K_i L_i \quad (3)$$

where N is the number of well screens associated with each PAS unit. Matynowski (2020) utilized the Theis curve matching and Cooper-Jacobs methods to estimate aquifer parameters at the SWIFT Research Center using on drawdown data at the conventional wells (MW-UPA, MW-MPA, and MW-LPA) during extended pumping events in May 2018 immediately prior to the start of recharge at TW-1. These unit-specific transmissivities were used to calculate screen-specific hydraulic conductivity using Equation 2.

Results for the nine uppermost for both pumping and recharge conditions based on the mean flow distributions from the flowmeter tests are shown in Figure 5-5. Because pumping test analysis showed that the LPA was not responsive during the duration of the test period (Matynowski 2020), hydraulic conductivity estimates were not calculated for Screens 10 and 11. Under pumping conditions, hydraulic conductivity ranged from 31.8 to 149.8 feet/day (9.7 to 45.7 meters/day) for UPA (Screen 1-4) and 45.3 to 297.0 feet/day (13.8 to 90.5 meters/day) for

the MPA (Screens 5-9). In general, the vertical distribution of strata-scale hydraulic conductivity determined from the recharge tests was similar.

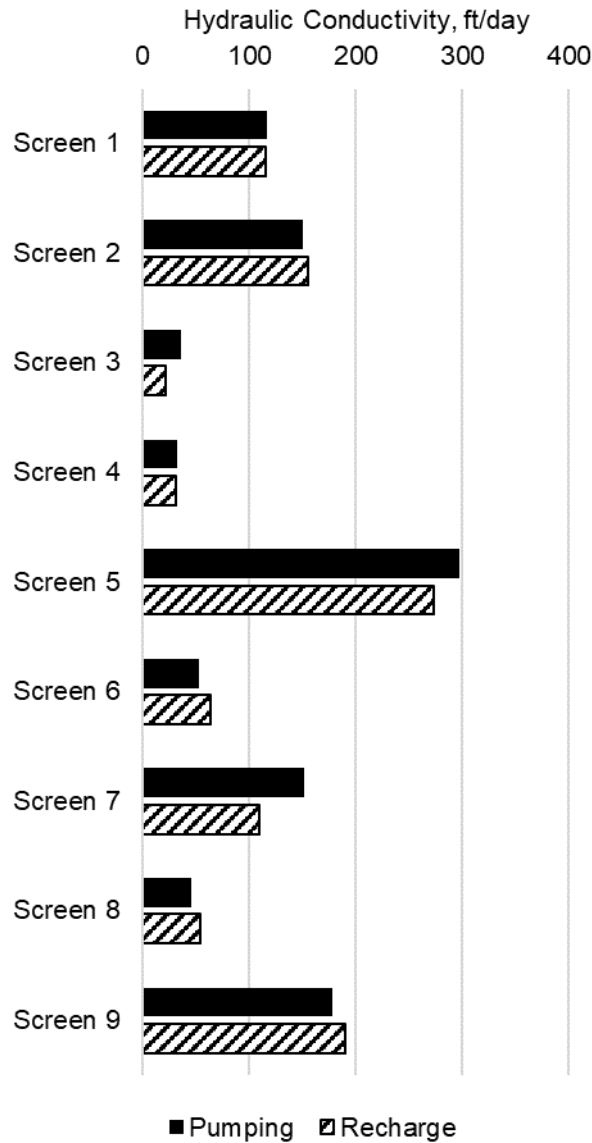


Figure 5-5. Hydraulic conductivity (ft/day) at each screen in the Upper Potomac Aquifer (Screens 1-4) and in the Middle Potomac Aquifer (Screens 5-9).

A comparison of results to previously estimated hydraulic conductivities in the PAS can be found in Table 5-4. Smith (1999) derived hydraulic conductivity for the UPA, MPA, and LPA

from transmissivity data from aquifer tests conducted by the City of Newport News in 1995 for their brackish groundwater development (BGD) project. Heywood and Pope (2009) acknowledge that the PAS is heterogeneous and that estimates of hydraulic conductivity based on aquifer-performance test results across the region range from 15 to 337 feet/day (4.6 to 102.7 meters/day). Their model of groundwater flow in the coastal plain of Virginia simulates hydraulic conductivity across the region based on pilot points placed within the model. The three well sites closest to the SWIFT Research Center in Suffolk had conductivity estimates of 175 ft/d (53.3 m/d), 59 ft/d (18.0 m/d), and 83 to 337 ft/d (25.3 to 102.7 m/d), demonstrating the variability of conductivity in the PAS (Heywood and Pope 2009). For the purpose of the groundwater flow model, hydraulic conductivities at pilot points were parameterized and estimated during model calibration, and conductivities between pilot points were spatially interpolated; conductivity at the SWIFT Research Center location was interpolated as 35 to 50 ft/d (10.7 to 15.2 m/d), though site specific conductivity may be significantly higher (Heywood and Pope 2009).

Table 5-4. Comparison of hydraulic conductivity estimates. All estimates are in ft/day.

Aquifer Unit	Smith 1999	Heywood and Pope 2009		Flowmeter Testing
		Model Simulation	PAS Pumping Tests	
UPA	74.1		59 - 175	94
MPA	40.0	35 - 50	83 - 337	133
LPA	6.9		--	--

Hydraulic conductivity distribution across individual screens was also calculated using the following modification of Equation 4:

$$K_i = \frac{T_s * Q_i}{z_i} \quad (4)$$

where T_s is the screen-specific transmissivity, Q_s is the screen-specific flow rate, Q_i is the change in flow rate over the vertical interval of measurement, and z_i is the vertical interval of measurement. Screen 2 was again chosen as a representative section. Under recharge conditions, hydraulic conductivity at screen 2 is an average of 155.3 ft/day (47.3 m/day) varies from 46 to 327 ft/day (14 to 99.7 m/day) with the highest conductivities in the upper section of the screen, decreasing with depth (Figure 5-6). Conductivity estimates during pumping are more distributed across the screen and range from 3 to 213 ft/day (0.9 to 64.9 m/day) with an average of 156 ft/day (47.5 m/day).

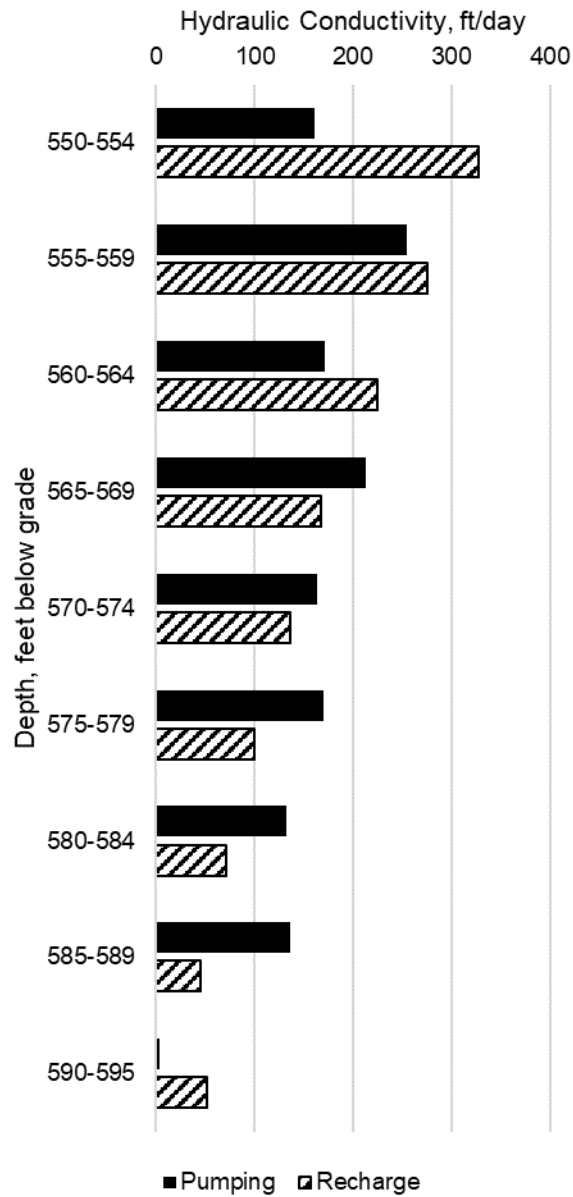


Figure 5-6. Conductivity distribution measured over five-foot intervals in screen 2.

5.3.4. Consideration of Turbulence Flow Within the Well

Flowmeter readings stabilized to an equilibrium value in well casing above each screen typically at a distance of 20 ft above the top of each screen. The source of instability was thought to result from turbulent flow in the well casing. The Reynolds number (Re) inside TW-1 ranged from 23,000 to 183,000 during recharge and 50,000 to 300,000 during pumping indicating

turbulent flow was prevalent (i.e., $Re > 2,000$) above Screen 10 (see Table C-3 and C-4 of Appendix C lists depth-depending Re using mean flow rates). This range and maximum are consistent with previous studies utilizing impeller flowmeters in high-capacity pumping wells in which maximum Re values varied from 420,000 to 650,000 in single-screened wells (Gossell et al. 1999 and Newhouse et al. 2005, respectively) and from 440,000 to 610,000 in multiple-screen wells (Hanson et al. 2003 and Fakhreddine et al. 2020, respectively). Head loss due to divergent flow before reaching each screen during recharge could potentially introduce error into the reading at the top of the screen (Houben 2015; van Lopik et al. 2021).

Under pumping conditions, flow lines in the well casing converge over the length of the well screen and in the casing above the screen creating a condition under turbulent flow in which the velocity profile is not fully developed. Empirical expressions for the required distance (L_{dev}) for development of fully-developed pipe flow with an upstream entrance conditions is dependent on the Reynolds number and diameter (Cengel and Cimbala 2017).

$$L_{dev} = 1.359DR_e^{1/4} \quad (5)$$

where D is the well pipe diameter. Although the experimental entrance condition associated with Equation 5 is not identical to the pattern of flow above a well screen during pumping, the expression provides an over-estimate of the length of well case over which a stable velocity profile is formed. Using the mean pumping rates in TW-1 (Table 2), L_{dev} varied from 21 ft above Screen 9 to 32 ft above Screen 1. This result provides one reasonable explanation for non-uniform flowmeter readings above well screens during pumping. This suggests additional research is needed to evaluate the impact of divergent and convergent flow in high-capacity wells under recharge and pumping conditions, respectively.

5.4 Discussion

Recharge at the SWIFT-RC began in May 2018 and has been relatively continuous with the exception of several periods of extended pumping or discontinuation of recharge for maintenance of the water treatment system or TW-1. From November 2018 to late April 2019, the SWIFT-RC was offline for treatment process repair and subsequent well rehabilitation due to the introduction of iron corrosion products into TW-1 via recharge. Well rehabilitation involved the removal of the pump column, wire brushing of the screens, air lifting from the bottom of the well, mechanical swabbing, chemical treatment, and chlorine disinfection. Flowmeter installation was completed in April 2019 immediately following well rehabilitation and flowmeter testing took place in May 2019. Therefore, multiple lines of evidence collected were employed to further evaluate the results and were modified as necessary to account for differences in the well condition at TW-1 over time.

Flow distribution measured using the impeller flowmeter was compared to previous site-specific measurements of flow distribution and transmissivity under recharge and pumping conditions (Table 5-5). The flow rate distribution shown for flowmeter testing represents the sum of mean values for Screens 1-4 (UPA) and Screens 5-9 (MPA). Bullard et al. (2019) estimated flow distribution during the initial recharge operations in May 2018 by modeling conductivity breakthrough of SWIFT Water at MW-SAT at each of the 11 screens. Although the results compare favorably (Table 5-5), changes in flow rate distribution between recharge operations in 2018 and post-rehabilitation in 2019 are apparent.

Table 5-5. Percent flow distribution (Qi/ total Q) during recharge and pumping conditions and percent transmissivity (Ti/ total T).

Aquifer	Recharge		Pumping	
	(Qi/ total Q) x 100%		(Ti/ total T) x 100%	
	SWIFT Water Breakthrough Modeling (2018)*	Flowmeter Testing (Recharge)	Flowmeter Testing (Pumping)	Water Level Analysis (2018)†
UPA	57	74±2	64±2	43
MPA	41	24±2	30±2	57
LPA	2.3	1.2	4	--

*Bullard et al. (2019); Flow distribution derived from conductivity breakthrough data
†Matynowski (2020); Transmissivity derived from analysis of drawdown data

Pre-rehabilitation transmissivity estimates based on analysis of pumping test data were used to estimate flow rate distribution to the UPA and MPA based on Equation 1 and compared to mean flowmeter-derived flow rate distribution pumping in Table 5-3. For both recharge and pumping conditions, the flowmeter testing produced flow rate distributions that considerably vary from the transmissivity ratios. The impact of well rehabilitation conducted from November 2018 to April 2019, which rehabilitated clogged screens and likely created preferential flow paths opening to the UPA undoubtedly contributed to differences between the flow distributions determined using pre-rehabilitation data (2018) and the flow meter results. However, these results suggest aquifer transmissivity is not a clear indicator of predicted flow distribution in a multi-screen, multiaquifer well under either pumping or recharge conditions.

Similar behavior was observed by Orange County Water District’s (OCWD) Groundwater Replenishment System, a 100 MGD (378,000 m³/d) advanced treatment project, which injects part of the product (approximately 1.5 MGD [5,678 m³/d]) into the local aquifer system. The system is stratified similarly to the PAS with interbedded sands and clays in a semiconsolidated confined aquifer system in California, USA (Fakhreddine et al. 2020).

According to Burris (2018), a 2015 spinner flowmeter test at the site conducted before, during, and after a backwash pumping period showed a difference in flow distribution between pumping and recharge conditions. The test also demonstrated a change in flow distribution as a result of the backwash pumping, although the pumping rates during the two injection tests were not constant so some difference may be attributed to the different flow rates used for the two injection tests (Burris 2018).

5.5 Conclusions

This investigation provides an evaluation of flow rate distribution in a multi-screen, multiaquifer recharge well during MAR operations and a site-specific comparison to previous estimates of flow and transmissivity distributions. Based on the results of this study, the following flowmeter operations-based conclusions can be drawn. Dynamic tests with a higher flowmeter speed had less variation of average influent flow and therefore were more representative as the flowmeter moved along the wellbore. Dynamic tests moving against the direction of flow (trolling up the well during recharge and trolling down the well during pumping) were more accurate, since there was not a period where the flowmeter was moving at the same speed as the water and therefore flow was not captured.

Flow rate distributions under recharge and pumping conditions were not identical. Well screens with a larger magnitude of flow tended to have a larger absolute difference between recharge and pumping flow distributions. Recharge in the multi-screen well tended to move preferentially through the uppermost screens and through the upper half of each well screen, while flow distribution under pumping conditions was more evenly distributed in the multi-screen well and specific screens. Moreover, this study provided a comparison of flow rate

distributions over time suggesting flow distribution in multi-screen wells is dynamic and should be monitored over the course of an MAR project. These results have implications for transport modeling given flow distribution is typically considered to be largely constant over time and does not vary under a range of operational conditions. Further research into the dynamic nature of flow distribution during MAR operations would provide insight into how recharge operations may impact groundwater flow and transport during MAR projects.

Acknowledgments

The authors would like to thank members of the HRSD SWIFT-RC team for their help in monitoring the status of the flowmeter at the SWIFT-RC, specifically Thomas Dziura and Dan Holloway. Additional design support for flowmeter installation for in-situ use was provided by Hazen and Sawyer. This work was supported by HRSD, the Potomac Aquifer Recharge Monitoring Laboratory, and the Charles E. Via, Jr. Department of Civil and Environmental Engineering at Virginia Tech.

Supplemental Information

Additional information can be found in Appendix C.

References

- Basiricò, S., G.B. Crosta, P. Frattini, A. Villa, and A. Godio. 2015. Borehole Flowmeter Logging for the Accurate Design and Analysis of Tracer Tests. *Groundwater* 53 (S1): 3–9. <https://doi.org/10.1111/gwat.12293>
- Bianchi, Marco. 2017. Validity of Flowmeter Data in Heterogeneous Alluvial Aquifers.” *Advances in Water Resources* 102: 29–44. <https://doi.org/10.1016/j.advwatres.2017.01.003>
- Boman, G.K., F.J. Molz, and K.D. Boone. 1997. Borehole Flowmeter Application in Fluvial Sediments: Methodology, Results, and Assessment. *Ground Water* 35 (3): 443–50. <https://doi.org/10.1111/j.1745-6584.1997.tb00104.x>
- Bryant, H.L. 1960. Production Well Logging Techniques. *Geophysics* XXV (4): 905–27.
- Bullard, H M, R.D. Clarke, and D.H. Rush. 1964. Production Logging as Applied to Post Primary Production. In *SPWLA 5th Annual Logging Symposium* 1964.
- Bullard, M.G., M. Widdowson, G. Salazar-Benites, J. Heisig-Mitchell, A. Nelson, and C. Bott. 2019. “Managed Aquifer Recharge: Transport and Attenuation in a Coastal Plain Aquifer.” In *Proceedings of the EWRI World Environmental and Water Resources Congress 2019: Groundwater, Sustainability, Hydro-Climates/Climate Change, and Environmental Engineering*, 1–14. Pittsburgh: EWRI. <https://doi.org/https://doi.org/10.1061/9780784482346.011>
- Burris, Debra L. 2018. Groundwater Replenishment System 2018 Annual Report. Irvine, CA: OCWD. <https://www.ocwd.com/media/7933/2018-gwrs-annual-report.pdf>.
- Cengel, Y.A., and J.M. Cimbala. 2017. *Fluid mechanics: Fundamentals and Applications* (4th ed.). McGraw-Hill Education.
- Datel, J.V., M. Kobr, and M. Prochazka. 2009. Well Logging Methods in Groundwater Surveys of Complicated Aquifer Systems: Bohemian Cretaceous Basin. *Environmental Geology* 57 (5): 1021–34. <https://doi.org/10.1007/s00254-008-1388-8>
- Dillon, P., P. Stuyfzand, T. Grischek, M. Lluria, R.D.G. Pyne, R.C. Jain, J. Bear, et al. 2019. Sixty Years of Global Progress in Managed Aquifer Recharge. *Hydrogeology Journal* 27: 1–30. <https://doi.org/10.1007/s10040-018-1841-z>.
- Dinwiddie, C.L., N.A. Foley, and F.J. Molz. 1999. In-Well Hydraulics of the Electromagnetic Borehole Flowmeter. *Ground Water* 37 (2): 305–15. <https://doi.org/10.1111/j.1745-6584.1999.tb00988.x>

- Fakhreddine, S., H. Prommer, S.M. Gorelick, J. Dadakis, and S. Fendorf. 2020. Controlling Arsenic Mobilization during Managed Aquifer Recharge: The Role of Sediment Heterogeneity. *Environmental Science and Technology* 54 (14): 8728–38. <https://doi.org/10.1021/acs.est.0c00794>.
- Gossell, M.A., T. Nishikawa, R.T. Hanson, J.A. Izbicki, M.A. Tabidian, and K. Bertine. 1999. Application of Flowmeter and Depth-Dependent Water Quality Data for Improved Production Well Construction. *Ground Water* 37 (5): 729–35. <https://doi.org/10.1111/j.1745-6584.1999.tb01165.x>.
- Guerin, R. 2005. Borehole and Surface-Based Hydrogeophysics. *Hydrogeology Journal* 13 (1): 251–54. <https://doi.org/10.1007/s10040-004-0415-4>.
- Halford, K.J. and R.T. Hanson. 2002. User guide for the drawdown-limited, multi-node well (MNW) package for the U.S. Geological Survey's modular three-dimensional finite-difference ground-water flow model, versions MODFLOW-96 and MODFLOW-2000. U.S. Geological Survey Open-File Report 2002-293.
- Hanson, R.T., and T. Nishikawa. 1996. Combined Use of Flowmeter and Time-Drawdown Data to Estimate Hydraulic Conductivities in Layered Aquifer Systems. *Ground Water* 34 (1): 84–94. <https://doi.org/10.1111/j.1745-6584.1996.tb01868.x>.
- Hanson, RT, P. Martin, and K.M. Koczot. 2003. Simulation of Ground-Water/Surface-Water Flow in the Santa Clara-Calleguas Ground-Water Basin, Ventura County, California. U.S. Geological Survey Water-Resources Investigations Report 02-4136. Sacramento. <https://pubs.usgs.gov/wri/wri024136/wrir024136.pdf>.
- Hearst, J.R., and P.H. Nelson. 1985. *Well Logging for Physical Properties*. 1st ed. McGraw-Hill Companies.
- Heywood, C.E, and J.P. Pope. 2009. Simulation of Groundwater Flow in the Coastal Plain Aquifer System of Virginia. U.S. Geological Survey Scientific Investigations Report 2009 – 5039. Reston, VA. <https://doi.org/10.3133/sir20095039>.
- Houben, G.J. 2015. Review: Hydraulics of Water Wells—Head Losses of Individual Components. *Hydrogeology Journal* 23 (8): 1659–75. <https://doi.org/10.1007/s10040-015-1313-7>.
- Izbicki, J.A, C.E. Petersen, K.J. Glotzbach, L.F. Metzger, A.H. Christensen, G.A. Smith, D. O’leary, M.S. Fram, T. Joseph, and H. Shannon. 2010. Aquifer Storage Recovery (ASR) of Chlorinated Municipal Drinking Water in a Confined Aquifer. *Applied Geochemistry* 25: 1133–52. <https://doi.org/10.1016/j.apgeochem.2010.04.017>.

- Konikow, L.F., G.Z. Hornberger, K.J. Halford, and R.T. Hanson. 2009. Revised multi-node well (MNW2) package for MODFLOW ground-water flow model: U.S. Geological Survey Techniques and Methods 6–A30, 67 p.
- Martinez, M.B., Widdowson, M.A., Bott, C., Holloway, D., Heisig-Mitchell, J. and Wilson, C. (2022), Demonstration of Managed Aquifer Recharge in a Coastal Plain Aquifer: Lessons Learned. *Groundwater*. Accepted Author Manuscript. <https://doi.org/10.1111/gwat.13197>
- Matynowski, E.D. 2020. Groundwater Modeling and Hydrogeological Parameter Estimation: Potomac Aquifer System, SWIFT Research Center. M.S. thesis, Department of Civil and Environmental Engineering, Virginia Tech.
- McFarland, E.R., and T.S. Bruce. 2006. The Virginia Coastal Plain Hydrogeologic Framework. U.S. Geological Survey Professional Paper 1731. <https://doi.org/10.3133/pp1731>.
- McFarland, E. R. 2013. Sediment Distribution and Hydrologic Conditions of the Potomac Aquifer in Virginia and Parts of Maryland and North Carolina. U.S. Geological Survey Scientific Investigations Report 2013–5116.
- Molz, F.J., R.H. Morin, A.E. Hess, J.G. Melville, and O. Güven. 1989. The Impeller Meter for Measuring Aquifer Permeability Variations: Evaluation and Comparison with Other Tests. *Water Resources Research* 25 (7): 1677–83. <https://doi.org/10.1029/WR025i007p01677>.
- Molz, F.J., G.K. Boman, S.C. Young, and W.R. Waldrop. 1994. Borehole Flowmeters: Field Application and Data Analysis. *Journal of Hydrology* 163 (3–4): 347–71. [https://doi.org/10.1016/0022-1694\(94\)90148-1](https://doi.org/10.1016/0022-1694(94)90148-1).
- Neville, C.J., and M.J. Tonkin. 2004, Modeling multiaquifer wells with MODFLOW. *Ground Water* 42 (6): 910–919. <https://doi.org/10.1111/j.1745-6584.2004.t01-9-.x>
- Newhouse, M.W., J.A. Izbicki, and G.A. Smith. 2005. Comparison of Velocity-Log Data Collected Using Impeller and Electromagnetic Flowmeters. *Ground Water* 43 (3): 434–38. <https://doi.org/10.1111/j.1745-6584.2005.0030.x>.
- Newman, J L, C. Waddell, and H.L. Sauder. 1956. A Flowmeter for Measuring Subsurface Flow Rates. *Journal of Petroleum Technology* 8 (7): 49–52.
- Pyne, R.D.G. 2006. *Groundwater Recharge and Wells: A Guide to Aquifer Storage Recovery*. 2nd ed. CRC Press, Inc.

- Rehfeldt, K.R., J.M. Boggs, and L.W. Gelhar. 1992. Field Study of Dispersion in a Heterogeneous Aquifer: 3. Geostatistical Analysis of Hydraulic Conductivity. *Water Resource Research*. 28 (12): 3309–24. <https://doi.org/10.1029/92WR01758>
- Ren, S., S. Gragg, Y. Zhang, B.J. Carr, and G. Yao. 2018. Borehole Characterization of Hydraulic Properties and Groundwater Flow in a Crystalline Fractured Aquifer of a Headwater Mountain Watershed, Laramie Range, Wyoming. *Journal of Hydrology* 561 (November 2017): 780–95. <https://doi.org/10.1016/j.jhydrol.2018.04.048>
- Ringleb, J., J. Sallwey, and C. Stefan. 2016. Assessment of Managed Aquifer Recharge through Modeling-A Review. *Water* 8 (12): 1–32. <https://doi.org/10.3390/w8120579>
- Riva, M., P. Ackerer, and A. Guadagnini. 2012. Interpretation of Flowmeter Data in Heterogeneous Layered Aquifers. *Journal of Hydrology* 452–453 (July): 76–82. <https://doi.org/10.1016/j.jhydrol.2012.05.040>
- Rumble, R.C., H.M. Buck, and B.A. Peters. 1959. A Subsurface Flowmeter for Determining Well Production or Injection Profiles. In *Third Symposium on Rock Mechanics : Papers and Discussions from the Third Symposium on Rock Mechanics Held at the Colorado School of Mines*, 115–19.
- Ruud, N.C., Z.J. Kabala, and F.J. Molz. 1999. Evaluation of Flowmeter-Head Loss Effects in the Flowmeter Test. *Journal of Hydrology* 224: 55–63. [https://doi.org/10.1016/S0022-1694\(99\)00119-5](https://doi.org/10.1016/S0022-1694(99)00119-5)
- Smith, B.S. 1999. The Potential for Saltwater Intrusion in the Potomac Aquifers of the York-James Peninsula, Virginia. U.S. Geological Survey Water-Resources Investigations Report 98-4187, 1–29.
- Trapp, H., and M.A. Horn. 1997. Ground Water Atlas of the United States: Segment 11, Delaware, Maryland, New Jersey, North Carolina, Pennsylvania, Virginia, West Virginia. U.S. Geological Survey Hydrologic Atlas 730-L.
- van Lopik, J. H., T. Sweijen, N. Hartog, and R.J. Schotting. 2021. Contribution to Head Loss by Partial Penetration and Well Completion: Implications for Dewatering and Artificial Recharge Wells. *Hydrogeology Journal* 29 (2): 875–93. <https://doi.org/10.1007/s10040-020-02228-5>.
- Xiang, J. 1995. The Evaluation of the Flowmeter Test in Three-Layer Aquifers and the Influence of Disturbed Zones. *Journal of Hydrology* 166 (1-2): 127-45. [https://doi.org/10.1016/0022-1694\(94\)02570-2](https://doi.org/10.1016/0022-1694(94)02570-2)

Young, S.C., H.K. Julian, H.S. Pearson, F.J. Molz, and G.K. Boman. 1998. Application of the Electromagnetic Borehole Flowmeter. USEPA Report. Vol. EPA/600/R-.

Zlotnik, V.A., and B.R. Zurbuchen. 2003. Estimation of Hydraulic Conductivity from Borehole Flowmeter Tests Considering Head Losses. *Journal of Hydrology* 281 (1–2): 115–28. [https://doi.org/10.1016/S0022-1694\(03\)00204-X](https://doi.org/10.1016/S0022-1694(03)00204-X).

6. Multiple Tracers to Evaluate Flow Through a Multi-Layered Aquifer Using a Novel Transport Approximation

Title

Multiple Tracers to Evaluate Flow Through a Multi-Layered Aquifer Using a Novel Transport Approximation

Abstract

Aquifer long-term replenishment (ALTR) is a water reuse sustainability strategy that recharges water via injection well to depleted aquifer systems in order to increase storage and raise the potentiometric surface over space and time. One implication of large-scale continuous recharge is a large radial impact and the need to quantify transport in radially extensive strata. The use of an artificial tracer can be cost-prohibitive as the radial front moves further from the injection well. To this end, the injectate serves as a valuable tool for characterizing distribution of flow in a multi-screen ALTR well and travel time within each receiving stratum. This work employs a novel approximation for quantifying tracer breakthrough under transient flow, dynamic flow distribution, and variable influent concentration conditions. Six constituents -- sulfate, TOC, chloride, fluoride, 1,4-dioxane and N-nitrosodimethylamine (NDMA) -- were chosen to evaluate conservative transport and semi-qualitatively assess attenuation of non-conservative constituents relative to a conservative tracer. Results indicate that sulfate acted as the most effective tracer for characterization of transport and travel times. Behavior of the remaining constituents is discussed, and qualities of an effective intrinsic tracer for future ALTR projects are identified. Moving forward, a robust monitoring plan with multiple intrinsic tracers will be an important part of ensuring the longevity of the project as well as understanding flow through large, complex aquifer systems.

6.1 Introduction

The global use of injection wells for water reuse strategies like aquifer storage and recovery (ASR) or aquifer storage transfer and recovery (ASTR) has been extensively described (Pyne 2006; Ringleb et al. 2016; Dillon et al. 2019). However, more recently, the application of injection wells has been expanded beyond the goal of short-term storage and recovery to the implementation of aquifer long-term replenishment (ALTR). ALTR involves continuous recharge of confined aquifer systems to return aquifers to pre-development conditions by increasing storage and raising the potentiometric surface over space and time. For ALTR to be successful, it requires a recharge well field with large pumping volumes (10-15 million gallons per day (MGD) [$3.78 \times 10^4 - 5.68 \times 10^4 \text{ m}^3 \text{d}^{-1}$] per site), likely over multiple sites. Injection into a confined aquifer system would be expected to involve multiple well screens and long screen lengths over multiple aquifer layers, although well design would largely depend on the site-specific hydrostratigraphy. Because ALTR would likely be implemented in a complex aquifer system, understanding flow distribution and transport through the aquifer system is of both engineering and regulatory importance.

Traditionally, tracer tests have been implemented to observe groundwater velocity, travel time, and hydrogeologic parameters in an aquifer system. Tracer selection depends on multiple considerations, and tracers are often chosen based on the native groundwater characteristics at the project site, the conservative nature of the tracer in the aquifer, detection methods, low aquifer interaction potential (i.e., the potential is low for the tracer to change the aquifer hydrogeologic properties), and the cost-effectiveness of the tracer. Davis et al. (1985) outline and discuss commonly used artificial and intrinsic tracers, including temperature, ions, dyes, dissolved gases, stable isotopes, and radionuclides.

In addition to serving as an alternative data collection strategy for flow distribution in a multi-screen well, tracer tests allow for the characterization of advective-dispersive transport and for the measurement of water quality impacts. High confidence is needed when communicating travel times to regulatory agencies and to the public about the transport of recharge water through an aquifer system during an ALTR project.

The experimental implementation of a tracer test depends on the goal. For an ALTR project, the nature of the project inherently creates conditions suitable for a forced gradient tracer test (FGTT). FGTTs have been used extensively in the past to characterize aquifer properties (Molz et al. 1988). These tests can use one well or two wells. For a single-well experiment, tracer is injected and recovered through the same well in a push-pull experiment. Work has been done at the Mobile Test Site in Alabama to interpret single well tracer tests in stratified aquifers, but these experiments use a single shallow screen well with multilevel samplers in a nearby observation well to observe and model transport (Güven et al. 1985; Molz et al. 1985). Using two wells for a tracer test, a separate injection well and pumping well operating at similar flow rates create a forced gradient where tracer is injected in one well and monitored/recovered in the other (Molz et al. 1986). An ALTR project would mimic a single-well tracer test where injectate is recharged at one well and occasional pumping occurs from the same well. Separate monitoring wells are used to measure breakthrough and aquifer characteristics.

Multi-tracer tests have also been used to characterize aquifer properties as well as flow between aquifer systems (Reimus et al. 2003; Goderniaux et al. 2010; Hillebrand et al. 2015; Hadi et al. 2016). Hadi et al. (2016) used a FGTT with rhodamine-WT, fluorescein, and sodium bromide at three separate injection wells in the Kuwait aquifer system to quantify inter- and intra-aquifer connectivity to determine aquifer characteristics and travel time. One tracer was

injected into three separate aquifers (Lower Kuwait, Upper Dammam, and Lower Dammam), and water from monitoring wells in each respective aquifer was analyzed for each of the three tracers (Hadi et al. 2016). Hillebrand et al. (2015) also employed multiple reference tracers (uranine, acesulfame, and carbamazepine) with reactive compounds to monitor mass transport and attenuation in a karst aquifer system in southwest Germany. Multiple tracers have the potential to be useful in increasing confidence in aquifer parameters and identifying potential water quality mechanisms in the aquifer system. Sanford et al. (2017) found that incorporating multiple tracer concentrations into an advective-transport model was useful to identify the existence of a dual-porosity system and constrain transport parameters. Gerenday et al. (2020) showed that the use of multiple tracers (sulfur hexafluoride and potassium bromide) was effective to assess hydrologic conditions such as porous media saturation in unconfined aquifers at managed aquifer recharge (MAR) sites where the primary method of recharge was infiltration basins supported by injection wells.

In the context of an ALTR project, artificial tracers like bromide or carbamazepine can be used as valuable means to determine aquifer characteristics, but an initial and long-term valuable tracer tool is the injectate itself. Multiple studies suggest that the water used for recharge in an ASR project is sufficient to be used for a large-scale tracer test (Williams 2000; Pavelic et al. 2006). Chloride and other intrinsic characteristics of recharge water like specific conductance have been employed as tracers on ASR projects (Mirecki et al. 1998; Pavelic et al. 2006). Provided that the recharge characteristics are significantly different from native groundwater characteristics, using recharge injectate eliminates the potential high cost associated with injecting large amounts of artificial tracer to characterize a whole site, since the recharge itself

becomes an intrinsic tracer. Using an intrinsic tracer is a more cost-effective method for large-scale recharge projects, especially with increasing injection time and distance.

One promising avenue of research is the use of multiple indicators within injectate for large-scale site characterization. In recharge wells where native groundwater characteristics vary by screen depth, identifying multiple intrinsic tracers to quantify breakthrough at all screens is important to understand transport fully. Furthermore, the use of an intrinsic tracer to quantify flow through a single multi-screen recharge well is a novel proposal, since most studies of multi-layer or multi-aquifer systems implement either multiple injection wells (Young and Benton 1990; Hadi et al. 2016), borehole dilution (West and Odling 2007), or pumping test drawdown analysis (Hunt 1986; Székely 1992; Wu et al. 2015) to characterize the aquifer system.

Multiple solutions for constituent transport have been developed to describe advective-dispersive axisymmetric transport in the case of pumping or recharge conditions (Chen 1985; Hsieh 1986; Moench 1989; Goltz and Oxley 1991; Novakowski 1992; Moench 1995; Lai et al. 2016). Of the axisymmetric analytical models that exist, most assume constant operating conditions (i.e., assume that the velocity field is not a temporal function) and constant influent concentrations. Chen et al. (2012) consider radial solute transport under variable flow and concentration conditions and provide a semi-analytical solution to evaluate the relative concentration by transforming the time domain to the cumulative flow domain within a recharge or pumping well. Chen et al.'s solution assumes a single screen well with synthetic test cases (Chen et al. 2012). There is no known approximation for variable flow and variable concentration conditions that does not involve Laplace transformation. Furthermore, the existing analytical solutions assume a single screen; in a well with multiple screens and dynamic flow

distributions that change over time, determining flow distribution through multiple screens would be computationally intensive.

This study examines flow behavior through a multi-screen well over a distance of 340 feet and a timespan of 3.5 years. Since the beginning of recharge in May 2018, operational conditions have varied at the eleven-screen recharge well and included multiple extended shutdowns, regular pumping to maintain injectivity, and one extended pumping event. The objective of this study was to use multiple tracers to characterize distribution of flow and delivery of injectate to a complex aquifer system and to evaluate travel time within each strata using a novel approximation for quantifying tracer breakthrough under transient flow, dynamic flow distribution, and variable influent concentration conditions. Furthermore, the study aims to describe attenuation of non-conservative constituents relative to a conservative tracer (e.g., sorption, biodegradation, mobile/immobile mass transfer); identify qualifying characteristics for effective tracers; and evaluate the reliability of the novel approximation. This study is unique in that it allows for comparison to a large-scale field experiment to aid in model validation.

6.2 Methods

6.2.1 Site and Project Description

In 2018 Hampton Roads Sanitation District (HRSD) initiated recharge at the Sustainable Water Initiative for Tomorrow (SWIFT) Research Center in Suffolk, Virginia. The SWIFT Project is a large-scale managed aquifer recharge project that treats effluent from HRSD's water reclamation facilities (WRFs) to drinking water standards and then recharges the Potomac Aquifer System (PAS) through injection wells located on site. The project background and location have been previously discussed by Martinez et al. (2022). As of June 2021, the SWIFT Research Center (SWIFT-RC) has one recharge well (TW-1), a depth discrete monitoring well

(MW-SAT), and three conventional wells screened in the Upper, Middle, and Lower Potomac Aquifer (MW-UPA, MW-MPA, and MW-LPA, respectively) (Figure 6-1). TW-1 has 11 discrete screens located in the UPA, MPA, and LPA (Table 6-1). MW-SAT is located 50 feet (15.2m) from TW-1 and is screened at identical depths. MW-UPA, MW-MPA, and MW-LPA are located 340 feet (104m), 390 feet (119m), and 440 feet (134m) from TW-1, respectively. The conventional wells were screened based on core samples taken during drilling and therefore do not match screen depths at TW-1 exactly, but they still reflect the most transmissive depths of the PAS (Table 6-2).

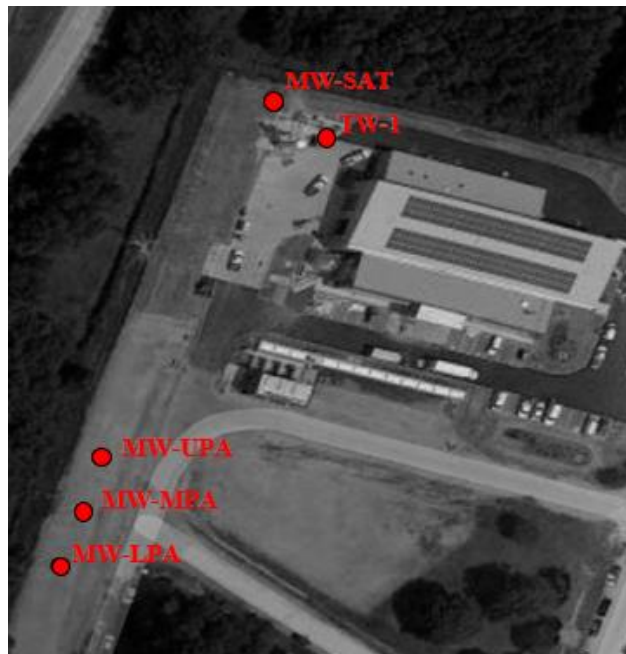


Figure 6-1. Site map of the SWIFT Research Center. TW-1 is the injection well location, MW-SAT is the depth discrete sampling system, and MW-UPA, MW-MPA, and MW-LPA are the Upper, Middle, and Lower Potomac conventional wells, respectively.

Table 6-1. Well Screen Depth and Length of Screen in TW-1 and MW-SAT.

Aquifer Zone	Starting Depth (fbg)	Ending Depth (fbg)	Length of Screen (ft)
Upper Potomac Aquifer (UPA)			
Screen 1	505	530	25
Screen 2	550	595	45
Screen 3	665	680	15
Screen 4	720	755	35
Middle Potomac Aquifer (MPA)			
Screen 5	820	835	15
Screen 6	860	890	30
Screen 7	905	920	15
Screen 8	965	990	25
Screen 9	1050	1090	40
Lower Potomac Aquifer (LPA)			
Screen 10	1230	1335	105
Screen 11	1370	1400	30
(fbg) – feet below grade			

Table 6-2. Well Screen Depth and Length of Screen in the Conventional Wells

Aquifer Zone	Starting Depth (fbg)	Ending Depth (fbg)	Length of Screen (ft)
MW-UPA (distance from TW-1 = 340')			
Screen 1	515	565	50
Screen 2	585	605	20
Screen 3	660	675	15
Screen 4	710	740	30
MW-MPA (distance from TW-1 = 390')			
Screen 1	860	920	60
Screen 2	975	990	15
Screen 3	1030	1090	60
MW-LPA (distance from TW-1 = 440')			
Screen 1	1260	1320	60
Screen 2	1350	1410	60
(fbg) – feet below grade			

The PAS is comprised up of primarily fluvial-deltaic coarse-grained sands and gravels with interbedded clays of varying thicknesses (E. Randolph et al. 2006). Because of the nature of the interbedded clays, confining units within the PAS function as local barriers but are not homogeneous and are often discontinuous across the extent of the PAS (E. Randolph et al. 2006;

Heywood and Pope 2009). For the purpose of this study, transport is local and site specific, and the Upper, Middle, and Lower Potomac (UPA, MPA, and LPA, respectively), are considered to be separate aquifers. Because of long travel times in the MPA and LPA, this study focuses on transport in the UPA only, though the discussion and conclusions will be extrapolated to the MPA and LPA. Preliminary data from MW-MPA will also be shared. A simplified figure of screen depths and hydrostratigraphy in the UPA is included in Appendix D (Figure D-1).

A key input to model and analysis is the operating conditions at the recharge well. This has been separated into nine phases, described in detail in Table 6-3. Recharge and pumping volumes for each test are listed in Table 6-4, and total duration in each operating condition per phase is provided in Table 6-5.

Table 6-3. General description of operating conditions for each phase of the SWIFT Project to date.

Phase	General Description of Operating Conditions
1	Normal operations with steady recharge and intermittent backflush. An initial ramp-up process was completed before recharge steadied at 700 gpm (1 MGD).
2	Extended backflush for removal of injectate with high nitrite concentrations.
3	Normal operations with steady recharge and intermittent backflush.
4	Well shutdown for rehabilitation due to clogging caused by the presence of iron corrosion products in injectate.
5	Post-rehabilitation extended backflush.
6	Normal operations with steady recharge and intermittent backflush. Two extended shutdowns (each ~ 1 month) occurred due to issues in the treatment process that had to be addressed before the SWIFT-RC could return to recharge
7	Well shutdown for rehabilitation to increase injectivity.
8	Post-rehabilitation extended backflush.
9	Normal operations with steady recharge and intermittent backflush.

Table 6-4. Recharge and pumping volumes during the length of the tracer test. All volumes are given in gallons. Parentheses indicate negative flow or pumping from the well.

Phase	Start Time	End Time	Length (days)	Total Recharge Volume	Total Pumping Volume	Net Recharge Volume
1	05/15/18 14:15	08/02/18 17:00	79.11	41,211,468	(1,179,749)	40,031,719
2	08/02/18 17:00	08/21/18 14:45	18.91	-	(26,445,142)	(26,445,142)
3	08/21/18 14:45	11/21/18 01:15	91.44	58,811,894	(1,040,690)	57,771,204
4	11/21/18 01:15	04/26/19 08:00	156.28	108,184	(756,285)	(648,101)
5	04/26/19 08:00	04/29/19 07:00	2.96	5,261	(4,511,581)	(4,506,320)
6	04/29/19 07:00	12/25/20 17:15	606.43	326,362,036	(33,715,618)	292,646,418
7	12/25/20 17:15	04/09/21 13:15	104.83	580,969	-	580,969
8	04/09/21 13:15	04/14/21 12:00	4.95	151,890	(6,596,367)	(6,444,477)
9	04/14/21 12:00	11/02/21 02:15	201.59	101,314,633	(14,112,802)	87,201,832

Table 6-5. Time split during each phase of the bromide tracer test. All units are in days.

Phase	Start Time	End Time	Total Length	Recharge	Shutdown	Pumping
1	05/15/18 14:15	08/02/18 17:00	79.11	54.06	24.34	0.71
2	08/02/18 17:00	08/21/18 14:45	18.91	-	2.01	16.90
3	08/21/18 14:45	11/21/18 01:15	91.44	58.79	31.98	0.67
4	11/21/18 01:15	04/26/19 08:00	156.28	0.17	155.59	0.52
5	04/26/19 08:00	04/29/19 07:00	2.96	0.01	0.07	2.87
6	04/29/19 07:00	12/25/20 17:15	606.43	338.79	246.91	20.56
7	12/25/20 17:15	04/09/21 13:15	104.83	0.77	104.06	-
8	04/09/21 13:15	04/14/21 12:00	4.95	0.18	0.89	3.86
9	04/14/21 12:00	11/02/21 02:15	201.59	133.19	60.22	8.04

6.2.2 Tracer Selection

Breakthrough at MW-SAT was identified using SWIFT Water as an intrinsic tracer (Bullard et al. 2019). Specific conductivity was used as an indicator of chloride in SWIFT Water due to the ability to measure at high frequencies and the availability of a cost-effective handheld conductivity probe. While specific conductivity served as an acceptable indicator at MW-SAT, the use of multiple tracers was suggested for MW-UPA due to the high variation in native groundwater characteristics between Screens 1-4. Specific conductivity at MW-UPA was not significantly different than SWIFT Water specific conductivity ($1247 \pm 184 \mu\text{S}/\text{cm}$). Though

conductivity may not be an acceptable indicator at MW-UPA, it will likely indicate preliminary breakthrough at MW-MPA and MW-LPA.

Consequently, a review of the sampled constituents was undertaken to identify other potential conservative or semi-conservative tracers. Of 88 potential constituents monitored by the Central Environmental Lab (CEL) at HRSD, candidates were narrowed by sample frequency, detection of the constituent above the detection limit in either SWIFT Water or the conventional well, and the nature of the constituent. Chloride, fluoride, sulfate, 1,4-dioxane, N-nitrosodimethylamine (NDMA), and TOC were identified as potential constituents of interest. Chloride, fluoride, and sulfate were chosen because of their potential to act as conservative tracers. Previous work on soil columns at this site indicated that TOC degrades during transport and 1,4-dioxane and NDMA may degrade during transport (Dziura 2020), providing an opportunity to compare a conservative transport model to observations at MW-UPA and semi-quantitatively assess the nature of the constituents within the aquifer system. Background concentrations of the chosen constituents at MW-SAT (Screens 1-11) and the conventional wells are listed in Table 6-6.

Table 6-6. Pre-recharge native groundwater concentrations of identified constituents of interest. Individual screens in MW-SAT are noted with S-[screen number] (e.g., MW-SAT S 1 for Screen 1). 1,4-Dioxane and NDMA are not included because both were below detection (0.06 µg/L and 2 ng/L, respectively) in every screen in MW-SAT and the conventional wells. For the detected constituents, one standard deviation is listed in parentheses. Measured TOC in MW-SAT is likely higher than actual native groundwater concentrations due to interference during installation.

Location	Constituents of Interest				
	Conductivity (µS/cm)	Chloride (mg/L)	Fluoride (mg/L)	Sulfate (mg/L)	TOC (mg/L)
MW-SAT S-1	1,463 (± 6)	162 (± 5)	4.40 (± 0.2)	23 (± 1)	1.09 (± 0.03)
MW-SAT S-2	3,696 (± 137)	1,450 (± 161)	2.76 (± 0.2)	89 (± 15)	1.08 (± 0.16)
MW-SAT S-3	7,690 (± 101)	2,030 (± 89)	1.74 (± 0.1)	122 (± 11)	1.05 (± 0.21)
MW-SAT S-4	7,790 (± 106)	1,900 (± 446)	1.52 (± 0.2)	129 (± 10)	1.05 (± 0.13)
MW-SAT S-5	9,873 (± 94)	3,716 (± 90)	ND*	235 (± 13)	0.99 (± 0.33)
MW-SAT S-6	12,548 (± 73)	3,227 (± 993)	ND*	203 (± 13)	1.16 (± 0.38)
MW-SAT S-7	12,088 (± 148)	3,593 (± 39)	ND*	154 (± 23)	4.88 (± 0.38)
MW-SAT S-8	5,806 (± 190)	2,070 (± 131)	ND*	149 (± 29)	1.63 (± 0.26)
MW-SAT S-9	5,768 (± 44)	1,947 (± 154)	ND*	93 (± 12)	2.30 (± 0.11)
MW-SAT S-10	13,551 (± 44)	3,800 (± 649)	ND*	248 (± 14)	2.76 (± 1.03)
MW-SAT S-11	16,763 (± 104)	5,290 (± 155)	0.43 (± 0.1)	279 (± 45)	5.02 (± 1.05)
MW-UPA	1,133 (± 223)	117 (± 2)	4.07 (± 0.04)	23 (± 0.3)	0.31 (± 0.04)
MW-MPA	4,743 (± 210)	1,133 (± 31)	0.67 (± 0.03)	92 (± 4)	ND [†]
MW-LPA	13,623 (± 1,669)	4,313 (± 255)	ND*	226 (± 13)	0.20 (± 0.01)

* Detection Limit = 0.50 mg/L
[†] Detection Limit = 0.20 mg/L

6.2.3. Tracer Monitoring

Fluoride, sulfate, and chloride samples were collected and analyzed for SWIFT Water and at MW-UPA using EPA Method 300.0. SWIFT Water samples for these three constituents were collected approximately once per day when the SWIFT-RC was recharging water to the PAS. Because fluoride was the originally selected constituent to monitor breakthrough based on its behavior at MW-SAT, samples were taken at MW-UPA daily. Sulfate and chloride samples were taken approximately once per week, though frequency did vary over time and with recharge status at TW-1. Because of cost-effectiveness of sampling, fluoride, sulfate, and chloride were the most frequently sampled constituents in this analysis. 1,4-Dioxane samples were collected and analyzed using EPA Method 522. NDMA samples were collected and analyzed using EPA

Method 521. QC samples were used to evaluate the quality of data according to each analyzation method. TOC data were collected and analyzed using Standard Methods 5310B. Exact numbers for the datapoints included in the breakthrough model are included in Table 6-7.

Table 6-7. Number of SWIFT Water influent and MW-UPA samples included in the breakthrough model.

Constituent	SWIFT Water Influent	MW-UPA
Sulfate	455	264
TOC	357	128
Chloride	456	147
Fluoride	594	874
1,4-Dioxane	97	71
NDMA	101	71

6.2.4. Radial Breakthrough Model Development

Operations at the SWIFT-RC are transient and include periods of recharge, backflush, and shutdown (no flow at the well). If operations were consistent with only short periods of pumping and no flow, the assumption that flow is constant would be relatively accurate, and the following equation could be used to describe the relative concentration, $C_i(r, t)$, during radial flow at each screened interval (modified from Charbeneau 2000):

$$C_s(r, t) = C_{B,s} + \frac{C_F}{2} * \operatorname{erfc} \left[\frac{r - R_s}{\sqrt{\frac{4}{3} \alpha_{L,s} R_s}} \right] \quad (1)$$

$$R_s(t) = \sqrt{\frac{Q_s t}{\pi n_s b_s}} \quad (2)$$

where $C_{B,s}$ is the background concentration within the screen of interest, C_F is the influent concentration, r is the radial distance from the injection well, t is the time since the start of

injection, $\alpha_{L,s}$ is the screen-specific longitudinal dispersivity, R_s is the mean displacement of the front, Q_s is the recharge flow rate to the individual well screen (which varies based on changes in flow distribution), n is the screen-specific effective porosity, and b is the thickness of the screen of interest. This model was used initially to describe transport assuming only minor stoppages and pumping events (Bullard et al. 2019). An approximation based on Equations 1 and 2 was developed to account for transient conditions where the mean displacement of the front is calculated using the method described in Bullard et al. 2019:

$$R_{s,i}^*(t) = \sqrt{\frac{V_{s,i}^*(t)}{\pi n_i b_i}} \quad (3)$$

where $V_{s,i}^*(t) = [Q_{s,i}(t_i - t_{i-1})] + V_{s,i-1}^*(t)$ and t_i is the actual time. Sign conventions for Q are positive during recharge and negative during pumping. To calculate the concentration measured at the monitoring well at a given time, $C_{s,i}(r, t)$, during transient flow conditions, Equation 1 can be adapted to produce:

$$C_{s,i}(r, t) = C_{B,s} + \frac{C_F}{2} * \operatorname{erfc} \left[\frac{r - R_{s,i}^*}{\sqrt{\frac{4}{3} \alpha_{L,s} R_{s,i}^*}} \right] \quad (4)$$

While the approximate model developed by Bullard et al. (2019) is a promising step forward in accounting for transient flow conditions, it assumes that the influent concentration at TW-1 is constant. Influent concentrations of SWIFT Water at TW-1 can vary significantly, and assuming a constant influent concentration is unlikely to account for variation in monitoring well samples (Figure 6-2). Because influent variability played a part in model effectiveness, more detail is provided regarding the variability of influent characteristics in Table 6-8.

Sulfate was consistently measured in SWIFT Water and was significantly different (> 3 standard deviations) from background concentrations of sulfate in MW-UPA. TOC has the most predictably variable influent concentration due to the use of granular activated carbon (GAC) during advanced treatment. Fresh GAC had high rates of TOC removal during the treatment process, but as the carbon was exhausted, TOC concentrations increased over time. During the 2018-2019 well rehabilitation process, which also included a treatment process shut down, the carbon in the two GAC contactors was replaced, and TOC concentrations dropped and increased again as treatment restarted. Once TOC concentrations reached 4 mg/L, flow was split between two carbon contactors to maintain a TOC concentration between 3.5 and 4.0 mg/L.

The average chloride concentration used for Model 2 was 202.86 mg/L. Influent chloride data showed an initial period (day 0 to 110) with an average concentration of 226 mg/L, followed by a second period (day 110 to 203) with average influent chloride concentration measuring 168.5 mg/L. Chloride concentrations after the well rehabilitation was an average of 206.6 mg/L with a standard deviation of 55.3 mg/L. Fluoride was measured daily at the SWIFT-RC, and concentrations were consistent and non-variable. Concentrations were significantly different from fluoride concentrations in MW-SAT Screens 1 through 4 and MW-UPA. 1,4-Dioxane and NDMA were measured at lower frequencies than the previous four constituents due to the cost of analysis.

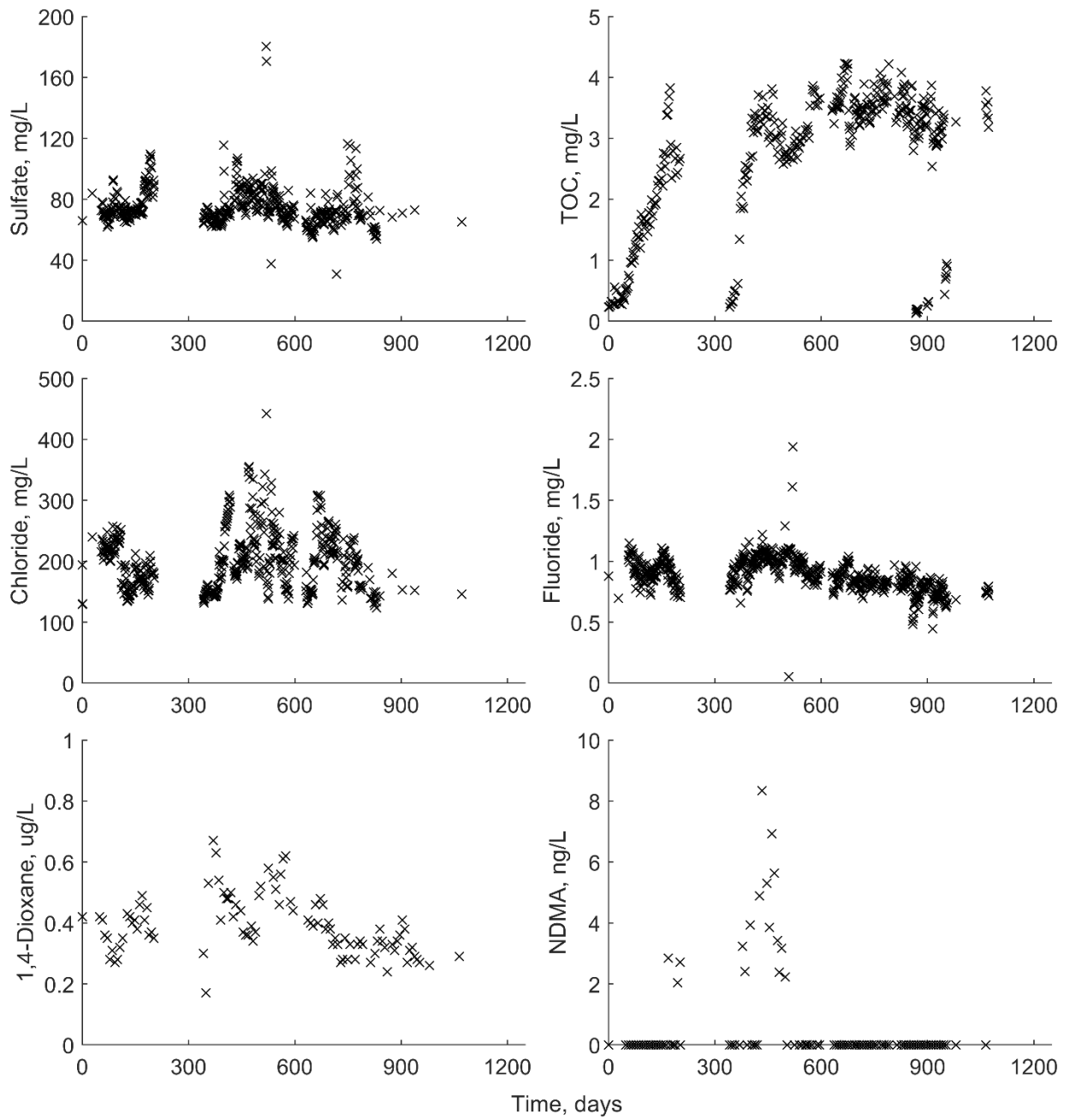


Figure 6-2. SWIFT Water concentrations of the constituents of interest.

Table 6-8. SWIFT Water characteristics for tracer constituents.

Constituent	Number of Measurements	Number of Detections	Average Value	Standard Deviation	Minimum Value	Maximum Value
Sulfate	455	455	75.23	12.89	30.80	180.30
TOC	357	357	2.73	1.12	0.13	4.23
Chloride	456	456	202.86	50.38	123.64	545.47
Fluoride	594	594	0.89	0.14	0.05	1.94
1,4-Dioxane*	97	97	0.39	0.10	0.17	0.67
NDMA [#]	101	16	3.96	1.76	0.00 [†]	8.34

* Concentration values are measured in µg/L
[#] Concentration values are measured in ng/L
[†] Indicates non-detect

To account for changing influent concentrations, Equation 4 can be modified to calculate each measured influent concentration:

$$\begin{aligned}
 t_i < t_j \quad & C_{s,i,j}(r,t) = 0 \\
 & R_{s,i}^*(t) = 0 \\
 & V_{s,i}^*(t) = 0
 \end{aligned} \tag{5}$$

$$\begin{aligned}
 t_i \geq t_j \quad & C_{s,i,j}(r,t) = \frac{\Delta C_F}{2} * \operatorname{erfc} \left[\frac{r - R_{s,i}^*}{\sqrt{\frac{4}{3} \alpha_{L,s} R_{s,i}^*}} \right] \\
 & R_{s,i}^*(t) = \sqrt{\frac{V_{s,i}^*(t)}{\pi n_s b_s}}
 \end{aligned} \tag{6}$$

$$V_{s,i}^*(t) = [Q_{s,i}(t_i - t_{i-1})] + V_{s,i-1}^*(t)$$

where t_i is the actual time, t_j is the time that the influent concentration was measured, and $\Delta C_F = C_{F,i} - C_{F,i-1}$ where j denotes a measured influent concentration at t_j . For the first iteration ($j = 1$), $\Delta C_F = C_{F,i} - C_B$, where C_B is the background concentration measured prior to

the start of recharge. At any time, t_i , the concentration at a monitoring well screen would be given as:

$$C_{s,i}(r,t) = C_B + \sum_{j=1}^j C_{s,i,j}(r,t) \quad (7)$$

For a well with multiple screens, the total concentration could be calculated using a length- or flow-weighted average of $C_{s,i}(r,t)$ for the relevant screens. Previous results at the SWIFT-RC reveal that flow distribution within the recharge well is dynamic. Flow of SWIFT Water to the aquifer was quantified with a Rosemount 8750W Magnetic Flowmeter System immediately prior to entering TW-1. Because the recharge rate entering each screen (Q_i) is calculated based on a percentage of the total flow measured entering the recharge well, analysis is required to (a) determine the flow distribution to each screen and (b) determine the variation in flow distribution over time.

Following the observation of breakthrough at MW-UPA, model development began with an assessment of sample bias at the conventional monitoring well. Obtaining representative water quality samples can be a challenge; sampling bias in wells with long screens is well documented in the literature (Reilly et al. 1989; Konikow and Hornberger 2006; Poulsen et al. 2019), and because the conventional monitoring wells lack depth-discrete sampling mechanisms, the initial step required is evaluating where samples originate based on observed breakthrough. Furthermore, low flow rates from the sampling pumps at the conventional wells (2 gallons per minute (7.6 L/min)) are likely to introduce bias in a well with multiple deep screens.

Because sulfate was the most reliable of the six tracers (i.e., low influent variability, high number of samples, and had a clear breakthrough), it was used to determine where samples were

collected at MW-UPA. First, a transport model for sulfate was calculated for each individual screen based on Equations 5-7. These models assume that the UPA is solely measuring from the screen of interest (only using the screen length and aquifer characteristics (n and α) from that screen, as determined from as-built diagrams and the original breakthrough work done in 2018).

Next, length- and flow-weighted averages were calculated using the transport models developed for each screen. Two separate flow-weighted averages were calculated, one based on pre-rehabilitation flow measured during initial conductivity breakthrough (Bullard et al. 2019), the other based on post-rehabilitation flow distribution measured during in-situ flowmeter testing in May 2019 (Chapter 5). Details regarding pre- and post-rehab flow distribution are documented in Table 6-9. Length and flow weighted distributions were applied using all screens and using Screens 1 and 2 only, since it was suspected that the upper screens were contributing more. Using Screens 1 and 2 proved to be the most effective in all cases. Further detail and full comparisons are included in Appendix D.

Table 6-9. Pre- and post-rehab flow distributions and aquifer characteristics for MW-UPA.

	Pre-Rehab Flow Distribution* (Conductivity Breakthrough)	Post Rehab Flow Distribution** (In-Situ Flowmeter)	Porosity	Longitudinal Dispersivity (ft)
Screen 1	18%	19%	0.20	5
Screen 2	24%	46%	0.25	10
Screen 3	6%	2%	0.27	10
Screen 4	9%	7%	0.35	20

* Chapter 4
** Chapter 5

6.3 Results

Four separate conditions are compared in this analysis: (1) constant concentration and constant flow, as derived by Charbeneau in Equation 1; (2) constant concentration, transient

flow, and variable flow distribution, as derived by Bullard et al. (2019) in Equation 3 and 4; (3) variable concentration, transient flow, and constant flow distribution as derived in Equations 5-7; and (4) variable concentration, transient flow, and variable flow distribution.

Condition (3) assumed that flow distribution is constant based on the pre-rehab value measured during initial conductivity breakthrough (Bullard et al. 2019). For comparison, variable flow distribution was used in Conditions (2) and (4) because flow distribution has been shown to be dynamic at the SWIFT-RC site. Two flow distributions were used, one based on the aforementioned pre-rehabilitation flow and the other based on post-rehabilitation flow distribution measured during in-situ flowmeter testing in May 2019. Conditions (2) and (4) assumed that flow distribution before $t = 344$ days (right before the restart of recharge after rehabilitation) is equal to the pre-rehab flow distribution. From $t = 344$ days until $t = 445$ days, flow distribution is equal to the post-rehab flow distribution. After 445 days, it was assumed that flow distribution returns to the original pre-rehab flow distribution. Additional discussion of the process for determining the switch-back time is available in Appendix D.

Model 1, while previously used at the SWIFT-RC to describe breakthrough, failed as a model on a larger spatial and time scale. The assumption that flow and concentration are constant was flawed based on the reality of operations at an ALTR site. Model 2 was similar to Models 3 and 4 with regard to predicting initial breakthrough, but because it assumed a constant influent concentration, it was unable to account for variations in concentration following initial breakthrough at MW-UPA. Model 4 provided the best fit for sulfate, which was determined to be the tracer that best described travel time and chemical transport (Figure 6-3). Coefficients of determination for Model 4 are included in Figure 6-4 and support sulfate as the most effective tracer. Model 2 and Model 4 (which account for dynamic flow distribution) were both able to

capture the peak of breakthrough after the shutdown since the flow distribution increased in the UPA following well rehabilitation. Model 4 also established the breakthrough time for TOC accurately but failed to account for decay within the aquifer system during transport. Model 2 originally seemed to be a fit for chloride transport while Model 4 fell short in predicting the original breakthrough. Fluoride concentrations in the UPA remained at background levels long after observed breakthrough at MW-UPA. Models 3 and 4 generally captured 1,4-dioxane concentrations following breakthrough. Concentrations of 1,4-dioxane and NDMA were not measured until breakthrough was already identified, and therefore the initial breakthrough is not supported by observed measurements at the recharge well.

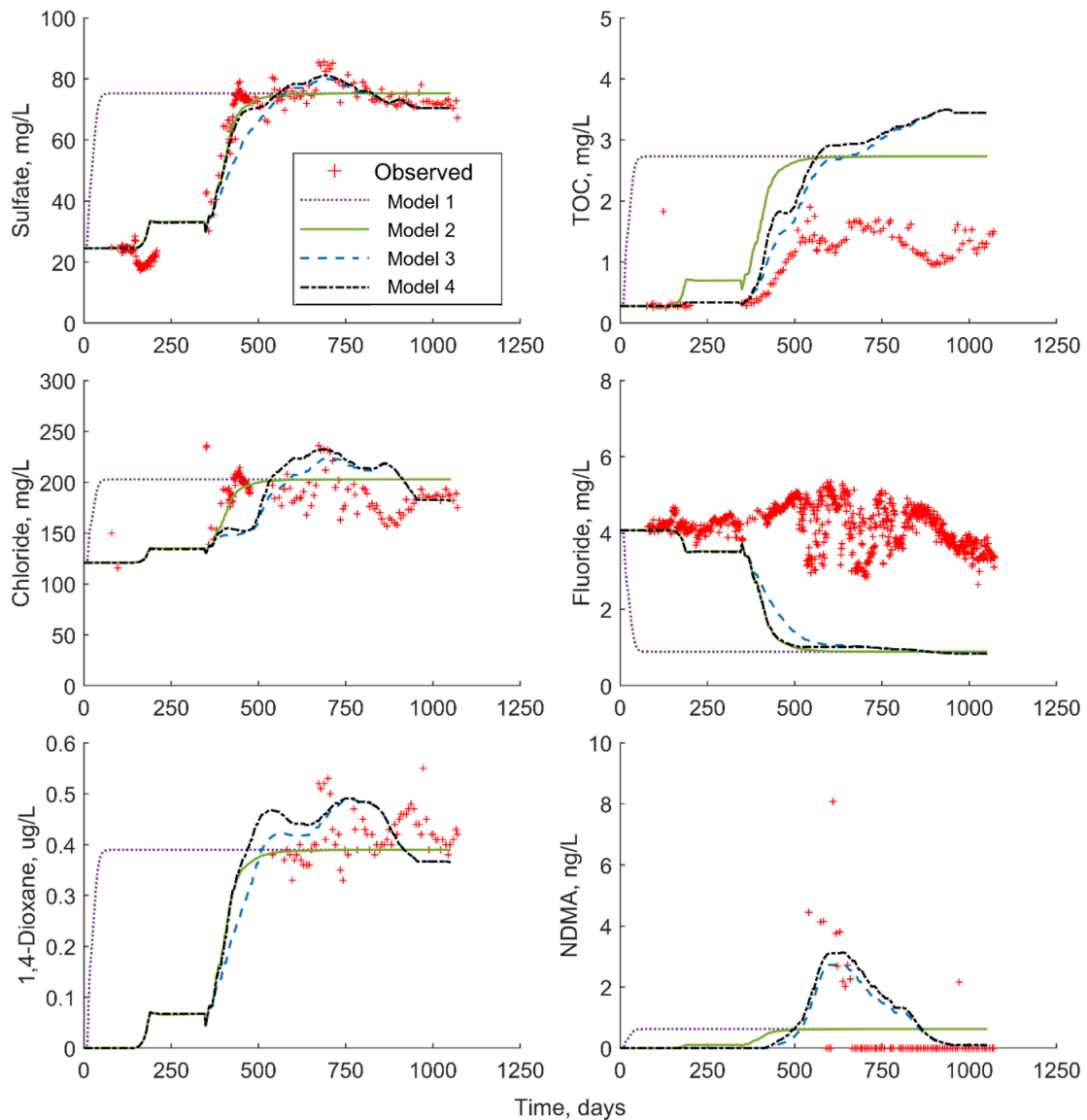


Figure 6-3. Modeled constituent concentrations. Four models are compared: (1) Model 1, which assumes a constant flow and constant concentration; (2) Model 2, which assumes a constant influent concentration but transient flow and variable flow distribution; (3) Model 3, which varies influent concentration and transient flow but maintains a constant flow distribution; and (4) Model 4, which varies influent concentration and flow distribution with time and accounts for transient flow.

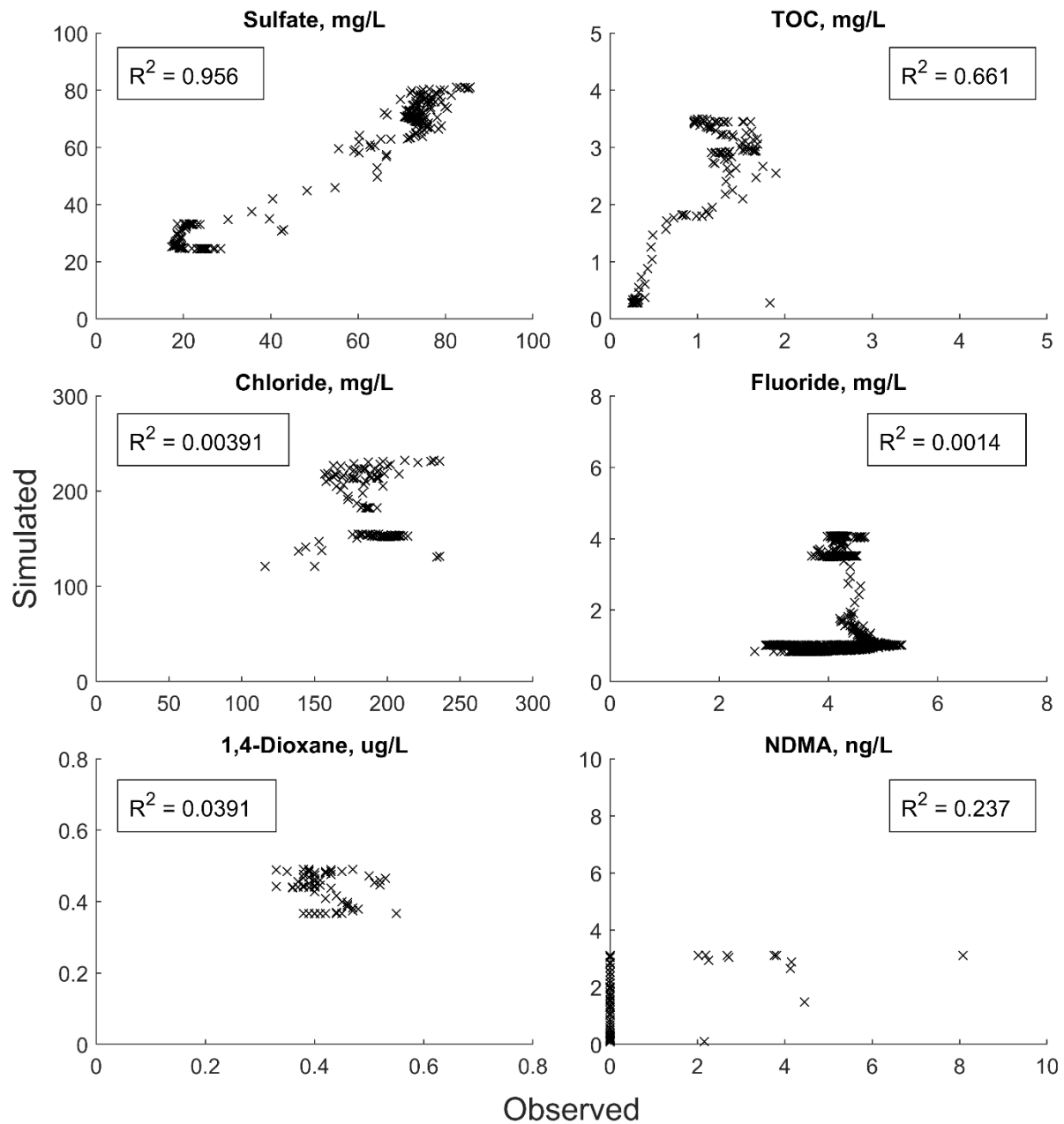


Figure 6-4. Coefficient of determination for each constituent under Condition (4) – variable concentration, variable flow, and variable flow distribution conditions.

6.4 Discussion

The effectiveness of each of the potential tracers sits along a range, from very effective to completely ineffective at characterizing delivery of injectate to the UPA and evaluating travel time. Each constituent will be discussed in the following subsections.

6.4.1. Sulfate

Sulfate was the most effective tracer with regard to capturing breakthrough and travel time. Multiple factors contribute to the efficacy of sulfate as a tracer in MW-UPA: (1) average sulfate concentrations in SWIFT Water are significantly different (> 3 standard deviations) than native groundwater concentrations, which allows for a clean breakthrough of SWIFT Water sulfate concentrations; (2) with a few exceptions, influent sulfate concentrations have low variability; and (3) high frequency of sulfate sampling allowed for more precise characterization of influent sulfate concentrations and therefore increased the accuracy of the model.

6.4.2. TOC

The existing approximation was able to capture TOC breakthrough at the appropriate time and with behavior expected related to the changes in influent concentration; however, the model did not account for decay of the constituent during transport. Departure from the conservative model was expected since TOC is a non-conservative constituent. The observed TOC concentrations reveal degradation but not sorption of the constituent within the system, which is common in direct injection conditions where the organic fraction of the soil is low (Patterson et al. 2011). Future work will aim to modify the approximation to include other mechanisms including degradation, retardation, and other aquifer interaction mechanisms.

6.4.3. Chloride

Chloride, while unable to capture initial breakthrough, was still shown to be somewhat effective in describing post-breakthrough conditions and travel time. Similar to what was observed at Screen 1 during initial breakthrough at MW-SAT, chloride concentrations were higher than expected based on SWIFT Water concentrations (Figure 6-5). Before the start of recharge, the PAS was conditioned with aluminum chlorohydrate (ACH) to stabilize the

interstitial clays within the aquifer and maintain aquifer permeability once recharge began. Failure to pretreat the aquifer will result in the loss of injectivity (Brown and Silvey 1977). It is likely that the higher chloride concentrations than expected in the initial breakthrough are a result of the remnants of this ACH treatment that was not fully recovered from Screen 1.

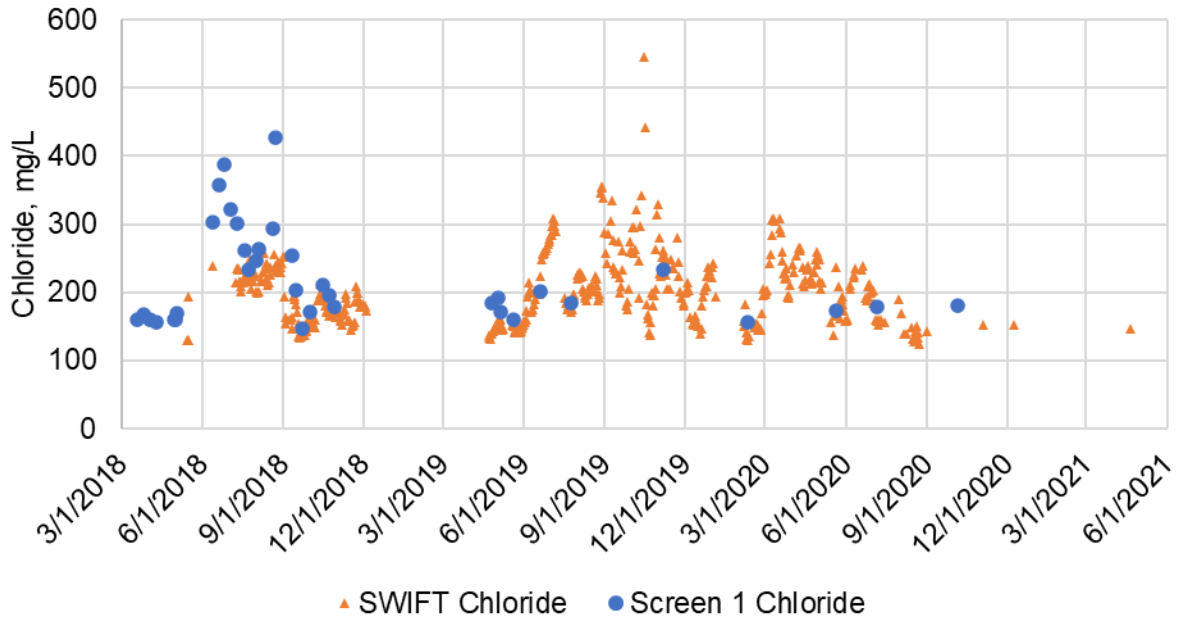
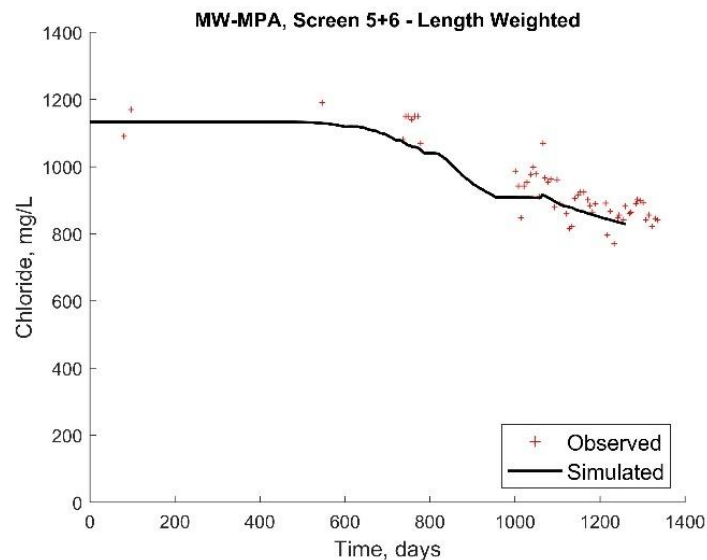


Figure 6-5. Chloride concentrations in SWIFT Water and MW-SAT Screen 1. In the initial breakthrough period (June 2018), observed concentrations at Screen 1 were higher than influent SWIFT Water concentrations.

The significant range of chloride concentrations as well as their closeness to native groundwater concentrations (within two standard deviations) is also a factor contributing to the lower effectiveness of the model after breakthrough was observed. In addition to the ACH, the two-phase concentration data before the shutdown for well rehabilitation could have also played a role in decreasing the efficacy of Models 3 and 4. The second period of concentration that was lower than average retarded the model and led to an inaccurate estimation of breakthrough.

Because background chloride concentration in the UPA (117 mg/L) was already close to SWIFT chloride, Model 4 was not a good fit.

Since increased chloride concentrations indicating remaining aluminum chlorohydrate were not observed in any other screens during the initial breakthrough and because native groundwater chloride concentrations are significantly higher in in MW-MPA and MW-LPA, chloride is expected to be a more reliable tracer for the remaining conventional monitoring wells. Preliminary chloride data from MW-MPA shows breakthrough of chloride that is also predicted by applying the existing model to a different aquifer layer (Figure 6-6). Breakthrough at MW-LPA has not yet been observed at the SWIFT-RC.



**Figure 6-6. Preliminary chloride breakthrough at MW-MPA.
This breakthrough is based on Model 4.**

6.4.4. Fluoride

While fluoride was initially expected to be a reliable and conservative tracer, observed concentrations at MW-UPA as well as previously observed breakthrough concentrations at MW-

SAT (Screen 1) indicate aquifer interaction that resulted in fluoride mobilization (Bullard et al. 2019). Fluoride mobilization during MAR projects has been attributed to multiple causes, including mineral dissolution (Gaus et al. 2002; Schafer et al. 2018) and interaction with low permeability sediments within the aquifer system (Gaus et al. 2002; Malcuit et al. 2014). Schafer et al. (2018) hypothesized that fluoride release during MAR experiments was a result of the dissolution of carbonate-rich fluorapatite due to the injection of injectate with low ionic strength. In another ASR project, dual porosity mixing of recharge and native groundwater before recovery and slow dissolution of fluorite both contributed to elevated fluoride concentrations in recovered injectate (Gaus et al. 2002). Malcuit et al. (2014) observed fluoride concentrations from low permeability units contributing to elevated fluoride concentrations in a single-screened, multi-layer aquifer around the city of Bordeaux, France.

Elevated fluoride concentrations have been observed in the UPA (Figure 6-7) and in the groundwater of the City of Suffolk (E.R. McFarland 2010). At the SWIFT-RC, the highest concentrations are located at screens 1 and 2, from 500 to 700 feet (152 to 215 meters) below land surface, which is consistent with previous observations across the Virginia Coastal Plain Aquifer System. Since the UPA is a fluvial-deltaic sediment system, it lacks the fluorapatite and other phosphatic material common in marine systems, which are a common contributor to fluoride mobilization. McFarland (2010) hypothesizes that the high fluoride belt located in the UPA is a result of high-fluoride groundwater flowing from the overlying marine sediments into the PAS and adsorbing to oxyhydroxides within the PAS sediments. As sea level rises, the location of the saltwater transition zone shifts and causes fluoride to desorb due to adsorption of other anions in the saltwater zone, leading to elevated concentrations within the saltwater transition zone at the observed locations in Figure 6-7 (McFarland 2010).

Though SWIFT Water fluoride concentrations are low, fluoride continues to show elevated values at MW-UPA, even following observed breakthrough based on other constituents. We hypothesize this is due to the continued desorption of fluoride from oxyhydroxides in the UPA due to increasing pH as SWIFT Water is transported through the aquifer (LaFayette et al. 2020). Because the mass of fluoride in the UPA is not increasing with time other than with the addition of SWIFT Water, we expect that once the fluoride in the native groundwater is desorbed, fluoride concentrations will decrease to SWIFT Water levels. Because of this, fluoride is not a reliable tracer for this project but may be a reliable tracer for other ALTR projects, depending on the local hydrogeochemistry and the difference between native fluoride and pH and recharge fluoride and pH.

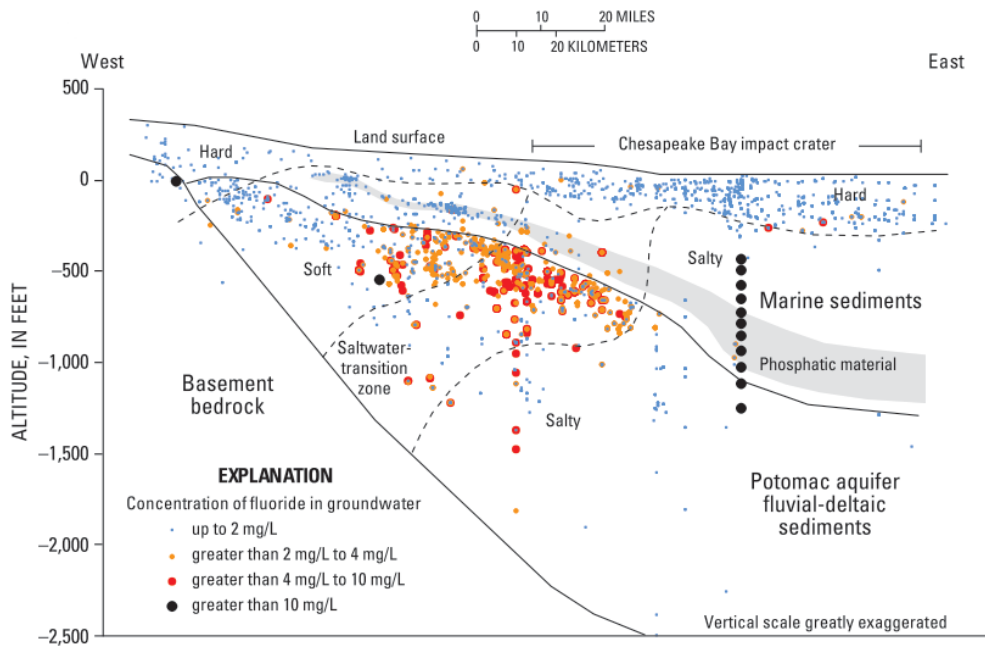


Figure 6-7. Generalized fluoride distribution in the Virginia Coastal Plain (McFarland 2010).

6.4.5. 1,4-Dioxane and NDMA

The efficacy of 1,4-dioxane and NDMA as tracers was limited by the frequency of influent sampling as well as the number of detections. Because only 16% of NDMA samples were above the 2ng/L detection limit, it is probable that the remaining 84% of non-detects ranged from 0-2 ng/L and that tracer mass was not accounted for in the model. Because of cost-effectiveness, sample frequency was lower for 1,4-dioxane and NDMA, and spikes or large variations in influent concentrations may not have been detected in the limited number of samples available. While previous work suggested that 1,4-dioxane and NDMA may degrade during transport (Dziura 2020), results from MW-UPA indicate that the two constituents are mostly conservative. This suggests that microbes that biodegrade these constituents may need a longer acclimation time with more consistent concentrations, and colonies large enough to degrade the constituents may not exist within the aquifer at the current time. Other studies have also indicated the need for a long acclimation period before degradation is observed (Drewes et al. 2006; Nalinakumari et al. 2010; Suzuki et al. 2015; Trussell et al. 2018).

6.5 Conclusions

The application of multiple intrinsic tracers to determine breakthrough in a multi-aquifer system at the SWIFT-RC demonstrates the significance of both a robust sampling plan and depth-discrete samples in a nearby multi-screen well for aquifer characterization. Comparing multiple tracers also aided in identifying tracer weaknesses and confirmed travel time to MW-UPA. For an intrinsic tracer, multiple factors contribute to the effectiveness of a constituent, including magnitude of difference between the tracer and native groundwater, variability of tracer concentrations, high frequency of influent sampling, and hydrogeochemical interaction potential.

The use of multiple tracers can confirm travel time with higher confidence, provide insight into aquifer interaction, and guide monitoring decisions while scaling up ALTR projects. In a multi-aquifer system like the PAS, tracer efficacy may vary by aquifer layer, and several background samples are beneficial to fully characterize the native groundwater before recharge begins. Furthermore, the use of a novel approximation that accounts for variable flow conditions, time-varying flow distribution, and variable influent concentration improved the fit of the sulfate transport model. Future model developments should address attenuation, which was not included in this initial model, though attenuation was observed in the TOC observational data. Existing radial models that include first-order decay do not account for transient conditions in influent concentration and flow. In future ALTR projects, where the use of an artificial tracer can be cost-prohibitive the further from the injection well being monitored, identification and monitoring of multiple, reliable intrinsic tracers will be an important part of ensuring the longevity of the project as well as understanding flow through large, complex aquifer systems.

Acknowledgments

The authors would like to thank members of the SWIFT Research Center team and the CEL team for collection and analysis of samples. This work was supported by HRSD and the Charles E. Via, Jr. Department of Civil and Environmental Engineering at Virginia Tech.

Supplemental Information

Additional information can be found in Appendix D.

References

- Brown, D.L., and W.D. Silvey. 1977. "Artificial Recharge to a Freshwater-Sensitive Brackish-Water Sand Aquifer, Norfolk, Virginia." U.S. Geological Survey Professional Paper 939. doi:10.3133/pp939
- Bullard, M.G., M. Widdowson, G. Salazar-Benites, J. Heisig-Mitchell, A. Nelson, and C. Bott. 2019. "Managed Aquifer Recharge: Transport and Attenuation in a Coastal Plain Aquifer." In *Proceedings of the EWRI World Environmental and Water Resources Congress 2019: Groundwater, Sustainability, Hydro-Climates/Climate Change, and Environmental Engineering*, 1–14. Pittsburgh: EWRI. doi:https://doi.org/10.1061/9780784482346.011
- Charbeneau, R.J. 2000. *Groundwater Hydraulics and Pollutant Transport*. Upper Saddle River, NJ: Prentice Hall.
- Chen, C.-S. 1985. "Analytical and Approximate Solutions to Radial Dispersion from an Injection Well to a Geological Unit With Simultaneous Diffusion Into Adjacent Strata." *Water Resources Research* 21 (8): 1069–76. doi:10.1029/WR021i008p01069.
- Chen, Y., C. Lu, and J. Luo. 2012. "Solute Transport in Divergent Radial Flow with Multistep Pumping." *Water Resources Research* 48 (2): 1–10. doi:10.1029/2011WR010692.
- Davis, S.N., D.J. Campbell, H.W. Bentley, and T.J. Flynn. 1985. "An Introduction to Ground-Water Tracers." Tuscon: EPA.
- Dillon, P., P. Stuyfzand, T. Grischek, M. Lluria, R.D.G. Pyne, R.C. Jain, J. Bear, et al. 2019. "Sixty Years of Global Progress in Managed Aquifer Recharge." *Hydrogeology Journal* 27: 1–30. doi:10.1007/s10040-018-1841-z.
- Drewes, J.E., C. Hoppe, and T. Jennings. 2006. "Fate and Transport of N -Nitrosamines Under Conditions Simulating Full-Scale Groundwater Recharge Operations." *Water Environment Research* 78 (13): 2466–73. doi:10.2175/106143006X115408.
- Dziura, T. 2020. "Evaluation of Contaminant Removal Through Soil Aquifer Treatment by a Lab Scale Soil Column Experiment Including a Trace Contaminant Spike Test." M.S. Thesis, Via Department of Civil and Environmental Engineering, Virginia Tech.
- Gaus, I., P. Shand, I.N. Gale, A.T. Williams, and J.C. Eastwood. 2002. "Geochemical Modelling of Fluoride Concentration Changes during Aquifer Storage and Recovery (ASR) in the Chalk Aquifer in Wessex, England." *Quarterly Journal of Engineering Geology and Hydrogeology* 35 (2): 203–8. doi:10.1144/1470-9236/2001-52.

- Gerenday, S.P., J.F. Clark, J. Hansen, I. Fischer, and J. Koreny. 2020. "Sulfur Hexafluoride and Potassium Bromide as Groundwater Tracers for Managed Aquifer Recharge." *Groundwater* 58 (5): 777–87. doi:10.1111/gwat.12983.
- Goderniaux, P., S. Brouyère, A. Gutierrez, and N. Baran. 2010. "Multi-Tracer Tests to Evaluate the Hydraulic Setting of a Complex Aquifer System (Brévilles Spring Catchment, France)." *Hydrogeology Journal* 18 (7): 1729–40. doi:10.1007/s10040-010-0633-x.
- Goltz, M.N., and M.E. Oxley. 1991. "Analytical Modeling of Aquifer Decontamination by Pumping When Transport Is Affected by Rate-Limited Sorption." *Water Resources Research* 27 (4): 547–56. doi:10.1029/90WR02760.
- Güven, O., R.W. Falta, F.J. Molz, and J.G. Melville. 1985. "Analysis and Interpretation of Single-Well Tracer Tests in Stratified Aquifers." *Water Resources Research* 21 (5): 676–84. doi:10.1029/WR021i005p00676.
- Hadi, K., U. Saravana Kumar, M. Al-Senafy, A. Mukhopadhyay, A. Al-Khalid, K. Al-Fahad, and H. Bhandary. 2016. "Multi-Well and Multi-Tracer Tests to Characterize the Groundwater Aquifers in Southern Kuwait." *Environmental Earth Sciences* 75 (20): 1340. doi:10.1007/s12665-016-6143-y.
- Heywood, C.E., and J.P. Pope. 2009. "Simulation of Groundwater Flow in the Coastal Plain Aquifer System of Virginia" U.S. Geological Survey Scientific Investigations Report 2009 – 5039. Reston, VA. doi:10.3133/sir20095039.
- Hillebrand, O., K. Nödler, M. Sauter, and T. Licha. 2015. "Multitracer Experiment to Evaluate the Attenuation of Selected Organic Micropollutants in a Karst Aquifer." *Science of The Total Environment* 506–507 (February): 338–43. doi:10.1016/j.scitotenv.2014.10.102.
- Hsieh, P.A. 1986. "A New Formula for the Analytical Solution of the Radial Dispersion Problem." *Water Resources Research* 22 (11): 1597–1605. doi:10.1029/WR022i011p01597.
- Hunt, B. 1986. "Solutions for Steady Groundwater Flow in Multi-Layer Aquifer Systems." *Transport in Porous Media*. Vol. 1.
- Konikow, L.F., and G.Z. Hornberger. 2006. "Modeling Effects of Multinode Wells on Solute Transport." *Ground Water* 44 (5): 648–60. doi:10.1111/j.1745-6584.2006.00231.x.
- LaFayette, G.N., P.S.K. Knappett, Y. Li, I. Loza-Aguirre, and M.L. Polizzotto. 2020. "Geogenic Sources and Chemical Controls on Fluoride Release to Groundwater in the Independence Basin, Mexico." *Applied Geochemistry* 123 (December 2019): 104787. doi:10.1016/j.apgeochem.2020.104787.

- Lai, K.-H., C.-W. Liu, C.-P. Liang, J.-S. Chen, and B.-R. Sie. 2016. “A Novel Method for Analytically Solving a Radial Advection-Dispersion Equation.” *Journal of Hydrology* 542. Elsevier B.V.: 532–40. doi:10.1016/j.jhydrol.2016.09.027.
- Malcuit, E., O. Atteia, F. Larroque, M. Franceschi, and A. Pryet. 2014. “On the Role of Low-Permeability Beds in the Acquisition of F and SO₄ Concentrations in a Multi-Layer Aquifer, South-West France.” *Journal of Contaminant Hydrology* 169: 37–49. doi:10.1016/j.jconhyd.2014.05.001.
- Martinez, M.B., Widdowson, M.A., Bott, C., Holloway, D., Heisig-Mitchell, J. and Wilson, C. (2022), Demonstration of Managed Aquifer Recharge in a Coastal Plain Aquifer: Lessons Learned. *Groundwater*. Accepted Author Manuscript. <https://doi.org/10.1111/gwat.13197>
- McFarland, E. R. 2010. “Groundwater-Quality Data and Regional Trends in the Virginia Coastal Plain, 1906 – 2007.” U.S. Geological Survey Professional Paper 1772. Reston: USGS, 86. <https://pubs.usgs.gov/pp/1772/>
- McFarland, E.R., and T.S. Bruce. 2006. “The Virginia Coastal Plain Hydrogeologic Framework.” U.S. Geological Survey Professional Paper 1731. Reston: USGS, 118.
- Mirecki, J.E., B.G. Campbell, K.J. Conlon, and M.D. Petkewich. 1998. “Solute Changes During Aquifer Storage Recovery Testing in a Limestone/Clastic Aquifer.” *Ground Water* 36 (3): 394–403. doi:10.1111/j.1745-6584.1998.tb02809.x.
- Moench, A.F. 1989. “Convergent Radial Dispersion: A Laplace Transform Solution for Aquifer Tracer Testing.” *Water Resources Research* 25 (3): 439–47. doi:10.1029/WR025i003p00439.
- . 1995. “Convergent Radial Dispersion in a Double-Porosity Aquifer with Fracture Skin: Analytical Solution and Application to a Field Experiment in Fractured Chalk.” *Water Resources Research* 31 (8): 1823–35. doi:10.1029/95WR01275.
- Molz, F.J., O. Güven, J.G. Melville, R.D. Crocker, and K.T. Matteson. 1986. “Performance, Analysis, and Simulation of a Two-Well Tracer Test at the Mobile Site.” *Water Resources Research* 22 (7): 1031–37. doi:10.1029/WR022i007p01031.
- Molz, F.J., O. Güven, J.G. Melville, J.S. Nohrstedt, and J.K. Overholtzer. 1988. “Forced-Gradient Tracer Tests and Inferred Hydraulic Conductivity Distributions at the Mobile Site.” *Ground Water* 26 (5): 570–79. doi:10.1111/j.1745-6584.1988.tb00790.x.
- Molz, F.J., J.G. Melville, O. Güven, R.D. Crocker, and K.T. Matteson. 1985. “Design and Performance of Single-Well Tracer Tests at the Mobile Site.” *Water Resources Research* 21 (10): 1497–1502. doi:10.1029/WR021i010p01497.

- Nalinakumari, B., W. Cha, and P. Fox. 2010. "Effects of Primary Substrate Concentration on NDMA Transport during Simulated Aquifer Recharge." *Journal of Environmental Engineering* 136 (4): 363–70. doi:10.1061/(ASCE)EE.1943-7870.0000168.
- Novakowski, K.S. 1992. "The Analysis of Tracer Experiments Conducted in Divergent Radial Flow Fields." *Water Resources Research* 28 (12): 3215–25.
- Patterson, B.M., M. Shackleton, A.J. Furness, E. Bekele, J. Pearce, K.L. Linge, F. Buseti, T. Spadek, and S. Toze. 2011. "Behaviour and Fate of Nine Recycled Water Trace Organics during Managed Aquifer Recharge in an Aerobic Aquifer." *Journal of Contaminant Hydrology* 122 (1–4): 53–62. doi:10.1016/j.jconhyd.2010.11.003.
- Pavelic, P., P.J. Dillon, and C.T. Simmons. 2006. "Multiscale Characterization of a Heterogeneous Aquifer Using an ASR Operation." *Ground Water* 44 (2): 155–64. doi:10.1111/j.1745-6584.2005.00135.x.
- Poulsen, D.L., P.G. Cook, C.T. Simmons, J.L. McCallum, and S. Dogramaci. 2019. "Effects of Intraborehole Flow on Purging and Sampling Long-Screened or Open Wells." *Groundwater* 57 (2): 269–78. doi:10.1111/gwat.12797.
- Pyne, R.D.G. 2006. *Groundwater Recharge and Wells: A Guide to Aquifer Storage Recovery*. 2nd ed. CRC Press, Inc.
- Reilly, E.T., O.L. Franke, G.D. Bennett. 1989. "Bias in Groundwater Samples Caused by Wellbore Flow." *Journal of Hydraulic Engineering* 115 (2): 270–76. doi:10.1061/(ASCE)0733-9429(1989)115:2(270).
- Reimus, P., G. Pohll, T. Mihevc, J. Chapman, M. Haga, B. Lyles, S. Kosinski, R. Niswonger, and P. Sanders. 2003. "Testing and Parameterizing a Conceptual Model for Solute Transport in a Fractured Granite Using Multiple Tracers in a Forced-Gradient Test." *Water Resources Research* 39 (12). doi:10.1029/2002WR001597.
- Ringleb, J., J. Sallwey, and C. Stefan. 2016. "Assessment of Managed Aquifer Recharge through Modeling-A Review." *Water (Switzerland)* 8 (12): 1–32. doi:10.3390/w8120579.
- Sanford, W.E., L.N. Plummer, G. Casile, E. Busenberg, D.L. Nelms, and P. Schlosser. 2017. "Using Dual-Domain Advective-Transport Simulation to Reconcile Multiple-Tracer Ages and Estimate Dual-Porosity Transport Parameters." *Water Resources Research* 53 (6): 5002–16. doi:10.1002/2016WR019469.
- Schafer, D., M. Donn, O. Atteia, J. Sun, C. MacRae, M. Raven, B. Pejicic, and H. Prommer. 2018. "Fluoride and Phosphate Release from Carbonate-Rich Fluorapatite during

- Managed Aquifer Recharge.” *Journal of Hydrology* 562 (July): 809–20.
doi:10.1016/j.jhydrol.2018.05.043.
- Suzuki, R., I. Kameda, Y. Takabe, F. Nishimura, and S. Itoh. 2015. “Removal of Dissolved Organic Matter and Disinfection By-Products Formation Potential in the Upper Layer during Soil Aquifer Treatment.” *Journal of Water and Environment Technology* 13 (2): 107–18. doi:10.2965/jwet.2015.107.
- Székely, F. 1992. “Pumping Test Data Analysis in Wells with Multiple or Long Screens.” *Journal of Hydrology* 132 (1-4): 137–56. doi:10.1016/0022-1694(92)90176-V
- Trussell, B., S. Trussell, Y. Qu, F. Geringer, S. Stanczak, T. Venezia, I. Monroy, F. Bacaro, and R. Trussell. 2018. “A Four-Year Simulation of Soil Aquifer Treatment Using Columns Filled with San Gabriel Valley Sand.” *Water Research* 144 (November): 26–35.
doi:10.1016/j.watres.2018.07.012.
- West, L.J., and N.E. Odling. 2007. “Characterization of a Multilayer Aquifer Using Open Well Dilution Tests.” *Ground Water* 45 (1): 74–84. doi:10.1111/j.1745-6584.2006.00262.x.
- Williams, A.T. 2000. “Using an Aquifer Storage and Recovery (ASR) Trial as a Large Scale Tracer Test.” In *Tracers and Modelling in Hydrogeology*, edited by A Dassargues, 195–99. Liege, Belgium: IAHS.
[https://books.google.com/books?hl=en&lr=&id=Uv439c4rqvsC&oi=fnd&pg=PA195&dq=Using+an+aquifer+storage+and+recovery+\(ASR\)+trial+as+a+large+scale+tracer+test&ots=iH1Ok5M2vb&sig=m2ZofzIHAWuCEL_8vGI52PCIVyE#v=twopage&q&f=false](https://books.google.com/books?hl=en&lr=&id=Uv439c4rqvsC&oi=fnd&pg=PA195&dq=Using+an+aquifer+storage+and+recovery+(ASR)+trial+as+a+large+scale+tracer+test&ots=iH1Ok5M2vb&sig=m2ZofzIHAWuCEL_8vGI52PCIVyE#v=twopage&q&f=false).
- Wu, Y.-X., H.-N. Wu, S.-L. Shen, and Y.-S. Xu. 2015. “Behaviour of Multi-Aquifer System during Pumping Test.” *Japanese Geotechnical Society Special Publication* 1 (4): 15–18.
doi:10.3208/jgssp.CPN-11.
- Young, S. C., and D.J. Benton. 1990. “The Usefulness of Multi-Well Aquifer Tests in Heterogeneous Aquifers.” Atomic Energy of Canada Limited, AECL Report.

7. Forced Gradient Tracer Test in a Multiscreen, Multi-Aquifer Recharge Well

Title

Forced Gradient Tracer Test in a Multiscreen, Multi-Aquifer Recharge Well

Abstract

Hampton Roads Sanitation District (HRSD) implemented a large-scale aquifer long-term replenishment (ALTR) project, the Sustainable Water Initiative for Tomorrow (SWIFT). The primary aim of the project is to raise the depleted regional potentiometric surface over space and time through deep well recharge to the Potomac Aquifer System (PAS), a deep, confined hydrostratigraphic unit with three distinct aquifer layers and eleven screens within the recharge well. Previous work has demonstrated the effectiveness of injectate as an intrinsic tracer to characterize flow behavior in the multi-screen well and transport in the PAS, but after the recharge front passes a monitoring well, injectate is no longer a useful tracer unless an artificial tracer is added. This unique study employs a forced gradient sodium bromide tracer test in the PAS during recharge operations to characterize flow distribution and evaluate chemical transport. A comparison of a Single-Zone and Two-Zone model, both accounting for variable influent concentration and transient flow over the course of the test, demonstrate the efficacy of a Two-Zone model within the PAS compared to a Single-Zone model. Results are contrasted to previously estimated flow distribution and suggest a dynamic flow distribution, which changes over time as a result of preferential clogging within the recharge well.

7.1 Introduction

Managed aquifer recharge (MAR) is the intentional increase of recharge rates for banking and/or treatment in an aquifer system (Dillon 2005; Maliva 2015). MAR serves as an umbrella term for a variety of recharge strategies. In deep, confined aquifer systems, the most commonly used MAR approaches are aquifer storage and recovery (ASR) and aquifer storage transfer and recovery (ASTR). ASR involves the injection of potable water into an aquifer for storage and recovery from the same well, while ASTR injects potable water into a well for recovery from a different well, usually with the expectation that the potable water receives additional treatment during transport (Dillon 2005; Pyne 2006). Both of these strategies are primarily storage-based, with the end goal of recovering water for reuse.

With groundwater usage outpacing the natural rate of recharge, the need for comprehensive strategies to increase the potentiometric surface over space and time is necessary to maintain a sustainable groundwater source (Wada et al. 2010; Aeschbach-Hertig and Gleeson 2012). Aquifer long-term replenishment (ALTR), which rehabilitates depleted aquifers via the injection of geochemically compatible water to confined aquifer systems, is one approach to increasing storage in confined aquifers to combat overuse of groundwater resources (Martinez et al. 2022). While the implementation is similar to ASR, short-term recovery is not a primary goal of an ALTR project. Because of this, the extent of the recharge front over the course of an ALTR project is significantly farther reaching than an ASR project. Quantifying the location of the recharge front and travel times off site is an important part of communicating the impact of an ALTR project on a region.

Historically, tracer tests have been used to measure groundwater flow and velocity, estimate hydrogeologic parameters, and approximate travel time in an aquifer system (Davis et

al. 1985). In MAR projects, tracers can be introduced via multiple methods (e.g., infiltration basins, injection wells), depending on the type of project. The use of a natural gradient tracer test (NGTT), where tracer is added over an aquifer thickness and moves with the pre-existing flow of groundwater based on the established hydraulic gradient, is commonly used to evaluate groundwater flow under natural flow conditions. In an ALTR project, however, which recharges directly into confined aquifers, tracers are typically added to the system via injection well under forced gradient tracer test (FGTT) conditions, which use either one or two wells to create a forced hydraulic gradient between the injection well (where the tracer is introduced) and nearby monitoring wells (Güven et al. 1985; Molz et al. 1985; Molz et al. 1986; Güven et al. 1986).

Previous work has shown injectate constituents serve as effective intrinsic tracers in a multi-aquifer recharge facility located at the HRSD SWIFT Research Center (SWIFT-RC) site (Chapters 4 and 6). Injectate has also been used to characterize other ASR sites (Williams 2000; Pavelic, Dillon, and Simmons 2006; Izbicki et al. 2010). However, following the passage of the recharge front past a monitoring well, the injectate itself can no longer be used as a tracer unless the injectate water quality significantly changes. Further characterization of the aquifer system once the injectate front has passed a monitoring well can be accomplished with the use of an artificial tracer.

Artificial tracers are added to injectate to differentiate between background concentrations and the recharge front. Tracer selection should be carefully considered based on the project purpose, scale, cost, site hydrogeology, and nature of the tracer (Davis et al. 1985). Salt-based tracers like chloride (NaCl) and bromide (NaBr) are commonly used as non-reactive, or conservative, tracers (Ptak et al. 2004; Zakhem and Hafez 2012; Mosthaf et al. 2018; Gerenday et al. 2020). Few ASR projects use artificial tracers to characterize sites, likely because

of the scale of the test and long travel times. Visser et al. (2014) conducted a 7-day artificial tracer test at an ASR site using xenon-enriched water to characterize transport in Woodland, CA4). The recharge well was approximately 600 feet deep (85 feet of screened interval) and was designed for a recharge rate of 2,000 gallons per minute (gpm) (City of Woodland 2013).

In heterogeneous media, the incorporation of multiple transport domains within a system can improve predictions of solute transport and tailing behavior observed at monitoring wells (Becker and Shapiro 2000; Liu, Zheng, and Gorelick 2007). A dual-porosity model, where multiple porosity domains exist, accounts for preferential flow paths (PFPs) during transport. Analytical solutions for dual-porosity transport have been a topic of research for some time (van Genuchten and Wierenga 1976; Bibby 1981; Małoszewski and Zuber 1985; Gerke and van Genuchten 1993; Haggerty and Gorelick 1995; Cihan and Tyner 2011; Knorr et al. 2016). While this paradigm is commonly applied to fractured rock and karst terrains, it can also be applied to alternating layers of sands and clays (Sanford et al. 2017; Saxena et al. 1994). Saxena et al. (1994) implement a chlorine isotope (^{36}Cl) tracer in conjunction with tritium (^3H) as tritiated water (HTO) to evaluate dual-porosity flow through lysimeters using a model developed by Jarvis et al. which accounts for transport under non-steady flow (Jarvis et al. 1991a; Jarvis et al. 1991b).

Few studies examine the potential impact of dual-porosity flow during MAR projects in deep, confined aquifers. Gaus et al. (2002) identified dual-porosity flow as a key contributor to fluoride release during an ASR project. The authors calibrated two models, a geochemical mass transport model (PHREEQC) and a physical model (SWIFT/486), using chloride as an intrinsic tracer over eight cycles of ASR and confirmed the impact of dual-porosity effects on fluoride release (Williams 2000; Gaus et al. 2002). Guo et al. (2015) investigated the impact of dual-

porosity conditions and aquifer heterogeneity on ASR recovery efficiency. However, this research is theoretical in nature and uses the Eclipse model in conjunction with manufactured input parameters to characterize simulated ASR performance (Guo et al. 2015).

This study is unique in its conception and complexity. The objective of this study was to implement a forced gradient tracer test using sodium bromide to characterize transport in a multiscreen, multi-aquifer well during ALTR operations. No known artificial tracer tests have been conducted in a multi-screen well situated in multiple hydrostratigraphic units during long-term recharge operations; the recharge well at this site contains 11 screens situated in 3 hydrostratigraphic units. Furthermore, the study aims to demonstrate the efficacy of a dual-porosity approximation to describe bromide transport through a multi-layered aquifer. It also compares results to previously measured estimates at the site to examine how flow distribution changes over the course of an ALTR project.

7.2 Methods

7.2.1. Site Description

The Sustainable Water Initiative for Tomorrow (SWIFT) Research Center (SWIFT-RC) is a large-scale MAR demonstration facility located at Nansemond Treatment Plant in Suffolk, Virginia, USA. The SWIFT-RC treats approximately 1 million gallons per day (MGD) (3,780 m³/d) of effluent from Hampton Road Sanitation District's (HRSD) water reclamation facilities (WRFs) to drinking water standards using advanced treatment methods (Figure 7-1) (Martinez et al. *in press*). Following treatment, this "SWIFT Water" is recharged to multiple hydrostratigraphic units of the Potomac Aquifer System (PAS) using a multi-screen recharge well (TW-1) that contains eleven screens ranging from 500 to 1400 feet below land surface. This study will focus on results observed at MW-SAT, a depth discrete monitoring well 50 feet (15.2

m) from TW-1. MW-SAT is screened at identical depths to TW-1. Samples are collected from each screen using a flexible liner underground technology (FLUTE) system, a multilevel sampling system that uses a well liner to eliminate mixing in the monitoring well.

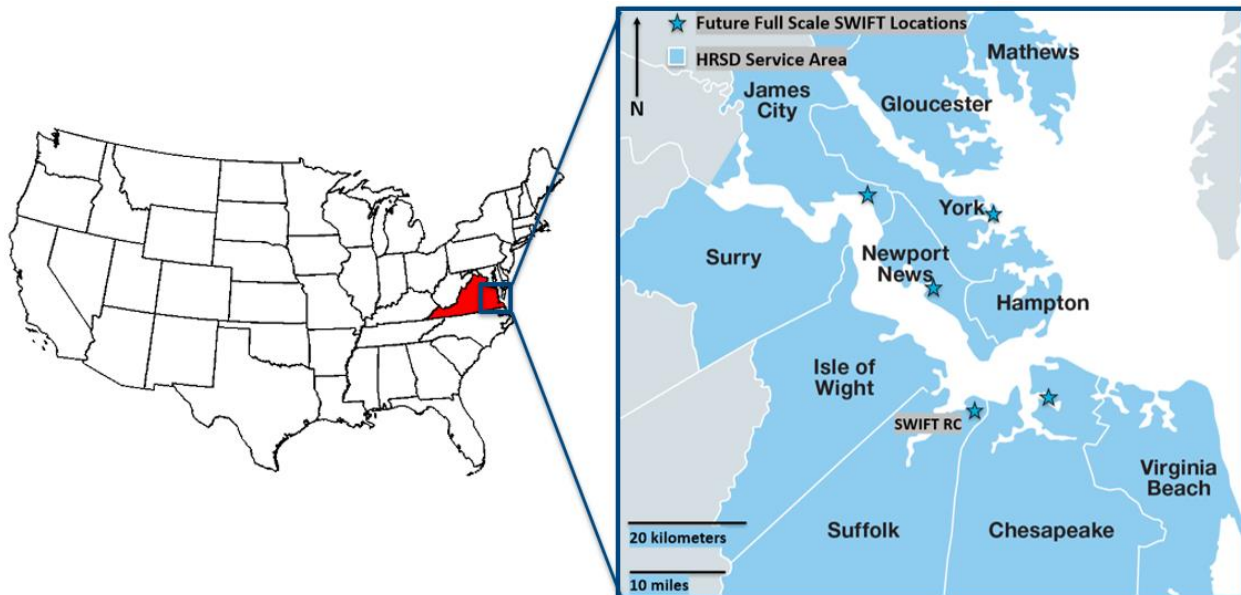


Figure 7-1. HRSD Service Area in eastern Virginia, USA. The existing demonstration facility (SWIFT-RC) in Suffolk is the study site, while future full-scale sites are marked by blue stars (Martinez et al. 2022).

The PAS is a confined aquifer that stretches in extent from New Jersey to the South Carolina coast (Trapp and Horn 1997; McFarland and Bruce 2006; Heywood and Pope 2009). U.S. Geological Survey (USGS) reports identify the Potomac aquifer as primarily fluvial-deltaic coarse-grained sands and gravels with interbedded clays of varying thicknesses (McFarland and Bruce 2006). The nature of the interbedded clays within the PAS leads to confining units functioning as local barriers without those confining units encompassing the extent of the PAS (McFarland and Bruce 2006; Heywood and Pope 2009). Despite three distinct aquifers having been recognized in past regional models, the three aquifers are interconnected. McFarland mentions that studies of the Virginia Coastal Plain between the 1940s-1980s designated the PAS

as a single aquifer; however, in the 1980s, investigations of the hydrogeologic framework differentiated between the Upper, Middle, and Lower Potomac aquifers (UPA, MPA, and LPA, respectively) to aid in vertical discretization in modeling projects. Since current modeling techniques allow multiple model layers within one aquifer to simulate vertical flow, more recent reports combine the three into one Potomac Aquifer while they may differentiate between the three locally (McFarland and Bruce 2006).

7.2.2. Experimental Setup and Field Sampling Procedures

Sodium bromide was selected as an artificial tracer because of its conservative behavior (i.e., low aquifer-interaction potential) and relatively low background concentration. Average concentration across all 11 screens was measured as 0.713 mg/L, with minimum and maximum concentrations measured as 0.212 mg/L at Screen 9 to 1.856 mg/L at Screen 10, and average SWIFT Water concentration (0.09 mg/L) compared to the target injection concentration. A concentrated sodium bromide solution was added to the recharge stream immediately before entering TW-1 via the use of a peristaltic pump configured to only add bromide under recharge conditions. Recharge at TW-1 during the injection phase occurred at a rate of 679 gpm with a target recharge time of 72 hours; flow at the recharge well was recorded using the SWIFT supervisory control and data acquisition (SCADA) system. The rate of mixing between SWIFT Water and the concentrated sodium bromide solution was designed to achieve a target injection concentration of approximately 200 mg/L of bromide. The concentration of bromide added was calculated incrementally using the drawdown in five 1000 L sodium bromide totes (measured approximately every hour) and confirmed with samples collected once per day during the injection phase. Measured concentration within the totes was 435,000 mg/L bromide. Following

the bromide injection phase, recharge continued at TW-1 using SWIFT Water with no bromide addition.

In the week preceding the tracer test, samples were taken once per day from SWIFT Water, MW-SAT, and the conventional wells at a consistent time to establish background bromide concentrations at each sample port and prevent interference of daily fluctuations. Samples were collected in 250 mL high density polyethylene (HDPE) containers and refrigerated before analysis was completed. Bromide samples were analyzed by the HRSD Central Environmental Lab (CEL) using Reference Method EPA 300.0. Following the start of the tracer test, bromide levels at MW-SAT were monitored multiple times per day.

Sampling at frequent increments (up to 4 times per day) was important, especially for screens where preliminary data indicated travel time < 7 days so that breakthrough would be monitored with a significant sample size. For screens with longer expected travel times based on initial breakthrough at MW-SAT or where the previously observed breakthrough was more gradual (Bullard et al. 2019), samples were collected at a lower frequency (1 to 2 times per day) until significant breakthrough (at least three times the background concentration observed at the screen) was observed. Once those screens passed the sample threshold, sampling frequency increased to 2 to 4 times per day. Sampling frequencies were decreased once a screen passed the threshold for the second time (i.e., after breakthrough was observed). In MW-SAT, following the return to within 10% of pre-test bromide concentrations, bromide was monitored once per day for one week and then once per week for one month to ensure that concentrations remained at the same level before ending bromide sampling at that screen at a frequency above the normal monitoring levels. More information on sampling frequency is described in Appendix E.

7.2.3. Modeling

A simplified analytical model (Model 1) based on the assumptions of variable influent concentration and constant flow was used to describe the breakthrough of bromide at MW-SAT and estimate flow distribution in the recharge well. Variable influent concentration was required to account for the bromide tracer pulse. If operations were consistent with only short periods of pumping and no flow, the assumption that flow is constant would be relatively accurate. Results of this initial model are available in Appendix E (Table E-3, Figures E-2 to E-12). The following equation could be used to describe the observed concentration, $C_i(r, t)$, during radial flow at each screened interval (modified from Charbeneau 2000):

$$C_s(r, t) = C_{B,s} + \frac{C_F}{2} * \operatorname{erfc} \left[\frac{r - R_s}{\sqrt{\frac{4}{3} \alpha_{L,s} R_s}} \right] \quad (1)$$

$$R_s(t) = \sqrt{\frac{Q_s t}{\pi n_s b_s}} \quad (2)$$

where $C_{B,s}$ is the background concentration within the screen of interest, C_F is the influent concentration, r is the radial distance from the injection well, t is the time since the start of injection, $\alpha_{L,s}$ is the screen-specific longitudinal dispersivity, R_s is the mean displacement of the front, Q_s is the recharge flow rate to the individual well screen (which varies based on changes in flow distribution), n is the screen-specific effective porosity, and b is the thickness of the screen of interest. To account for variable influent concentration, the model is modified as such with the following boundary conditions:

$$\begin{aligned}
t_i < t_j & \quad C_{s,i,j}(r,t) = 0 \\
& \quad R_{s,i}^*(t) = 0 \\
& \quad V_{s,i}^*(t) = 0
\end{aligned} \tag{3}$$

$$\begin{aligned}
t_i \geq t_j & \quad C_{s,i,j}(r,t) = \frac{\Delta C_F}{2} * \operatorname{erfc} \left[\frac{r - R_s}{\sqrt{\frac{4}{3} \alpha_{L,s} R_s}} \right] \\
& \quad R_s(t) = \sqrt{\frac{Q_s(t_i - t_j)}{\pi n_s b_s}}
\end{aligned} \tag{4}$$

where t_i is the total elapsed time, t_j is the time that the influent concentration was measured, and $\Delta C_F = C_{F,i} - C_{F,i-1}$ where j denotes a measured influent concentration at t_j . For the first iteration ($j = 1$), $\Delta C_F = C_{F,i} - C_B$, where C_B is the background concentration measured prior to the start of recharge. At any time, t_i , the concentration at a monitoring well screen would be given as:

$$C_{s,i}(r,t) = C_B + \sum_{j=1}^j C_{s,i,j}(r,t) \tag{5}$$

Though the initial estimates were based on constant flow, recharge during a large-scale ALTR project is not continuous and included frequent pumping to maintain injectivity and shut down due to treatment process adjustments and well rehabilitation. A MATLAB model (Model

2) was used to account for variable influent concentration and transient flow conditions, which have been shown in Chapter 4 and Chapter 6 to represent transport in changing operating conditions. Model 2 has been used to analyze breakthrough of SWIFT Water as an intrinsic tracer and is discussed in depth by Martinez and Widdowson in previous work (Chapter 6):

$$\begin{aligned}
 t_i < t_j & \quad C_{s,i,j}(r, t) = 0 \\
 & \quad R_{s,i}^*(t) = 0 \\
 & \quad V_{s,i}^*(t) = 0
 \end{aligned} \tag{6}$$

$$\begin{aligned}
 t_i \geq t_j & \quad C_{s,i,j}(r, t) = \frac{\Delta C_F}{2} * \operatorname{erfc} \left[\frac{r - R_{s,i}^*}{\sqrt{\frac{4}{3} \alpha_{L,s} R_{s,i}^*}} \right] \\
 & \quad R_{s,i}^*(t) = \sqrt{\frac{V_{s,i}^*(t)}{\pi n_s b_s}}
 \end{aligned} \tag{7}$$

$$V_{s,i}^*(t) = [Q_{s,i}(t_i - t_{i-1})] + V_{s,i-1}^*(t)$$

where $R_{s,i}^*$ is the mean displacement of the front based on $V_{s,i}^*(t)$, the incremental volume, which is calculated from the flow to the screen, $Q_{s,i}(t_i)$. At any time, t_i , the concentration at a monitoring well screen would be given as:

$$C_{s,i}(r,t) = C_B + \sum_{j=1}^j C_{s,i,j}(r,t) \quad (7)$$

The estimates of flow distribution from Model 1 were used as a starting estimate to calibrate the initial breakthrough of bromide at MW-SAT under Model 2, considering transient flow and variable influent concentration. To increase the likelihood of convergence, the flow and porosity parameters were combined, and a range of estimated porosities was used to determine the range of possible flow rates to each screen. Two parameters were used, $\left(\frac{Q}{n}\right)_1$ and α_1 , where $\left(\frac{Q}{n}\right)_1$ is the flow/porosity term and α_1 is the longitudinal dispersivity. MATLAB's Optimize tool was used to vary the two parameters to minimize the residual sum of squares (RSS)

$$RSS = \sum_{i=1}^n (C_{obs,i,s} - C_{sim,i,s})^2$$

where C_{obs} is the observed concentration and C_{sim} is the simulated concentration at a given time, i for a given screen, s . Full results from the Single-Zone optimization model are included in Appendix E (Table E-5).

To further investigate breakthrough behavior, the model was extended to incorporate two zones, a high permeability/flow zone and a low permeability/flow zone. This involved delineating the thickness for each zone as a model variable, calculating the concentration breakthrough over time in each zone using Model 2, and using a length-weighted concentration to calculate the total concentration value over time:

$$C_s(t) = \frac{(C_s(t)_1 * [b_1 * b_{tot}]) + (C_s(t)_2 * [(1 - b_1) * b_{tot}])}{b_{tot}}$$

where the parameter b_1 is the percent thickness of Zone 1 relative to the total thickness of the hydrostratigraphic unit (b_{tot}), and $C_s(t)_1$ and $C_s(t)_2$ are the time-dependent concentrations at the screen of interest based on Model 2 in Zone 1 and Zone 2, respectively. Zone 1 is considered to be the high permeability/flow zone, and Zone 2 is the low permeability/flow zone. The MATLAB Optimize tool was used to solve for five parameters: b_1 , $\left(\frac{Q}{n}\right)_1$, α_1 , $\left(\frac{Q}{n}\right)_2$, and α_2 . Upper and lower boundaries for each term were initially estimated based on the minimum and maximum values previously observed at the site (Bullard et al. 2019) (Table 7-1). The results of the single zone estimate were used as initial estimates in the two-zone model. The results of two models were compared to determine the best fit: (1) Single-Zone, Transient Flow and (2) Two-Zone, Transient Flow.

Table 7-1. Upper and lower parameter estimates for the two-zone model. The same boundaries for $\left(\frac{Q}{n}\right)_1$ and α_1 are applied to the single-zone model.

Term	Lower Boundary	Upper Boundary
b_1	0.1	0.99
$\left(\frac{Q}{n}\right)_1$	0.001	1
α_1	0.5	50
$\left(\frac{Q}{n}\right)_2$	0.001	1
α_2	0.5	50

7.3. Results and Discussion

7.3.1. Tracer Test Operational Conditions

Phases of the tracer test were (1) bromide injection phase, which lasted approximately 3.5 days; (2) steady recharge operations with intermittent backflush; (3) shutdown of recharge

operations for well rehabilitation; (4) post-rehabilitation pumping; and (5) normal operations with steady recharge and intermittent backflush. Recharge and pumping volumes for each test are listed in Table 7-2, and length in each operating condition per phase is provided in Table 7-3. The non-constant state of recharge confirms the need for Model 2 to account for transient flow conditions. Since all screen breakthroughs occurred before shutdown and because previous work suggested changes in the flow rate distribution at TW-1 following Phase 3 (Chapter 5), the focus of the data analysis is the first 100 days of the tracer test.

Table 7-2. Recharge and pumping volumes during the length of the tracer test. All volumes are given in gallons. Parentheses indicate negative flow or pumping from the well.

Phase	Start Time	End Time	Length (days)	Total Recharge Volume	Total Pumping Volume	Net Recharge Volume
1	09/29/20 09:25	10/02/20 20:45	3.47	3,153,322	(236,863)	2,916,459
2	10/02/20 20:45	12/25/20 17:00	83.84	63,069,435	(9,923,412)	53,146,023
3	12/25/20 17:00	04/09/21 13:15	104.84	581,869	-	581,869
4	04/09/21 13:15	04/14/21 12:00	4.95	351,625	(13,192,734)	(12,841,108)
5	04/14/21 12:00	10/26/21 16:45	195.20	99,276,534	(13,693,403)	85,583,131

Table 7-3. Time split during each phase of the bromide tracer test. All units are in days.

Phase	Start Time	End Time	Total Length	Recharge	Shutdown	Pumping
1	09/29/20 09:25	10/02/20 20:45	3.47	3.23	0.10	0.14
2	10/02/20 20:45	12/25/20 17:00	83.84	63.20	14.82	5.81
3	12/25/20 17:00	04/09/21 13:15	104.84	0.83	104.01	-
4	04/09/21 13:15	04/14/21 12:00	4.95	0.22	0.86	3.86
5	04/14/21 12:00	10/26/21 16:45	195.20	131.10	56.29	7.80

7.3.2. Single-Zone and Two-Zone Models

Background concentration of bromide and peak observed concentration during the tracer test are provided in Table 7-4. The highest concentration observed at MW-SAT was 160.0 mg/L at Screen 9, which was the quickest screen to peak, with a travel time of approximately 3 days. Travel time at each screen differed from previous data collected at the site (Bullard et al. 2019), especially in the LPA, where travel time decreased from over 180 days to approximately 13 days. Following the tracer testing, water level response was evaluated, and relevant flow contributions were identified from each of the hydrostratigraphic units, in contrast to water level analyses completed in 2018, which indicated little to no response from the LPA.

Table 7-4. Background concentration, peak observed bromide concentration, and travel time measured at each screen.

Screen	Background Bromide Concentration (mg/L)	Peak Observed Bromide Concentration (mg/L)	Travel Time (days)
1	0.295	90.8	8.7
2	0.236	72.1	7.6
3	0.647	25.3	39.7
4	0.319	36.3	17.9
5	0.710	44.0	12.5
6	1.614	13.8	44.8
7	0.430	22.3	27.3
8	0.314	48.1	15.6
9	0.212	160.0	2.9
10	1.856	37.0	13.7
11	1.211	47.6	11.7

Following the parameter estimation process, the single-zone models underestimated the observed peak breakthrough at each screen and did not account for tailing behavior observed after peak breakthrough at some screens. Comparisons of model fit between the Single-Zone and Two-Zone model are provided for Screen 1 and 2 (Figure 7-2), 3 and 4 (Figure 7-3), 5 and 6 (Figure 7-4), 7 and 8 (Figure 7-5), and 10 and 11 (Figure 7-6). The Two-Zone model improved

the fit for all screens except Screen 9, where the Single-Zone model was able to capture the peak breakthrough and travel time (Figure 7-7).

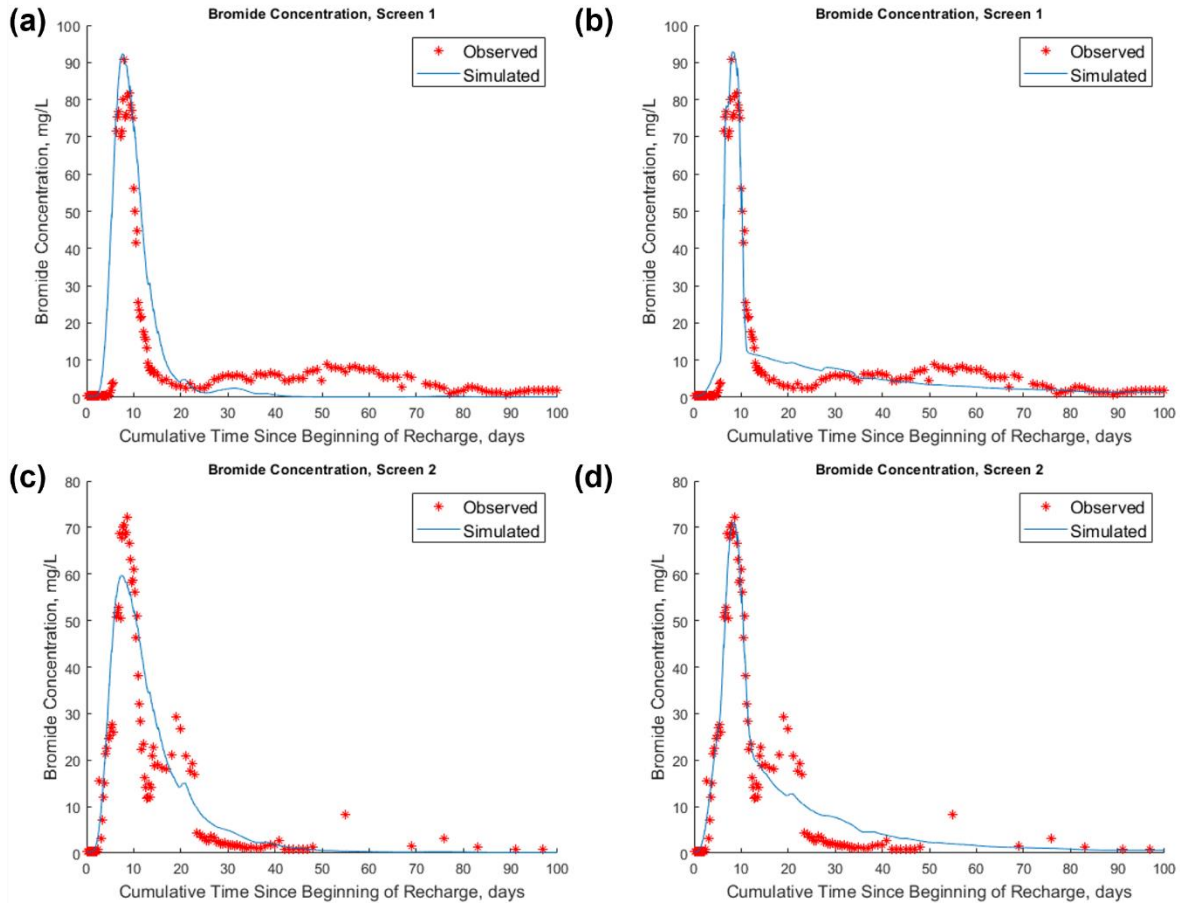


Figure 7-2. Bromide transport in Screen 1 [(a) and (b)] and Screen 2 [(c) and (d)] for the Single-Zone model [(a) and (c)] and the Two-Zone model [(b) and (d)]. The Two-Zone model increases the capability to fit both the initial peak and the steep drop in concentration after initial breakthrough.

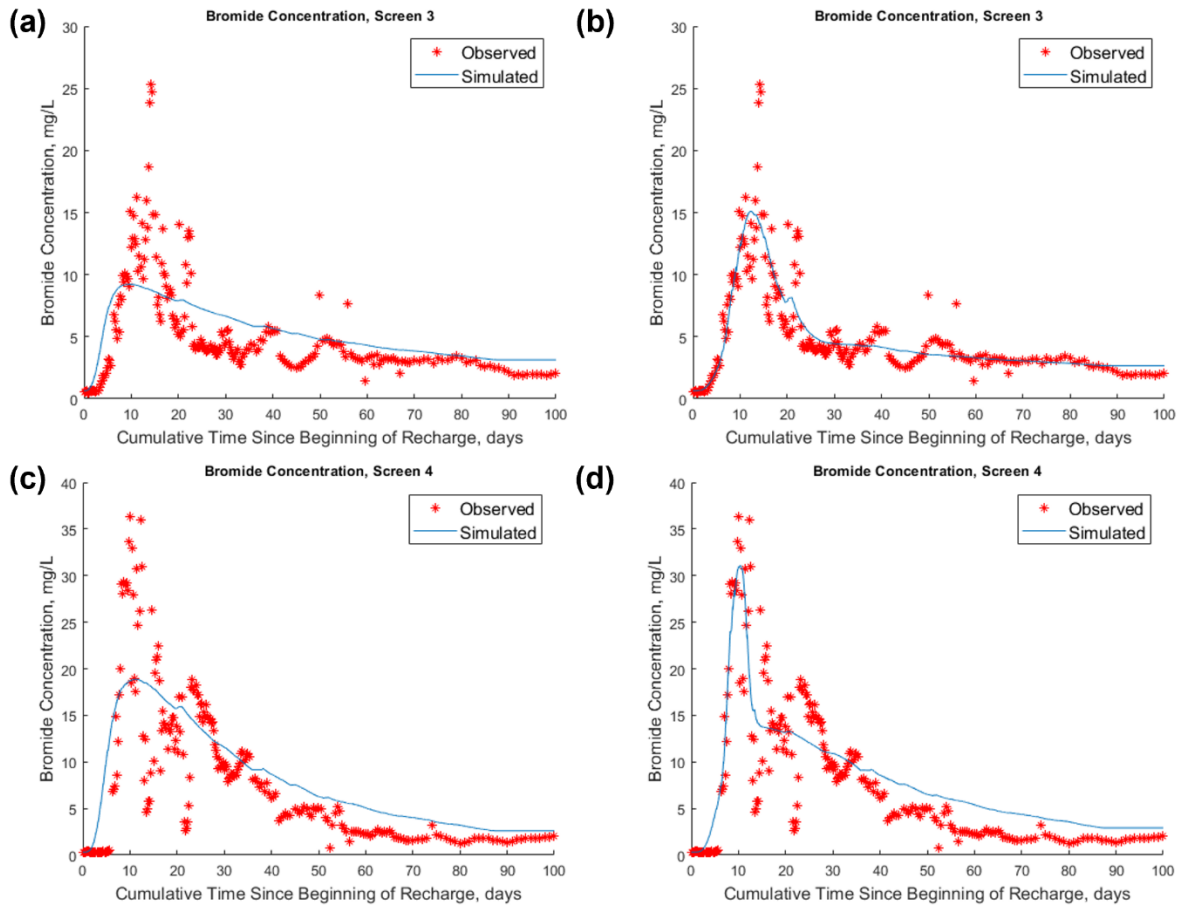


Figure 7-3. Bromide transport in Screen 3 [(a) and (b)] and Screen 4 [(c) and (d)] for the Single-Zone model [(a) and (c)] and the Two-Zone model [(b) and (d)]. The Two-Zone model increases the capability to fit both the steep initial peak and the tailing effect after initial breakthrough.

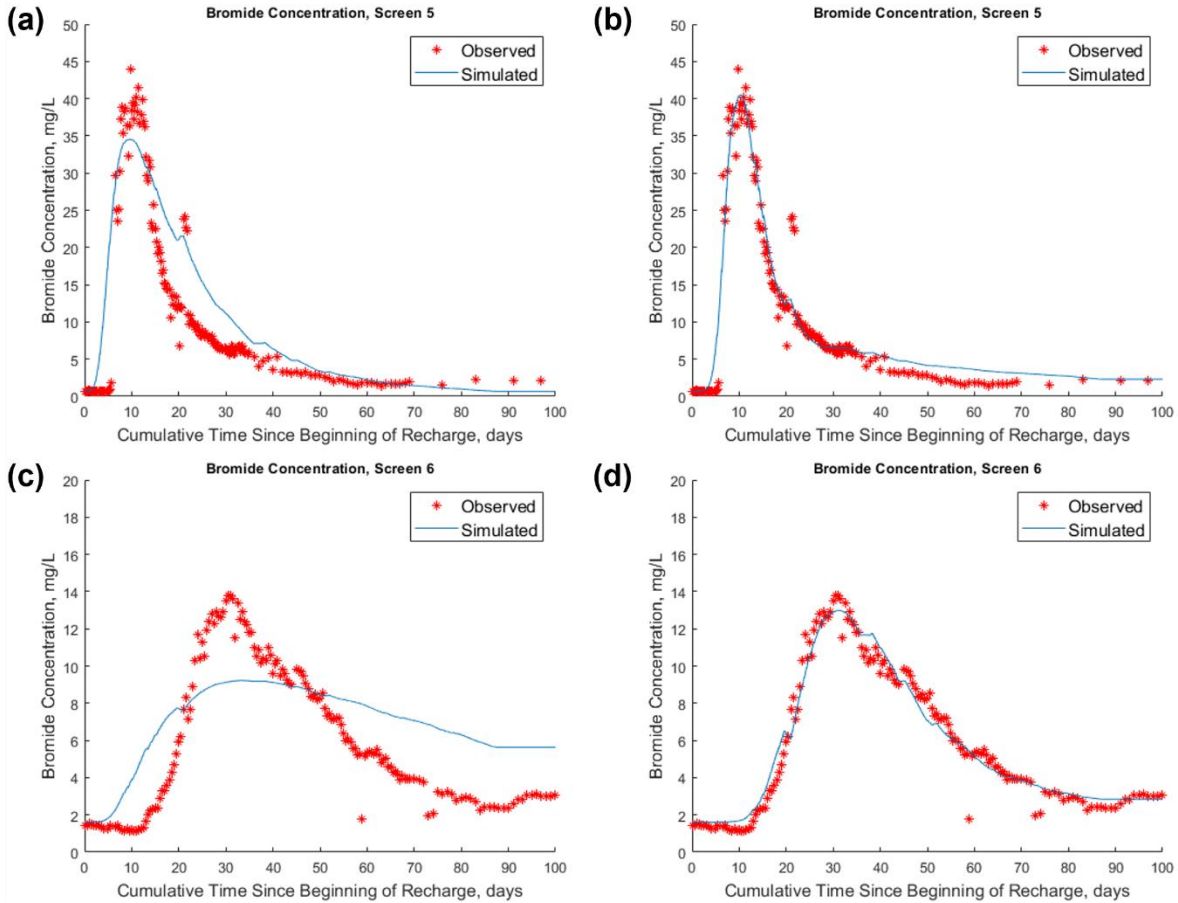


Figure 7-4. Bromide transport in Screen 5 [(a) and (b)] and Screen 6 [(c) and (d)] for the Single-Zone model [(a) and (c)] and the Two-Zone model [(b) and (d)]. The Two-Zone model increases the capability to fit both the initial peak and the steep drop in concentration after initial breakthrough at Screen 5 and is able to accurately capture the entire breakthrough in Screen 6.

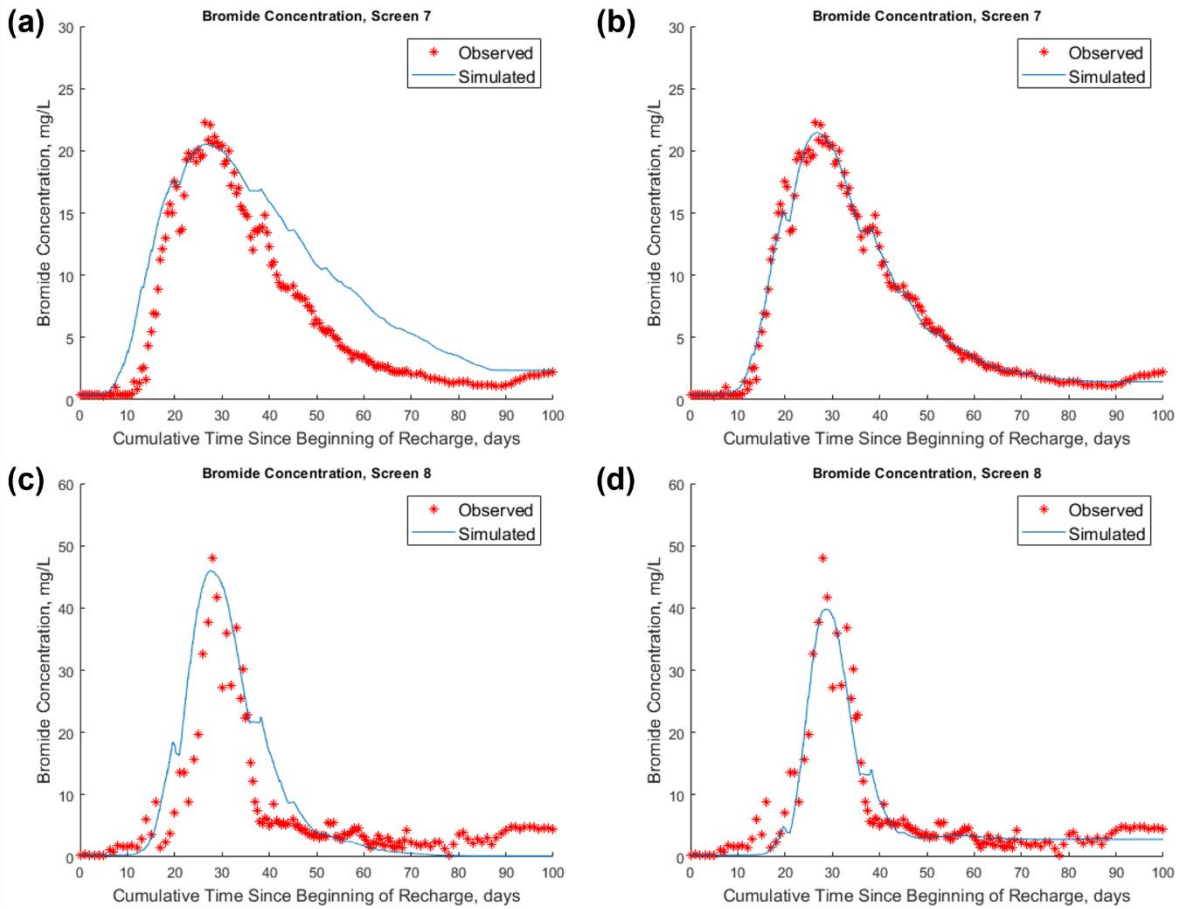


Figure 7-5. Bromide transport in Screen 7 [(a) and (b)] and Screen 8 [(c) and (d)] for the Single-Zone model [(a) and (c)] and the Two-Zone model [(b) and (d)]. The Two-Zone model is able to accurately capture the entire breakthrough in Screen 7 and captures the narrow initial breakthrough and the tailing effect in Screen 8 following breakthrough.

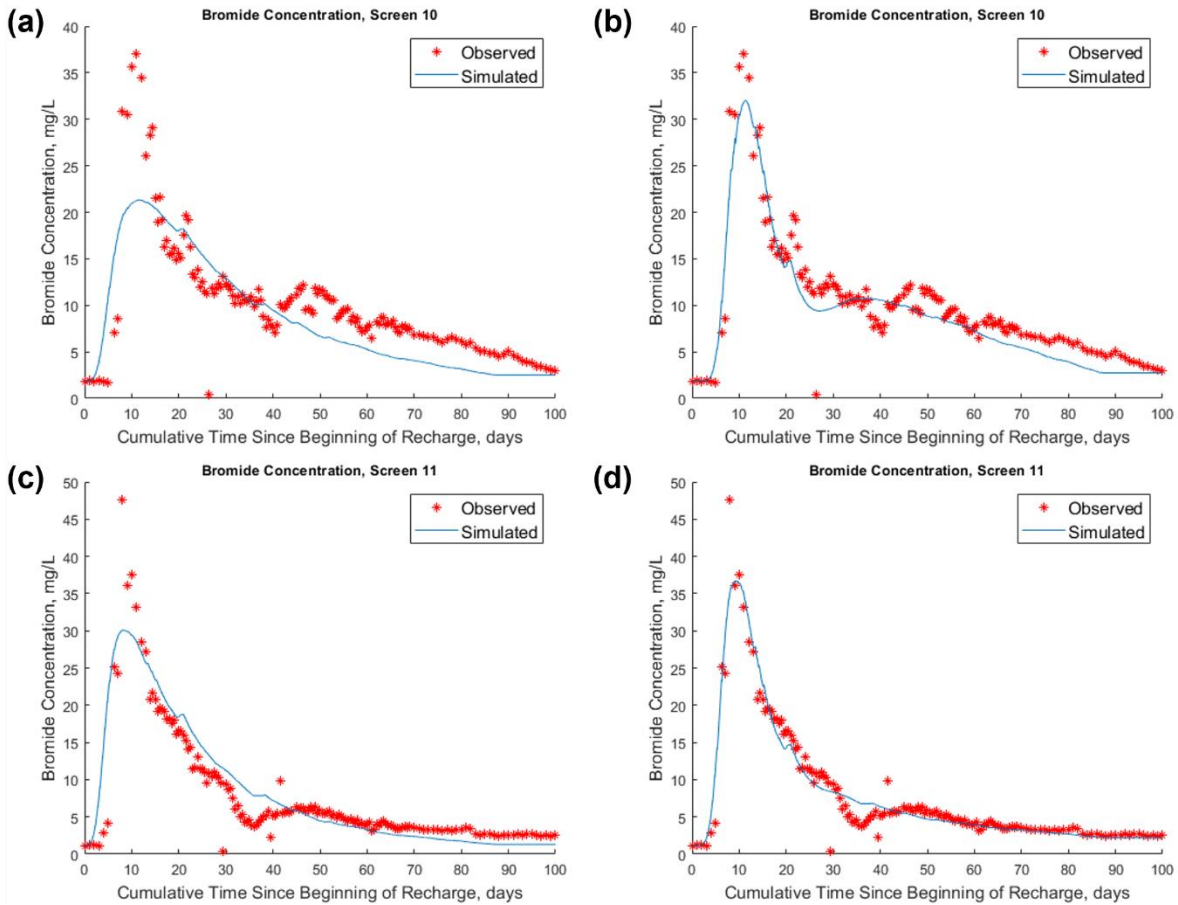


Figure 7-6. Bromide transport in Screen 10 [(a) and (b)] and Screen 11 [(c) and (d)] for the Single-Zone model [(a) and (c)] and the Two-Zone model [(b) and (d)]. The Two-Zone model increases the capability to fit both the initial peak breakthrough and the tailing effect following breakthrough.

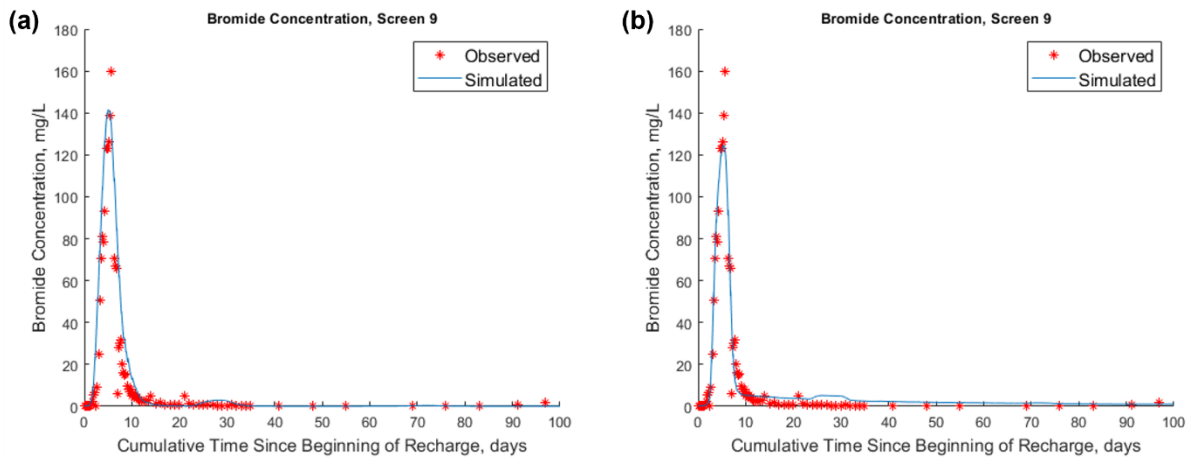


Figure 7-7. Bromide transport in Screen 9 for (a) Single-Zone model and (b) Two-Zone model. The Single-Zone model better captures peak breakthrough.

Parameter estimates and a range of estimated flow distribution for each screen are provided in Table 7-5. Single-Zone results are located in Appendix E (Table E-5), and the results from Screen 9 are included in Table 7-5. Using the Two-Zone model for each screen, with the exception of the Single-Zone model results for screen 9, the model captures between 44.8% to 99.1% of total flow through the PAS. It is likely that the actual flow distribution to each screen is between these two boundary values since these values are estimated based on the minimum and maximum porosity and assume constant porosity over the entire depth of the screen. Larger figures of individual screen results are included in Appendix E (Figures E-13 to E-34).

Table 7-5. Two-Zone solution parameters and total flow estimates. The variable b_1 indicates the percentage of the total thickness that makes up the high permeability/flow zone, Zone 1. Screen 9 is a single-zone solution, denoted by $b_1 = 100\%$. For the total flow estimate, the low estimate assumes porosity in both zones is 0.20, and the high estimate assumes porosity in both zones is 0.45.

Screen	b_1 (%)	Zone 1		Zone 2		Total Flow (%)	
		$\frac{Q}{n}$ (%)	α_1 (ft)	$\frac{Q}{n}$ (%)	α_2 (ft)	Low Est.	High Est.
1	41	0.115	0.1	0.052	18.5	3.3	7.5
2	75	0.225	14.6	0.119	0.3	6.9	15.5
3	14	0.014	1.6	0.008	40.0	0.4	1.0
4	89	0.081	14.8	0.034	0.2	2.3	5.2
5	47	0.056	2.4	0.015	15.9	1.4	3.2
6	40	0.031	2.1	0.008	12.4	0.8	1.8
7	63	0.029	2.1	0.003	12.5	0.6	1.4
8	62	0.047	0.5	0.009	5.3	1.1	2.5
9	100	0.797	3.0	--	--	15.9	34.3
10	47	0.341	2.7	0.107	3.3	8.9	20.1
11	45	0.112	3.6	0.038	13.3	3.0	6.7
						44.8	99.1

A comparison of Q/n values over time indicates that flow distribution is dynamic (Table 7-6). The most noticeable change is the transition from little to no flow in the LPA in the original breakthrough analysis to a significant portion of the flow going to the LPA, which overall

experienced a 675% increase in Q/n between the initial estimate and the Two-Zone model estimate. This is compensated for by a decrease in the Q/n estimate to the UPA and MPA of 69% and 41%, respectively. A comparison of longitudinal dispersivity values over time reveals that while some screens change significantly (e.g., 10 ft to 34.6 ft in screen 3), most of the length-averaged values are within the same order of magnitude as the original (Table 7-7). The change in dispersivity is a result of the variability of groundwater velocity within each screen layer over time.

Table 7-6. Comparison of Q/n values between original estimate in 2018 (Bullard et al. 2019), extrapolated values from an in-situ flowmeter test in 2019 (Chapter 5), and Single-Zone and Two-Zone results. Flowmeter values are extrapolated based on the estimated porosity from the original work.

Screen	Original	Flowmeter	Single Zone Model	Two-Zone Model			Percent Change (%)
				Zone 1	Zone 2	Sum	
1	0.667	0.950	0.262	0.052	0.115	0.167	-75
2	0.960	1.840	0.400	0.119	0.225	0.344	-64
3	0.222	0.074	0.018	0.008	0.014	0.022	-90
4	0.257	0.200	0.113	0.034	0.081	0.114	-56
5	0.160	0.240	0.084	0.056	0.015	0.070	-56
6	0.117	0.100	0.040	0.031	0.008	0.039	-67
7	0.043	0.071	0.039	0.003	0.029	0.032	-26
8	0.023	0.063	0.077	0.009	0.047	0.056	143
9	1.348	0.478	0.797	0.033	0.538	0.571	-41
10	0.067	0.040	0.360	0.107	0.341	0.447	567
11	0.010	0.000	0.152	0.038	0.112	0.150	1400

Table 7-7. Longitudinal dispersivity comparison between the original estimate (Bullard et al. 2019) and the bromide tracer analysis. The thickness-averaged value of longitudinal dispersivity in the Two-Zone model is also included with the individual zone values.

Screen	Original	Single-Zone Model	Two-Zone Model		
			Zone 1	Zone 2	Length Averaged
1	5	2.8	18.5	10.3	10.9
2	10	6.4	0.3	33.9	11.1
3	10	40.9	40.0	2.1	34.6
4	20	16.8	0.2	31.2	13.3
5	8	9.9	2.4	8.0	9.6
6	20	12.7	2.1	18.1	8.3
7	30	4.8	12.5	9.5	5.9
8	2	1.0	5.3	15.4	2.3
9	10	3.0	34.0	25.7	12.6
10	0.05	14.5	3.3	49.3	3.0
11	3	14.2	13.3	13.5	8.9

Using the best fit results from Table 7-5, bromide mass discharge was estimated at MW-SAT (Table 7-8). During the tracer test, the average bromide concentration at TW-1 was 203.8 mg/L, resulting in a total of 2,250.4 kg of bromide was recharged into the aquifer during Phase 1. Three estimates for mass discharge at MW-SAT were made based on the Q/n value: (1) flow distribution based on the original porosities estimated in the 2018 breakthrough study (Bullard et al. 2019), where 58% of the flow is accounted for; (2) a low estimate, assuming porosity at each screen is 0.20, where 44.8% of the flow is accounted for; and (3) a high estimate, assuming porosity at each screen is 0.45, where 99.1% of the flow is accounted for. Between the low and high estimate, recovery efficiency ranges from 48.8% to 82.8%. The actual value is likely between those two, since the two zones likely have two different porosities, and these estimates assume constant porosity over the entire screened depth.

Table 7-8. Mass discharge at MW-SAT. Original indicates the flow distribution based on porosities estimated by Bullard et al. (2019), Low Estimate assumes porosity in both zones is 0.20, and High Estimate assumes porosity in both zones is 0.45.

Screen	Original		Low Estimate		High Estimate	
	Estimated Q (%)	Bromide Recovered (kg)	Estimated Q (%)	Bromide Recovered (kg)	Estimated Q (%)	Bromide Recovered (kg)
1	3.3%	63.5	3.3%	63.5	7.5%	143.0
2	8.6%	164.6	6.9%	131.7	15.5%	296.3
3	0.6%	131.9	0.4%	130.7	1.0%	135.0
4	4.0%	159.3	2.3%	136.6	5.2%	174.5
5	1.8%	26.9	1.4%	21.5	3.2%	48.4
6	1.2%	53.0	0.8%	49.7	1.8%	58.0
7	0.9%	109.3	0.6%	106.0	1.4%	116.3
8	1.8%	30.9	1.1%	19.3	2.5%	43.5
9	13.1%	180.4	15.9%	218.9	34.3%	470.6
10	11.2%	210.3	8.9%	168.2	20.1%	378.5
11	4.0%	69.8	3.0%	51.7	6.7%	116.4
Total Mass Recovered (kg)		1200.1	1098.0		1980.5	
Recovery Efficiency		53.3%	48.8%		88.0%	

Regardless of the estimate, the mass balance indicates only partial recovery of the bromide tracer at MW-SAT. This is likely due to issues related to sample collection at MW-SAT. Samples collected from the FLUTE system are assumed to be representative of the entire length of the screen, though the sample collection port is small compared to the full length of the screen. The FLUTE system contains an annular spacer within the identified monitoring interval, but it is likely that the sample preferentially flows from the depth nearest the sample port. In a long screen that could be impacted by density driven flow (i.e., the sample water flows preferentially through one part of the screen), the sample collected may not be representative of the total mass traveling through the screen.

7.4. Conclusions

This study executed a bromide tracer test in a multi-screen, multi-aquifer recharge well during ALTR operations. Results of Single-Zone and Two-Zone models to explain bromide transport were compared to evaluate the existence and impact of a dual-porosity transport paradigm within the aquifer system. The study confirmed the existence of a mobile/immobile zone in most layers of the PAS, indicated by the improvement in model fit using a Two-Zone model. A mass balance completed on the system showed a low recovery efficiency for bromide at the depth-discrete monitoring well, MW-SAT, likely due to sampling bias within each screen. The recovery efficiency also explains the inability of the Single-Zone or Two-Zone model to capture 100% of the total flow distribution.

Model results were also compared to previous estimates of flow distribution at the site. Previous studies at this site established that flow distribution is dynamic, though the change observed was likely immediate as a result of well rehabilitation (Chapter 5). This study, however, indicated that flow distribution changed since the last measurement without a discernible singular precipitating event, indicating that flow distribution is also likely to change over time as a result of non-constant well operations and preferential clogging. This was further supported by a water level analysis at conventional wells screened in the UPA, MPA, and LPA on site. Conventionally, studies of multi-layered aquifers used for MAR purposes measure flow distribution once and assume for modeling purposes that the flow distribution is constant over time. Evaluating changes in flow distribution over time should be a priority for transport modeling purposes in multi-layer aquifer systems to quantify chemical transport and travel times in any MAR project.

Acknowledgments

The authors would like to thank members of the SWIFT Research Center team, operators at Nansemond Treatment Plant, and members from the HRSD Technical Services Division for their help in collecting samples onsite at the SWIFT Research Center. This work was supported by HRSD and the Charles E. Via, Jr. Department of Civil and Environmental Engineering at Virginia Tech.

Supplemental Information

Additional information can be found in Appendix E.

References

- Aeschbach-Hertig, W., and T. Gleeson. 2012. "Regional Strategies for the Accelerating Global Problem of Groundwater Depletion." *Nature Geoscience* 5 (12): 853–61. <https://doi.org/10.1038/ngeo1617>.
- Becker, M.W., and A.M. Shapiro. 2000. "Tracer Transport in Fractured Crystalline Rock: Evidence of Nondiffusive Breakthrough Tailing." *Water Resources Research* 36 (7): 1677–86. <https://doi.org/10.1029/2000WR900080>.
- Bibby, R. 1981. "Mass Transport of Solutes in Dual-Porosity Media." *Water Resources Research* 17 (4): 1075–81. <https://doi.org/10.1029/WR017i004p01075>.
- Bullard, M.G, M. Widdowson, G. Salazar-Benites, J. Heisig-Mitchell, A. Nelson, and C. Bott. 2019. Managed Aquifer Recharge: Transport and Attenuation in a Coastal Plain Aquifer. *Proceedings of the EWRI World Environmental and Water Resources Congress 2019: Groundwater, Sustainability, Hydro-Climates/Climate Change, and Environmental Engineering*, 1–14. Pittsburgh: EWRI. doi: 10.1061/9780784482346.011.
- Charbeneau, R.J. (2000) *Groundwater Hydraulics and Pollutant Transport*. Upper Saddle River, Prentice-Hall, Inc.
- Cihan, A., and J.S. Tyner. 2011. "2-D Radial Analytical Solutions for Solute Transport in a Dual-Porosity Medium." *Water Resources Research* 47 (4). <https://doi.org/10.1029/2009WR008969>.

- City of Woodland. 2013. "Drinking Water Source Assessment." Woodland, CA.
[https://www.cityofwoodland.org/DocumentCenter/View/1575/Drinking-Water-Source-Assessment-PDF?bidId=.](https://www.cityofwoodland.org/DocumentCenter/View/1575/Drinking-Water-Source-Assessment-PDF?bidId=)
- Davis, S.N., D.J. Campbell, H.W. Bentley, and T.J. Flynn. 1985. "An Introduction to Ground-Water Tracers." Tuscon: EPA.
<https://nepis.epa.gov/Exe/ZyPURL.cgi?Dockey=20012NZD.txt>
- Dillon, P. 2005. "Future Management of Aquifer Recharge." *Hydrogeology Journal* 13 (1): 313–16. <https://doi.org/10.1007/s10040-004-0413-6>.
- Gaus, I., P. Shand, I.N. Gale, A.T. Williams, and J.C. Eastwood. 2002. "Geochemical Modelling of Fluoride Concentration Changes during Aquifer Storage and Recovery (ASR) in the Chalk Aquifer in Wessex, England." *Quarterly Journal of Engineering Geology and Hydrogeology* 35 (2): 203–8. <https://doi.org/10.1144/1470-9236/2001-52>.
- Genuchten, M.Th. van, and P.J. Wierenga. 1976. "Mass Transfer Studies in Sorbing Porous Media I. Analytical Solutions." *Soil Science Society of America Journal* 40 (4): 473–80. <https://doi.org/10.2136/sssaj1976.03615995004000040011x>.
- Gerenday, S.P., J.F. Clark, J. Hansen, I. Fischer, and J. Koreny. 2020. "Sulfur Hexafluoride and Potassium Bromide as Groundwater Tracers for Managed Aquifer Recharge." *Groundwater* 58 (5): 777–87. <https://doi.org/10.1111/gwat.12983>.
- Gerke, H.H., and M.T. van Genuchten. 1993. "A Dual-Porosity Model for Simulating the Preferential Movement of Water and Solutes in Structured Porous Media." *Water Resources Research* 29 (2): 305–19. <https://doi.org/10.1029/92WR02339>.
- Guo, W., K. Coulibaly, and R.G. Maliva. 2015. "Simulated Effects of Aquifer Heterogeneity on ASR System Performance." *Environmental Earth Sciences* 73 (12): 7803–9. <https://doi.org/10.1007/s12665-014-3822-4>.
- Güven, O., R.W. Falta, F.J. Molz, and J.G. Melville. 1986. "A Simplified Analysis of Two-Well Tracer Tests in Stratified Aquifers." *Ground Water* 24 (1): 63–71. <https://doi.org/10.1111/j.1745-6584.1986.tb01460.x>.
- Güven, O., R.W. Falta, F.J. Molz, and J.G. Melville. 1985. "Analysis and Interpretation of Single-Well Tracer Tests in Stratified Aquifers." *Water Resources Research* 21 (5): 676–84. <https://doi.org/10.1029/WR021i005p00676>.
- Haggerty, R., and S.M. Gorelick. 1995. "Multiple-Rate Mass Transfer for Modeling Diffusion and Surface Reactions in Media with Pore-Scale Heterogeneity." *Water Resources Research* 31 (10): 2383–2400. <https://doi.org/10.1029/95WR10583>.

- Heywood, C.E., and J.P. Pope. 2009. "Simulation of Groundwater Flow in the Coastal Plain Aquifer System of Virginia" U.S. Geological Survey Scientific Investigations Report 2009–5039. Reston, VA. <https://doi.org/10.3133/sir20095039>.
- Izbicki, J.A., C.E. Petersen, K.J. Glotzbach, L.F. Metzger, A.H. Christensen, G.A. Smith, D. O’leary, M.S. Fram, T. Joseph, and H. Shannon. 2010. "Aquifer Storage Recovery (ASR) of Chlorinated Municipal Drinking Water in a Confined Aquifer." *Applied Geochemistry* 25 (8): 1133–52. <https://doi.org/10.1016/j.apgeochem.2010.04.017>.
- Jarvis, N. J., L. Bergström, and P.E. Dik. 1991a. "Modelling Water and Solute Transport in Macroporous Soil. II. Chloride Breakthrough under Non-Steady Flow." *Journal of Soil Science* 42 (1): 71–81. <https://doi.org/10.1111/j.1365-2389.1991.tb00092.x>.
- Jarvis, N.J., P.-E. Jansson, P.E. Dik, and I. Messing. 1991b. "Modelling Water and Solute Transport in Macroporous Soil. I. Model Description and Sensitivity Analysis." *Journal of Soil Science* 42 (1): 59–70. <https://doi.org/10.1111/j.1365-2389.1991.tb00091.x>.
- Knorr, B., P. Maloszewski, F. Krämer, and C. Stumpp. 2016. "Diffusive Mass Exchange of Non-Reactive Substances in Dual-Porosity Porous Systems - Column Experiments under Saturated Conditions." *Hydrological Processes* 30 (6): 914–26. <https://doi.org/10.1002/hyp.10620>.
- Liu, G., C. Zheng, and S.M. Gorelick. 2007. "Evaluation of the Applicability of the Dual-Domain Mass Transfer Model in Porous Media Containing Connected High-Conductivity Channels." *Water Resources Research* 43 (12). <https://doi.org/10.1029/2007WR005965>.
- Maliva, R.G. 2015. "Managed Aquifer Recharge: State-of-the-Art and Opportunities." *Water Science and Technology: Water Supply* 15 (3): 578–88. <https://doi.org/10.2166/ws.2015.009>.
- Małoszewski, P., and A. Zuber. 1985. "On the Theory of Tracer Experiments in Fissured Rocks with a Porous Matrix." *Journal of Hydrology* 79 (3–4): 333–58. [https://doi.org/10.1016/0022-1694\(85\)90064-2](https://doi.org/10.1016/0022-1694(85)90064-2).
- Martinez, M.B., Widdowson, M.A., Bott, C., Holloway, D., Heisig-Mitchell, J. and Wilson, C. (2022), Demonstration of Managed Aquifer Recharge in a Coastal Plain Aquifer: Lessons Learned. *Groundwater*. Accepted Author Manuscript. <https://doi.org/10.1111/gwat.13197>
- McFarland, E.R., and T.S. Bruce. 2006. "The Virginia Coastal Plain Hydrogeologic Framework." U.S. Geological Survey Professional Paper 1731, 118. Reston, VA. <https://doi.org/10.3133/pp1731>

- Molz, F.J., O. Güven, J.G. Melville, R.D. Crocker, and K.T. Matteson. 1986. “Performance, Analysis, and Simulation of a Two-Well Tracer Test at the Mobile Site.” *Water Resources Research* 22 (7): 1031–37. <https://doi.org/10.1029/WR022i007p01031>.
- Molz, F.J., J.G. Melville, O. Güven, R.D. Crocker, and K.T. Matteson. 1985. “Design and Performance of Single-Well Tracer Tests at the Mobile Site.” *Water Resources Research* 21 (10): 1497–1502. <https://doi.org/10.1029/WR021i010p01497>.
- Mosthaf, K., B. Brauns, A.S. Fjordbøge, M.M. Rohde, H. Kern-Jespersen, P.L. Bjerg, P.J. Binning, and M.M. Broholm. 2018. “Conceptualization of Flow and Transport in a Limestone Aquifer by Multiple Dedicated Hydraulic and Tracer Tests.” *Journal of Hydrology* 561 (June): 532–46. <https://doi.org/10.1016/j.jhydrol.2018.04.011>.
- Pavelic, P., P.J. Dillon, and C.T. Simmons. 2006. “Multiscale Characterization of a Heterogeneous Aquifer Using an ASR Operation.” *Ground Water* 44 (2): 155–64. <https://doi.org/10.1111/j.1745-6584.2005.00135.x>.
- Ptak, T., M. Piepenbrink, and E. Martac. 2004. “Tracer Tests for the Investigation of Heterogeneous Porous Media and Stochastic Modelling of Flow and Transport—a Review of Some Recent Developments.” *Journal of Hydrology* 294 (1–3): 122–63. <https://doi.org/10.1016/j.jhydrol.2004.01.020>.
- Pyne, R.D.G. 2006. *Groundwater Recharge and Wells: A Guide to Aquifer Storage Recovery*. 2nd ed. CRC Press, Inc.
- Sanford, W.E., L.N. Plummer, G. Casile, E. Busenberg, D.L. Nelms, and P. Schlosser. 2017. “Using Dual-Domain Advective-Transport Simulation to Reconcile Multiple-Tracer Ages and Estimate Dual-Porosity Transport Parameters.” *Water Resources Research* 53 (6): 5002–16. <https://doi.org/10.1002/2016WR019469>.
- Saxena, R.K., N.J. Jarvis, and L. Bergström. 1994. “Interpreting Non-Steady State Tracer Breakthrough Experiments in Sand and Clay Soils Using a Dual-Porosity Model.” *Journal of Hydrology* 162 (3–4): 279–98. [https://doi.org/10.1016/0022-1694\(94\)90232-1](https://doi.org/10.1016/0022-1694(94)90232-1).
- Trapp, H., and M.A. Horn. 1997. “Ground Water Atlas of the United States: Segment 11, Delaware, Maryland, New Jersey, North Carolina, Pennsylvania, Virginia, West Virginia.” U.S. Geological Survey Hydrologic Investigations Atlas 730-L. <https://doi.org/10.3133/ha730L>
- Visser, A., M. Singleton, and B. Esser. 2014. “Xenon Tracer Test at Woodland Aquifer Storage and Recovery Well.” Lawrence Livermore National Laboratory Report. Vol. LLNL-TR-65. Livermore, CA (United States). <https://doi.org/10.2172/1162248>.

- Wada, Y., L.P.H. van Beek, C.M. van Kempen, J.W.T.M. Reckman, S. Vasak, and M.F.P. Bierkens. 2010. "Global Depletion of Groundwater Resources." *Geophysical Research Letters* 37 (20). <https://doi.org/10.1029/2010GL044571>.
- Williams, A.T. 2000. "Using an Aquifer Storage and Recovery (ASR) Trial as a Large Scale Tracer Test." In *Tracers and Modelling in Hydrogeology*, edited by A Dassargues, 195–99. Liege, Belgium: IAHS.
[https://books.google.com/books?hl=en&lr=&id=Uv439c4rqvsC&oi=fnd&pg=PA195&dq=Using+an+aquifer+storage+and+recovery+\(ASR\)+trial+as+a+large+scale+tracer+test&ots=iH1Ok5M2vb&sig=m2ZofzlHAWuCEL_8vGI52PCIVyE#v=twopage&q&f=false](https://books.google.com/books?hl=en&lr=&id=Uv439c4rqvsC&oi=fnd&pg=PA195&dq=Using+an+aquifer+storage+and+recovery+(ASR)+trial+as+a+large+scale+tracer+test&ots=iH1Ok5M2vb&sig=m2ZofzlHAWuCEL_8vGI52PCIVyE#v=twopage&q&f=false).
- Zakhem, B.A., and R. Hafez. 2012. "Chemical and Isotopic Methods for Management of Artificial Recharge in Mazraha Station (Damascus Basin, Syria)." *Hydrological Processes* 26 (24): 3712–24. <https://doi.org/10.1002/hyp.8446>.

8. Conclusions

Chapters 4 through 7 of this dissertation provide new insights into assessing the impact of long-term recharge operations on the Potomac Aquifer System (PAS) at the SWIFT Research Center (SWIFT-RC) on chemical transport through the PAS and travel time. The following sections summarize the major findings of each chapter, synthesize the results, provide a broader context, and discuss future research directions.

8.1. Objectives and Findings

Chapter 4. The objective of this investigation was to characterize flow distribution and aquifer characteristics at MW-SAT (50-ft travel distance from multi-screen recharge well TW-1) based on initial breakthrough of conductivity (serving as an indicator of chloride). Major findings were:

- An incremental flow model was able to improve fit and capture changes in conductivity breakthrough behavior by incorporating extended pumping and shutdown periods at the SWIFT Research Center.
- Advection is the prevailing transport mechanism in the aquifer system during operations, while diffusion from low-permeability zones occurs during shutdown conditions, causing measured concentrations at the monitoring well to change.

Chapter 5. The objective of this study was to implement an impeller flowmeter to measure flow rate distribution in a multi-screen well during ALTR operations (recharge and pumping). An additional objective was to quantify differences in flow behavior across single screens under recharge and pumping conditions. Major findings include:

- Flowmeter readings stabilized above each screen at approximately 20 feet above the well screen; the stabilized reading accounted for the full flow, while unstable readings

underestimated or overestimated the flow to the screens. The source of instability was hypothesized to result from turbulent flow in the well casing above each screen.

- In a multi-screen well, recharge flow moves preferentially through the uppermost well screens and the upper portion of individual screens. Flow rates during pumping are more evenly distributed along the well screens and individual screens.
- A comparison of flow distribution measurements with the findings from Chapter 4 and with water level analysis performed by Matynowski (Matynowski 2020) suggests a dynamic flow distribution at TW-1 and a single measurement in time cannot be assumed to be constant over the length of an entire project. This change in flow distribution is hypothesized to be a result of the well rehabilitation that took place immediately before the testing but transient conditions in the wells screens and gravel pack are also considered to influence flow distribution.

Chapter 6. The objective of this phase of the research was to evaluate multiple tracers for characterizing flow in the UPA, a multi-screen system, using a novel approximation for quantifying breakthrough under variable flow, dynamic flow distributions, and variable influent tracer concentration conditions. The work also identifies characteristics of effective intrinsic tracers for large-scale aquifer characterization. Finally, the efficacy of the novel approximation was evaluated. Major findings were:

- Multiple factors contribute to intrinsic tracer effectiveness as an indicator of travel time, including significant differences between the constituent concentration between native groundwater and injectate, aquifer interaction potential, and variability of the injectate constituent concentration combined with frequency of influent sampling.

- Tracer efficacy varies by aquifer layer, especially when native groundwater characteristics vary significantly by depth. Sulfate was the most effective tracer for the Upper Potomac Aquifer (well MW-UPA), but chloride is estimated to be effective for the Middle and Lower Potomac Aquifer (wells MW-MPA and MW-LPA, respectively).
- An approximation to account for three operational factors at TW-1: (1) variable flow conditions, (2) time-varying flow distribution, and (3) variable influent concentration improves the fit of the transport model.

Chapter 7. The objective of this study was to use a bromide tracer test to demonstrate the efficacy of a Two-Zone approximation to describe transport through a multi-screen, multi-layered aquifer. Results are also compared to previous estimates of flow distribution to evaluate how flow distribution changes over the course of the project. Major findings were:

- A comparison between a Single-Zone and Two-Zone model demonstrated that the Two-Zone model was more effective at characterizing transport in all screens except Screen 9, supporting the existence of a mobile/immobile zone within the aquifer.
- Changes in flow distribution were compared to previous estimates at the site. Observed changes in flow distribution indicate that the dynamic nature of flow distribution at the site is gradual, likely as a result of preferential clogging in screens which receive high amounts of flow.

8.2. Major Themes and Engineering Significance

The SWIFT Research Center is a 1 MGD demonstration facility for an aquifer long-term replenishment (ALTR) project that aims to replenish the overused PAS. This work shows that the use of injectate as an intrinsic tracer is a cost-effective way to characterize flow in a multi-

screen, multiaquifer well (Chapter 4, Chapter 6). A consistent and robust monitoring plan should be established before the start of recharge, and a water quality background should be verified at the nearby monitoring wells. Multiple potential tracers should be identified in case unexpected interaction happens within the system, as was the case with fluoride in Screen 1 and MW-UPA. Furthermore, the use of a depth-discrete sampling system near the recharge well is critical for a full characterization of the aquifer. Characterization at the conventional wells was possible because of screen-specific work from MW-SAT, where a Flexible Liner Underground Technology (FLUTE) system was installed to collect depth-discrete samples. Samples collected at MW-UPA showed a sample bias towards the upper screens, which was accounted for in the model with the individual screen data from MW-SAT. Without the individual screen characterization, the characterization of MW-UPA would have resulted in an underestimation of flow to the aquifer and skewed estimates of aquifer characteristics.

Perhaps the most significant finding of this work is the dynamic nature of flow rate distribution and travel time (Table 8-1). Typically, flow distribution in multi-screen wells is estimated once over the length of a project and assumed to remain constant for modeling purposes (e.g., Fakhreddine et al. 2020). By measuring flow distribution using multiple methods over the course of the project, this work shows that is not the case. Flow distribution is transformed over time in two ways: (1) gradual shifts in flow distribution caused by normal recharge and pumping operations, and (2) rapid changes as a result of well rehabilitation or change in operating conditions. The flowmeter testing took place in April/May 2019 immediately after the extended shutdown for well rehabilitation in 2018-2019. It is likely that the significant changes in flow distribution that favored the upper screens were a result of preferential treatment of those screens during well rehabilitation. Bromide tracer testing started

in October 2020, well after the rehabilitation. While regular backflushing took place at the well to maintain injectivity, it is likely that the screens that received the most flow initially after the 2019 well rehabilitation were preferentially clogged, which resulted in flow gradually shifting to slower screens. This would explain the high flow to screens 9-11 during the tracer test, especially when the LPA had not been initially responsive.

Table 8-1. Estimated travel time (days) for individual screens at MW-SAT (50-ft radial distance) assuming constant recharge flow (700 gpm) at the recharge well (TW-1). Actual travel times will be longer, and in some cases may be significantly longer depending on operating conditions on site.

Screen*	Intrinsic Tracer** (2018)	Flowmeter (2019)	Bromide Tracer (2020)
1	1.6	2.1	8.7
2	2.7	1.4	7.6
3	3.9	11.8	39.7
4	7.9	10.2	17.9
5	5.5	2.7	12.5
6	15.0	26.2	44.8
7	20.4	4.9	27.3
8	37.3	14.0	15.6
9	1.7	3.6	2.9
10	91.8	183.6	13.7
11	181.6	181.6	11.7

* Screens 1-4: UPA; Screens 5-9: MPA; Screens 10-11: LPA

**Travel time at Screens 10 and 11 are different than those listed in Chapter 4 due to improved fit (i.e., breakthrough occurred at these screens after the chapter was published).

8.3. Future Research Directions

Plans for additional flowmeter testing are currently underway at a new full-scale recharge well (NP-MAR-01) on site at the SWIFT Research Center. This testing will continue to evaluate differences between recharge, no-flow, and pumping conditions. Furthermore, additional investigation into the turbulent behavior above the well screens could provide new insights into flow behavior in turbulent conditions in a recharge well.

Further research potential also exists in the area of model enhancement. Currently, the approximation used to describe transport accounts for changes in operating conditions, time-varying flow distribution, and variable influent concentrations. However, the approximation does not account for non-conservative constituents. This is discussed in Chapter 6, where the approximation was able to demonstrate the correct breakthrough time and behavior but not the correct concentration of TOC due to decay during transport. While the approximation developed in this dissertation could be modified to account for decay during transport, the difficulty lies in maintaining decay behavior during non-recharge periods. The model could be enhanced to account for additional transport behavior during shut down, including natural background flow, constituent decay, and aquifer interaction (e.g., sorption/desorption, microbial behavior).

Finally, the development of a method that could estimate changes in flow distribution based on water level analysis (Theis 1935; Cooper and Jacob 1946) at the conventional wells could provide a real-time and cost-effective way to monitor changes in flow distribution. The use of injectate as an intrinsic tracer is very useful, especially on a large scale, but once the recharge front passes a monitoring well, it can no longer be used as a tracer unless water quality characteristics change significantly. Flowmeters can be used to directly measure flow distribution, and artificial tracer tests can also be used to characterize flow behavior, but both of these undertakings are expensive and require additional time to collect and analyze data. Semi-regular pumping tests, which would measure drawdown over time in nearby monitoring wells, could indicate well clogging or changes in preferential flow within a multi-screen well. These tests would be relatively straightforward to perform, and testing could be done under recharge and pumping conditions.

References

- Cooper, H. H., and C. E. Jacob. 1946. "A Generalized Graphical Method for Evaluating Formation Constants and Summarizing Well-Field History." *Transactions, American Geophysical Union* 27 (4): 526. <https://doi.org/10.1029/TR027i004p00526>.
- Fakhreddine, S., H. Prommer, S.M. Gorelick, J. Dadakis, and S. Fendorf. 2020. "Controlling Arsenic Mobilization during Managed Aquifer Recharge: The Role of Sediment Heterogeneity." *Environmental Science and Technology* 54 (14): 8728–38. <https://doi.org/10.1021/acs.est.0c00794>.
- Matynowski, E.D. 2020. "Groundwater Modeling and Hydrogeological Parameter Estimation: Potomac Aquifer System, SWIFT Research Center." M.S. thesis, Via Department of Civil and Environmental Engineering, Virginia Tech.
- Theis, C.V. 1935. "The Relation between the Lowering of the Piezometric Surface and the Rate and Duration of Discharge of a Well Using Ground-Water Storage." *Transactions, American Geophysical Union* 16 (2): 519. <https://doi.org/10.1029/TR016i002p00519>.

Appendices

Appendix A: SWIFT Research Center Site Description and Initial Aquifer Characterization

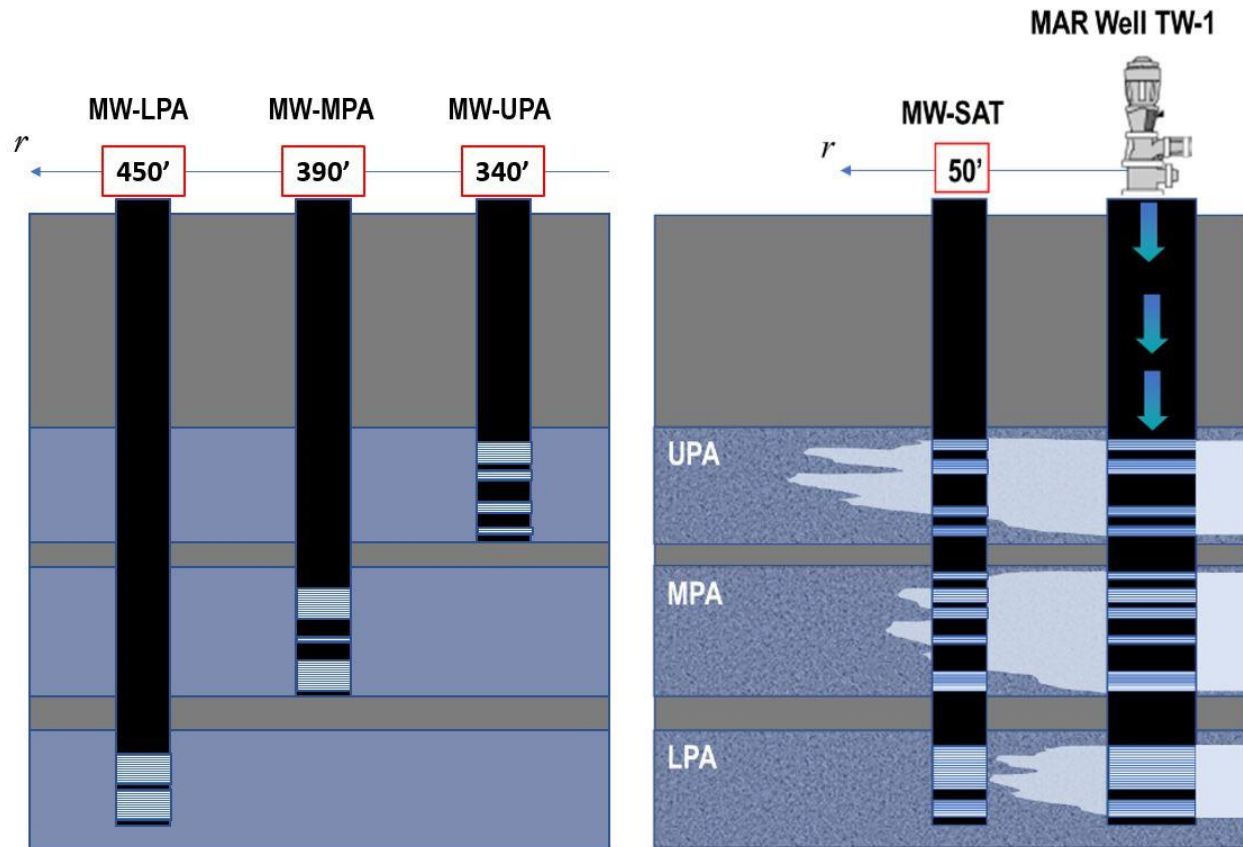


Figure A-1. Screen Depths at TW-1, MW-SAT, and Conventional Wells

Table A-1. Well Screen Depth and Length of Screen in TW-1 and MW-SAT.

Aquifer Zone		Starting Depth (fbg)	Ending Depth (fbg)	Length of Screen (ft)
Upper Potomac Aquifer (UPA)				
	Screen 1	505	530	25
	Screen 2	550	595	45
	Screen 3	665	680	15
	Screen 4	720	755	35
Middle Potomac Aquifer (MPA)				
	Screen 5	820	835	15
	Screen 6	860	890	30
	Screen 7	905	920	15
	Screen 8	965	990	25
	Screen 9	1050	1090	40
Lower Potomac Aquifer (LPA)				
	Screen 10	1230	1335	105
	Screen 11	1370	1400	30
(fbg) – feet below grade				

Table A-2. Well Screen Depth and Length of Screen in the Conventional Wells

Aquifer Zone		Starting Depth (fbg)	Ending Depth (fbg)	Length of Screen (ft)
MW-UPA (distance from TW-1 = 340')				
	Screen 1	515	565	50
	Screen 2	585	605	20
	Screen 3	660	675	15
	Screen 4	710	740	30
MW-MPA (distance from TW-1 = 390')				
	Screen 1	860	920	60
	Screen 2	975	990	15
	Screen 3	1030	1090	60
MW-LPA (distance from TW-1 = 440')				
	Screen 1	1260	1320	60
	Screen 2	1350	1410	60
(fbg) – feet below grade				

Figure A-2. TW-1 Well Completion Report. This includes well location information, screen depths, well diameter, and soil type with depth. (Includes the next 6 pages.)

Form GW-2
Revised 7/1/2015
Page 1 of 4

COMMONWEALTH OF VIRGINIA
UNIFORM WATER WELL COMPLETION REPORT

DEQ Well # 161-597
USGS Local # 59 0 33
VDH HDIN #
VDH PWSID #

1. Contact Information

Contact:	Name	Address	Phone
Owner	HRSD	1436 Air Rail Ave. Virginia Beach, VA 23455	757460-4242
Driller	William Howe, ACSM	8221 Cloverleaf Drive, Millersville, MD 21108	410-841-6710
System Provider	HRSD	6909 Armstead Rd. Suffolk, VA 23435	757-636-7363

2. Well Location

Physical Address: 6909 Armstead Rd.		County/City: Suffolk	
Subdivision Name: Nansemond WWTP		Section:	Block: Lot:
Tax Map/GPIN #: 0499-01-5074		Well Designation or Number: Injection TW #1	
Latitude: 36.5339.549	N	Longitude: -76.2531.351	W
Datum Source	Horizontal: <input checked="" type="checkbox"/> WGS84 <input type="checkbox"/> NAD83 <input type="checkbox"/> NAD27	Vertical: <input type="checkbox"/> NGVD29 <input type="checkbox"/> NAVD88	
Lat/Long Source (Check One): <input type="checkbox"/> Map <input checked="" type="checkbox"/> GPS <input type="checkbox"/> PPDGPS <input type="checkbox"/> Survey <input type="checkbox"/> Imagery <input type="checkbox"/> WASS			
Location Information Collected By : Scott Bruce			
Physical Location Description: Tax map 6 Parcel 1D			

3. Facility & Use

Type of Facility (Check One):		Type of Use (Check All That Apply):	
<input checked="" type="checkbox"/> Waterworks	<input type="checkbox"/> Drinking/Domestic Use	<input type="checkbox"/> Food Processing	<input type="checkbox"/> Cooling/Heating
<input type="checkbox"/> Observation/Monitoring Well	<input type="checkbox"/> Agricultural	<input type="checkbox"/> Manufacturing	<input checked="" type="checkbox"/> Injection
<input type="checkbox"/> Private Well	<input type="checkbox"/> Irrigation	<input type="checkbox"/> Fire Safety	<input type="checkbox"/> Geothermal

4. Well Construction

Well designation, Name or Number: Injection TW #1			
Date Started: 5/8/16		Date Completed: 8/23/16	
Class Well (Check One): <input type="checkbox"/> I <input type="checkbox"/> IIA <input type="checkbox"/> IIB <input type="checkbox"/> IIIA <input type="checkbox"/> IIIB <input type="checkbox"/> IIIC <input type="checkbox"/> IIID <input type="checkbox"/> IIIE <input type="checkbox"/> IV		Type Rig: SS40 Mud Rotary	
Construction Type (Check One): <input checked="" type="checkbox"/> New <input type="checkbox"/> Existing-Modified			
Well Depth: 1410 ft.		Borehole Depth: 1420 ft.	
Hole Size (include reamed zones): 28" inches from 0 to 100 ft.		Depth to Bedrock: N/A ft.	
Height of Casing above Land Surface: 3 ft. inches			
Casing Size (I.D.) and Materials: (below)		Total Depth of Casing: ft.	
20 inches from 0 to 100 ft.	Material Steel	Weight per ft. 78.6 or wall thickness .375 in.	
12 inches from 0 to 505 ft.	Material Steel	Weight per ft. 49.56 or wall thickness .375 in.	
12 inches from 530 to 550 ft.	Material Steel	Weight per ft. 49.56 or wall thickness .375 in.	
12 inches from 595 to 665 ft.	Material Steel	Weight per ft. 49.56 or wall thickness .375 in.	
12 inches from 660 to 720 ft.	Material Steel	Weight per ft. 49.56 or wall thickness .375 in.	
Screen Size & Mesh:			
12 inches from 505 to 530 ft.	Mesh Size .040	Type 304 SS	
12 inches from 550 to 595 ft.	Mesh Size .040	Type 304 SS	
12 inches from 665 to 680 ft.	Mesh Size .040	Type 304 SS	
Water Zones: from 475 to 680 ft.		from 720 to 1090 ft.	from 1230 to 1400 ft.
Gravel Pack: from 475 to 790 ft.		from 800 to 1150 ft.	from 1160 to 1420 ft.
Grout Type: from 0 to 100 ft.		Grouting Method: Tremie	Type of Seal: Cement
This information was collected by Camera Survey: <input type="checkbox"/> Yes <input checked="" type="checkbox"/> No Date Conducted:			
Additional Well Construction Form Information Attached: <input checked="" type="checkbox"/> Yes <input type="checkbox"/> No			

COMMONWEALTH OF VIRGINIA
 UNIFORM WATER WELL COMPLETION REPORT

DEQ Well # 161-597
 USGS Local # 59033
 VDH HDIN #
 VDH PWSID #

Well designation, Name or Number: Injection TW #1

5. Disinfection

Well Disinfected: <input checked="" type="checkbox"/> Yes <input type="checkbox"/> No	Date: 8/11/20216
---	------------------

6. Abandonment (*When abandoning a well, Sections 1 thru 6 are required to be completed) N/A

Date Started:	Date Completed:	Type Rig:
Static Water Level (unpumped level measured):		ft.
Casing Size (I.D.) and Materials:	Casing Pulled: <input type="checkbox"/> Yes <input type="checkbox"/> No <input type="checkbox"/> Uncased Well	
Depth of Fill:	Type and Source of Fill:	
Grout: From 790 to 800 Type:	From 1150 to 1160 Type:	
Method of permanently marking location:		

7. Pump Test

Static Water Level (unpumped level measured): 95.17		ft.
Date: 8-3-16	Method (Check One): <input type="checkbox"/> Water Tape <input type="checkbox"/> Airline <input checked="" type="checkbox"/> Transducer <input type="checkbox"/> Other	
Stabilized measured pumping water level: 127.3		ft.
Date: 8-4-16	Method (Check One): <input type="checkbox"/> Top of Well <input checked="" type="checkbox"/> Top of Casing <input type="checkbox"/> Surface Level	
Test Pump Intake Depth: 260	ft	Stabilized Yield: 1100 gpm after 24 hours
Natural Flow: <input type="checkbox"/> Yes <input checked="" type="checkbox"/> No	Flow Rate	gpm

8. Pump Data N/A

Type:	Motor HP:
Production Pump Intake Depth: ft	Rated Capacity: gpm at ft TDH

9. Geologic Information Potomac

Formation: Upper, Middle, Lower	Type Logs: Electric and Gemma
Lithology:	Cuttings: Ditch
Province:	Aquifer Test Performed: Yes 24 hr.
Geologic Map Used:	
Water Quality Results Attached: Yes <input type="checkbox"/> No <input checked="" type="checkbox"/>	

Comments:

COMMONWEALTH OF VIRGINIA
 UNIFORM WATER WELL COMPLETION REPORT

DEQ Well # 161-597
 USGS Local # 55 C 32
 VDH HDIN # _____
 VDH PWSID # _____

10. Driller's Log (Use additional sheets if necessary)

Well designation, Name or Number: <u>Injection TW#1</u>					
Depth (feet)		Type of Rock or Soil	Remarks	Drilling Time (Min.)	Diagram of Well Construction (with dimensions)
From	To	(Color, material, fossils, hardness, etc.)	(Water, caving, cavities, etc.)		
0	30	Yellow clay and sand			(See Attached)
30	40	Yellow clay and sand with shells			
40	60	Red, sandy clay and shell			
60	80	Shells and sand			
80	90	Gray clay and shells			
90	207	Gray clay with shells and sand			
207	210	Hard layer			
210	366	Green clay with shells			
366	371	Silty sand			
371	400	Green clay with shells			
400	401	Hard layer			
401	406	Clay			
406	407	Hard layer			
407	433	Silty sand and clay			
433	465	Clay green and gray			
465	492	Sand			
492	504	Hard clay with sand streaks			
504	515	Sand with clay layer			
515	537	Sand			
537	546	Clay			
546	617	Sand			
617	640	Sand			
640	648	Sand with clay layers			
648	655	clay and sand			
655	680	Sand			
680	691	Hard clay			
691	709	Sandy clay with sand			
709	710	Clay			
710	741	Silty clay, sand and clay layers			
741	764	Sand			
764	767	Silty clay			
767	772	Clay med hard			
772	794	Sand			
794	795	Soft clay			
795	814	Hard clay			

I certify that the information contained herein is true and correct and that this well and/or system has been installed and constructed in accordance with the applicable permit and further that the well complies with all applicable federal, state and local regulations, ordinances and laws.

Signature: Walter Hovs

Date: 9/20/12

License Number: 2719000622

COMMONWEALTH OF VIRGINIA
 UNIFORM WATER WELL COMPLETION REPORT

DEQ Well # 161-597
 USGS Local # 88 D 88
 VDH HDIN # _____
 VDH PWSID # _____

10. Driller's Log (Use additional sheets if necessary)

Well designation, Name or Number:					
Depth (feet)		Type of Rock or Soil	Remarks	Drilling Time (min.)	Diagram of Well Construction (with dimensions)
From	To	(Color, material, fossils, hardness, etc.)	(Water, casing, cavities, etc.)		
814	834	Soft green clay and sand			(See Attached)
834	855	Clay with layer of sand			
855	865	Sand with clay streaks			
865	885	Clay & sand mix, more clay			
885	895	Harder clay with sand streaks			
895	921	Soft clay with sand layers			
921	926	Med hard clay			
926	934	Hard, red clay			
934	947	Red and gray clay hard			
947	958	Hard red and gray clay			
958	968	Gray and red clay			
968	973	Gray clay			
973	989	Sand and gray clay			
989	1020	Med hard clay			
1020	1026	Med hard clay			
1026	1050	Sand and sandy clay			
1050	1077	Good sand			
1077	1085	Sand with clay layers			
1085	1097	Sand and clay layer 50/50 mix			
1097	1113	Hard red and gray clay			
1113	1122	Hard clay with sand layers			
1122	1139	Good sand			
1139	1141	Hard clay			
1141	1142	Sand			
1142	1156	Very hard clay			
1156	1164	Softer clay			
1164	1180	Sandy clay and sand			
1180	1191	Hard red and gray clay			
1191	1205	Sandy clay and sand			
1205	1209	Sand			
1209	1231	Med hard red & gray clay w/sand streaks			
1231	1235	Hard clay			
1235	1239	Med hard clay			
1239	1256	Sand			

I certify that the information contained herein, is true and correct and that this well and/or system has been installed and constructed in accordance with the applicable permit and further that the well complies with all applicable federal, state and local regulations, ordinances and laws.

Signature: Will Howe Date: 9/20/16

License Number: 2719000622

COMMONWEALTH OF VIRGINIA
 UNIFORM WATER WELL COMPLETION REPORT

DEQ Well # 161-597
 USGS Local # 59 C 32
 VDH HDIN # _____
 VDH PWSID # _____

10. Driller's Log (Use additional sheets if necessary)

Well designation, Name or Number:					
Depth (feet)		Type of Rock or Soil	Remarks	Drilling Time (Min.)	Diagram of Well Construction (with dimensions)
From	To	(Color, material, fossils, hardness, etc.)	(Water, caving, cavities, etc.)		
1258	1261	Clay with sand layers			(See Attached)
1261	1266	Sand with clay streaks			
1266	1297	Sand with clay layers			
1297	1325	Sand with clay layers			
1325	1328	Clay with sand streaks			
1328	1340	Sand			
1340	1353	Hard clay			
1353	1358	Softer clay with sand layers			
1358	1368	Sand			
1368	1388	Sand with clay streaks			
1388	1389	Clay			
1389	1398	Sand			
1398	1416	Clay and sand			
1416	1420	Tight, dense clay			

I certify that the information contained herein is true and correct and that this well and/or system has been installed and constructed in accordance with the applicable permit and further that the well complies with all applicable federal, state and local regulations, ordinances and laws.

Signature: Walter Howe Date: 9/20/12

License Number: 2719000622

Additional Well Construction Data

Well designation, Name or Number: Injection TW #1											
Physical Location: 6909 Armstead Rd.				Date Started: 5/8/16				Date Completed: 8/23/16			
Hole Size (Include reamed zones):											
inches	from	to	ft.	inches	from	to	ft.	inches	from	to	ft.
inches	from	to	ft.	inches	from	to	ft.	inches	from	to	ft.
inches	from	to	ft.	inches	from	to	ft.	inches	from	to	ft.
Casing Size (I.D.) and Materials:											
12	inches	from	755	to	820	ft.	Material	Steel	Weight per ft.	49.56	or wall thickness .375 in.
12	inches	from	835	to	860	ft.	Material	Steel	Weight per ft.	49.56	or wall thickness .375 in.
12	inches	from	890	to	905	ft.	Material	Steel	Weight per ft.	49.56	or wall thickness .375 in.
12	inches	from	920	to	965	ft.	Material	Steel	Weight per ft.	49.56	or wall thickness .375 in.
12	inches	from	990	to	1050	ft.	Material	Steel	Weight per ft.	49.56	or wall thickness .375 in.
12	inches	from	1090	to	1230	ft.	Material	Steel	Weight per ft.	49.56	or wall thickness .375 in.
12	inches	from	1335	to	1370	ft.	Material	Steel	Weight per ft.	49.56	or wall thickness .375 in.
12	inches	from	1400	to	1410	ft.	Material	Steel	Weight per ft.	49.56	or wall thickness .375 in.
	inches	from		to		ft.	Material		Weight per ft.		or wall thickness in.
	inches	from		to		ft.	Material		Weight per ft.		or wall thickness in.
	inches	from		to		ft.	Material		Weight per ft.		or wall thickness in.
Screen Size & Mesh:											
12	inches	from	720	to	755	ft.	Mesh Size	.040	Type	304 SS	
12	inches	from	820	to	835	ft.	Mesh Size	.040	Type	304 SS	
12	inches	from	860	to	890	ft.	Mesh Size	.040	Type	304 SS	
12	inches	from	905	to	920	ft.	Mesh Size	.040	Type	304 SS	
12	inches	from	965	to	990	ft.	Mesh Size	.040	Type	304 SS	
12	inches	from	1050	to	1090	ft.	Mesh Size	.040	Type	304 SS	
12	inches	from	1230	to	1335	ft.	Mesh Size	.040	Type	304 SS	
12	inches	from	1370	to	1400	ft.	Mesh Size	.040	Type	304 SS	
	inches	from		to		ft.	Mesh Size		Type		
	inches	from		to		ft.	Mesh Size		Type		
	inches	from		to		ft.	Mesh Size		Type		
Water Zones:											
From	to	ft.	From	to	ft.	From	to	ft.	From	to	ft.
From	to	ft.	From	to	ft.	From	to	ft.	From	to	ft.
From	to	ft.	From	to	ft.	From	to	ft.	From	to	ft.
From	to	ft.	From	to	ft.	From	to	ft.	From	to	ft.
Gravel Pack:											
From	to	ft.	From	to	ft.	From	to	ft.			
From	to	ft.	From	to	ft.	From	to	ft.			
From	to	ft.	From	to	ft.	From	to	ft.			
Grout: Type: Neat Cement Slurry from 790 to 800 ft.											
Grout: Type: Neat Cement Slurry from 1150 to 1160 ft.											
Grout: Type: Neat cement slurry from 0 to 475 ft.											

Figure A-3. MW-SAT Well Completion Report. This includes well location information, screen depths, well diameter, and soil type with depth. (Includes the next 6 pages.)

Form GW-2
Revised 7/1/2015
Page 1 of 4

COMMONWEALTH OF VIRGINIA
UNIFORM WATER WELL COMPLETION REPORT

DEQ Well # 161-606
USGS Local # _____
VDH HDIN # _____
VDH PWSID # _____

1. Contact Information

Contact:	Name	Address	Phone
Owner	HRSD	1436 Air Rail Ave. Virginia Beach, VA 23455	757460-4242
Driller	Keegan Hartman, ACSM	8221 Cloverleaf Drive, Millersville, MD 21108	410-841-6710
System Provider	HRSD	5909 Armstead Rd. Suffolk, VA 23435	757-638-7363

2. Well Location

Physical Address: 6909 Armstead Rd. County/City: Suffolk
 Subdivision Name: Nansemond WWTP Section: Block: Lot:
 Tax Map/GPIN #: 0499-01-5074 Well Designation or Number: MW01-SAT
 Latitude: 36.53397935 N Longitude: -76.253181452 W
 Datum Source Horizontal: WGS84 NAD83 NAD27 Vertical: NGVD29 NAVD88
 Lat/Long Source (Check One): Map GPS PPDGPS Survey Imagery WASS
 Location Information Collected By: Scott Bruce
 Physical Location Description: Tax map 6 Parcel 1D

3. Facility & Use

Type of Facility (Check One):	Type of Use (Check All That Apply):
<input checked="" type="checkbox"/> Waterworks	<input type="checkbox"/> Drinking/Domestic Use <input type="checkbox"/> Food Processing <input type="checkbox"/> Cooling/Heating
<input type="checkbox"/> Observation/Monitoring Well	<input type="checkbox"/> Agricultural <input type="checkbox"/> Manufacturing <input checked="" type="checkbox"/> Injection
<input type="checkbox"/> Private Well	<input type="checkbox"/> Irrigation <input type="checkbox"/> Fire Safety <input type="checkbox"/> Geothermal

4. Well Construction

Well designation, Name or Number: MW01-SAT
 Date Started: 5/4/2017 Date Completed: 8/1/2017 Type Rig: CF-15 Mud Rotary
 Class Well (Check One): I IIA IIB IIIA IIIB IIIC IIID IIIE IV
 Construction Type (Check One): New Existing-Modified
 Well Depth: 1410 ft. Borehole Depth: 1420 ft. Depth to Bedrock: N/A ft.
 Hole Size (include reamed zones): 20 inches from 0 to 104 ft. 13 inches from 100 to 1420 ft.
 Height of Casing above Land Surface: 2.5 ft. inches
 Casing Size (I.D.) and Materials: (below) Total Depth of Casing: ft.

14 inches from 0 to 103 ft.	Material Steel	Weight per ft. 54.57 or wall thickness 375 in.
6 inches from 0 to 505 ft.	Material Steel	Weight per ft. 18.99 or wall thickness 280 in.
6 inches from 530 to 550 ft.	Material Steel	Weight per ft. 18.99 or wall thickness 280 in.
6 inches from 595 to 665 ft.	Material Steel	Weight per ft. 18.99 or wall thickness 280 in.
6 inches from 680 to 720 ft.	Material Steel	Weight per ft. 18.99 or wall thickness 280 in.

 Screen Size & Mesh:

6 inches from 505 to 530 ft.	Mesh Size .040	Type 304 SS
6 inches from 550 to 595 ft.	Mesh Size .040	Type 304 SS
6 inches from 665 to 680 ft.	Mesh Size .040	Type 304 SS

 Water Zones: from 475 to 680 ft. from 720 to 1090 ft. from 1230 to 1400 ft.
 Gravel Pack: from 475 to 790 ft. from 800 to 1150 ft. from 1160 to 1420 ft.
 Grout Type: Cement from 0 to 104 ft. Grouting Method: Tremie Type of Seal: Cement
 This information was collected by Camera Survey: Yes No Date Conducted:
 Additional Well Construction Form Information Attached: Yes No

COMMONWEALTH OF VIRGINIA
 UNIFORM WATER WELL COMPLETION REPORT

DEQ Well # 161-606
 USGS Local # _____
 VDH HDIN # _____
 VDH PWSID # _____

Well designation, Name or Number: MW01-SAT

5. Disinfection

Well Disinfected: Yes No Date: 8/11/20216

6. Abandonment (*When abandoning a well, Sections 1 thru 6 are required to be completed) N/A

Date Started:	Date Completed:	Type Rig:
Static Water Level (unpumped level measured):		ft.
Casing Size (L.D.) and Materials:		Casing Pulled: <input type="checkbox"/> Yes <input type="checkbox"/> No <input type="checkbox"/> Uncased Well
Depth of Fill:	Type and Source of Fill:	
Grout: From 790 to 800 Type:	From 1150 to 1160 Type:	
Method of permanently marking location:		

7. Pump Test

Static Water Level (unpumped level measured): 95.17		ft.	
Date: 8-3-16	Method (Check One): <input type="checkbox"/> Water Tape <input type="checkbox"/> Airline <input checked="" type="checkbox"/> Transducer <input type="checkbox"/> Other		
Stabilized measured pumping water level: 127.3		ft.	
Date: 8-4-16	Method (Check One): <input type="checkbox"/> Top of Well <input checked="" type="checkbox"/> Top of Casing <input type="checkbox"/> Surface Level		
Test Pump Intake Depth: 260	ft.	Stabilized Yield: 1100	gpm after 24 hours
Natural Flow: <input type="checkbox"/> Yes <input checked="" type="checkbox"/> No	Flow Rate	gpm	

8. Pump Data N/A

Type:	Motor HP:
Production Pump Intake Depth: _____	ft. Rated Capacity: _____
	gpm at _____ ft TDH

9. Geologic Information Potomac

Formation: Upper, Middle, Lower	Type Logs: Electric and Gemma
Lithology:	Cuttings: Ditch
Province:	Aquifer Test Performed: Yes 24 hr.
Geologic Map Used:	
Water Quality Results Attached: Yes <input type="checkbox"/> No <input checked="" type="checkbox"/>	

Comments:

Airlifted the well to test yield.

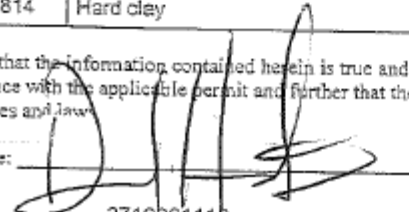
COMMONWEALTH OF VIRGINIA
 UNIFORM WATER WELL COMPLETION REPORT

DEQ Well # 161-806
 USGS Local # _____
 VDH HDIN # _____
 VDH PWSID # _____

10. Driller's Log (Use additional sheets if necessary)

Well designation, Name or Number: MW01-SAT					
Depth (feet)		Type of Rock or Soil	Remarks	Drilling Time (Min.)	Diagram of Well Construction (with dimensions)
From	To	(Color, material, fossils, hardness, etc.)	(Water, casing, cavities, etc.)		
0	30	Yellow clay and sand			(See Attached)
30	40	Yellow clay and sand with shells			
40	60	Red, sandy clay and shell			
60	80	Shells and sand			
80	90	Gray clay and shells			
90	207	Gray clay with shells and sand			
207	210	Hard layer			
210	366	Green clay with shells			
366	371	Silty sand			
371	400	Green clay with shells			
400	401	Hard layer			
401	406	Clay			
406	407	Hard layer			
407	433	Silty sand and clay			
433	465	Clay green and gray			
465	492	Sand			
492	504	Hard clay with sand streaks			
504	515	Sand with clay layer			
515	537	Sand			
537	546	Clay			
546	617	Sand			
617	640	Sand			
640	648	Sand with clay layers			
648	655	clay and sand			
655	680	Sand			
680	691	Hard clay			
691	709	Sandy clay with sand			
709	710	Clay			
710	741	Silty clay, sand and clay layers			
741	764	Sand			
764	767	Silty clay			
767	772	Clay med hard			
772	794	Sand			
794	795	Soft clay			
795	814	Hard clay			

I certify that the information contained herein is true and correct and that this well and/or system has been installed and constructed in accordance with the applicable permit and further that the well complies with all applicable federal, state and local regulations, ordinances and laws.

Signature: 

Date: 10/6/2017

License Number: 2719001110

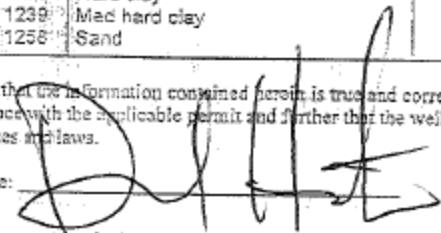
COMMONWEALTH OF VIRGINIA
 UNIFORM WATER WELL COMPLETION REPORT

DEQ Well # 161-606
 USGS Local # _____
 VDH HDIN # _____
 VDH PWSID # _____

10. Driller's Log (Use additional sheets if necessary)

Well designation, Name or Number: <u>MWD1-SAT</u>					
Depth (feet)		Type of Rock or Soil	Remarks	Drilling Time (Min.)	Diagram of Well Construction (with dimensions)
From	To	(Color, material, fossils, hardness, etc.)	(Water, casing, cavities, etc.)		
814	834	Soft green clay and sand			(See Attached)
834	859	Clay with layer of sand			
855	865	Sand with clay streaks			
865	885	Clay & sand mix, more clay			
885	896	Harder clay with sand streaks			
895	921	Soft clay with sand layers			
921	926	Med. hard clay			
926	934	Hard, red clay			
934	947	Red and gray clay hard			
947	958	Hard red and gray clay			
958	968	Gray and red clay			
968	973	Gray clay			
973	989	Sand and gray clay			
989	1020	Med hard clay			
1020	1025	Med hard clay			
1025	1050	Sand and sandy clay			
1050	1077	Good sand			
1077	1085	Sand with clay layers			
1085	1097	Sand and clay layer 50/50 mix			
1097	1113	Hard red and gray clay			
1113	1122	Hard clay with sand layers			
1122	1139	Good sand			
1139	1141	Hard clay			
1141	1142	Sand			
1142	1156	Very hard clay			
1156	1164	Softer clay			
1164	1180	Sandy clay and sand			
1180	1191	Hard red and gray clay			
1191	1205	Sandy clay and sand			
1205	1209	Sand			
1209	1231	Med hard red & gray clay w/sand streaks			
1231	1235	Hard clay			
1235	1239	Med hard clay			
1239	1258	Sand			

I certify that the information contained herein is true and correct and that this well and/or system has been installed and constructed in accordance with the applicable permit and further that the well complies with all applicable federal, state and local regulations, ordinances and laws.

Signature:  Date: 10/6/2017

License Number: 2719001110

COMMONWEALTH OF VIRGINIA
 UNIFORM WATER WELL COMPLETION REPORT

DEQ Well # 161-606
 USGS Local # _____
 VDH HDIN # _____
 VDH PWSID # _____

10. Driller's Log (Use additional sheets if necessary)

Well designation, Name or Number: MW01-SAT					
Depth (feet)		Type of Rock or Soil	Remarks	Drilling Time (Min.)	Diagram of Well Construction (with dimensions)
From	To	(Color, material, fossils, hardness, etc.)	(Water, caving, cavities, etc.)		
1258	1261	Clay with sand layers			(See Attached)
1261	1266	Sand with clay streaks			
1266	1297	Sand with clay layers			
1297	1325	Sand with clay layers			
1325	1328	Clay with sand streaks			
1328	1340	Sand			
1340	1353	Hard clay			
1353	1358	Softer clay with sand layers			
1358	1368	Sand			
1368	1388	Sand with clay streaks			
1388	1389	Clay			
1389	1398	Sand			
1398	1416	Clay and sand			
1416	1420	Tight, dense clay			

I certify that the information contained herein is true and correct and that this well and/or system has been installed and constructed in accordance with the applicable permit and further that the well complies with all applicable federal, state and local regulations, ordinances and laws.

Signature: _____

Date: _____

10/16/2017

License Number: 2719001110

Additional Well Construction Data

Well designation, Name or Number: MW01-SAT														
Physical Location: 6909 Armstead Rd.				Date Started: 5/4/2017				Date Completed: 8/1/2017						
Hole Size (Include reamed zones):														
13	inches	from	104	to	1,420	ft.	inches	from	to	ft.	inches	from	to	ft.
	inches	from	to	ft.	inches	from	to	ft.	inches	from	to	ft.		
	inches	from	to	ft.	inches	from	to	ft.	inches	from	to	ft.		
Casing Size (I.D.) and Materials:														
6	inches	from	755	to	820	ft.	Material	Steel	Weight per ft.	18.99	or wall thickness	.280	in.	
6	inches	from	835	to	860	ft.	Material	Steel	Weight per ft.	18.99	or wall thickness	.280	in.	
6	inches	from	890	to	905	ft.	Material	Steel	Weight per ft.	18.99	or wall thickness	.280	in.	
6	inches	from	920	to	965	ft.	Material	Steel	Weight per ft.	18.99	or wall thickness	.280	in.	
6	inches	from	990	to	1050	ft.	Material	Steel	Weight per ft.	18.99	or wall thickness	.280	in.	
6	inches	from	1090	to	1230	ft.	Material	Steel	Weight per ft.	18.99	or wall thickness	.280	in.	
6	inches	from	1335	to	1370	ft.	Material	Steel	Weight per ft.	18.99	or wall thickness	.280	in.	
6	inches	from	1400	to	1410	ft.	Material	Steel	Weight per ft.	18.99	or wall thickness	.280	in.	
	inches	from	to	ft.	Material		Weight per ft.	18.99	or wall thickness	.280	in.			
	inches	from	to	ft.	Material		Weight per ft.	18.99	or wall thickness	.280	in.			
	inches	from	to	ft.	Material		Weight per ft.	18.99	or wall thickness	.280	in.			
Screen Size & Mesh:														
6	inches	from	720	to	755	ft.	Mesh Size	.040	Type	304 SS				
6	inches	from	820	to	835	ft.	Mesh Size	.040	Type	304 SS				
6	inches	from	860	to	890	ft.	Mesh Size	.040	Type	304 SS				
6	inches	from	905	to	920	ft.	Mesh Size	.040	Type	304 SS				
6	inches	from	965	to	990	ft.	Mesh Size	.040	Type	304 SS				
6	inches	from	1050	to	1090	ft.	Mesh Size	.040	Type	304 SS				
6	inches	from	1230	to	1335	ft.	Mesh Size	.040	Type	304 SS				
6	inches	from	1370	to	1400	ft.	Mesh Size	.040	Type	304 SS				
	inches	from	to	ft.	Mesh Size		Type							
	inches	from	to	ft.	Mesh Size		Type							
	inches	from	to	ft.	Mesh Size		Type							
Water Zones:														
From	to	ft.	From	to	ft.	From	to	ft.	From	to	ft.			
From	to	ft.	From	to	ft.	From	to	ft.	From	to	ft.			
From	to	ft.	From	to	ft.	From	to	ft.	From	to	ft.			
From	to	ft.	From	to	ft.	From	to	ft.	From	to	ft.			
Gravel Pack:														
From	to	ft.	From	to	ft.	From	to	ft.						
From	to	ft.	From	to	ft.	From	to	ft.						
From	to	ft.	From	to	ft.	From	to	ft.						
Grout: Type: Neat Cement Slurry from 0 to 475 ft.														
Grout: Type: Bentonite from 790 to 800 ft.														
Grout: Type: Bentonite from 1,150 to 1,160 ft.														

Figure A-4. MW-UPA Well Completion Report. This includes well location information, screen depths, well diameter, and soil type with depth. (Includes the next 4 pages.)

Form GW-2
 Revised 8/19/2016
 Page 1 of 4

COMMONWEALTH OF VIRGINIA
 UNIFORM WATER WELL COMPLETION REPORT

DEQ Well # 161-609
 USGS Local #59D44
 VDH HDIN # _____
 VDH PWSID # _____

*Indicates required field or section
 **Indicates required field or section, if applicable

1. Contact Information*

Contact:	Name	Address	Phone
Owner	Hampton Rds Sanitation Distr	1434 Air Rail Avenue Virginia Beach, VA 23455	(757) 460-2491
Driller	A.C. Schultes of Maryland, Inc	8221 Cloverleaf Drive Millersville, MD 21108	(410) 841-6710
System Provider	Hampton Rds Sanitation Distr	1434 Air Rail Avenue Virginia Beach, VA 23455	(757) 460-2491

2. Well Location*

Physical Address: 6909 Armstead Road Suffolk, VA 23435		County/City: Suffolk	
Subdivision Name: Nansemond WWTP		Section:	Block: Lot:
Tax Map/GPIN #: 0499-01-5074			
Latitude: 36.5336648		N	Longitude: -76.2533444
Datum Source		Horizontal: <input checked="" type="checkbox"/> WGS84 <input type="checkbox"/> NAD83 <input type="checkbox"/> NAD27	W
Lat/Long Source (Check One): <input type="checkbox"/> Map <input type="checkbox"/> GPS <input type="checkbox"/> PPDGPS <input type="checkbox"/> Survey <input type="checkbox"/> Imagery <input checked="" type="checkbox"/> WAAS			
Location Information Collected By : Scott Bruce			
Physical Location Description: Tax map 6 Parcel 1D			

3. Facility & Use*

Type of Facility (Check One):	Type of Use (Check All That Apply):
<input type="checkbox"/> Private	<input type="checkbox"/> Drinking/Domestic Use <input type="checkbox"/> Agricultural <input type="checkbox"/> Food Processing
<input checked="" type="checkbox"/> Waterworks	<input type="checkbox"/> Manufacturing <input type="checkbox"/> Irrigation <input checked="" type="checkbox"/> Injection
<input type="checkbox"/> Observation/Monitoring Well	<input type="checkbox"/> Geothermal (Cooling/Heating) <input type="checkbox"/> Fire Safety
	<input type="checkbox"/> Closed
	<input type="checkbox"/> Open: <input type="checkbox"/> Returned to Surface
	<input type="checkbox"/> Returned to Aquifer

4. Well Construction*

Well designation, Name or Number: MW04-UPA			
Date Started: 2/12/2018		Date Completed: 3/23/2018	
		Type Rig: Mud rotary	
Class Well (Check One): <input type="checkbox"/> I <input type="checkbox"/> IIA <input type="checkbox"/> IIB <input type="checkbox"/> IIIA <input type="checkbox"/> IIIB <input type="checkbox"/> IIIC <input type="checkbox"/> IIID <input type="checkbox"/> IIIE <input type="checkbox"/> IV			
Construction Type (Check One): <input checked="" type="checkbox"/> New <input type="checkbox"/> Existing-Modified: <input type="checkbox"/> Well <input type="checkbox"/> Pump: Date: _____			
Well Depth: 750 ft.		Total Hole (borehole) Depth: 760 ft.	
Hole Size (Include reamed zones): 18 inches from 0 to _____ ft.		Inches from _____ to _____ ft.	
Height of Casing above Land Surface: 2 ft. inches			
Casing Size (I.D.) and Materials: (below)		Total Depth of Casing: _____ ft.	
12 inches from 0 to 42 ft. <input type="checkbox"/> infilled		Material steel	
8 inches from 0 to 515 ft. <input type="checkbox"/> infilled		Material steel	
6 inches from 565 to 585 ft. <input type="checkbox"/> infilled		Material steel	
Screen Size & Mesh:		Weight per ft. or wall thickness .375n.	
6 inches from 515 to 585 ft. <input type="checkbox"/> infilled		Mesh Size .040	
6 inches from 585 to 605 ft. <input type="checkbox"/> infilled		Mesh Size .040	
6 inches from 660 to 675 ft. <input type="checkbox"/> infilled		Mesh Size .040	
Water Zones: from 510 to 570 ft.		from 580 to 610 ft. from 655 to 680 ft.	
Gravel Pack:			
Size: #2 Type: _____		from 495 to 760 ft. Size: _____ Type: _____	
Grout Type:		from 5 to 5 ft.	
<input type="checkbox"/> Bentonite Slurry <input checked="" type="checkbox"/> Neat Cement		Grouting Method:	
<input type="checkbox"/> Bentonite pellets/chips <input type="checkbox"/> Concrete		<input type="checkbox"/> Poured from surface	
<input type="checkbox"/> Neat Cement (5% bentonite)		<input type="checkbox"/> Poured through tremmie pipe	
from 0 to 495 ft.		<input checked="" type="checkbox"/> Pumped from bottom upward	
from 0 to 42 ft.		Type of Seal:	
		<input type="checkbox"/> pitless adapter	
		<input checked="" type="checkbox"/> sanitary seal	
Camera Survey: <input type="checkbox"/> Yes <input checked="" type="checkbox"/> No		Date Conducted: _____	
Additional Well Construction Form Information Attached: <input checked="" type="checkbox"/> Yes <input type="checkbox"/> No			

Well designation, Name or Number*: MW04-UPA

5. Disinfection

Well Disinfected: <input checked="" type="checkbox"/> Yes <input type="checkbox"/> No	Date: 3/15/2018
---	-----------------

6. Abandonment (*When abandoning the well, Sections 1 thru 4 must be completed and/or attach original GW-2) n/a

Date Started:	Date Completed:
Static Water Level (unpumped level measured):	ft.
Casing Size (I.D.) and Materials:	Casing Pulled: <input type="checkbox"/> Yes <input type="checkbox"/> No <input type="checkbox"/> Uncased Well
Depth of Fill:	Type and Source of Fill:
Grout: From to Type:	From to Type:
Method of permanently marking location:	

7. Pump Test**

Static Water Level (unpumped level measured):	96	ft.
Date:	3/20/2018	Method (Check One): <input checked="" type="checkbox"/> Water Tape <input type="checkbox"/> Airline <input checked="" type="checkbox"/> Transducer <input type="checkbox"/> Other
Stabilized measured pumping water level:	n/a	ft.
Date:		Method (Check One): <input type="checkbox"/> Top of Well <input checked="" type="checkbox"/> Top of Casing <input type="checkbox"/> Surface Level
Test Pump Intake Depth:		ft Stabilized Yield: 120 gpm after _____ hours
Natural Flow:	<input type="checkbox"/> Yes <input checked="" type="checkbox"/> No	Flow Rate _____ gpm
Estimated Well Yield:	120	gpm

8. Pump Data** n/a

Type: <input type="checkbox"/> submersible <input type="checkbox"/> Turbine <input type="checkbox"/> Shallow Jet <input type="checkbox"/> Deep Jet <input type="checkbox"/> Other: _____	Motor HP:
Production Pump Intake Depth:	ft Rated Capacity: _____ gpm at _____ ft TDH

9. Geologic Information

Type Logs: Electric and gamma	Aquifer Test Performed: No
Water Quality Results Attached: Yes <input type="checkbox"/> No <input checked="" type="checkbox"/>	

Comments:

Monitoring well for 12" injection well.

Formation _____	Lithology _____	Province _____	Geologic Map Used _____
Elevation _____			
For Office Use			

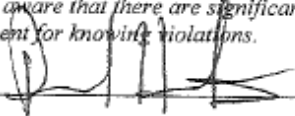
*Indicates required field or section
 **Indicates required field or section, if applicable

10. Driller's Log (Use additional sheets if necessary)*

Well designation, Name or Number: MW04-UPA					
Depth (feet)		Type of Rock or Soil	Remarks	Drilling Time (Min.)	Diagram of Well Construction (with dimensions)
From	To	(Color, material, fossils, hardness, etc.)	(Water, caving, cavities, etc.)		
0	1	Topsoil			Please see attached well "as built" diagram
1	27	Tan, sandy clay			
27	38	Tan/orange, very sandy clay with gravel			
38	97	Thick shell layers with blue/green silt becoming more clay			
97	145	Very soft silty, olive clay			
145	210	Silty, olive clay with salt and pepper sand			
210	353	Olive/blue clay some shell streaks			
353	498	Tight blue clay with some hard layers			
498	510	Red/brown clay			
510	570	Mixed sand with white streaks			
570	583	Clay			
583	678	Mixed sand with teal streaks			
678	708	Hard light blue clay			
708	752	Mixed sand with white streaks			
752	760	Hard, light blue clay			

11. Certification

I certify under penalty of law that this document and all attachments were prepared under my direction or supervision in accordance with a system designed to assure that qualified personnel properly gather and evaluate the information submitted. Based on my inquiry of the person or persons who manage the system or those persons directly responsible for gathering the information, the information submitted is to the best of my knowledge and belief true, accurate, and complete. I am aware that there are significant penalties for submitting false information including the possibility of fine and imprisonment for knowing violations.

Signature*: 

Date: 5/4/18

License Number: 2719001110

*Indicates required field or section
 **Indicates required field or section, if applicable

Additional Well Construction Data

(Use and submit only if additional space is needed)

12. Additional Well Construction Data

Well designation, Name or Number: MW04-UPA																
Physical Location: Tax map 6 Parcel 1D				Date Started: 2/12/2018				Date Completed: 3/23/2018								
Hole Size (Include reamed zones):																
18	inches	from	0	to	760	ft.		inches	from	to	ft.		inches	from	to	ft.
12	inches	from		to		ft.		inches	from	to	ft.		inches	from	to	ft.
	inches	from		to		ft.		inches	from	to	ft.		inches	from	to	ft.
Casing Size (I.D.) and Materials:																
6	inches	from	605	to	660	ft.	<input type="checkbox"/> infilled	Material	steel	Weight per ft.	or wall thickness	.322	in.			
6	inches	from	675	to	710	ft.	<input type="checkbox"/> infilled	Material	steel	Weight per ft.	or wall thickness	.322	in.			
6	inches	from	740	to	750	ft.	<input type="checkbox"/> infilled	Material	steel	Weight per ft.	or wall thickness	.322	in.			
	inches	from		to		ft.	<input type="checkbox"/> infilled	Material		Weight per ft.	or wall thickness		in.			
	inches	from		to		ft.	<input type="checkbox"/> infilled	Material		Weight per ft.	or wall thickness		in.			
	inches	from		to		ft.	<input type="checkbox"/> infilled	Material		Weight per ft.	or wall thickness		in.			
	inches	from		to		ft.	<input type="checkbox"/> infilled	Material		Weight per ft.	or wall thickness		in.			
	inches	from		to		ft.	<input type="checkbox"/> infilled	Material		Weight per ft.	or wall thickness		in.			
	inches	from		to		ft.	<input type="checkbox"/> infilled	Material		Weight per ft.	or wall thickness		in.			
	inches	from		to		ft.	<input type="checkbox"/> infilled	Material		Weight per ft.	or wall thickness		in.			
	inches	from		to		ft.	<input type="checkbox"/> infilled	Material		Weight per ft.	or wall thickness		in.			
Screen Size & Mesh:																
6	inches	from	710	to	740	ft.	<input type="checkbox"/> infilled	Mesh Size	.040	Type	304 stainless					
	inches	from		to		ft.	<input type="checkbox"/> infilled	Mesh Size		Type						
	inches	from		to		ft.	<input type="checkbox"/> infilled	Mesh Size		Type						
	inches	from		to		ft.	<input type="checkbox"/> infilled	Mesh Size		Type						
	inches	from		to		ft.	<input type="checkbox"/> infilled	Mesh Size		Type						
	inches	from		to		ft.	<input type="checkbox"/> infilled	Mesh Size		Type						
	inches	from		to		ft.	<input type="checkbox"/> infilled	Mesh Size		Type						
	inches	from		to		ft.	<input type="checkbox"/> infilled	Mesh Size		Type						
	inches	from		to		ft.	<input type="checkbox"/> infilled	Mesh Size		Type						
	inches	from		to		ft.	<input type="checkbox"/> infilled	Mesh Size		Type						
Water Zones:																
From	735	to	755	ft.	From		to	ft.	From		to	ft.	From		to	ft.
From		to	ft.	From		to	ft.	From		to	ft.	From		to	ft.	
From		to	ft.	From		to	ft.	From		to	ft.	From		to	ft.	
From		to	ft.	From		to	ft.	From		to	ft.	From		to	ft.	
Gravel Pack:																
Size:	Type:	From		to	ft.	Size:	Type:	From		to	ft.					
Size	Type:	From		to	ft.	Size:	Type:	From		to	ft.					
Size:	Type:	From		to	ft.	Size:	Type:	From		to	ft.					
Grout Type:						Grouting Method:										
<input type="checkbox"/> Bentonite Slurry						<input type="checkbox"/> Neat Cement										
<input type="checkbox"/> Bentonite pellets/chips						<input type="checkbox"/> Concrete										
<input type="checkbox"/> Neat Cement (6% bentonite)						<input type="checkbox"/> Poured from surface										
						<input type="checkbox"/> Poured through tremmie pipe										
						<input type="checkbox"/> Pumped from bottom upward										

Figure A-5. MW-MPA Well Completion Report. This includes well location information, screen depths, well diameter, and soil type with depth. (Includes the next 4 pages.)

Form GW-2
Revised 8/19/2016
Page 1 of 4

COMMONWEALTH OF VIRGINIA
UNIFORM WATER WELL COMPLETION REPORT

DEQ Well # 161-608
USGS Local #59D43
VDH HDIN #
VDH PWSID #

*Indicates required field or section
**Indicates required field or section, if applicable

1. Contact Information*

Contact:	Name	Address	Phone
Owner	Hampton Rds Sanitation Distr	1434 Air Rail Avenue Virginia Beach, VA 23455	(757) 460-2491
Driller	A.C. Schultes of Maryland, Inc	8221 Cloverleaf Drive Millersville, MD 21108	(410) 841-6710
System Provider	Hampton Rds Sanitation Distr	1434 Air Rail Avenue Virginia Beach, VA 23455	(757) 460-2491

2. Well Location*

Physical Address: 6909 Armstead Road		County/City: Suffolk	
Subdivision Name: Nansemond WWTP		Section:	Block: Lot:
Tax Map/GPIN #: 0499-01-5074			
Latitude: 36.5336170		N	Longitude: -76.2533593
Datum Source		Horizontal: <input checked="" type="checkbox"/> WGS84 <input type="checkbox"/> NAD83 <input type="checkbox"/> NAD27	W
Lat/Long Source (Check One): <input type="checkbox"/> Map <input type="checkbox"/> GPS <input type="checkbox"/> PPDGPS <input type="checkbox"/> Survey <input type="checkbox"/> Imagery <input checked="" type="checkbox"/> WAAS			
Location Information Collected By : Scott Bruce			
Physical Location Description: Tax map 6 Parcel 1D			

3. Facility & Use*

Type of Facility (Check One):	Type of Use (Check All That Apply):
<input type="checkbox"/> Private	<input type="checkbox"/> Drinking/Domestic Use <input type="checkbox"/> Agricultural <input type="checkbox"/> Food Processing
<input type="checkbox"/> Waterworks	<input type="checkbox"/> Manufacturing <input type="checkbox"/> Irrigation <input checked="" type="checkbox"/> Injection
<input type="checkbox"/> Observation/Monitoring Well	<input type="checkbox"/> Geothermal (Cooling/Heating) <input type="checkbox"/> Fire Safety
	<input type="checkbox"/> Closed
	<input type="checkbox"/> Open: <input type="checkbox"/> Returned to Surface
	<input type="checkbox"/> Returned to Aquifer

4. Well Construction*

Well designation, Name or Number: MW03-MPA			
Date Started: 11/7/2017		Date Completed: 2/7/2018	
Class Well (Check One): <input type="checkbox"/> I <input type="checkbox"/> IIA <input type="checkbox"/> IIB <input type="checkbox"/> IIIA <input type="checkbox"/> IIIB <input type="checkbox"/> IIIC <input type="checkbox"/> IIID <input type="checkbox"/> IIIE <input type="checkbox"/> IV		Type Rig: Mud rotary	
Construction Type (Check One): <input checked="" type="checkbox"/> New <input type="checkbox"/> Existing-Modified: <input type="checkbox"/> Well <input type="checkbox"/> Pump: Date 0			
Well Depth: 1,100 ft.		Total Hole (borehole) Depth: 1,340 ft.	
Hole Size (Include reamed zones): 18 inches from 0 to ft.		Depth to Bedrock: ft.	
Height of Casing above Land Surface: 2 ft. inches			
Casing Size (I.D.) and Materials: (below)		Total Depth of Casing: ft.	
12 inches from 0 to 98 ft. <input type="checkbox"/> infilled		Material black steel	
6 inches from 0 to 860 ft. <input type="checkbox"/> infilled		Weight per ft. or wall thickness .375n.	
6 inches from 920 to 975 ft. <input type="checkbox"/> infilled		Material steel	
		Weight per ft. or wall thickness .322n.	
Screen Size & Mesh:			
6 inches from 860 to 920 ft. <input type="checkbox"/> infilled		Mesh Size 0.045 slot	
6 inches from 975 to 990 ft. <input type="checkbox"/> infilled		Type 304 stainless	
6 inches from 1,030 to 1,090 ft. <input type="checkbox"/> infilled		Mesh Size 0.045 slot	
		Type 304 stainless	
Water Zones: from 857 to 923 ft. from 970 to 994 ft. from 1,026 to 1,095 ft.			
Gravel Pack:			
Size: #2 Type:		from 820 to 1,100 ft. Size: Type: from 0 to 0 ft.	
Grout Type:		Grouting Method:	
<input type="checkbox"/> Bentonite Slurry <input type="checkbox"/> Neat Cement		<input type="checkbox"/> Poured from surface	
<input type="checkbox"/> Bentonite pellets/chips <input type="checkbox"/> Concrete		<input type="checkbox"/> Poured through tremmie pipe	
<input type="checkbox"/> Neat Cement (6% bentonite)		<input type="checkbox"/> Pumped from bottom upward	
from 0 to 820 ft.		Type of Seal:	
from 0 to 30 ft.		<input type="checkbox"/> pitless adapter	
		<input checked="" type="checkbox"/> sanitary seal	
Camera Survey: <input type="checkbox"/> Yes <input checked="" type="checkbox"/> No			Date Conducted:
Additional Well Construction Form Information Attached: <input checked="" type="checkbox"/> Yes <input type="checkbox"/> No			

Well designation, Name or Number*: MW03-MPA

5. Disinfection

Well Disinfected: <input checked="" type="checkbox"/> Yes <input type="checkbox"/> No	Date: 2/2/2018
---	----------------

6. Abandonment (*When abandoning the well, Sections 1 thru 4 must be completed and/or attach original GW-2) n/a

Date Started:	Date Completed:
Static Water Level (unpumped level measured):	ft.
Casing Size (I.D.) and Materials:	Casing Pulled: <input type="checkbox"/> Yes <input type="checkbox"/> No <input type="checkbox"/> Uncased Well
Depth of Fill:	Type and Source of Fill:
Grout: From to Type:	From to Type:
Method of permanently marking location:	

7. Pump Test**

Static Water Level (unpumped level measured):	97	ft.
Date:	2/3/2018	Method (Check One): <input checked="" type="checkbox"/> Water Tape <input type="checkbox"/> Airline <input type="checkbox"/> Transducer <input type="checkbox"/> Other
Stabilized measured pumping water level:	n/a	ft.
Date:		Method (Check One): <input type="checkbox"/> Top of Well <input checked="" type="checkbox"/> Top of Casing <input type="checkbox"/> Surface Level
Test Pump Intake Depth:	n/a	ft. Stabilized Yield: 150 gpm after 8 hours
Natural Flow:	<input type="checkbox"/> Yes <input checked="" type="checkbox"/> No	Flow Rate gpm
Estimated Well Yield: 150 est. gpm		

8. Pump Data** n/a

Type: <input type="checkbox"/> submersible <input type="checkbox"/> Turbine <input type="checkbox"/> Shallow Jet <input type="checkbox"/> Deep Jet <input type="checkbox"/> Other: _____	Motor HP:
Production Pump Intake Depth:	ft. Rated Capacity: gpm at ft TDH

9. Geologic Information

Type Logs: Electric and gamma	Aquifer Test Performed: No
Water Quality Results Attached: Yes <input type="checkbox"/> No <input checked="" type="checkbox"/>	

Comments:

Monitoring well for 12" injection well

Formation _____	Lithology _____	Province _____	Geologic Map Used _____
Elevation _____			
For Office Use			

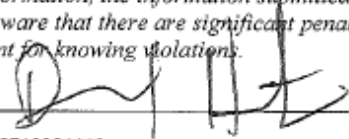
*Indicates required field or section
 **Indicates required field or section, if applicable

10. Driller's Log (Use additional sheets if necessary)*

Well designation, Name or Number: MW03-MPA					
Depth (feet)		Type of Rock or Soil	Remarks	Drilling Time (Min.)	Diagram of Well Construction (with dimensions)
From	To	(Color, material, fossils, hardness, etc.)	(Water, caving, cavities, etc.)		
0	2	Topsoil			Please see attached well "as built" diagram
2	25	Tan/gray, sandy clay			
25	35	Fine/med sand with shell			
35	96	Shell with sand and some silt layers			
96	142	Very silty olive green clay with shell			
142	248	Olive green silty clay with fine sand			
248	354	Olive/blue clay with shell			
354	373	Sandy silt, dark			
373	472	Blue clay w/cemented layers			
472	498	Med sand with light blue and white clay			
498	506	Red/brown clay			
506	570	Mixed sand w/white streaks			
570	593	White/green clay			
593	638	Mixed sand w/white clay			
638	656	Soft, light blue sandy silt			
656	684	Mixed sand			
684	708	Hard, light blue clay			
708	796	Mixed sand with white streaks			
796	810	Hard, teal clay			
810	923	Mixed sand with whitish blue			
923	955	Red/brown clay			
955	980	Soft, red/gray clay			
980	1,041	Red with light blue clay, sandy			
1,041	1,100	Mixed sand, some white clay			

11. Certification

I certify under penalty of law that this document and all attachments were prepared under my direction or supervision in accordance with a system designed to assure that qualified personnel properly gather and evaluate the information submitted. Based on my inquiry of the person or persons who manage the system or those persons directly responsible for gathering the information, the information submitted is to the best of my knowledge and belief true, accurate, and complete. I am aware that there are significant penalties for submitting false information including the possibility of fine and imprisonment for knowing violations.

Signature*: 

Date: 5/1/2018

License Number: 2719001110

*Indicates required field or section
 **Indicates required field or section, if applicable

Additional Well Construction Data

(Use and submit only if additional space is needed)

12. Additional Well Construction Data

Well designation, Name or Number: MW03-MPA													
Physical Location: Tax map 6 Parcel 1D				Date Started: 11/7/2017				Date Completed: 2/7/2018					
Hole Size (Include reamed zones):													
18	inches	from	0	to	ft.	inches	from	to	ft.	inches	from	to	ft.
12	inches	from		to	ft.	inches	from	to	ft.	inches	from	to	ft.
	inches	from		to	ft.	inches	from	to	ft.	inches	from	to	ft.
Casing Size (I.D.) and Materials:													
6	inches	from	990	to	1,030	ft.	<input type="checkbox"/> infilled	Material	Steel	Weight per ft.	or wall thickness	.322	in.
6	inches	from	1,090	to	1,100	ft.	<input type="checkbox"/> infilled	Material	Steel	Weight per ft.	or wall thickness	.322	in.
	inches	from		to	ft.	<input type="checkbox"/> infilled	Material		Weight per ft.	or wall thickness		in.	
	inches	from		to	ft.	<input type="checkbox"/> infilled	Material		Weight per ft.	or wall thickness		in.	
	inches	from		to	ft.	<input type="checkbox"/> infilled	Material		Weight per ft.	or wall thickness		in.	
	inches	from		to	ft.	<input type="checkbox"/> infilled	Material		Weight per ft.	or wall thickness		in.	
	inches	from		to	ft.	<input type="checkbox"/> infilled	Material		Weight per ft.	or wall thickness		in.	
	inches	from		to	ft.	<input type="checkbox"/> infilled	Material		Weight per ft.	or wall thickness		in.	
	inches	from		to	ft.	<input type="checkbox"/> infilled	Material		Weight per ft.	or wall thickness		in.	
	inches	from		to	ft.	<input type="checkbox"/> infilled	Material		Weight per ft.	or wall thickness		in.	
	inches	from		to	ft.	<input type="checkbox"/> infilled	Material		Weight per ft.	or wall thickness		in.	
Screen Size & Mesh:													
	inches	from		to	ft.	<input type="checkbox"/> infilled	Mesh Size		Type				
	inches	from		to	ft.	<input type="checkbox"/> infilled	Mesh Size		Type				
	inches	from		to	ft.	<input type="checkbox"/> infilled	Mesh Size		Type				
	inches	from		to	ft.	<input type="checkbox"/> infilled	Mesh Size		Type				
	inches	from		to	ft.	<input type="checkbox"/> infilled	Mesh Size		Type				
	inches	from		to	ft.	<input type="checkbox"/> infilled	Mesh Size		Type				
	inches	from		to	ft.	<input type="checkbox"/> infilled	Mesh Size		Type				
	inches	from		to	ft.	<input type="checkbox"/> infilled	Mesh Size		Type				
	inches	from		to	ft.	<input type="checkbox"/> infilled	Mesh Size		Type				
	inches	from		to	ft.	<input type="checkbox"/> infilled	Mesh Size		Type				
	inches	from		to	ft.	<input type="checkbox"/> infilled	Mesh Size		Type				
Water Zones:													
From	to	ft.	From	to	ft.	From	to	ft.	From	to	ft.		
From	to	ft.	From	to	ft.	From	to	ft.	From	to	ft.		
From	to	ft.	From	to	ft.	From	to	ft.	From	to	ft.		
From	to	ft.	From	to	ft.	From	to	ft.	From	to	ft.		
Gravel Pack:													
Size:	Type:	From	to	ft.	Size:	Type:	From	to	ft.				
Size:	Type:	From	to	ft.	Size:	Type:	From	to	ft.				
Size:	Type:	From	to	ft.	Size:	Type:	From	to	ft.				
Grout Type:				from	to	ft.	Grouting Method:						
<input type="checkbox"/> Bentonite Slurry				<input type="checkbox"/> Neat Cement		from	to	ft.	<input type="checkbox"/> Poured from surface				
<input type="checkbox"/> Bentonite pellets/chips				<input type="checkbox"/> Concrete		from	to	ft.	<input type="checkbox"/> Poured through tremmie pipe				
<input type="checkbox"/> Neat Cement (6% bentonite)				from	to	ft.	<input type="checkbox"/> Pumped from bottom upward						

Figure A-6. MW-LPA Well Completion Report. This includes well location information, screen depths, well diameter, and soil type with depth. (Includes the next 5 pages.)

Form GW-2
Revised 7/1/2015
Page 1 of 4

COMMONWEALTH OF VIRGINIA
UNIFORM WATER WELL COMPLETION REPORT

DEQ Well # 161-607
USGS Local # 59 D 42
VDH HDIN # _____
VDH PWSID # _____

1. Contact Information

Contact:	Name	Address	Phone
Owner	Hampton Roads Sanitation District	1436 Air Rail Ave. Virginia Beach, VA 23455	(757) 460-4242
Driller	Keegan Hartman, ACSM	8221 Cloverleaf Drive Millersville, MD 21108	(410) 841-6710
System Provider	Hampton Roads Sanitation District	6909 Armstead Road Suffolk, VA 23435	(757) 638-7363

2. Well Location

Physical Address: 6909 Armstead Road		County/City: Suffolk	
Subdivision Name: Nansemond WWTP		Section:	Block: Lot:
Tax Map/GPIN #: 0499-01-5074		Well Designation or Number: MW02-LPA	
Latitude: 36.5335718 N		Longitude: -76.2533757 W	
Datum Source	Horizontal: <input type="checkbox"/> WGS84 <input type="checkbox"/> NAD83 <input type="checkbox"/> NAD27	Vertical: <input type="checkbox"/> NGVD29 <input type="checkbox"/> NAVD88	
Lat/Long Source (Check One): <input type="checkbox"/> Map <input checked="" type="checkbox"/> GPS <input type="checkbox"/> PPDGPS <input type="checkbox"/> Survey <input type="checkbox"/> Imagery <input type="checkbox"/> WASS			
Location Information Collected By: Scott Bruce			
Physical Location Description: Tax map 6 Parcel 1D			

3. Facility & Use

Type of Facility (Check One):	Type of Use (Check All That Apply):		
<input checked="" type="checkbox"/> Waterworks	<input type="checkbox"/> Drinking/Domestic Use	<input type="checkbox"/> Food Processing	<input type="checkbox"/> Cooling/Heating
<input type="checkbox"/> Observation/Monitoring Well	<input type="checkbox"/> Agricultural	<input type="checkbox"/> Manufacturing	<input checked="" type="checkbox"/> Injection
<input type="checkbox"/> Private Well	<input type="checkbox"/> Irrigation	<input type="checkbox"/> Fire Safety	<input type="checkbox"/> Geothermal

4. Well Construction

Well designation, Name or Number: MW02-LPA			
Date Started: 8/24/2017	Date Completed: 9/22/2017	Type Rig: SS40 Mud Rotary	
Class Well (Check One): <input type="checkbox"/> I <input type="checkbox"/> IIA <input type="checkbox"/> IIB <input type="checkbox"/> IIIA <input type="checkbox"/> IIIB <input type="checkbox"/> IIIC <input type="checkbox"/> IIID <input type="checkbox"/> IIIE <input type="checkbox"/> IV			
Construction Type (Check One): <input checked="" type="checkbox"/> New <input type="checkbox"/> Existing-Modified			
Well Depth: 1,422 ft.	Borehole Depth: 1,440 ft.	Depth to Bedrock: ft.	
Hole Size (Include reamed zones): inches from 0 to 93 ft.		13 inches from 100 to 1,440 ft.	
Height of Casing above Land Surface: 3 ft. inches			
Casing Size (I.D.) and Materials: (below)		Total Depth of Casing: ft.	
14 inches from 0 to 93 ft.	Material	Weight per ft.	or wall thickness in.
6 inches from 0 to 1,260 ft.	Material	Weight per ft.	or wall thickness in.
6 inches from 1,320 to 1,350 ft.	Material	Weight per ft.	or wall thickness in.
6 inches from 1,410 to 1,422 ft.	Material	Weight per ft.	or wall thickness in.
6 inches from to ft.	Material	Weight per ft.	or wall thickness in.
Screen Size & Mesh:			
6 inches from 1,260 to 1,320 ft.	Mesh Size	Type	
6 inches from 1,350 to 1,410 ft.	Mesh Size	Type	
6 inches from to ft.	Mesh Size	Type	
Water Zones: from 1,258 to 1,412 ft.		from to ft.	from to ft.
Gravel Pack: from 1,240 to 1,440 ft.		from to ft.	from to ft.
Grout Type: from 0 to 93 ft.		Grouting Method: Tremie	Type of Seal: Cement
This information was collected by Camera Survey: <input type="checkbox"/> Yes <input checked="" type="checkbox"/> No			Date Conducted:
Additional Well Construction Form Information Attached: <input checked="" type="checkbox"/> Yes <input type="checkbox"/> No			

COMMONWEALTH OF VIRGINIA
 UNIFORM WATER WELL COMPLETION REPORT

DEQ Well # 161-607
 USGS Local # 59 D 42
 VDH HDIN # _____
 VDH PWSID # _____

Well designation, Name or Number: MW02-LPA

5. Disinfection

Well Disinfected: Yes No Date: 9/29/2017

6. Abandonment (*When abandoning a well, Sections 1 thru 6 are required to be completed)

Date Started:	Date Completed:	Type Rig:
Static Water Level (unpumped level measured): _____ ft.		
Casing Size (I.D.) and Materials:	Casing Pulled: <input type="checkbox"/> Yes <input type="checkbox"/> No <input type="checkbox"/> Uncased Well	
Depth of Fill:	Type and Source of Fill:	
Grout: From _____ to _____ Type: _____	From _____ to _____	Type: _____
Method of permanently marking location:		

7. Pump Test

Static Water Level (unpumped level measured):		96	ft.
Date: <u>8/3/2016</u>	Method (Check One): <input checked="" type="checkbox"/> Water Tape <input type="checkbox"/> Airline <input type="checkbox"/> Transducer <input type="checkbox"/> Other		
Stabilized measured pumping water level:		158	ft.
Date: <u>10/4/2017</u>	Method (Check One): <input type="checkbox"/> Top of Well <input checked="" type="checkbox"/> Top of Casing <input type="checkbox"/> Surface Level		
Test Pump Intake Depth:	315	ft	Stabilized Yield: 215 gpm after 3 hours
Natural Flow:	<input type="checkbox"/> Yes <input checked="" type="checkbox"/> No	Flow Rate	gpm

8. Pump Data

Type:	Motor HP:
Production Pump Intake Depth: _____ ft	Rated Capacity: _____ gpm at _____ ft TDH

9. Geologic Information Potomac

Formation: Upper, Middle, Lower	Type Logs: Electric and gamma
Lithology:	Cuttings: Ditch
Province:	Aquifer Test Performed: Yes, 24 hours
Geologic Map Used:	
Water Quality Results Attached: Yes <input type="checkbox"/> No <input checked="" type="checkbox"/>	

Comments:

10. Driller's Log (Use additional sheets if necessary)

Well designation, Name or Number: MW02-LPA					
Depth (feet)		Type of Rock or Soil	Remarks	Drilling Time (Min.)	Diagram of Well Construction (with dimensions)
From	To	(Color, material, fossils, hardness, etc.)	(Water, caving, cavities, etc.)		
0	2	Top soil			
2	25	Tan/gray, very sandy clay			
25	35	Fine/med sand with shell			
35	96	Shell with shell and blue silt			
96	142	Very silty clay w/shell olive green			
142	248	Olive green silty clay with salt and pepper fine sand			
248	354	Olive green/blue clay with some shell			
354	373	Sandy silt			
373	405	Tight clay			
405	406	Hard layer			
406	413	Olive green/blue clay			
413	414	Hard layer			
414	472	Blue/olive green clay			
472	498	Med-fine sand with light blue and white clay			
498	506	Reddish brown/blue clay			
506	570	Mixed sand with some clay streaks			
570	593	Clay			
593	638	Mixed sand with clay streaks			
638	656	Soft sandy silt, light blue			
656	684	Mixed sand			
684	708	Hard, light blue clay			
708	796	Mixed sand with clay streaks			
796	810	Hard, light blue clay			
810	923	Mixed sand with clay streaks			
923	955	Red/brown/light blue clay			
955	980	Soft red/gray clay			
980	1,013	Hard red/light blue clay			
1,013	1,041	Soft silty light blue, red, tan			
1,041	1,099	Mixed sand			
1,099	1,111	Hard red/gray clay			
1,111	1,123	Softer red/gray/light blue clay			
1,123	1,145	Sand and gravel			
1,145	1,173	Hard gray clay			
1,173	1,198	Softer light blue, gray, reddish/brown clay			

I certify that the information contained herein is true and correct and that this well and/or system has been installed and constructed in accordance with the applicable permit and further that the well complies with all applicable federal, state and local regulations, ordinances and laws.

Signature: _____

Date: 12/09/17

License Number: 2719001110

COMMONWEALTH OF VIRGINIA
 UNIFORM WATER WELL COMPLETION REPORT

DEQ Well # 161-607
 USGS Local # 59 D 42
 VDH HDIN # _____
 VDH PWSID # _____

10. Driller's Log (Use additional sheets if necessary)

Well designation, Name or Number: <u>MW02-LPA</u>					
Depth (feet)		Type of Rock or Soil	Remarks	Drilling Time (Min.)	Diagram of Well Construction (with dimensions)
From	To	(Color, material, fossils, hardness, etc.)	(Water, caving, cavities, etc.)		
1,198	1,228	Sandy layers between tight clay			
1,228	1,330	Sand/gravel/stone, some white	sandy clay streaks		
1,330	1,335	Very hard clay			
1,335	1,348	Dark, gray sandy silt			
1,348	1,425	Sand/gravel with sandy white	clay streaks		
1,425	1,440	Hard, reddish brown clay			

I certify that the information contained herein is true and correct and that this well and/or system has been installed and constructed in accordance with the applicable permit and further that the well complies with all applicable federal, state and local regulations, ordinances and laws.

Signature: _____

Date: 10/09/17

License Number: 2719001110

Additional Well Construction Data

Well designation, Name or Number: MW02-LPA											
Physical Location: Nansemond WWTP						Date Started: 8/24/2017			Date Completed: 9/22/2017		
Hole Size (Include reamed zones):											
inches	from	to	ft.	inches	from	to	ft.	inches	from	to	ft.
inches	from	to	ft.	inches	from	to	ft.	inches	from	to	ft.
inches	from	to	ft.	inches	from	to	ft.	inches	from	to	ft.
Casing Size (I.D.) and Materials:											
inches	from	to	ft.	Material	Weight per ft.	or wall thickness	in.				
inches	from	to	ft.	Material	Weight per ft.	or wall thickness	in.				
inches	from	to	ft.	Material	Weight per ft.	or wall thickness	in.				
inches	from	to	ft.	Material	Weight per ft.	or wall thickness	in.				
inches	from	to	ft.	Material	Weight per ft.	or wall thickness	in.				
inches	from	to	ft.	Material	Weight per ft.	or wall thickness	in.				
inches	from	to	ft.	Material	Weight per ft.	or wall thickness	in.				
inches	from	to	ft.	Material	Weight per ft.	or wall thickness	in.				
inches	from	to	ft.	Material	Weight per ft.	or wall thickness	in.				
inches	from	to	ft.	Material	Weight per ft.	or wall thickness	in.				
Screen Size & Mesh:											
inches	from	to	ft.	Mesh Size	Type						
inches	from	to	ft.	Mesh Size	Type						
inches	from	to	ft.	Mesh Size	Type						
inches	from	to	ft.	Mesh Size	Type						
inches	from	to	ft.	Mesh Size	Type						
inches	from	to	ft.	Mesh Size	Type						
inches	from	to	ft.	Mesh Size	Type						
inches	from	to	ft.	Mesh Size	Type						
inches	from	to	ft.	Mesh Size	Type						
inches	from	to	ft.	Mesh Size	Type						
Water Zones:											
From	to	ft.	From	to	ft.	From	to	ft.	From	to	ft.
From	to	ft.	From	to	ft.	From	to	ft.	From	to	ft.
From	to	ft.	From	to	ft.	From	to	ft.	From	to	ft.
From	to	ft.	From	to	ft.	From	to	ft.	From	to	ft.
Gravel Pack:											
From	to	ft.	From	to	ft.	From	to	ft.			
From	to	ft.	From	to	ft.	From	to	ft.			
From	to	ft.	From	to	ft.	From	to	ft.			
Grout: Type: Neat cement slurry				from	0	to	1,240	ft.			
Grout: Type:				from		to		ft.			
Grout: Type:				from		to		ft.			

Figure A-7. NP-MAR-1 Well Completion Report. This includes well location information, screen depths, well diameter, and soil type with depth. (Includes the next 7 pages.)

Form GW-2
Revised 7/1/2015
Page 1 of 5

COMMONWEALTH OF VIRGINIA
UNIFORM WATER WELL COMPLETION REPORT

DEQ Well # 161-00623
USGS Local # 59D45
VDH HDIN # _____
VDH PWSID # _____

1. Contact Information

Contact:	Name	Address	Phone
Owner	HRSD	1436 Air Rail Ave. Virginia Beach, VA 23455	(757) 460 - 4242
Driller	Sam Hartman	8221 Cloverleaf Drive; Millersville, MD 21108	(410) 841 - 6710
System Provider	HRSD	6909 Armstead Road; Suffolk, MD 23435	(757) 638 - 7363

2. Well Location

Physical Address: 6909 Armstead Road; Suffolk, MD 23435		County/City:	
Subdivision Name: Nansemond WWTP		Section:	Block: Lot:
Tax Map/GPIN #: 0499-01-5074		Well Designation or Number: NP_MAR_01	
Latitude: 36.89419 N		Longitude: 76.42558 W	
Datum Source	Horizontal: <input checked="" type="checkbox"/> WGS84 <input type="checkbox"/> NAD83 <input type="checkbox"/> NAD27	Vertical: <input type="checkbox"/> NGVD29 <input type="checkbox"/> NAVD88	
Lat/Long Source (Check One): <input type="checkbox"/> Map <input checked="" type="checkbox"/> GPS <input type="checkbox"/> PPDGPS <input type="checkbox"/> Survey <input type="checkbox"/> Imagery <input type="checkbox"/> WASS			
Location Information Collected By: Sam Hartman			
Physical Location Description: Tax Map 6 Parcel ID			

3. Facility & Use

Type of Facility (Check One):	Type of Use (Check All That Apply):		
<input checked="" type="checkbox"/> Waterworks	<input type="checkbox"/> Drinking/Domestic Use	<input type="checkbox"/> Food Processing	<input type="checkbox"/> Cooling/Heating
<input type="checkbox"/> Observation/Monitoring Well	<input type="checkbox"/> Agricultural	<input type="checkbox"/> Manufacturing	<input checked="" type="checkbox"/> Injection
<input type="checkbox"/> Private Well	<input type="checkbox"/> Irrigation	<input type="checkbox"/> Fire Safety	<input type="checkbox"/> Geothermal

4. Well Construction

Well designation, Name or Number: Nansemond WWTP ; NP_MAR_01		
Date Started: 03/01/2021	Date Completed: 11/19/2021	Type Rig: SS40 Mud Rotary
Class Well (Check One): <input type="checkbox"/> I <input type="checkbox"/> IIA <input type="checkbox"/> IIB <input type="checkbox"/> IIIA <input type="checkbox"/> IIIB <input type="checkbox"/> IIIC <input type="checkbox"/> IIID <input type="checkbox"/> IIIE <input type="checkbox"/> IV		
Construction Type (Check One): <input checked="" type="checkbox"/> New <input type="checkbox"/> Existing-Modified		
Well Depth: 1426 ft.	Borehole Depth: 1470 ft.	Depth to Bedrock: N/A ft.
Hole Size (Include reamed zones): 48 inches from 0 to 72 ft.		40 inches from 72 to 500 ft.
Height of Casing above Land Surface: 3 ft. 0 inches		
Casing Size (I.D.) and Materials: (below)		Total Depth of Casing: ft.
42 inches from 0 to 72 ft.	Material Steel	Weight per ft. 167 or wall thickness .375 in.
30 inches from 0 to 500 ft.	Material Steel	Weight per ft. 119 or wall thickness .375 in.
18 inches from 0 to 510 ft.	Material 316L Stainless Steel	Weight per ft. 71 or wall thickness .375 in.
inches from to ft.	Material	Weight per ft. or wall thickness in.
inches from to ft.	Material	Weight per ft. or wall thickness in.
Screen Size & Mesh:		
18 inches from 510 to 528 ft.	Mesh Size .040"	Type 316L 20x18 Prepacked
18 inches from 544 to 564 ft.	Mesh Size .040"	Type 316L 20x18 Prepacked
18 inches from to ft.	Mesh Size .040"	Type 316L 20x18 Prepacked
Water Zones: from 475 to 790 ft.		from 824 to 1140 ft. from 1295 to 1390 ft.
Gravel Pack (US Silica Size #4): from 430 to 805 ft.		from 815 to 1180 ft. Type of Seal:
Grout Type (Neat Cement): from 0 to 72 ft.		from 0 to 500 ft. Grouting Method: Pumped from bottom upward
This information was collected by Camera Survey: <input checked="" type="checkbox"/> Yes <input type="checkbox"/> No		Date Conducted: 11/17/2021
Additional Well Construction Form Information Attached: <input checked="" type="checkbox"/> Yes <input type="checkbox"/> No		

Well designation, Name or Number: NP_MAR_01

5. Disinfection

Well Disinfected: <input checked="" type="checkbox"/> Yes <input type="checkbox"/> No	Date: 11/15/2021
---	------------------

6. Abandonment (*When abandoning a well, Sections 1 thru 6 are required to be completed) N/A

Date Started: <u>N/A</u>	Date Completed: <u>N/A</u>	Type Rig: <u>N/A</u>
Static Water Level (unpumped level measured): <u>N/A</u> ft.		
Casing Size (I.D.) and Materials: <u>N/A</u>	Casing Pulled: <input type="checkbox"/> Yes <input type="checkbox"/> No <input type="checkbox"/> Uncased Well	
Depth of Fill: <u>N/A</u>	Type and Source of Fill: <u>N/A</u>	
Grout: From to Type: <u>N/A</u>	From to Type: <u>N/A</u>	
Method of permanently marking location: <u>N/A</u>		

7. Pump Test

Static Water Level (unpumped level measured): <u>102.18</u> ft.	
Date: <u>11/10/2021</u>	Method (Check One): <input checked="" type="checkbox"/> Water Tape <input type="checkbox"/> Airline <input checked="" type="checkbox"/> Transducer <input type="checkbox"/> Other
Stabilized measured pumping water level: <u>138.01</u> ft.	
Date: <u>11/11/2021</u>	Method (Check One): <input type="checkbox"/> Top of Well <input checked="" type="checkbox"/> Top of Casing <input type="checkbox"/> Surface Level
Test Pump Intake Depth: <u>287</u> ft	Stabilized Yield: <u>2388</u> gpm after <u>24</u> hours
Natural Flow: <input type="checkbox"/> Yes <input checked="" type="checkbox"/> No	Estimated Well Yield: <u>6000</u> gpm

8. Pump Data

Type: <u>Turbine</u>	Motor HP: <u>100</u>
Production Pump Intake Depth: <u>310</u> ft	Rated Capacity: <u>1450</u> gpm at <u>185</u> ft TDH

9. Geologic Information

Formation:	Type Logs:
Lithology:	Cuttings:
Province:	Aquifer Test Performed:
Geologic Map Used:	
Water Quality Results Attached: Yes <input type="checkbox"/> No <input checked="" type="checkbox"/>	

<p>Comments: Electric & Gamma Logs</p> <p style="text-align: center;">Gyroscopic Log</p>

10. Driller's Log (Use additional sheets if necessary)

Well designation, Name or Number: NP_MAR_01					
Depth (feet)		Type of Rock or Soil	Remarks	Drilling Time (Min.)	Diagram of Well Construction (with dimensions)
From	To	(Color, material, fossils, hardness, etc.)	(Water, caving, cavities, etc.)		
0	30	Yellow Clay with Sand			
30	40	Yellow Clay with Sand & Shells			
40	60	Red Sandy Clay with Shells			
60	80	Shells & Sand			
80	91	Silty Clay Green Sandy, Some Shell Layers			
91	98	Clay, Silty, Sandy, Light Blue			
98	103	Light Blue Silty Clay with Shells			
103	127	Tight Clay Layers			
127	161	Silty Clay with Shell Layers, Sandy Stripes			
161	180	Sand, Fine, Coarse with Soft Blue			
180	182.5	Shell/Gravel Layers			
182.5	191	Sandy Silty Clay, Some Shell Layers			
191	192	Shell Layers			
192	201	Sandy Silt, Blue with Gravel/Shell			
201	216	Silty Clay, Sandy, BUT Mostly Clay			
216	322	Tight Clay Gray/Olive Streaks			
322	324	Softer Light Blue Sand Silty Clay			
324	335	Hard Gray/Olive Clay			
335	338.5	Shell			
338.5	343	Gray Clay with Olive Streaks			
343	347	Blue Clay/Sandy Silt			
347	353	Fine-Medium Sand Light Blue			
353	360	Gray/Olive Clay			
360	369	Fine-Med., Lt. Blue/Gray Silt, Med./Coarse/Shell			
369	372	Silty Clay with Fine Sand			
372	380	Mixed Sand, Light Blue/Shell			
380	401	Gray/Olive Clay, Tight			
401	403	Mixed Sand Gravel, Shell			
403	408	Light Blue Very Sandy Silt			
408	410	Hard Cemented Shell Layer, Basalt Flakes/Gravel			
410	420	Mixed Sand, Light Blue Silty Clay			
420	465	Hard Blue Clay			
465	478	Fine Sand Silty Light Blue Clay			
478	493	Mixed Sand, Gravel, Shell, Mica Lignite			
493	507	Gray, Olive, Tan, Blue Clay			
507	509	Light Blue Sandy Clay Silt			
509	527	Mixed Sand, Gravel, Mica			
527	546	Gray, Blue, Tan, Purple Clay			

(*Please see the (2) additional pages, attached.)

I certify that the information contained herein is true and correct and that this well and/or system has been installed and constructed in accordance with the applicable permit and further that the well complies with all applicable federal, state and local regulations, ordinances and laws.

Signature: _____
 Samuel E. Hartman

Date: _____

License Number: 2719001123

10. Driller's Log (continued)

<u>DEPTH (Feet)</u>		<u>Type of Rock or Soil</u>
<u>FROM</u>	<u>TO</u>	<u>(Color, material, fossils, etc.)</u>
546	570	mixed Sand, Mica
570	579	Light Gray/Gray Clay with Gravel
579	581	Gray Silty Clay, Gravel, Shell
581	600	Mixed Sand, Mica
600	603	Gray, Tan, Black Silty Clay
603	635	Mixed Sand Mica
635	641	Gray Silty clay, Mixed Sand, Gravel, Pea Gravel
641	654	Mixed Sand, Gravel
654	673	Light Green/Gray Sandy Clay, Mixed Sand, Gravel
673	675	Gray Clay, Mixed Sand
675	681	Mixed Sand, Lignite
681	695	Olive Clay, Gravel, Peet Gravel, Gray Clay
695	705	Tight Gray Clay, Shell, Stone, Gravel, Pea Gravel
705	735	Fine Sand Mica
735	755	Gray, Olive Gray, Light Gray Clay, Gravel, Mixed Sand
755	778	Mixed Sand, Mica
778	793	Mixed Sand, Mica, Gravel, Pea Gravel
793	800	Gray, Light Gray Clay, Gravel
800	827	Gray, Light Brown, Red, Light Green Clay
827	843	White Sandy Silt, Gravel
843	858	Blue, Green, White
858	889	Mixed Sand, Some Gravel, Mica, White Silt, Stone
889	898	Clay, Brown, Gray
898	924	Mixed Sand, Gravel, Stone, White Silt
924	941	Tight Clay Brown, Red
941	966	Slightly Softer Brown, Red Clay

<u>DEPTH (Feet)</u>		<u>Type of Rock or Soil</u>
<u>FROM</u>	<u>TO</u>	<u>(Color, material, fossils, etc.)</u>
966	995	Mixed Sand, Gravel, White Silt
995	1011	White/Light Blue Sandy Clay-like Silt
1011	1031	Clay, Brown, Red
1031	1042	Clay, Green Grays, Brown, Gravel
1042	1139	Soft Sandy Clay, Gravel, Gray, Green, Black
1139	1157	Red Tight Clay, Gray, Brown, Green
1157	1168	Clay, Hard, Tight Gray, Brown
1168	1178	Soft Sandy Clay/Gray/Gravel
1178	1191	Hard Clay, Brown, Red, Dark Gray
1191	1206	Softer Clay, White/Light Green
1206	1210	Very Sandy/Gravelly, White/Blue, Sandy
1210	1247	Clay, Blue
1247	1260	Fine – Med. Sand, White/Green Sandy, Clay-like Silt
1260	1353	Mixed Sand Large Stone Gravel
1353	1362	Soft Clay White Light Blue/Gray
1362	1416	Sand, Gravel, Stone, Cobbles, Soft Clay, Sand Light Gray/Brown
1416	1424	Hard Tighter Clay
1424	1470	Soft Clay/Gravel, Pea Gravel, Cobble White Gray Green, Red with hard Clay Layers

Additional Well Construction Data

Well designation, Name or Number: Nansemond NP_MAR_01	
Physical Location: Nansemond WWTP	Date Started: 03/08/2021 Date Completed: 11/19/2021
Hole Size (Include reamed zones):	
28 inches from 500 to 1440 ft.	inches from to ft.
inches from to ft.	inches from to ft.
inches from to ft.	inches from to ft.
Casing Size (I.D.) and Materials: (*Please see the additional page, attached.)	
18 inches from 528 to 544 ft.	Material: 316L Stainless Steel Weight per ft. 71 or wall thickness .375 in.
18 inches from 564 to 576 ft.	Material: 316L Stainless Steel Weight per ft. 71 or wall thickness .375 in.
18 inches from 642 to 664 ft.	Material: 316L Stainless Steel Weight per ft. 71 or wall thickness .375 in.
18 inches from 680 to 760 ft.	Material: 316L Stainless Steel Weight per ft. 71 or wall thickness .375 in.
18 inches from 790 to 824 ft.	Material: 316L Stainless Steel Weight per ft. 71 or wall thickness .375 in.
18 inches from 840 to 858 ft.	Material: 316L Stainless Steel Weight per ft. 71 or wall thickness .375 in.
18 inches from 888 to 902 ft.	Material: 316L Stainless Steel Weight per ft. 71 or wall thickness .375 in.
18 inches from 920 to 970 ft.	Material: 316L Stainless Steel Weight per ft. 71 or wall thickness .375 in.
18 inches from 990 to 1046 ft.	Material: 316L Stainless Steel Weight per ft. 71 or wall thickness .375 in.
18 inches from 1072 to 1084 ft.	Material: 316L Stainless Steel Weight per ft. 71 or wall thickness .375 in.
18 inches from 1100 to 1126 ft.	Material: 316L Stainless Steel Weight per ft. 71 or wall thickness .375 in.
Screen Size & Mesh:	
18 inches from 664 to 680 ft.	Mesh Size: .040" Type: 316L 20" x 18" Pre-packed
18 inches from 760 to 790 ft.	Mesh Size: .060" Type: 316L 20" x 18" Pre-packed
18 inches from 824 to 840 ft.	Mesh Size: .060" Type: 316L 20" x 18" Pre-packed
18 inches from 858 to 888 ft.	Mesh Size: .060" Type: 316L 20" x 18" Pre-packed
18 inches from 902 to 920 ft.	Mesh Size: .060" Type: 316L 20" x 18" Pre-packed
18 inches from 970 to 990 ft.	Mesh Size: .040" Type: 316L 20" x 18" Pre-packed
18 inches from 1048 to 1072 ft.	Mesh Size: .060" Type: 316L 20" x 18" Pre-packed
18 inches from 1084 to 1100 ft.	Mesh Size: .060" Type: 316L 20" x 18" Pre-packed
18 inches from 1126 to 1140 ft.	Mesh Size: .040" Type: 316L 20" x 18" Pre-packed
18 inches from 1298 to 1338 ft.	Mesh Size: .060" Type: 316L 20" x 18" Pre-packed
18 inches from 1372 to 1386 ft.	Mesh Size: .060" Type: 316L 20" x 18" Pre-packed
Water Zones:	
From to ft.	From to ft.
From to ft.	From to ft.
From to ft.	From to ft.
From to ft.	From to ft.
Gravel Pack: US Silica Size #4	
From 1190 to 1470 ft.	From to ft.
From to ft.	From to ft.
From to ft.	From to ft.
Grout Type: Bentonite Slurry	from 805 to 815 ft.
Grout Type: Bentonite Slurry	from 1180 to 1190 ft.
Grouting Method: Pumped From The Bottom Upward	

Additional Well Construction Data

Well designation, Name or Number: Nansemond NP MAR 01	
Physical Location: Nansemond WWTP	Date Started: 03/08/2021 Date Completed: 11/19/2021
Hole Size (Include reamed zones):	
inches from to ft.	inches from to ft.
inches from to ft.	inches from to ft.
inches from to ft.	inches from to ft.
Casing Size (I.D.) and Materials:	
18 inches from 1140 to 1298 ft.	Material: 316L Stainless Steel Weight per ft. 71 or wall thickness .375 in.
18 inches from 1338 to 1372 ft.	Material: 316L Stainless Steel Weight per ft. 71 or wall thickness .375 in.
18 inches from 1386 to 1426 ft.	Material: 316L Stainless Steel Weight per ft. 71 or wall thickness .375 in.
inches from to ft.	Material Weight per ft. or wall thickness in.
inches from to ft.	Material Weight per ft. or wall thickness in.
inches from to ft.	Material Weight per ft. or wall thickness in.
inches from to ft.	Material Weight per ft. or wall thickness in.
inches from to ft.	Material Weight per ft. or wall thickness in.
inches from to ft.	Material Weight per ft. or wall thickness in.
inches from to ft.	Material Weight per ft. or wall thickness in.
inches from to ft.	Material Weight per ft. or wall thickness in.
inches from to ft.	Material Weight per ft. or wall thickness in.
Screen Size & Mesh:	
inches from to ft.	Mesh Size: Type:
inches from to ft.	Mesh Size: Type:
inches from to ft.	Mesh Size: Type:
inches from to ft.	Mesh Size: Type:
inches from to ft.	Mesh Size: Type:
inches from to ft.	Mesh Size: Type:
inches from to ft.	Mesh Size: Type:
inches from to ft.	Mesh Size: Type:
inches from to ft.	Mesh Size: Type:
inches from to ft.	Mesh Size: Type:
inches from to ft.	Mesh Size: Type:
Water Zones:	
From to ft.	From to ft. From to ft. From to ft.
From to ft.	From to ft. From to ft. From to ft.
From to ft.	From to ft. From to ft. From to ft.
From to ft.	From to ft. From to ft. From to ft.
Gravel Pack:	
From to ft.	From to ft. From to ft.
From to ft.	From to ft. From to ft.
From to ft.	From to ft. From to ft.
Grout Type: from to ft.	
Grout Type: from to ft.	
Grouting Method:	

Appendix B: Initial Conductivity Work Results

The initial conductivity work was completed in 2018, and in this section, only the breakthrough observed in the first 250 days after the start of recharge will be included. In most screens, breakthrough is observed before 250 days. Note that some error may have been introduced over time because a relative concentration was used, and the influent conductivity concentration was assumed to be constant while in reality it fluctuated as a result of changes in the advanced treatment process.

Screen 1. As discussed in the conference paper, the initial intrinsic tracer decision for screen 1 was to use fluoride as a tracer, since native conductivity was not significantly different than SWIFT Water conductivity. Conductivity values at Screen 1 initially spiked, which we hypothesize was due to the movement of water previously treated with aluminum chlorohydrate (as part of the well treatment to prevent clogging). Considering this to be the initial slug of SWIFT Water provided good results (as discussed in Chapter 4).

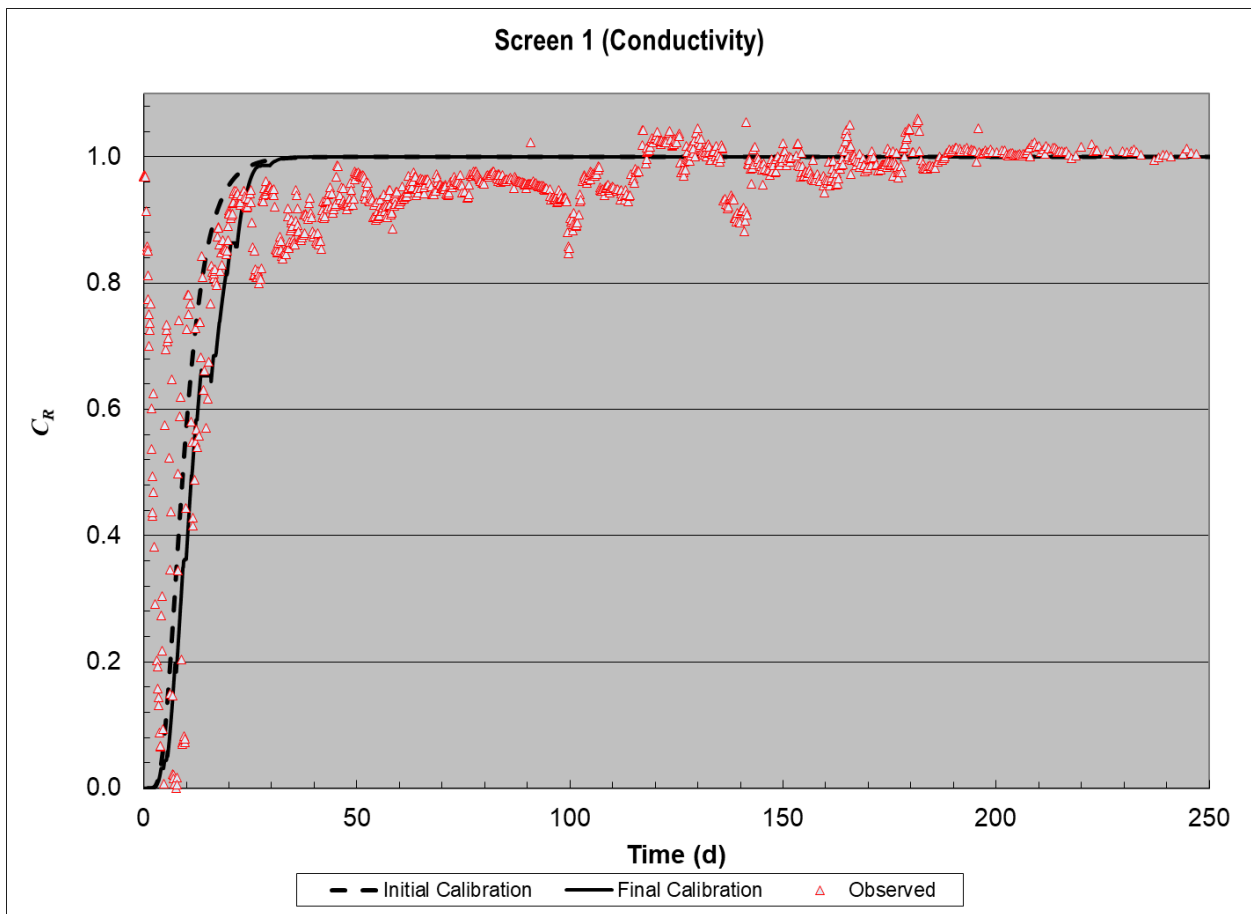


Figure B-1. Conductivity breakthrough in the first 250 days at Screen 1.

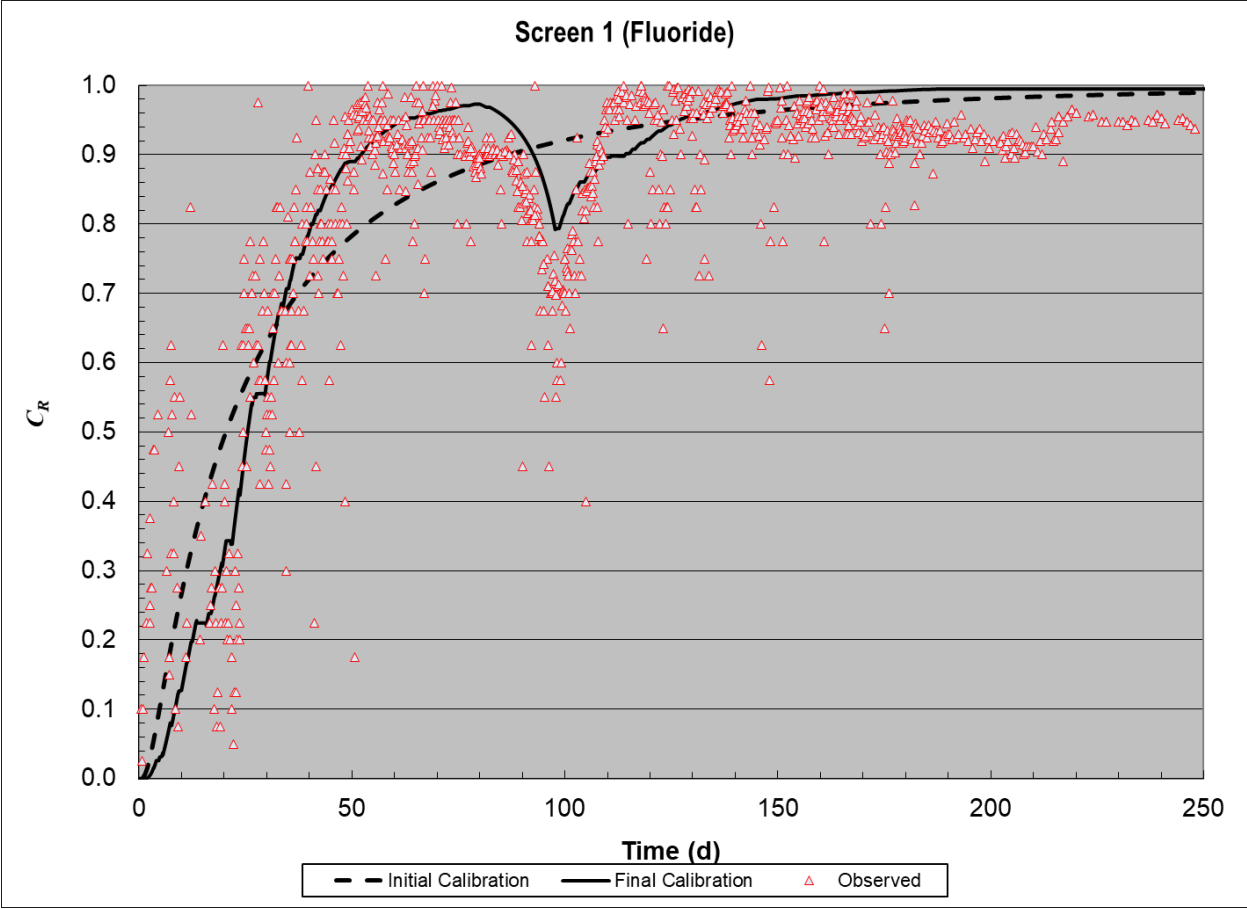


Figure B-2. Fluoride breakthrough in the first 250 days at Screen 1.

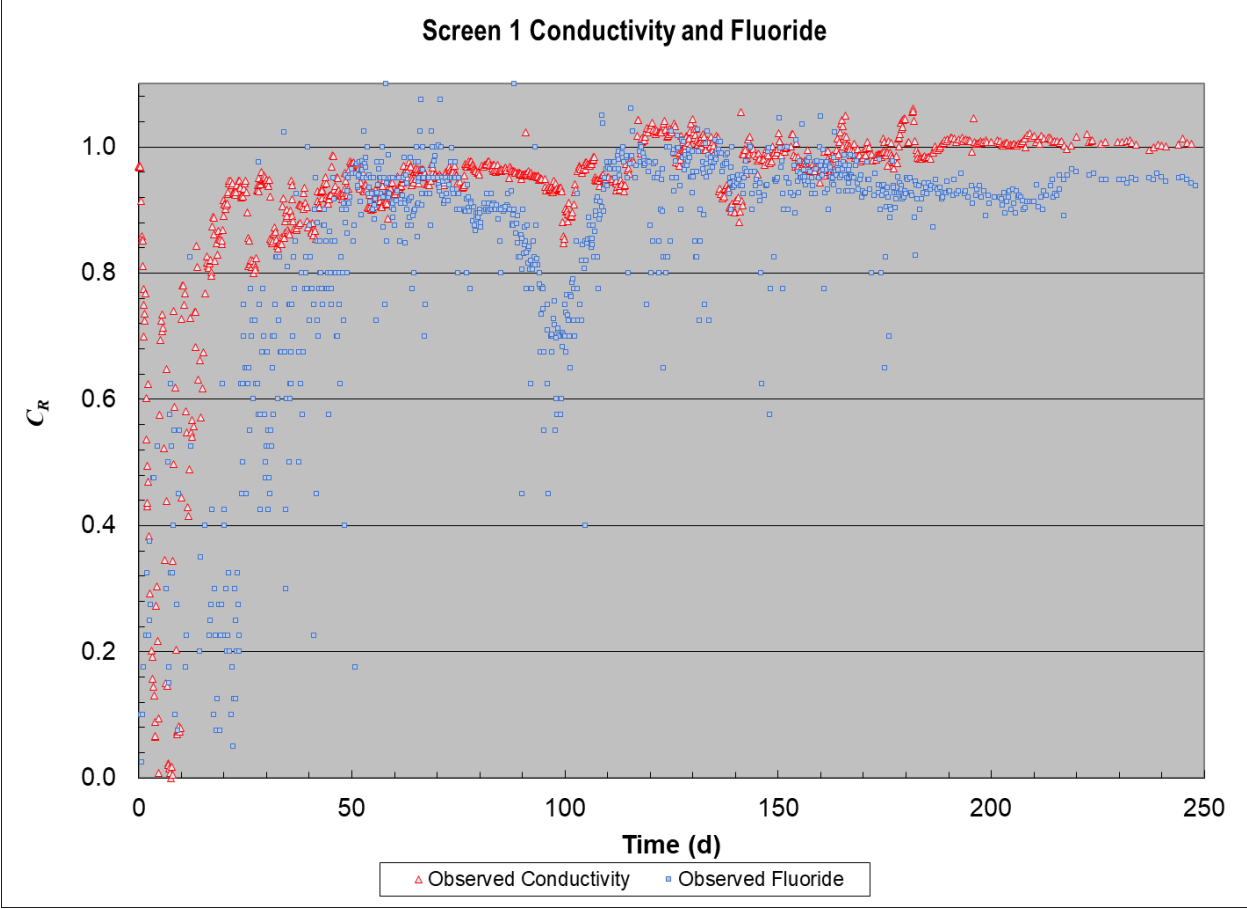


Figure B-3. Comparison of conductivity and fluoride measurements at Screen 1.

Screen 2. A similar behavior was seen in screen 2 with conductivity initially increasing (similar to the spike observed in screen 1) and then decreasing to SWIFT Water conductivity values. The model failed to account for the change in concentration observed during backflush around t=100 days.

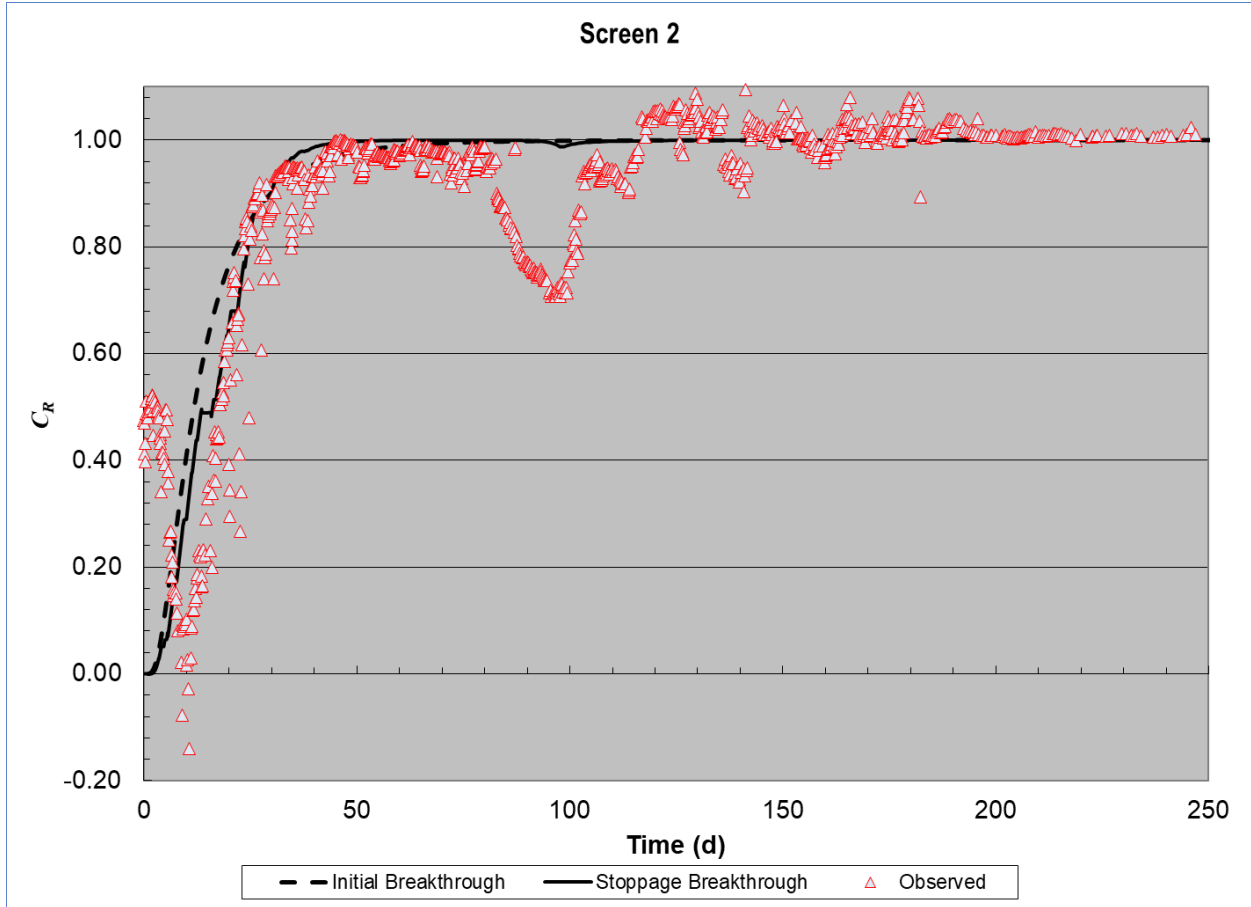


Figure B-4. Conductivity breakthrough in the first 250 days at Screen 2.

Screen 3: A similar behavior was seen in screen 3 with conductivity initially increasing and then decreasing to SWIFT Water conductivity values. The model failed to completely account for the change in concentration observed during backflush around $t=100$ days, though there was a slight change observed.

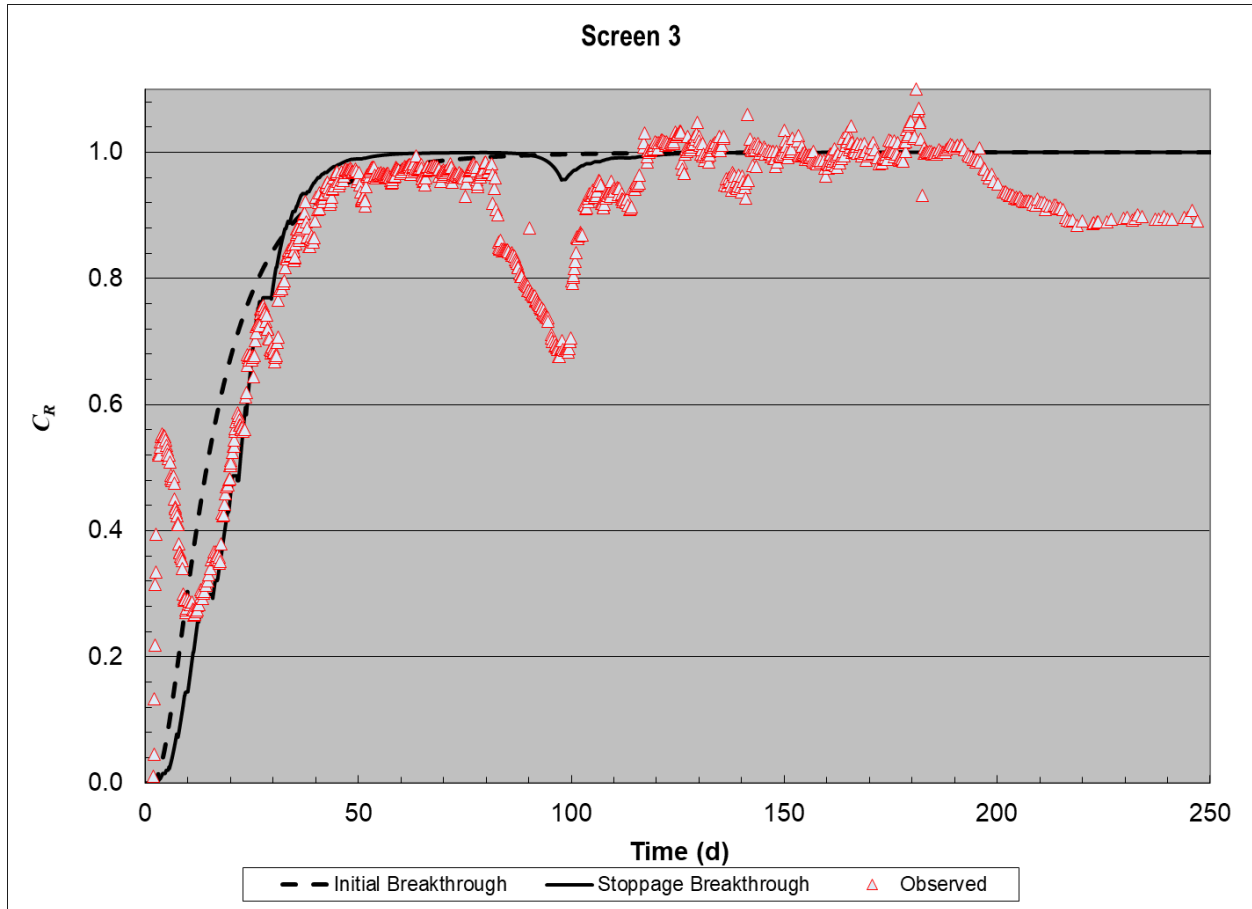


Figure B-5. Conductivity breakthrough in the first 250 days at Screen 3.

Screen 4: To a degree, the model accounted for the change in concentration observed during backflush around $t=100$ days, though the initial breakthrough wasn't completely captured. It is likely this is because the model doesn't account for varying influent concentrations.

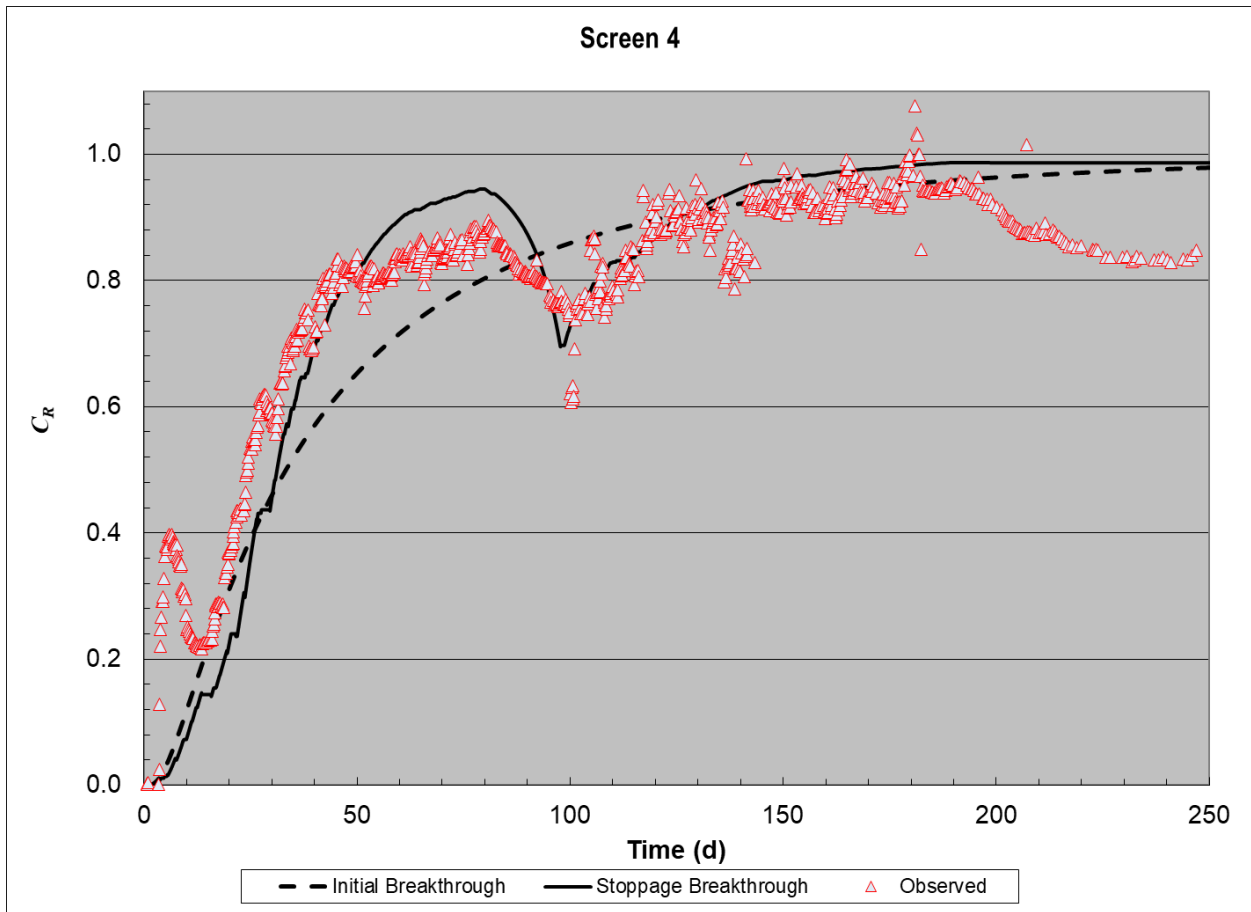


Figure B-6. Conductivity breakthrough in the first 250 days at Screen 4.

Screen 5: Breakthrough at screen 5 is well captured, with the exception of the initial spike in conductivity. Significant reversion is observed during the pumping phase which is unexplained by the original model.

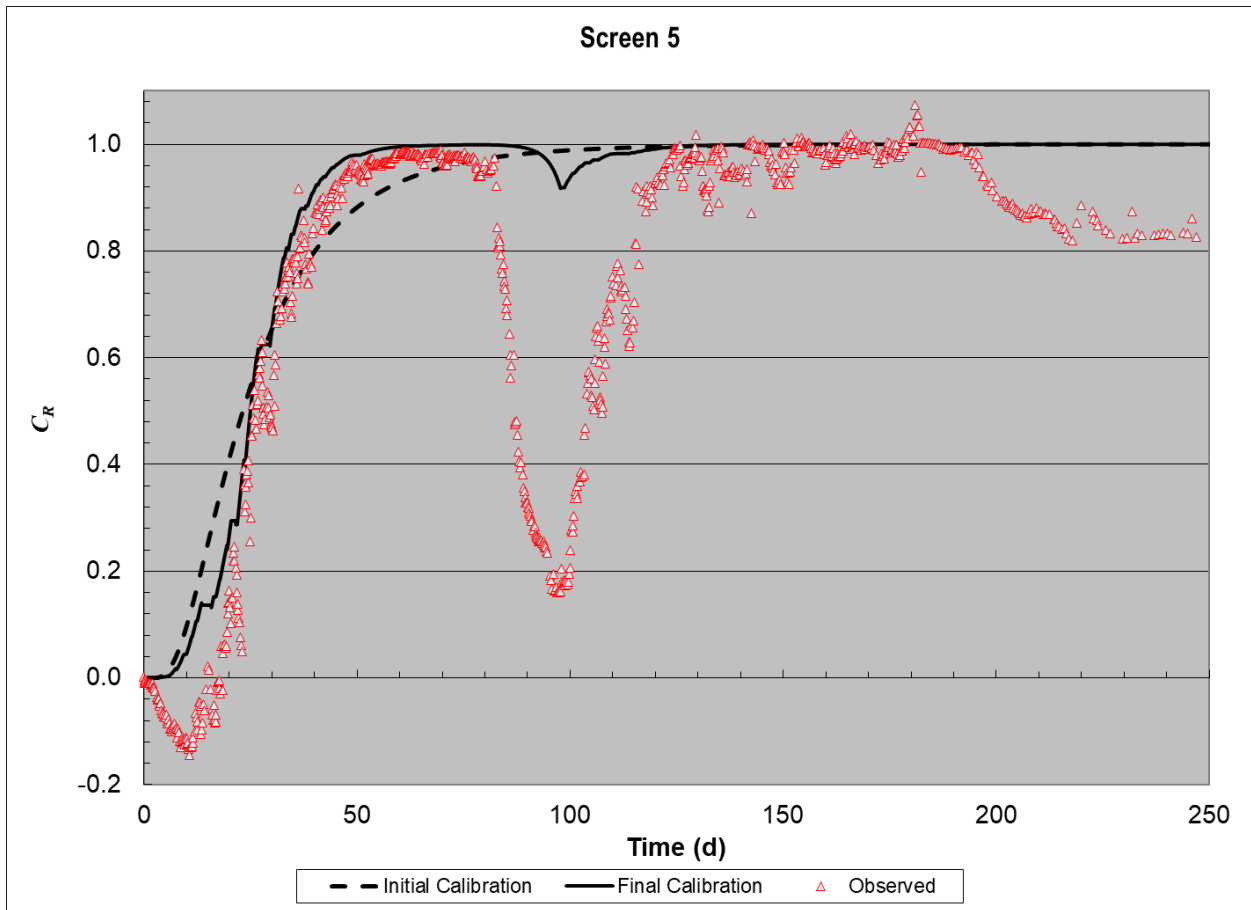


Figure B-7. Conductivity breakthrough in the first 250 days at Screen 5.

Screen 6:

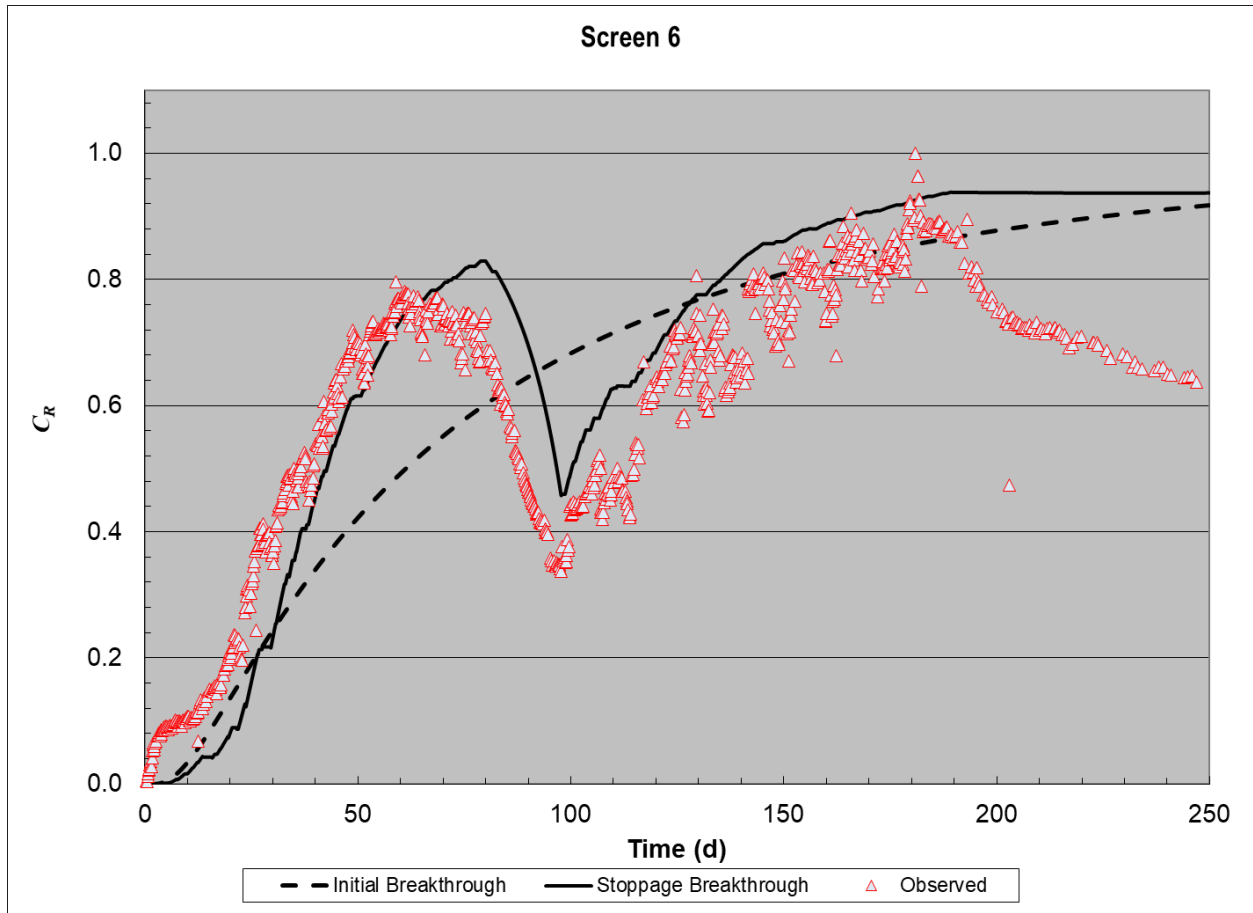


Figure B-8. Conductivity breakthrough in the first 250 days at Screen 6.

Screen 7:

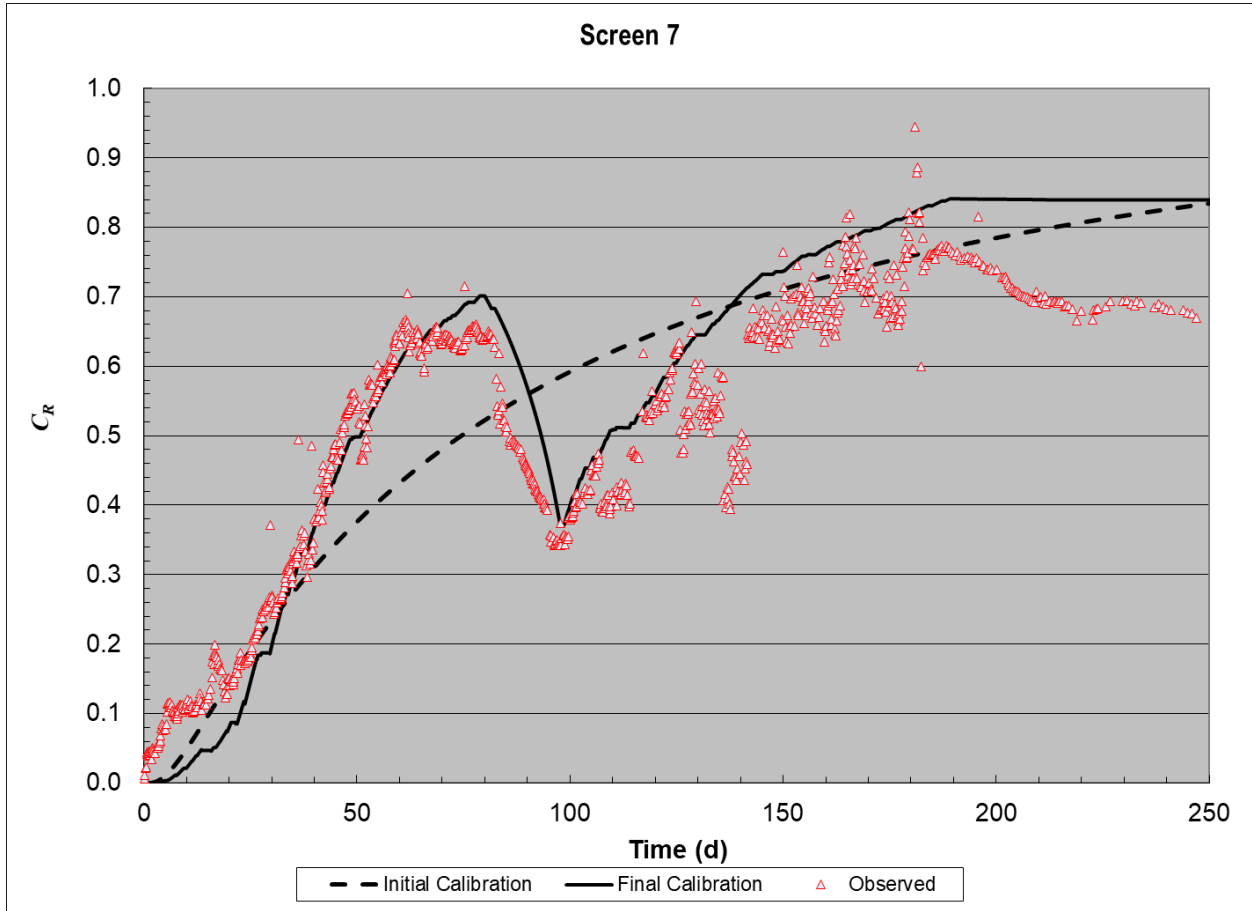


Figure B-9. Conductivity breakthrough in the first 250 days at Screen 7.

Screen 8:

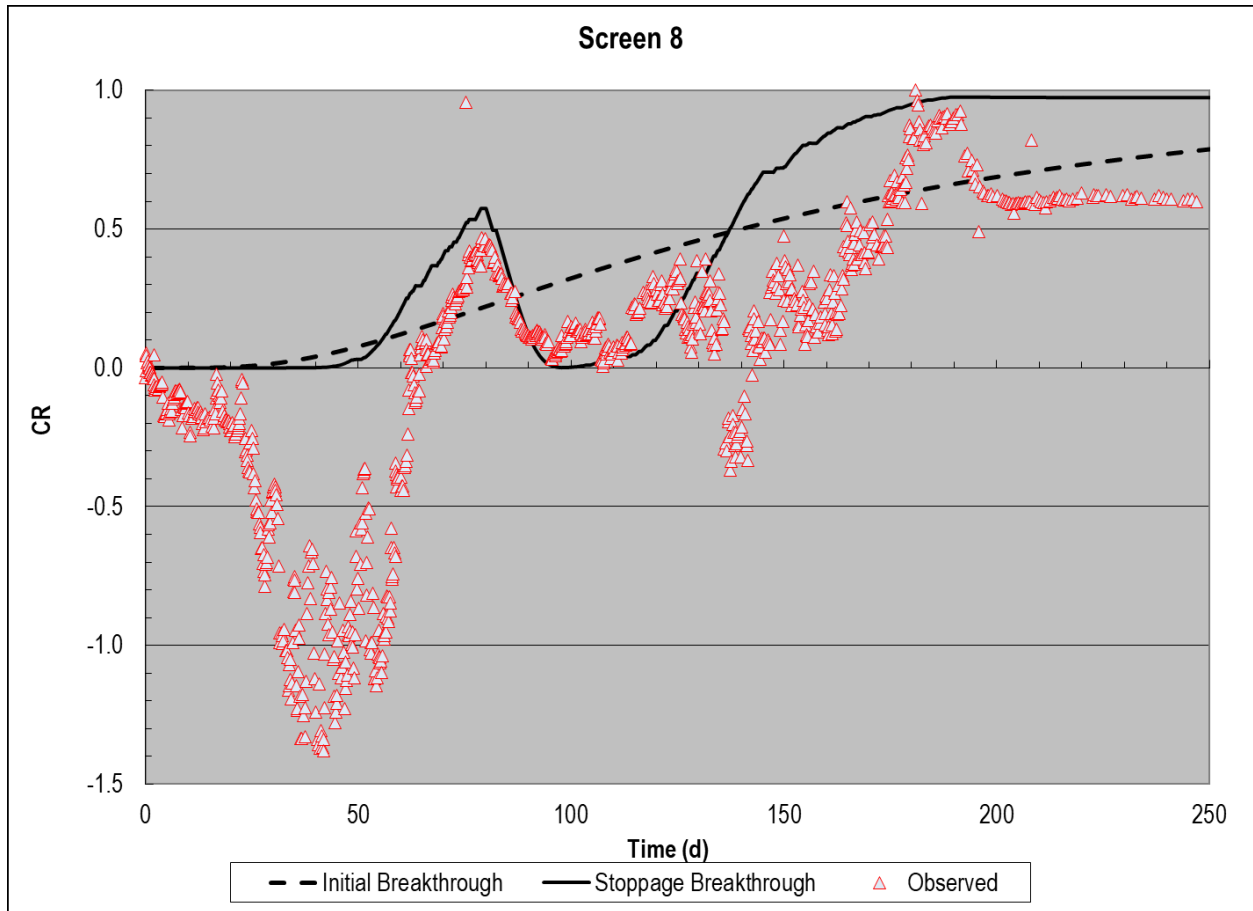


Figure B-10. Conductivity breakthrough in the first 250 days at Screen 8.

Screen 9:

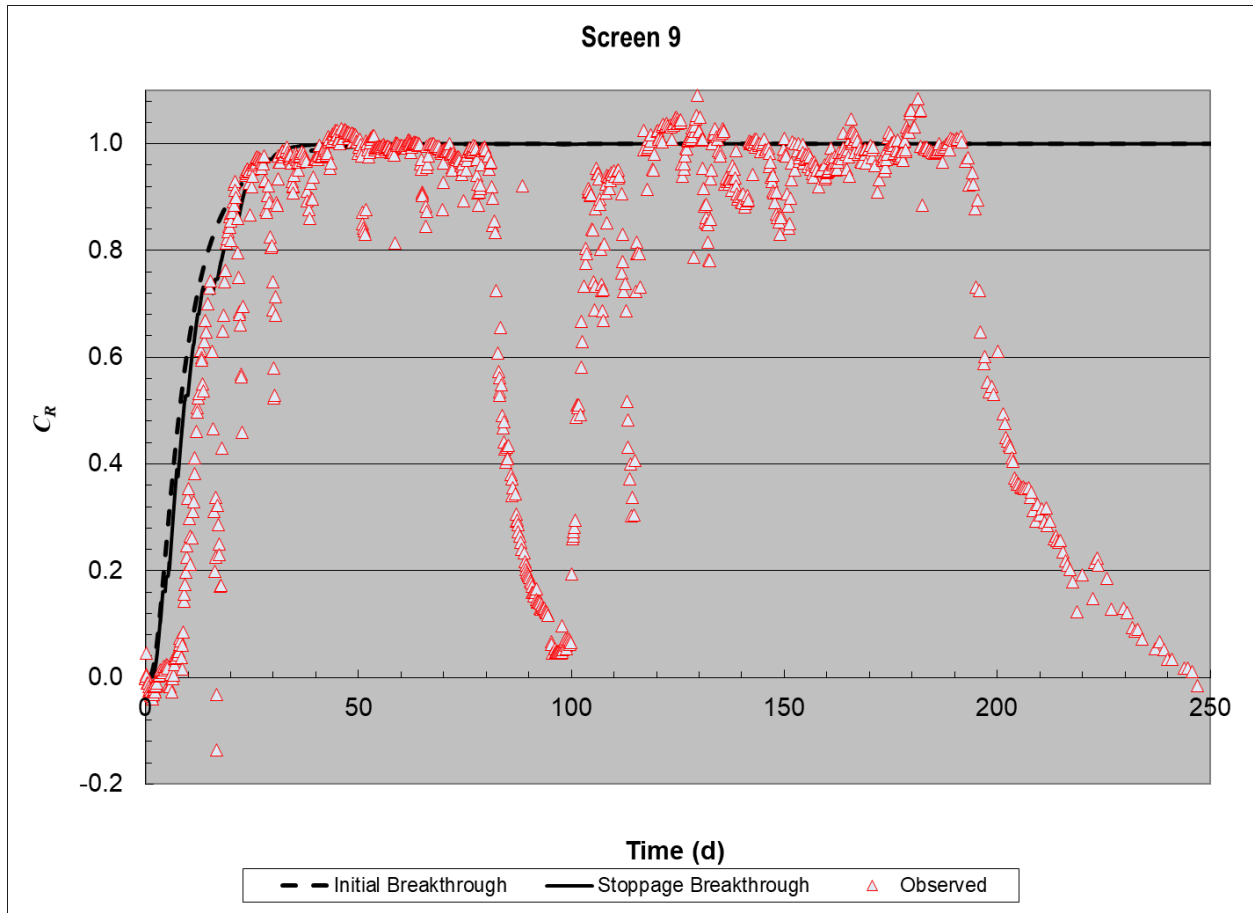


Figure B-11. Conductivity breakthrough in the first 250 days at Screen 9.

Screen 10:

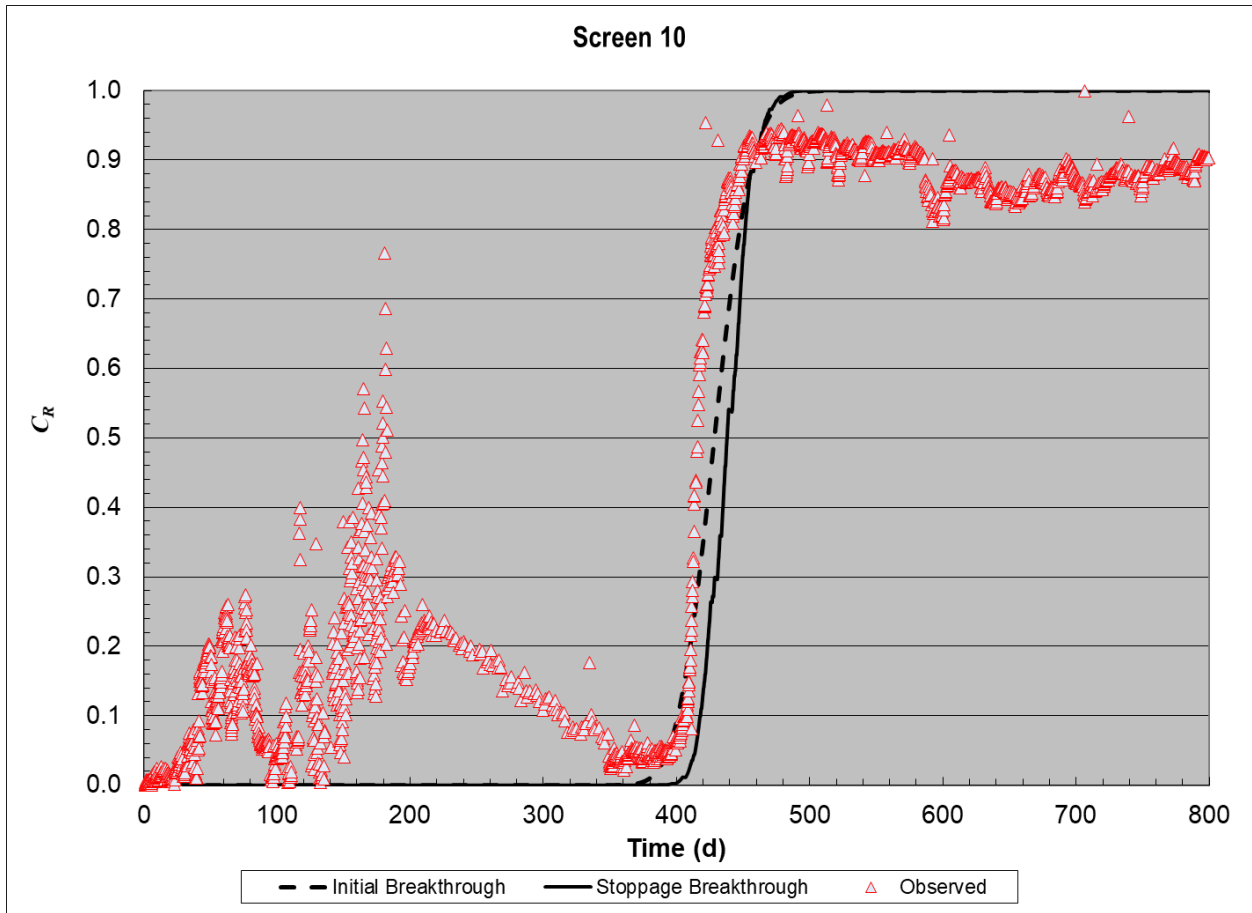


Figure B-12. Conductivity breakthrough in the first 800 days at Screen 10.

Screen 11:

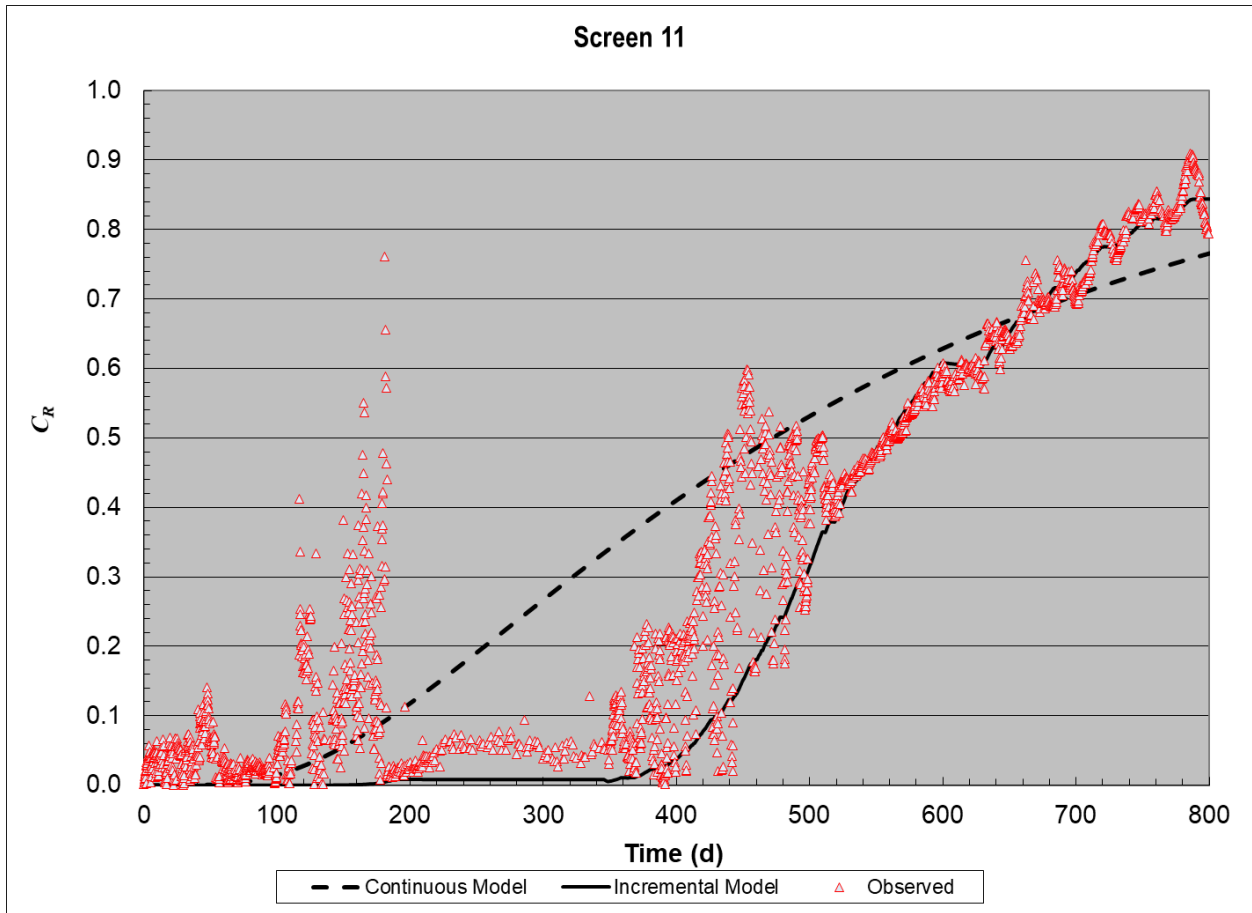


Figure B-13. Conductivity breakthrough in the first 800 days at Screen 11.

Appendix C: Flowmeter Supplemental Information

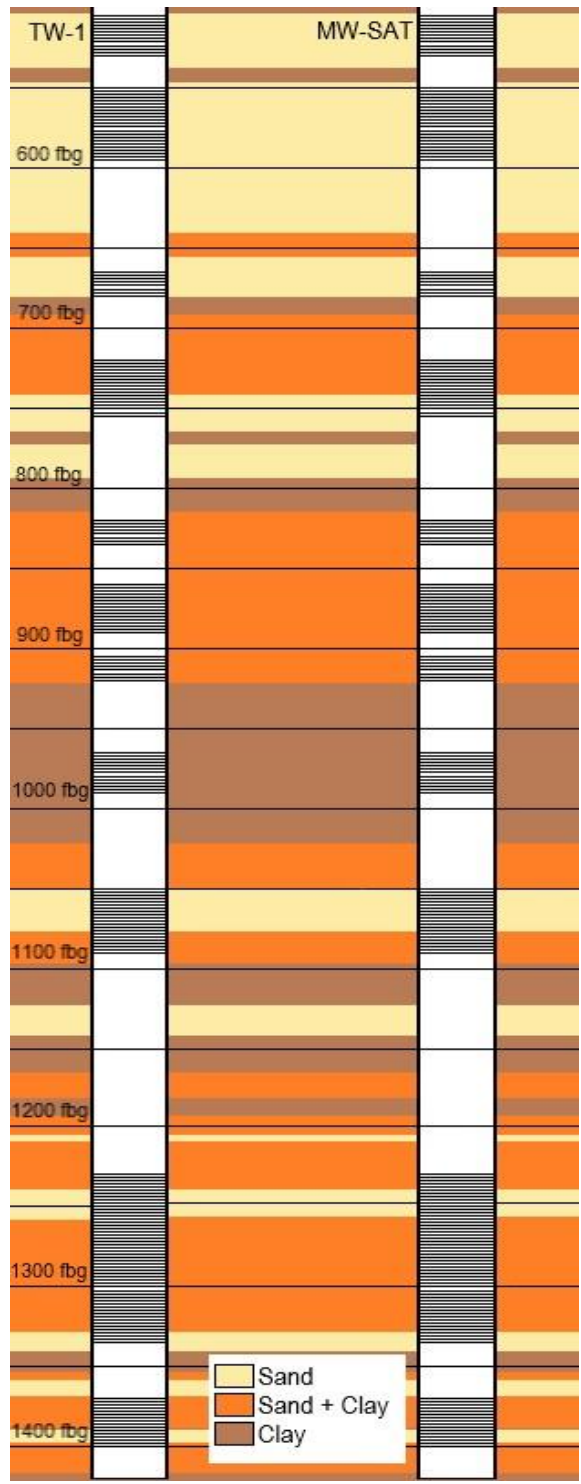


Figure C-1. Schematic of the recharge well (TW-1) and monitoring well (MW-SAT) 50 feet away showing the screen depths and hydrostratigraphy at the SWIFT Research Center site surrounding TW-1 and MW-SAT. This figure is vertically to scale, but not horizontally to scale.

Flowmeter Calibration

The flowmeter was calibrated during recharge and backflush conditions. The flowmeter was lowered to -475 fbg (above screen 1) where it would measure 100% of the flow. A range of flows were introduced at TW-1 and the counts per second (cps) at the flowmeter was measured (Figure C-2). Noise was removed by identifying periods of constant flow and averaging the spinner count values during those periods (Figure C-3). The same method was used for the recharge calibration (Figure C-4).

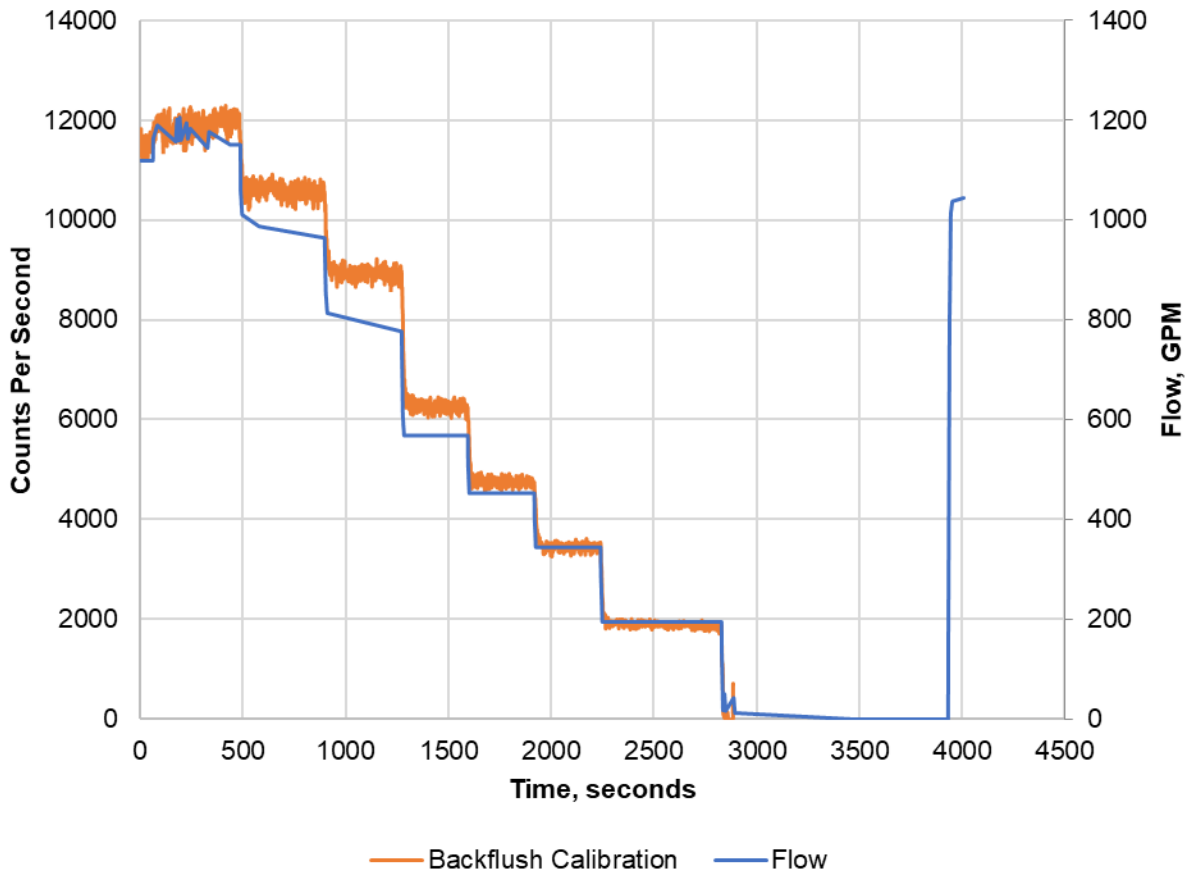


Figure C-2. Flowmeter response to step backflush calibration.

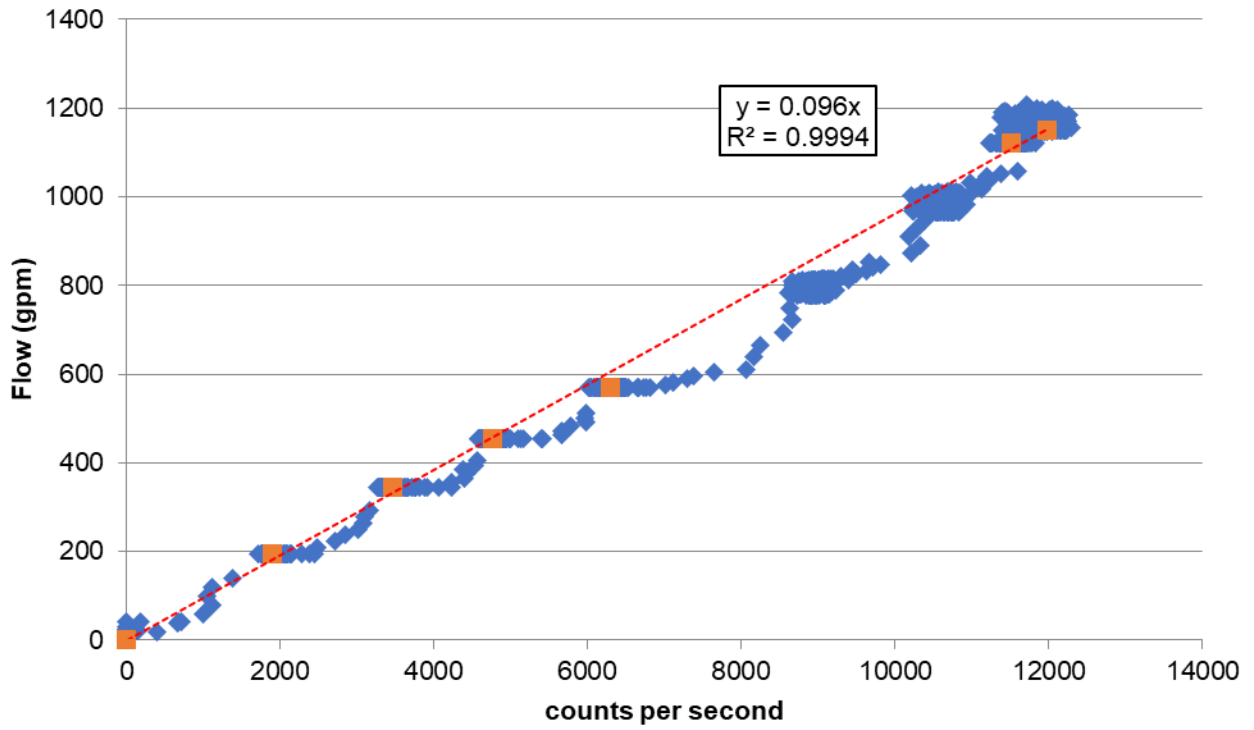


Figure C-3. Backflush calibration. The data used for calibration is in orange.

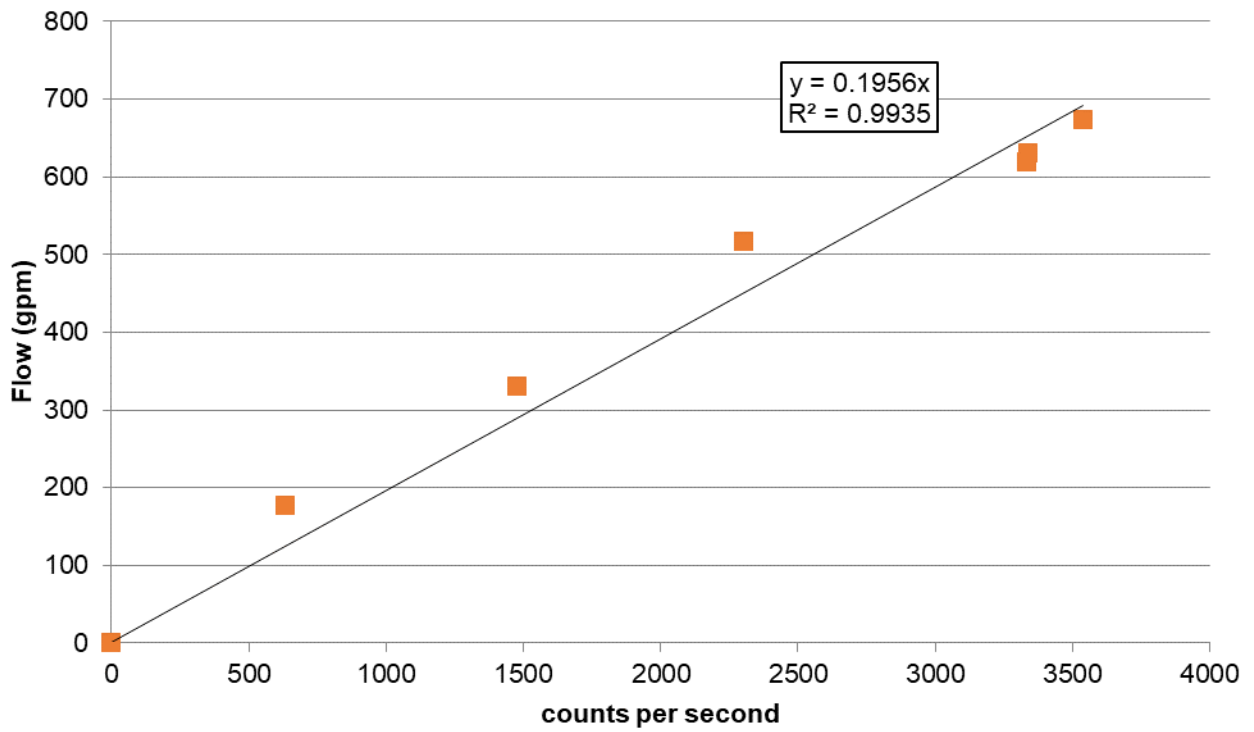


Figure C-4. Recharge calibration.

Static Testing

Static flowmeter testing performed during recharge conditions at the beginning of the experiment indicated that flow was changing between screens, as indicated by the non-zero values of the percent of total flow measured between the top of a lower screen and the bottom of the screen above it (Table C-3). In the manuscript, the flow distribution to each screen is calculated as the sum of the percent of total flow measured at the top of a screen and the percent of the total measured at the bottom of the above screen. For example, at screen 2, $Q_2(\%) = TOS_2 + BOS_1 = 32 + 20 = 52\%$. The remainder of flow is assumed to go to Screen 1, since a measurement of flow wasn't taken above that screen. These results reinforce the flow behavior observed above the screens during dynamic testing.

Table C-3. Static flowmeter testing results.

Screen	Location	Depth (fbg)	Measured Flow (gpm)	Change in Flow (gpm)	Percent of Total Flow (%)
-	Interim Space	450	586.24	-27.37	-
1	TOS	505	613.61	48.79	7
	BOS	530	564.82	135.06	20
2	TOS	550	429.76	218.27	32
	BOS	595	211.49	2.60	0
3	TOS	665	208.89	9.00	1
	BOS	680	199.89	14.75	2
4	TOS	720	185.24	39.65	6
	BOS	755	145.60	44.37	6
5	TOS	820	101.22	-0.06	0
	BOS	835	101.29	10.05	1
6	TOS	860	91.23	15.51	2
	BOS	890	75.72	5.94	1
7	TOS	905	69.78	7.07	1
	BOS	920	62.71	4.36	1
8	TOS	965	58.34	7.16	1
	BOS	990	51.19	51.17	7
9	TOS	1050	0.01	0.01	0
	BOS	1090	0.00	0.00	0
10	TOS	1230	0.00	0.00	0
	BOS	1335	0.00	0.00	0
SUM					88

Dynamic Testing Results

Flow distribution was calculated based on the difference between flow measured at the bottom of a screen (BOS) and flow measured 20 feet above the same screen (TFAS). This stabilization length was used because using the difference between the top of screen (TOS) and BOS did not sufficiently capture the flow going to the PAS. The difference in flow between the bottom of the screen and the bottom of the above screen (BOSa/BOS) was also calculated for comparison. With the exception of screen 7, which only has 15 feet between the above screen and the start of the screen, TFAS/BOS was used for flow distribution calculations.

During recharge tests, TOS/BOS measurements were consistently lower than using either TFAS/BOS or BOSa/BOS (Figure C-5). Using TOS/BOS resulted in an average of 50% of the total flow being captured, whereas using TFAS/BOS or BOSa/BOS resulted in averages of 99% and 102% of recharge flow captured, respectively. During backflush tests, TOS/BOS measurements were consistently higher than using either TFAS/BOS or BOSa/BOS (Figure C-6). Using TOS/BOS resulted in an average of 110% of the total flow being captured, whereas using TFAS/BOS or BOSa/BOS resulted in averages of 99% and 99% of backflush flow captured, respectively.

Using TFAS/BOS as the calculation method made both recharge and backflush flow distribution estimations more accurate at capturing the total flow to the aquifer during the test (Figure C-7). Spreadsheet results of a comparison between the three methods (TOS/BOS, TFAS/BOS, and BOSa/BOS) are also provided in Figure C-8 - Figure C-10.



Figure C-5. Flow distribution to screens during recharge tests using multiple calculation methods.



Figure C-6. Flow distribution to screens during backflush tests using multiple calculation methods.

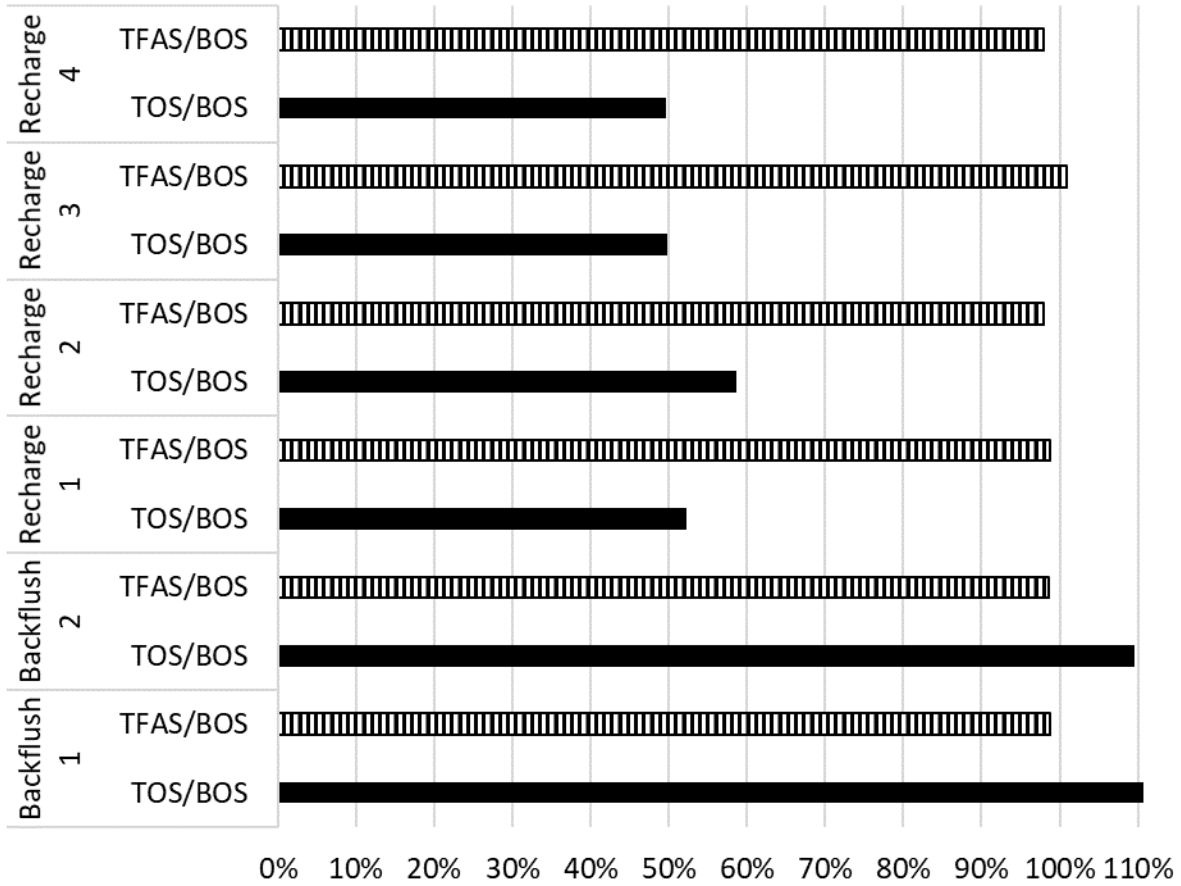


Figure C-7. Comparison of TFAS/BOS and TOS/BOS measurements at capturing the total pump flow at TW-1.

Test:	Test R1 - 5 ft/min against flow				Test R2 - 20 ft/min against flow			
Screen	5/15/2019				5/15/2019			
	Average Flow = 684 gpm; STDEV = 2.82				Average Flow = 687 gpm; STDEV = 0.52			
	Location	Depth fbg	Average Flow	Flow Distribution	Location	Depth fbg	Average Flow	Flow Distribution
1	20' Above Screen	485	652.12	6.6%	20' Above Screen	485	676.40	6.9%
	TOS	505	580.69	16.7%	TOS	505	575.14	21.6%
	BOS	530	543.22	16.7%	BOS	530	530.01	22.4%
2	20' Above Screen	530	543.22	31.2%	20' Above Screen	530	530.01	33.8%
	TOS	550	403.09	49.3%	TOS	550	425.83	44.1%
	BOS	595	221.59	49.3%	BOS	595	231.89	45.7%
3	20' Above Screen	645	219.96	1.9%	20' Above Screen	645	224.93	0.3%
	TOS	665	215.63	2.5%	TOS	665	221.05	1.3%
	BOS	680	203.89	2.7%	BOS	680	216.38	2.4%
4	20' Above Screen	700	205.75	7.0%	20' Above Screen	700	213.18	5.7%
	TOS	720	196.16	7.6%	TOS	720	188.57	8.6%
	BOS	755	155.91	7.4%	BOS	755	154.90	9.4%
5	20' Above Screen	800	152.94	0.0%	20' Above Screen	800	161.92	1.0%
	TOS	820	116.38	5.5%	TOS	820	135.35	4.5%
	BOS	835	116.77	6.0%	BOS	835	131.17	3.6%
6	20' Above Screen	840	116.27	1.0%	20' Above Screen	840	127.36	0.1%
	TOS	860	101.15	3.2%	TOS	860	112.81	2.1%
	BOS	890	95.24	3.3%	BOS	890	113.37	2.7%
7	15' Above Screen	890	95.24	1.2%	15' Above Screen	890	113.37	-1.4%
	TOS	905	87.93	2.2%	TOS	905	96.32	1.5%
	BOS	920	81.11	2.2%	BOS	920	103.33	1.5%
8	20' Above Screen	945	82.78	1.1%	20' Above Screen	945	103.56	3.4%
	TOS	965	75.71	2.0%	TOS	965	97.08	3.3%
	BOS	990	69.45	1.8%	BOS	990	81.48	3.4%
9	20' Above Screen	1030	71.90	2.1%	20' Above Screen	1030	85.71	4.5%
	TOS	1050	22.66	9.2%	TOS	1050	42.41	10.6%
	BOS	1090	11.87	8.8%	BOS	1090	14.35	10.3%
10	20' Above Screen	1210	3.36	0.2%	20' Above Screen	1210	2.86	2.9%
	TOS	1230	1.17	0.5%	TOS	1230	15.23	0.4%
	BOS	1335	0.00	1.8%	BOS	1335	0.00	2.2%
SUM	TOS/BOS			52.2%	TOS/BOS			57.2%
	TFAS/BOS			98.8%	TFAS/BOS			97.9%
	BOSa/BOS			100.0%	BOSa/BOS			103.7%

Figure C-8. Comparison of flow distribution calculation methods for tests R1 and R2 under recharge conditions. TOS/BOS in red, TFAS/BOS in yellow, BOSa/BOS in green for each screen.

Test:	Test R3 - 20 ft/min against flow				Test R4 - 20 ft/min against flow			
Screen	6/3/2019				6/5/2019			
	Average Flow = 684 gpm; STDEV = 12.4				Average Flow = 682 gpm; STDEV = 2.52			
	Location	Depth fbg	Average Flow	Flow Distribution	Location	Depth fbg	Average Flow	Flow Distribution
1	20' Above Screen	485	659.66	8.2%	20' Above Screen	485	674.74	10.7%
	TOS	505	614.63	15.5%	TOS	505	591.29	21.2%
	BOS	530	557.63	15.6%	BOS	530	531.59	22.0%
2	20' Above Screen	530	557.63	19.4%	20' Above Screen	530	531.59	19.3%
	TOS	550	365.56	47.6%	TOS	550	371.24	41.2%
	BOS	595	243.86	48.1%	BOS	595	253.91	42.6%
3	20' Above Screen	645	231.49	-1.9%	20' Above Screen	645	246.72	2.3%
	TOS	665	223.06	0.3%	TOS	665	231.42	4.6%
	BOS	680	229.77	2.2%	BOS	680	215.99	5.8%
4	20' Above Screen	700	233.96	6.2%	20' Above Screen	700	225.59	3.2%
	TOS	720	212.67	8.8%	TOS	720	218.53	3.9%
	BOS	755	175.70	8.3%	BOS	755	199.43	2.5%
5	20' Above Screen	800	175.69	2.2%	20' Above Screen	800	177.94	-0.7%
	TOS	820	135.60	7.9%	TOS	820	134.01	5.8%
	BOS	835	123.52	8.0%	BOS	835	138.53	9.3%
6	20' Above Screen	840	126.14	1.3%	20' Above Screen	840	135.81	1.0%
	TOS	860	119.10	2.2%	TOS	860	116.85	3.5%
	BOS	890	111.39	1.9%	BOS	890	111.86	4.1%
7	15' Above Screen	890	111.39	1.8%	15' Above Screen	890	111.86	1.0%
	TOS	905	103.28	3.0%	TOS	905	99.99	2.9%
	BOS	920	91.87	3.0%	BOS	920	92.20	3.0%
8	20' Above Screen	945	92.92	0.2%	20' Above Screen	945	100.14	1.5%
	TOS	965	89.65	0.7%	TOS	965	94.51	1.9%
	BOS	990	88.31	0.5%	BOS	990	87.27	0.8%
9	20' Above Screen	1030	87.96	7.1%	20' Above Screen	1030	87.35	6.2%
	TOS	1050	48.33	12.7%	TOS	1050	44.57	11.8%
	BOS	1090	4.02	12.9%	BOS	1090	7.76	12.2%
10	20' Above Screen	1210	14.80	3.4%	20' Above Screen	1210	7.43	4.4%
	TOS	1230	22.22	2.2%	TOS	1230	21.61	1.1%
	BOS	1335	0.00	0.6%	BOS	1335	0.00	1.2%
SUM	TOS/BOS			47.9%	TOS/BOS			48.9%
	TFAS/BOS			100.9%	TFAS/BOS			97.9%
	BOSa/BOS			101.2%	BOSa/BOS			103.5%

Figure C-9. Comparison of flow distribution calculation methods for tests R3 and R4 under recharge conditions. TOS/BOS in red, TFAS/BOS in yellow, BOSa/BOS in green for each screen.

Test:	Backflush - 20 ft/min AGAINST				Backflush - 20 ft/min WITH			
	5/14/2019				5/14/2019			
	Average Flow = 1123 gpm; STDEV = 1.76				Average Flow = 1130 gpm; STDEV = 4.29			
Screen	Location	Depth fbg	Average Flow	Flow Distribution	Location	Depth fbg	Average Flow	Flow Distribution
1	20' Above Screen	485	1247.58948	22.7%	20' Above Screen	485	1129.92379	23.9%
	TOS	505	1344.91908	17.02%	TOS	505	1218.61579	17.67%
	BOS	530	1035.25788	17.02%	BOS	530	930.295272	17.67%
2	20' Above Screen	530	1035.25788	41.5%	20' Above Screen	530	930.295272	44.1%
	TOS	550	1125.16788	37.59%	TOS	550	980.372592	42.94%
	BOS	595	566.2674003	37.59%	BOS	595	445.058352	42.94%
3	20' Above Screen	645	586.6765203	3.6%	20' Above Screen	645	466.950312	4.3%
	TOS	665	602.6716803	2.77%	TOS	665	479.254632	3.57%
	BOS	680	552.1118403	1.13%	BOS	680	426.600912	1.63%
4	20' Above Screen	700	549.7302003	8.2%	20' Above Screen	700	418.998192	8.3%
	TOS	720	576.5004003	6.64%	TOS	720	448.960152	6.38%
	BOS	755	466.9358403	6.83%	BOS	755	346.935072	7.05%
5	20' Above Screen	800	460.4186403	8.0%	20' Above Screen	800	336.212112	8.8%
	TOS	820	475.0336803	7.88%	TOS	820	354.143232	8.05%
	BOS	835	362.0920803	8.40%	BOS	835	245.214072	9.00%
6	20' Above Screen	840	364.8963603	3.8%	20' Above Screen	840	252.331512	4.9%
	TOS	860	391.6808403	1.84%	TOS	860	269.782872	3.84%
	BOS	890	341.8953603	1.62%	BOS	890	208.971192	3.21%
7	15' Above Screen	890	341.8953603	2.5%	15' Above Screen	890	208.971192	2.3%
	TOS	905	321.4917603	4.62%	TOS	905	198.831792	3.53%
	BOS	920	284.2521603	4.62%	BOS	920	169.123512	3.53%
8	20' Above Screen	945	279.7140003	3.9%	20' Above Screen	945	174.721392	4.6%
	TOS	965	315.3870003	1.57%	TOS	965	202.768032	2.52%
	BOS	990	260.1759603	1.93%	BOS	990	146.264232	2.02%
9	20' Above Screen	1030	241.4022003	12.6%	20' Above Screen	1030	114.801072	8.0%
	TOS	1050	229.4641203	14.75%	TOS	1050	105.921828	9.75%
	BOS	1090	57.35964028	16.26%	BOS	1090	4.67982515	12.53%
10	20' Above Screen	1210	51.35700028	3.9%	20' Above Screen	1210	4.83064684	0.4%
	TOS	1230	52.60524028	4.06%	TOS	1230	4.93390602	0.42%
	BOS	1335	0.757800276	4.54%	BOS	1335	0.07946018	0.41%
SUM	TOS/BOS			110.8%	TOS/BOS			109.6%
	TFAS/BOS			98.71%	TFAS/BOS			98.69%
	BOSa/BOS			98.74%	BOSa/BOS			98.66%

Figure C-10. Comparison of flow distribution calculation methods under backflush conditions. TOS/BOS in red, TFAS/BOS in yellow, BOSa/BOS in green for each screen.

Flow profiles for the remaining recharge and backflush tests not shown in the paper are shown below:

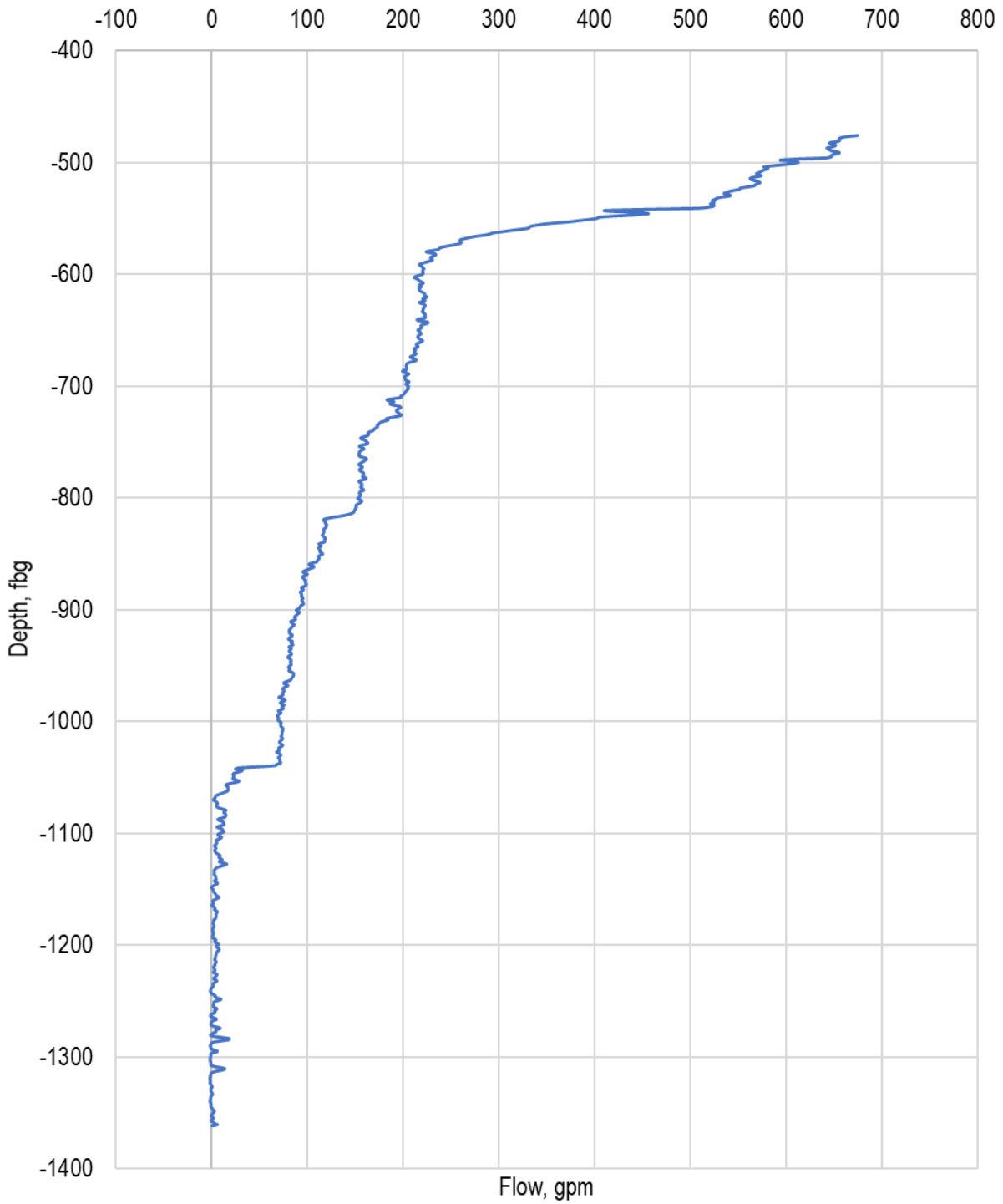


Figure C-11. Flow profile for Test R1. Results are shown with 1-foot precision.

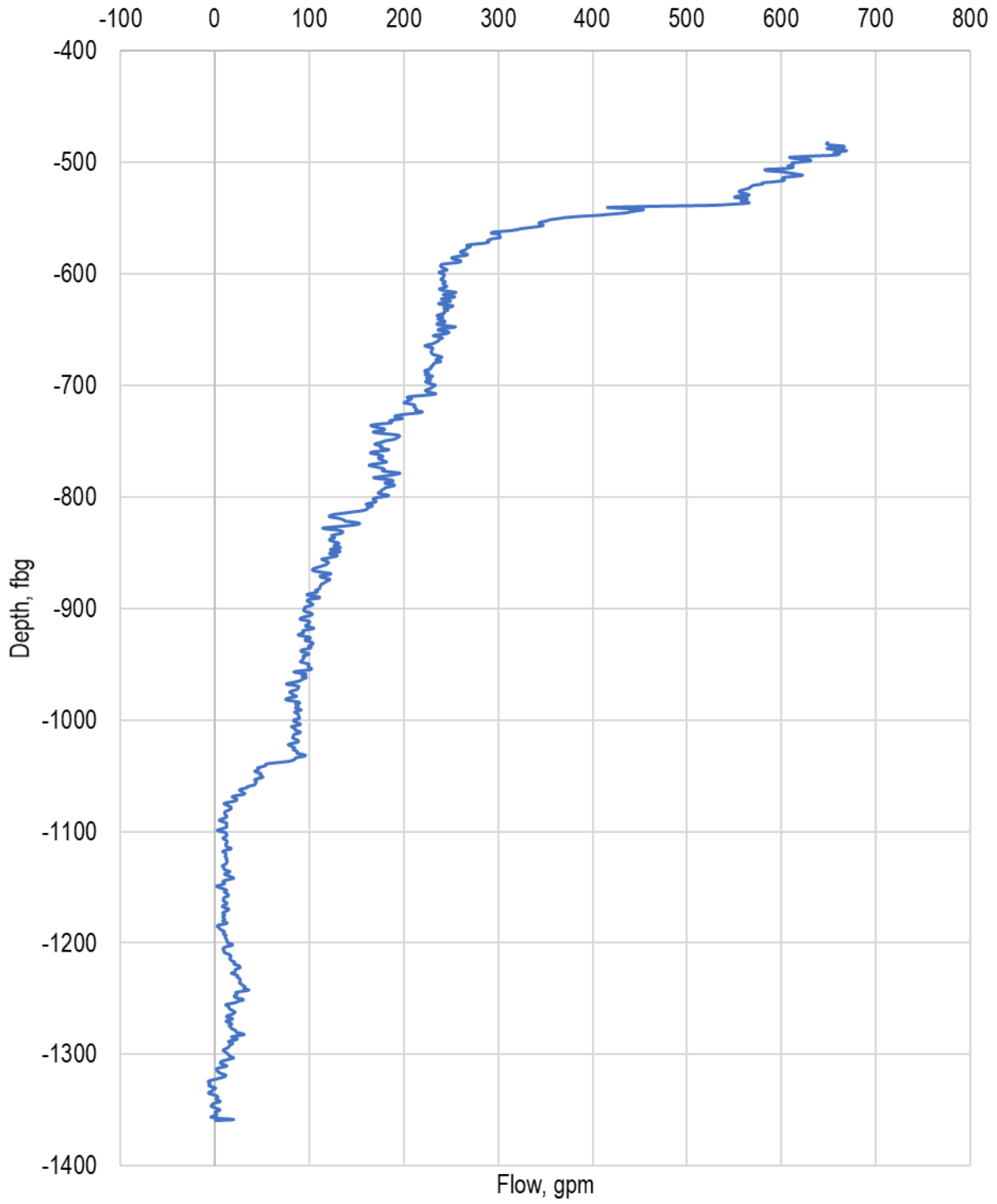


Figure C-12. Flow profile for Test R3. Results are shown with 1-foot precision.

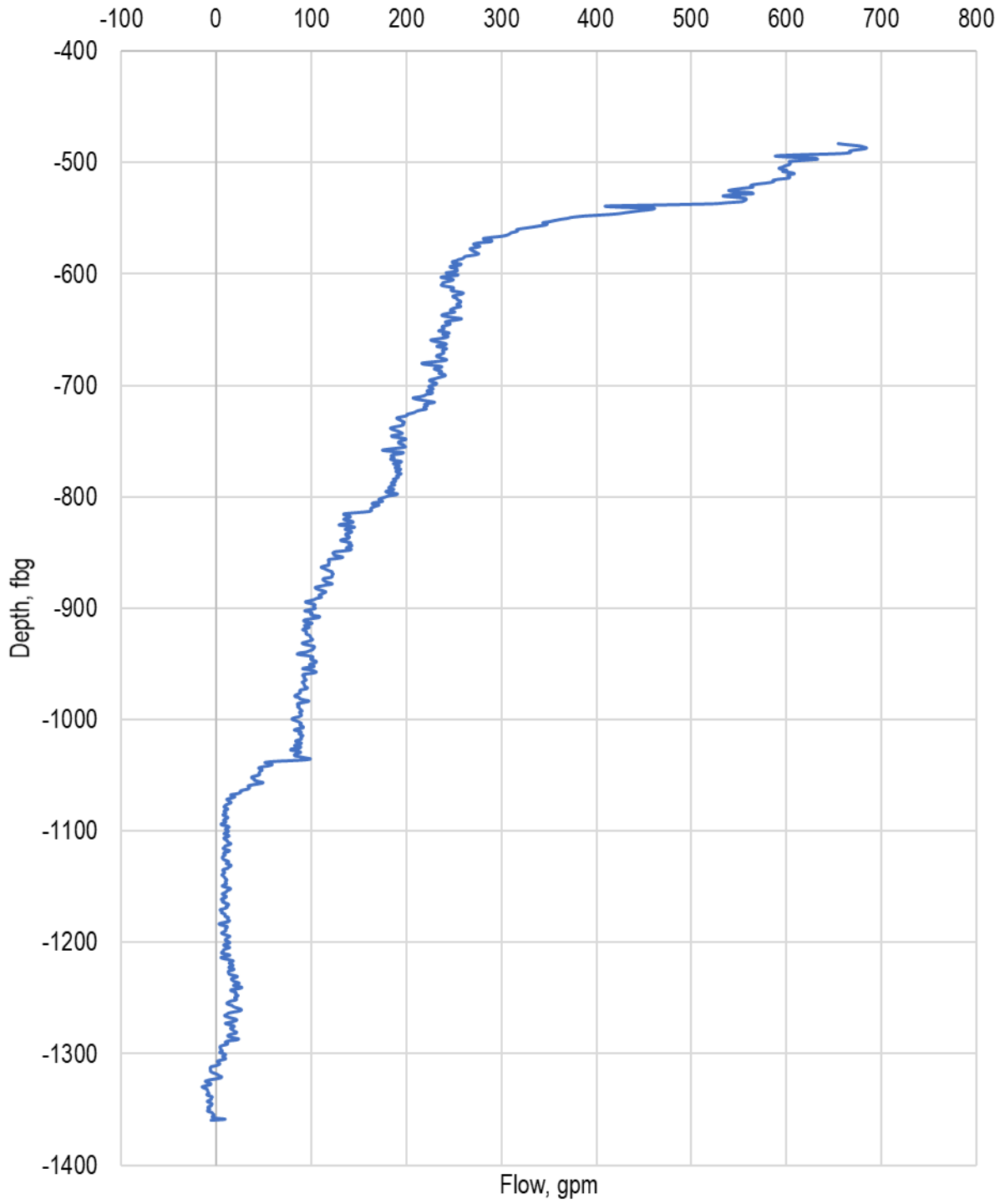


Figure C-13. Flow profile for Test R4. Results are shown with 1-foot precision.

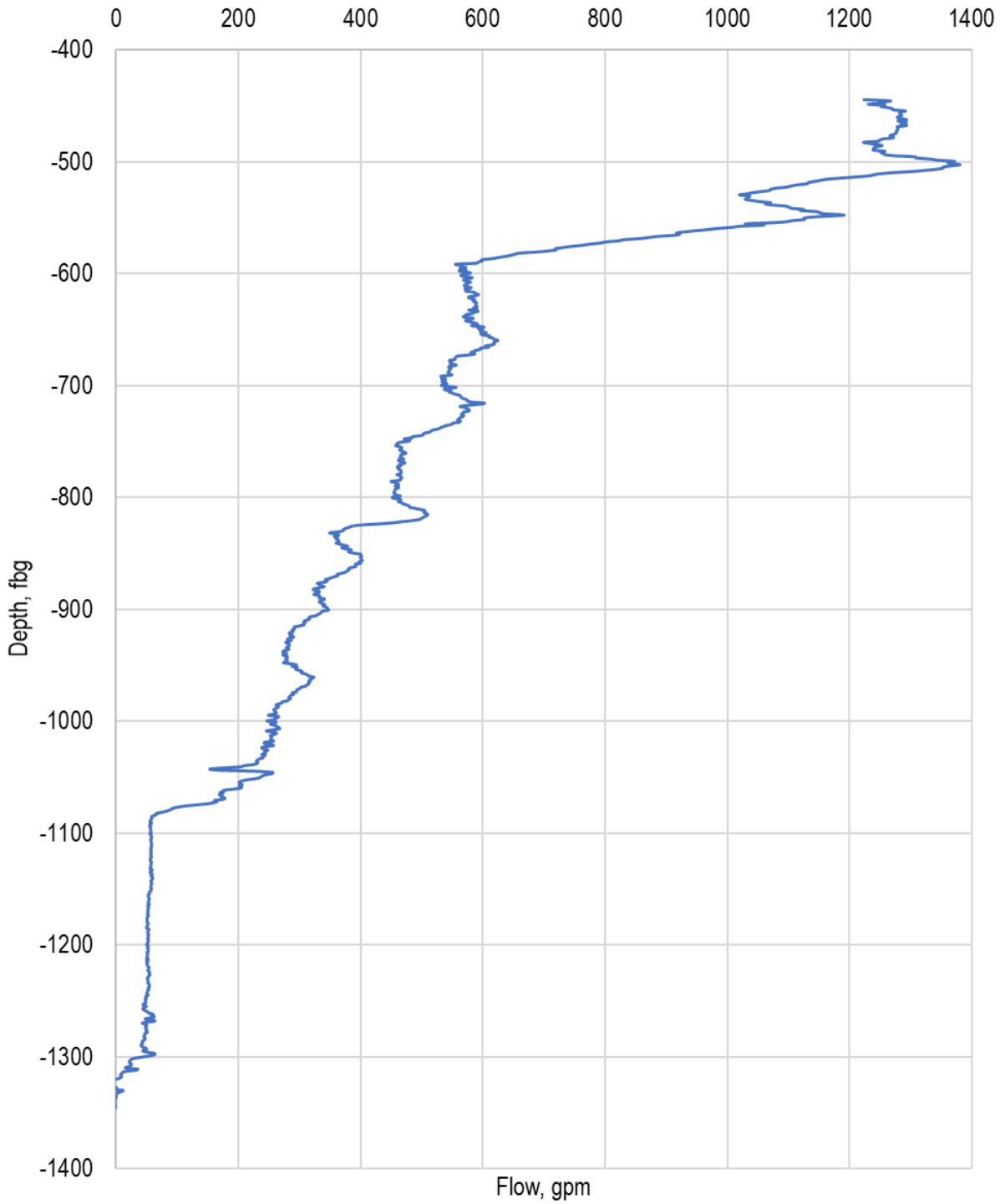


Figure C-14. Flow profile for Test B1. Results are shown with 1-foot precision.

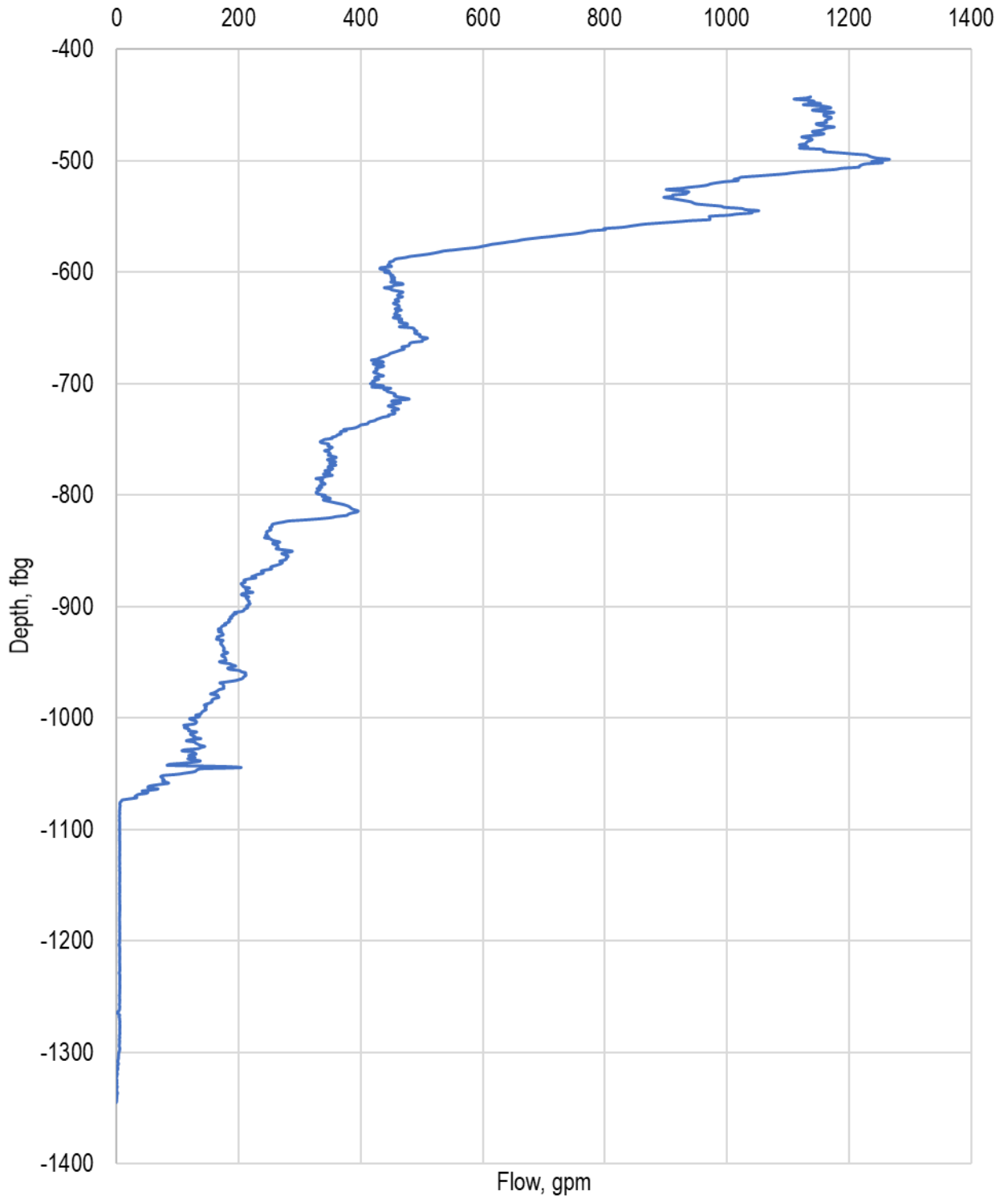


Figure C-15. Flow profile for Test B2. Results are shown with 1-foot precision.

Reynolds Number

An initial overview of the literature provided field studies where in-situ flowmeters had been used to measure flow in wells (Table C-4). Available data including maximum flow, total screen length, number of well screens, and well diameter were listed from the methods available. This was used to calculate Q/L and the maximum Reynolds Number in the well. Based on the flowmeter results, the Reynolds number was calculated at the top of each screen under recharge and backflush conditions (Table C-5, Table C-6).

Table C-4. Review of relevant field studies.

Citation	Publication Year	Max Flow	Total Screen Length	Number of Screens	Well Diameter	Q/L	Max Reynolds Number
		L/min	ft		inches	gal/min/ft	
Basirico et al.	2015	7	23	0	4	0.08	1,497
Boman et al.	1997	5.9	20	1	NL	0.08	--
		9.2	40	1	NL	0.06	--
Datel et al.	2009	35	200	0	NL	0.05	--
Fakreddine et al.	2020	11356	135	8	16	22.22	607,253
		4164	135	8	16	8.15	222,660
Gossell et al.	1999	7800	1060	1	16	1.94	423,764
Hanson and Nishiwaka	1996	7813	1060	1	18	1.95	371,369
Izbiki et al.	2010	30	151	1	NL	0.05	--
Molz et al.	1989	227	70	1	4	0.86	48,554
Mukhopadhyay	1995	4092	465	0	12.5	2.32	280,056
Pavelic et al.	2006	NL	164	1	NL	--	--
Rehfeldt et al.	1992	NL	NL	1	2	--	--
Ruud et al.	1999	20.83	148	1	4	0.04	4,455
Zlotnik and Zurbuchen	2003	57	50	1	4	0.30	12,132
SWIFT		4542	380	11	12	3.16	323,868
		2593	380	11	12	1.80	184,875

NL = not listed

Table C-5. Reynold's Number at the top of each screen during recharge.

Screen	Estimated Recharge Flow	Cumulative Recharge Flow	Flow at Top of Screen	Velocity at Top of Screen	Reynolds Number
	%	%	gpm	ft/sec	--
1	18.76%	98.99%	678.09	1.92	183,011
2	45.53%	80.24%	549.61	1.56	148,335
3	2.14%	34.71%	237.74	0.67	64,164
4	7.24%	32.57%	223.11	0.63	60,216
5	5.96%	25.33%	173.51	0.49	46,828
6	2.77%	19.37%	132.68	0.38	35,808
7	2.38%	16.60%	113.70	0.32	30,687
8	1.98%	14.22%	97.40	0.28	26,286
9	11.07%	12.24%	83.84	0.24	22,628
10	1.07%	1.17%	8.02	0.02	2,165
11	0.00%	0.10%	0.69	0.00	185

Table C-6. Reynold's Number at the top of each screen during backflush.

Screen	Estimated Backflush Flow	Cumulative Backflush Flow	Flow at Top of Screen	Velocity at Top of Screen	Reynolds Number
	%	%	gpm	ft/sec	--
1	16.93%	98.65%	1110.27	3.15	299,651
2	39.32%	81.72%	919.76	2.61	248,233
3	3.18%	42.40%	477.18	1.35	128,787
4	6.49%	39.22%	441.41	1.25	119,132
5	7.61%	32.72%	368.31	1.04	99,404
6	2.73%	25.12%	282.71	0.80	76,300
7	3.88%	22.39%	251.99	0.71	68,010
8	1.93%	18.51%	208.37	0.59	56,237
9	12.15%	16.58%	186.63	0.53	50,370
10	4.33%	4.43%	49.86	0.14	13,458
11	0.00%	0.10%	1.13	0.00	304

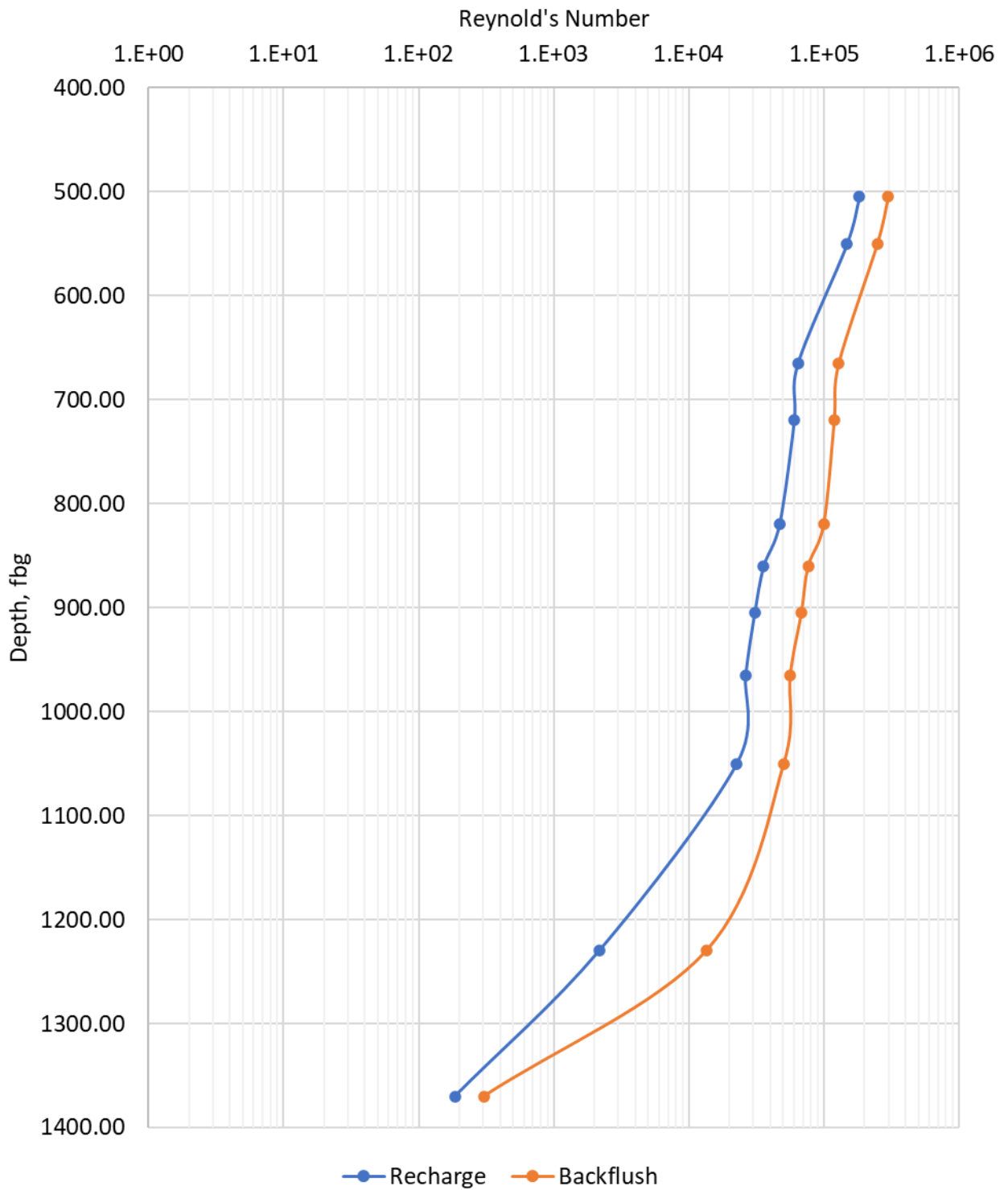


Figure C-16. Reynold's Number at the top of each screen.

Appendix D: Multi Tracer Supplemental Information

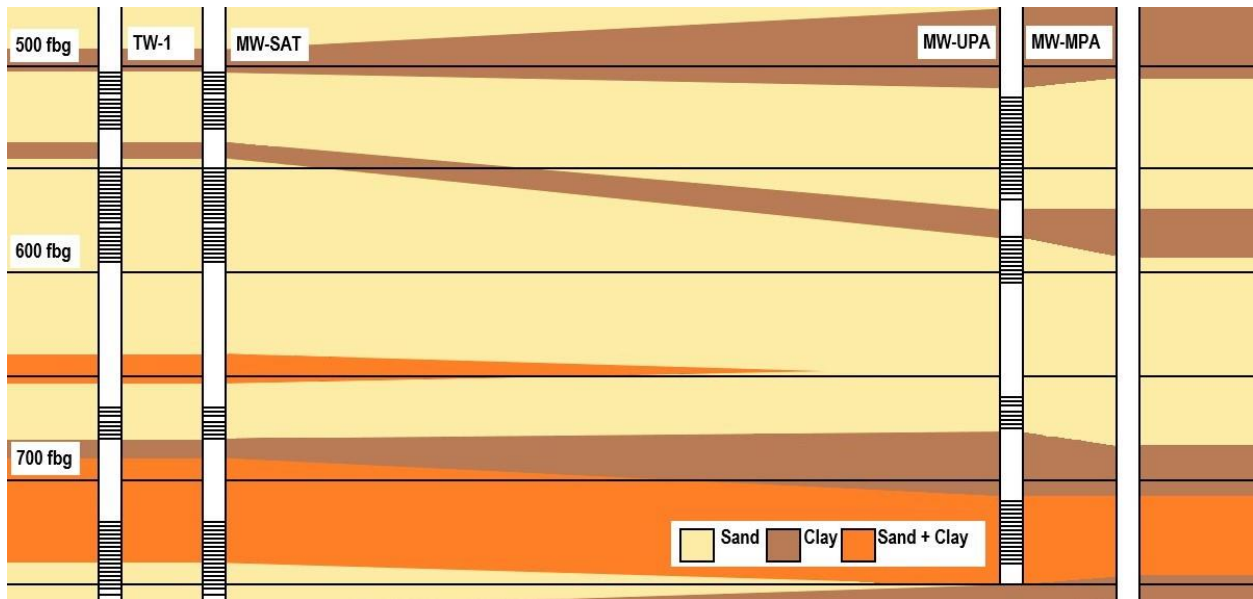


Figure D-17. Well locations and screen depths of wells at the SWIFT Research Center. Screen depths range from 500 to 1400 feet (152 to 427 m) below grade, but this study focuses on the UPA, which contains screens 1-4. Horizontal distance between wells is not shown to scale.

Upper Potomac Aquifer (UPA)

First, a breakthrough model for sulfate was calculated for each individual screen (Figure D-18). We applied the length and flow weighted distributions using all screens (Figure D-19) and using Screens 1 and 2 only (Figure D-20), since we suspected that the upper screens were contributing more. Using Screens 1 and 2 proved to be the most effective in all cases.

After flowmeter testing, drawdown at the conventional wells indicated that response in the UPA was decreasing, and the assumption could not be made that the flow distribution measured by the in-situ flowmeter was constant. For the initial comparisons, flow distribution before $t=344$ days (right before the restart of recharge after rehabilitation) is equal to the pre-rehab flow distribution. From $t=344$ days until $t=445$ days, flow distribution is equal to the post-rehab flow distribution. After 500 days, we assume that flow distribution returns to the original pre-rehab flow distribution, since there was not a direct measurement of flow distribution, but we know that it decreased.

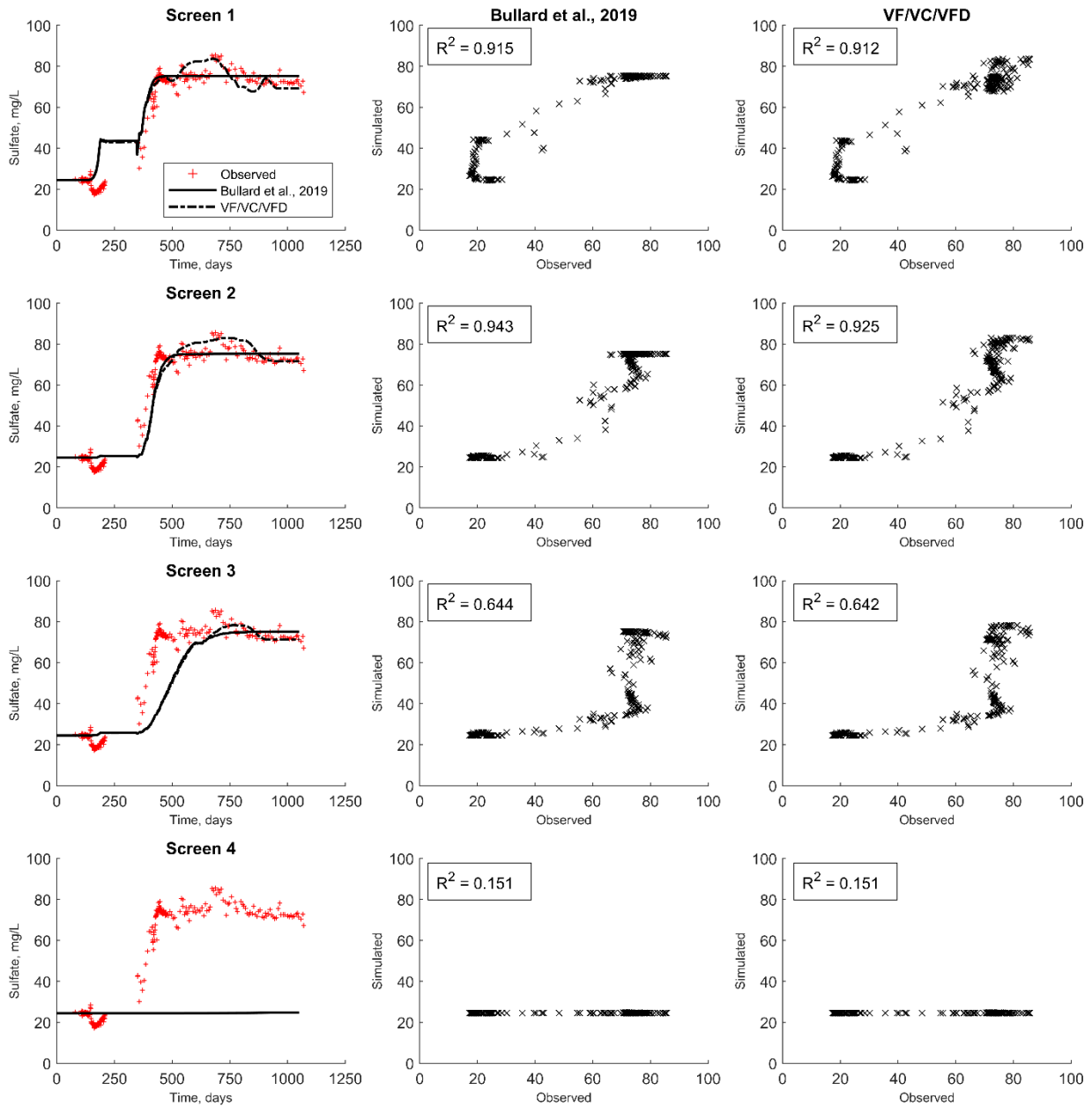


Figure D-18. Breakthrough calculated at each screen using aquifer characteristics (n and α) determined in Bullard et al. (2019). Coefficients of determination are shown for the constant concentration model (labeled Bullard et al. 2019) and the variable concentration model (labeled VF/VC/VFD). Both models account for variable flow and variable flow distribution.

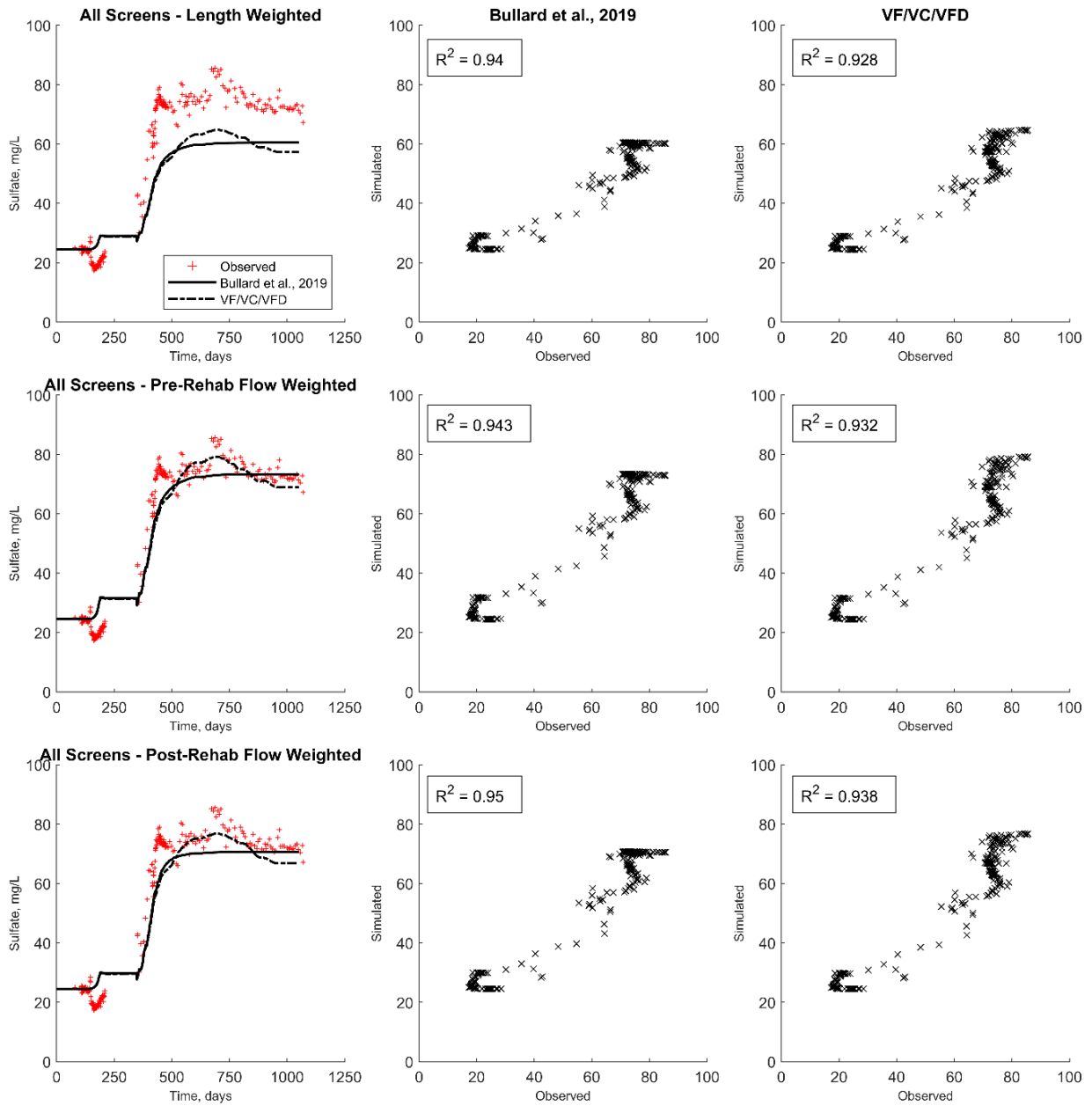


Figure D-19. Flow- and length-weighted models using screens 1-4. Coefficients of determination are shown for the constant concentration model (labeled Bullard et al. 2019) and the variable concentration model (labeled VF/VC/VFD). Both models account for variable flow and variable flow distribution.

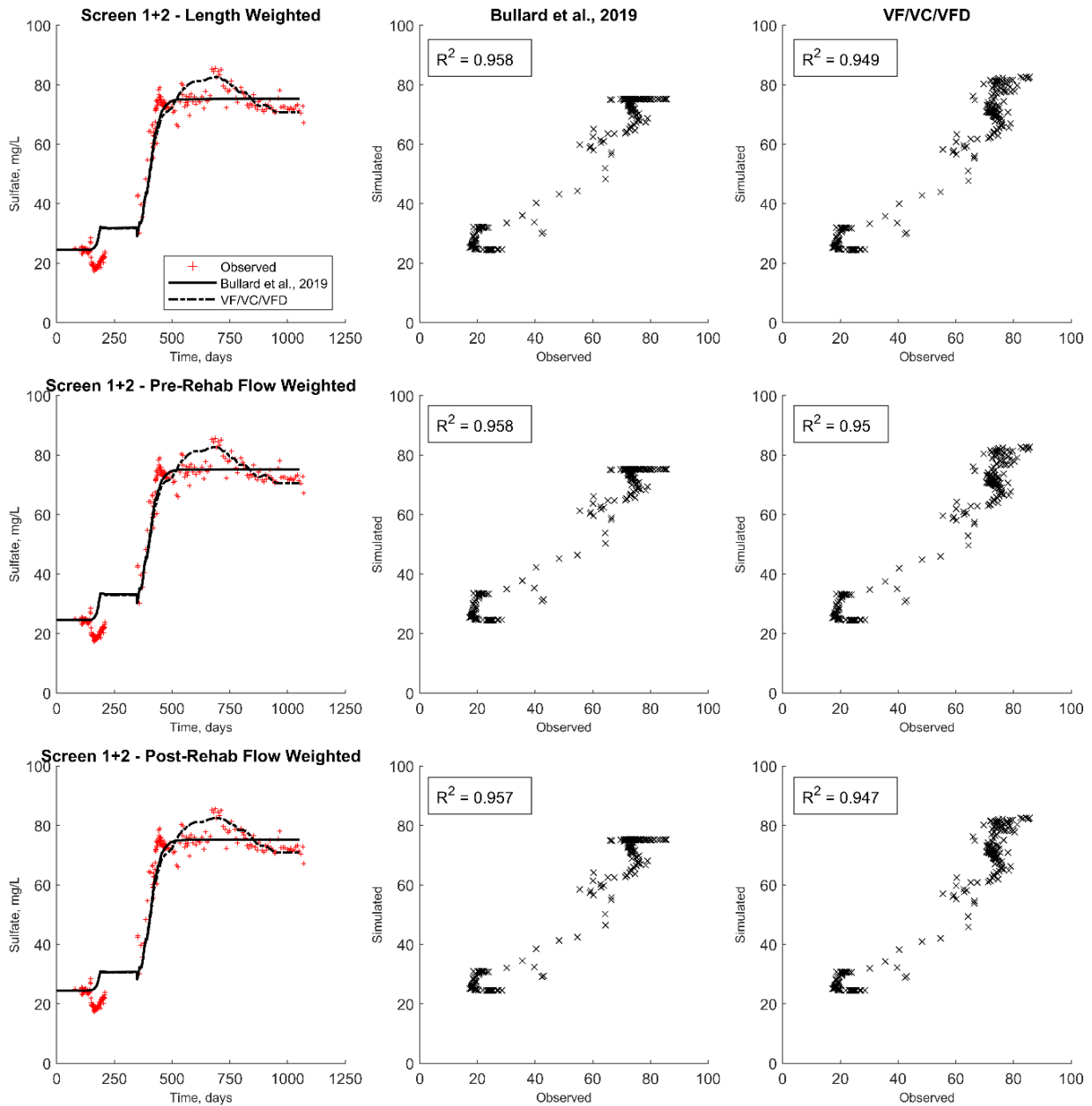


Figure D-20. Flow- and length-weighted models using screens 1 and 2 only. Coefficients of determination are shown for the constant concentration model (labeled Bullard et al. 2019) and the variable concentration model (labeled VF/VC/VFD). Both models account for variable flow and variable flow distribution.

Once it was determined that a combination of Screens 1 and 2 was most accurate, a secondary investigation was conducted to determine whether the length of time that the model used the post-rehab flow distribution impacted the fit of the model. This involved varying the transition day for post-rehab flow distribution back to pre-rehab flow distribution from 400 days

to 600 days and measuring the coefficient of determination for the variable influent concentration model (Figure D-21). Because the difference in fit between the length and flow weighted models were minimal, only the length weighted model was used for this part of the analysis. The optimal switchback time to pre-rehab flow distribution was 445 days, which produced a R^2 value of 0.9566.

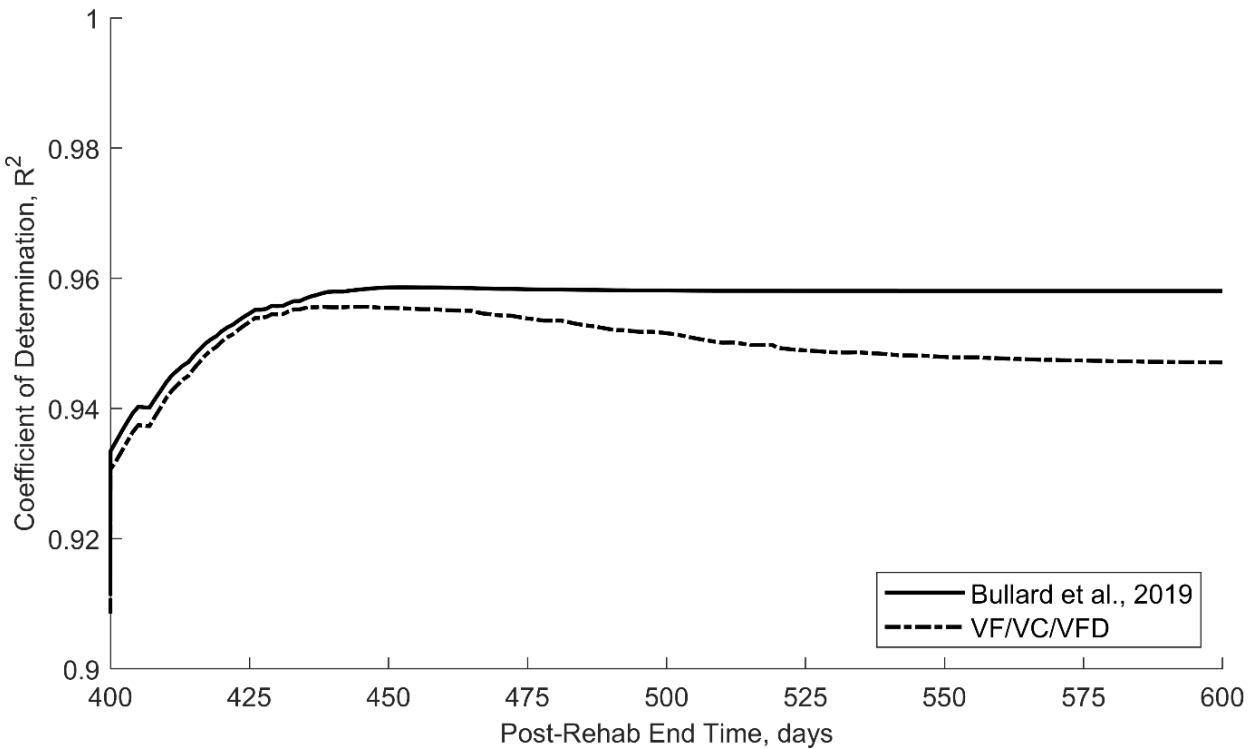


Figure D-21. Coefficient of determination

Following the determination of the optimal switchback time, the full model was run for all constituents using Screen 1 and 2 length weighted, pre-rehab flow weighted, and post-rehab flow weighted values (Figure D-22, Figure D-24, Figure D-26). Coefficients of determination were calculated for each constituent over each model run (Figure D-23, Figure D-25, Figure D-27). Since the results were not significantly different, the pre-rehab flow-weighted model was chosen for inclusion in the article.

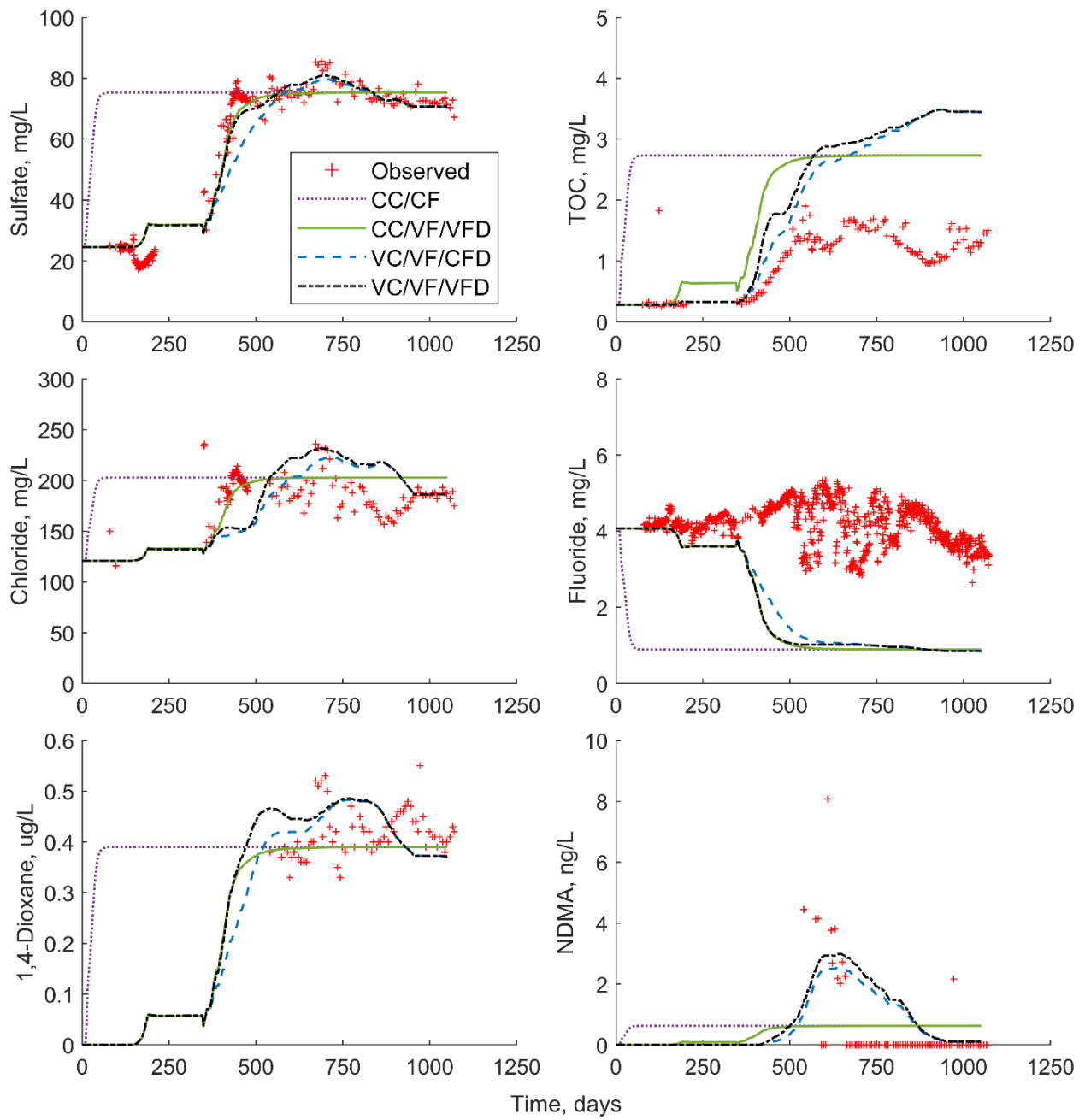


Figure D-22. Length-weighted model using Screens 1 and 2.

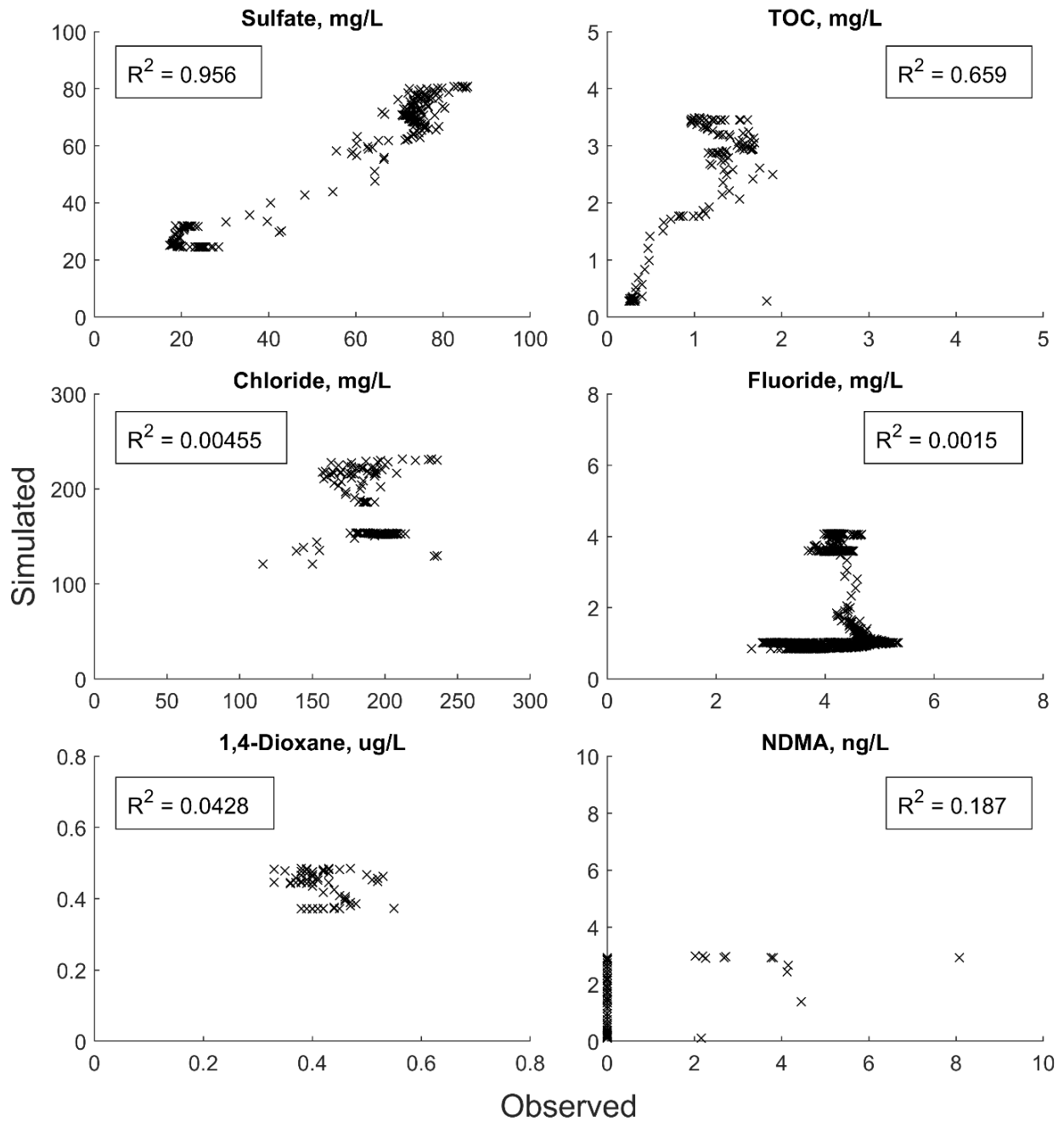


Figure D-23. Length-weighted model coefficients of determination.

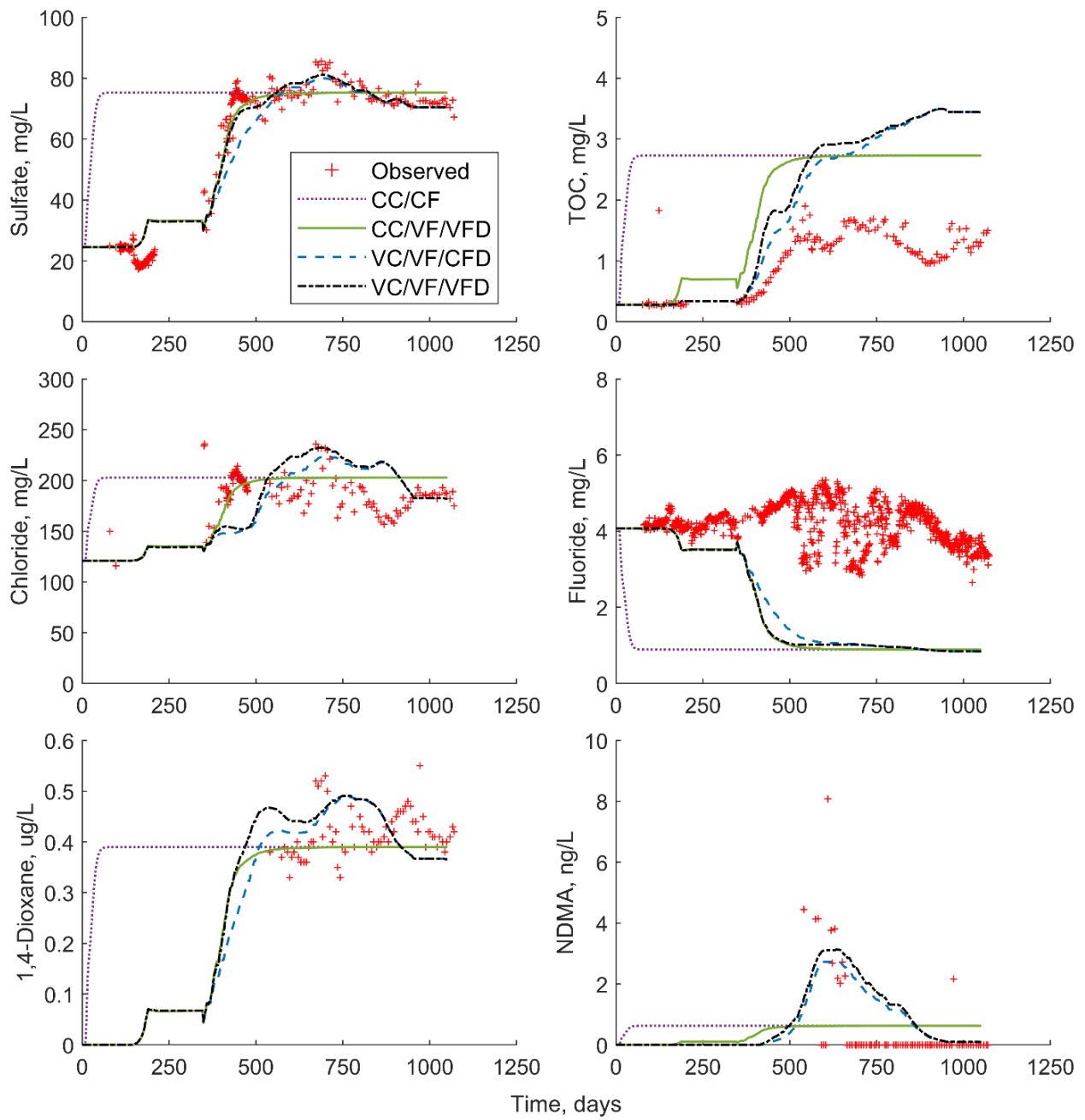


Figure D-24. Pre-rehab flow weighted model using Screens 1 and 2.

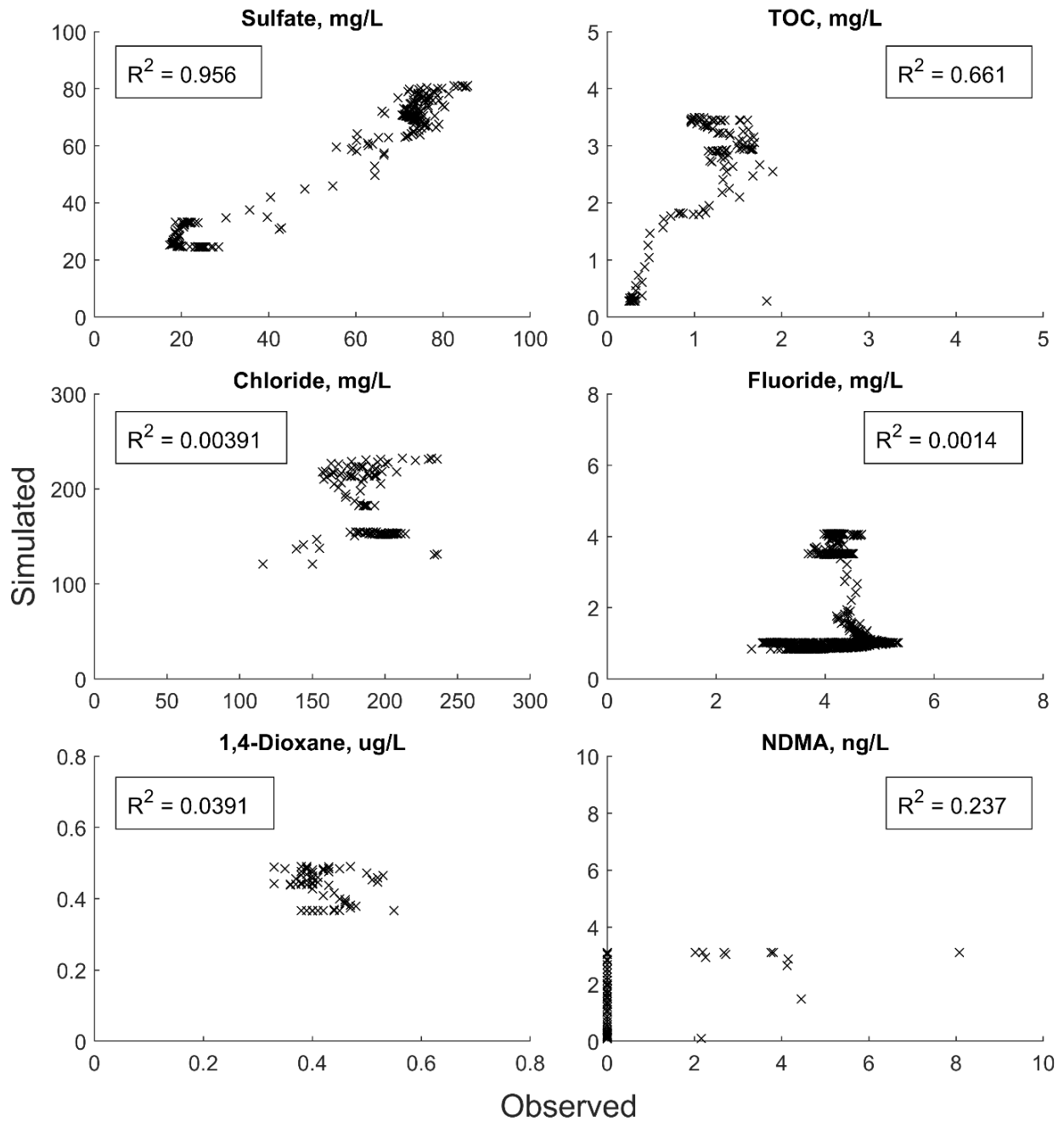


Figure D-25. Pre-rehab flow-weighted model coefficients of determination.

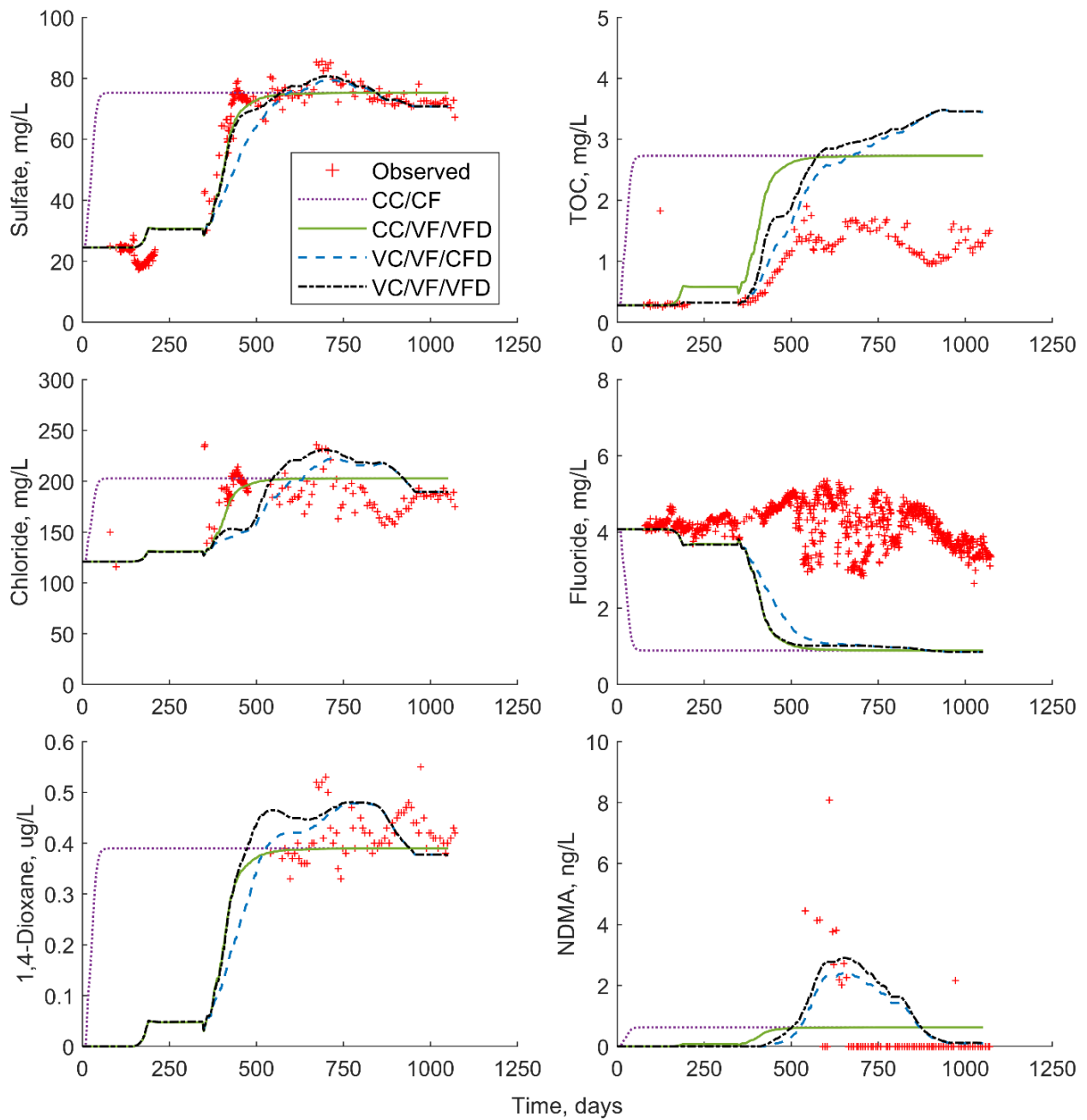


Figure D-26. Post-rehab flow weighted model using Screens 1 and 2.

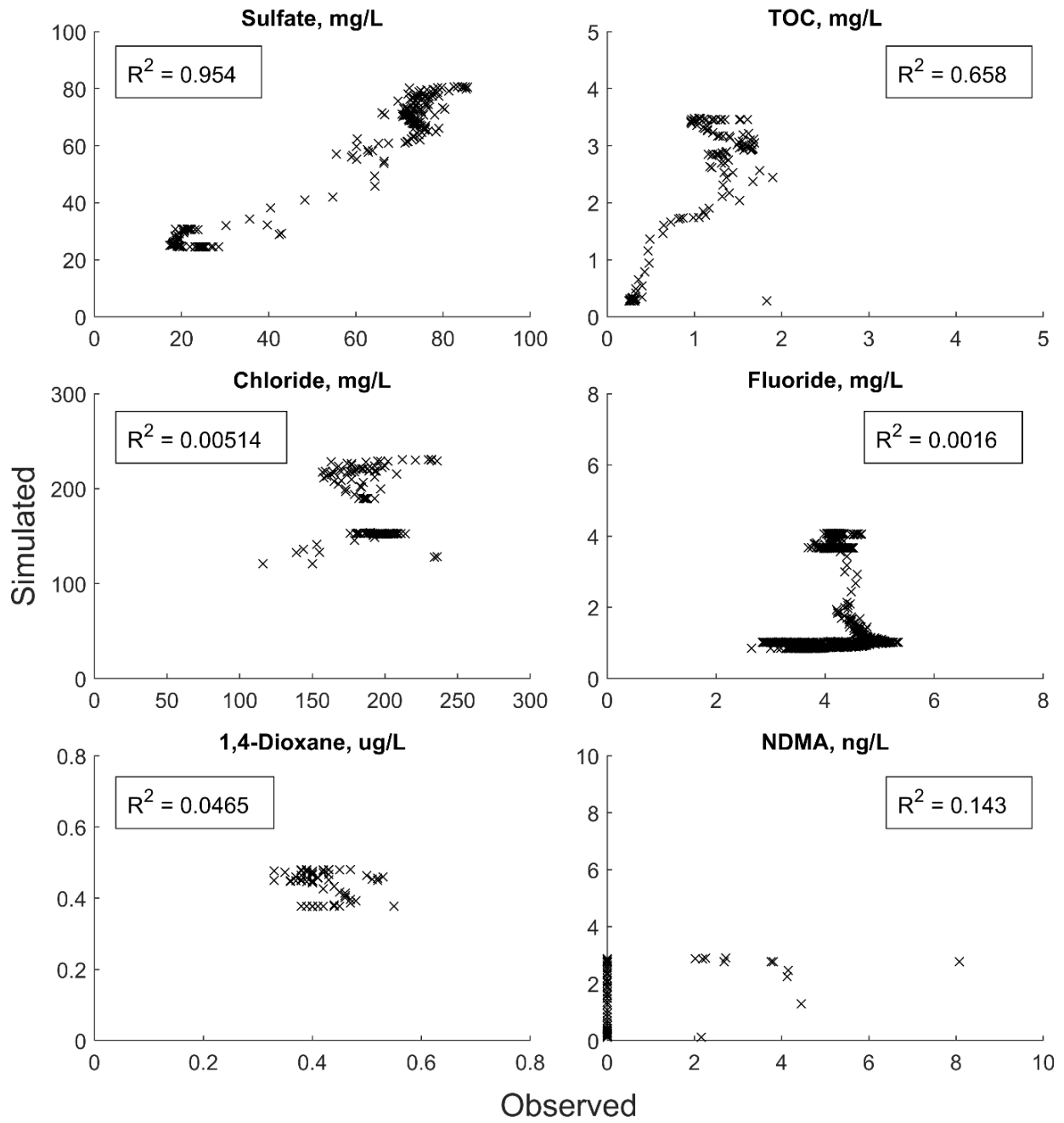


Figure D-27. Post-rehab flow-weighted model coefficients of determination.

Middle Potomac Aquifer (MPA)

A similar approach was used for chloride breakthrough in MW-MPA. First, a breakthrough model for chloride was calculated for each individual screen (Figure D-28). These models assume that the MPA is solely measuring from that screen alone (only using the screen length and aquifer characteristics (n and α) from that screen, as determined from as-built diagrams and the original breakthrough work done in 2018).

Next, length- and flow-weighted averages were calculated using the breakthrough models developed for each screen. Two separate flow-weighted averages were calculated, one based on pre-rehabilitation flow measured during initial conductivity breakthrough (Bullard et al. 2019), the other based on post-rehabilitation flow distribution measured during in-situ flowmeter testing in May 2019. Details regarding pre- and post-rehab flow distribution and individual screen characteristics are documented in Table D-1.

Table D-1. Pre- and post-rehab flow distributions and aquifer characteristics for MW-MPA.

	Pre-Rehab Flow Distribution (Conductivity Breakthrough)	Post Rehab Flow Distribution (In-Situ Flowmeter)	Porosity	Longitudinal Dispersivity (ft)
Screen 5	4.0%	6%	0.25	8
Screen 6	3.5%	3%	0.30	20
Screen 7	1.2%	2%	0.28	30
Screen 8	0.8%	2%	0.32	10
Screen 9	31%	11%	0.23	10

The results of the length- and flow-weighted model using all the screens confirms the same conclusion made in the UPA – that sample bias exists within the monitoring well and that the sample collected is not representative of all of the screens (Figure D-29). If the sample was representative of all of the screens, chloride from screen 9 would have caused the breakthrough to occur much faster. The process was repeated for combinations of the remainder of the screens – Screen 5 and 6 (Figure D-30), Screens 5-7 (Figure D-31), and Screens 5-8 (Figure D-32). While this data is preliminary, it seems to confirm the choice of a flow-weighted combination of screens 5-8. The choice of pre- or post-rehab in this case is not important since the difference

between the two is insignificant to the results. Further conclusions should not be drawn without continued observation and analysis.

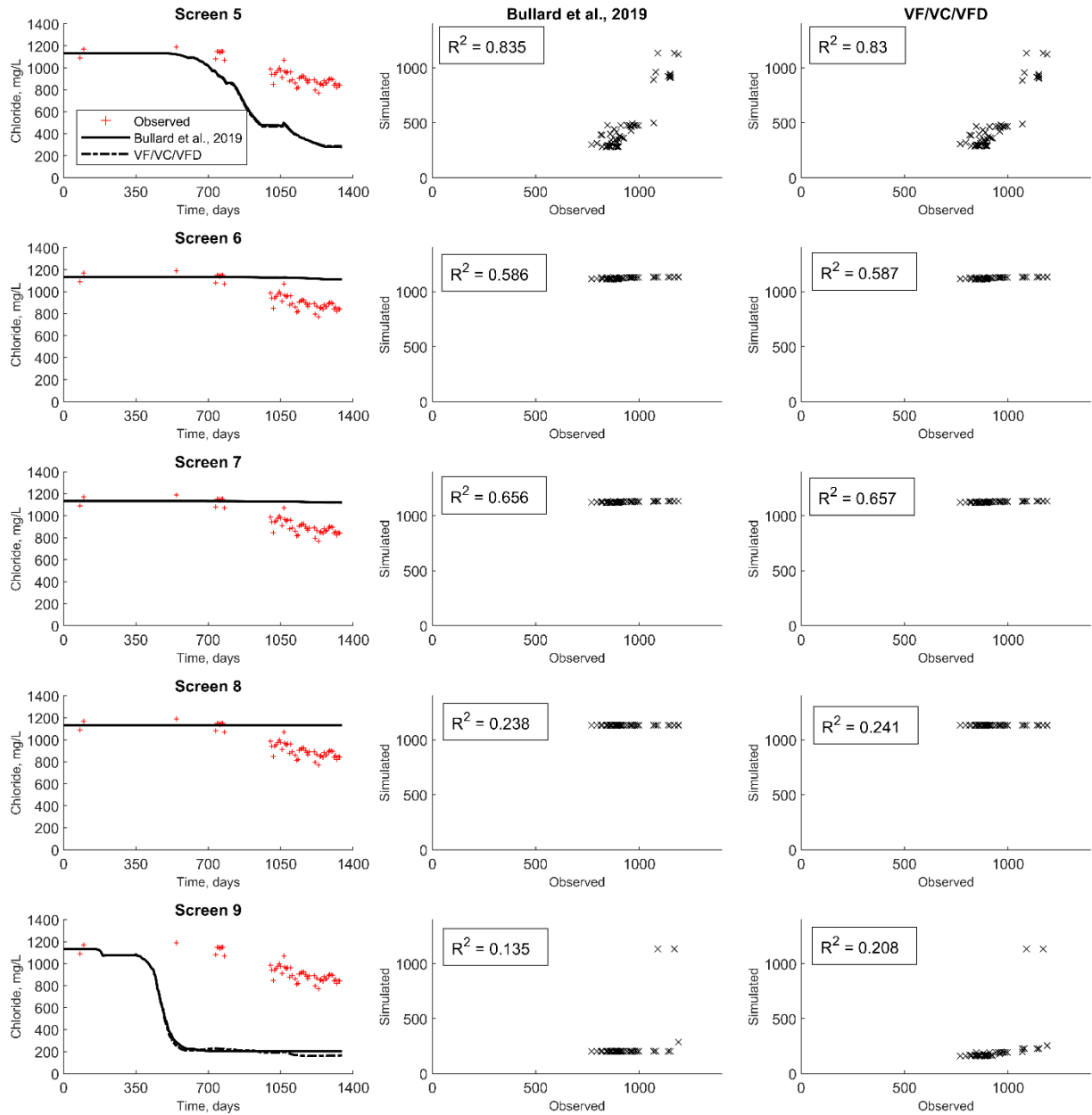


Figure D-28. Breakthrough calculated at each individual screen (5-9) using aquifer characteristics (n and α) determined in Bullard et al. (2019). Coefficients of determination are shown for the constant concentration model (labeled Bullard et al. 2019) and the variable concentration model (labeled VF/VC/VFD). Both models account for variable flow and variable flow distribution.

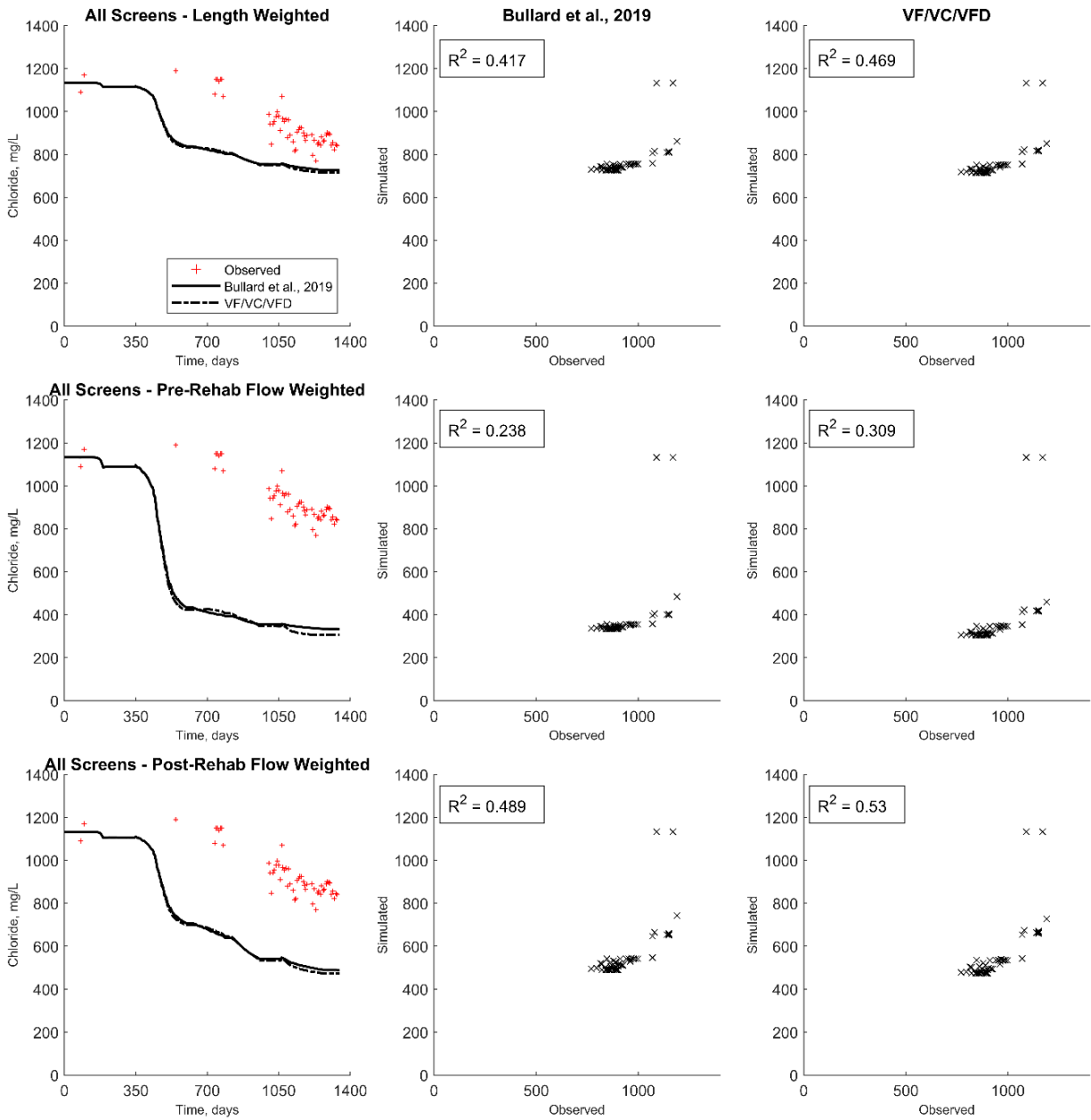


Figure D-29. Flow- and length-weighted models using screens 5-9. Coefficients of determination are shown for the constant concentration model (labeled Bullard et al. 2019) and the variable concentration model (labeled VF/VC/VFD). Both models account for variable flow and variable flow distribution.

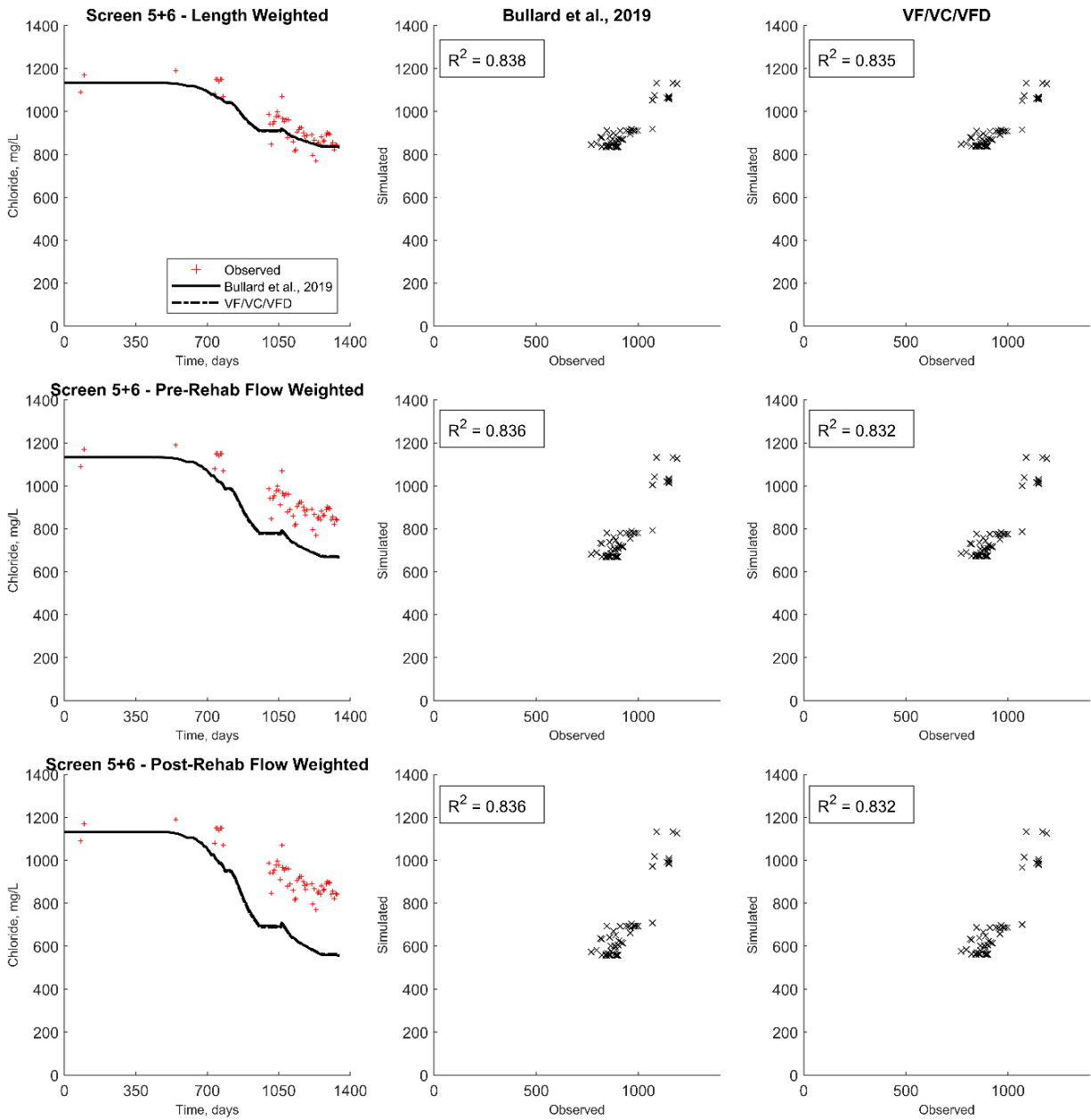


Figure D-30. Flow- and length-weighted models using screens 5-6. Coefficients of determination are shown for the constant concentration model (labeled Bullard et al. 2019) and the variable concentration model (labeled VF/VC/VFD). Both models account for variable flow and variable flow distribution.

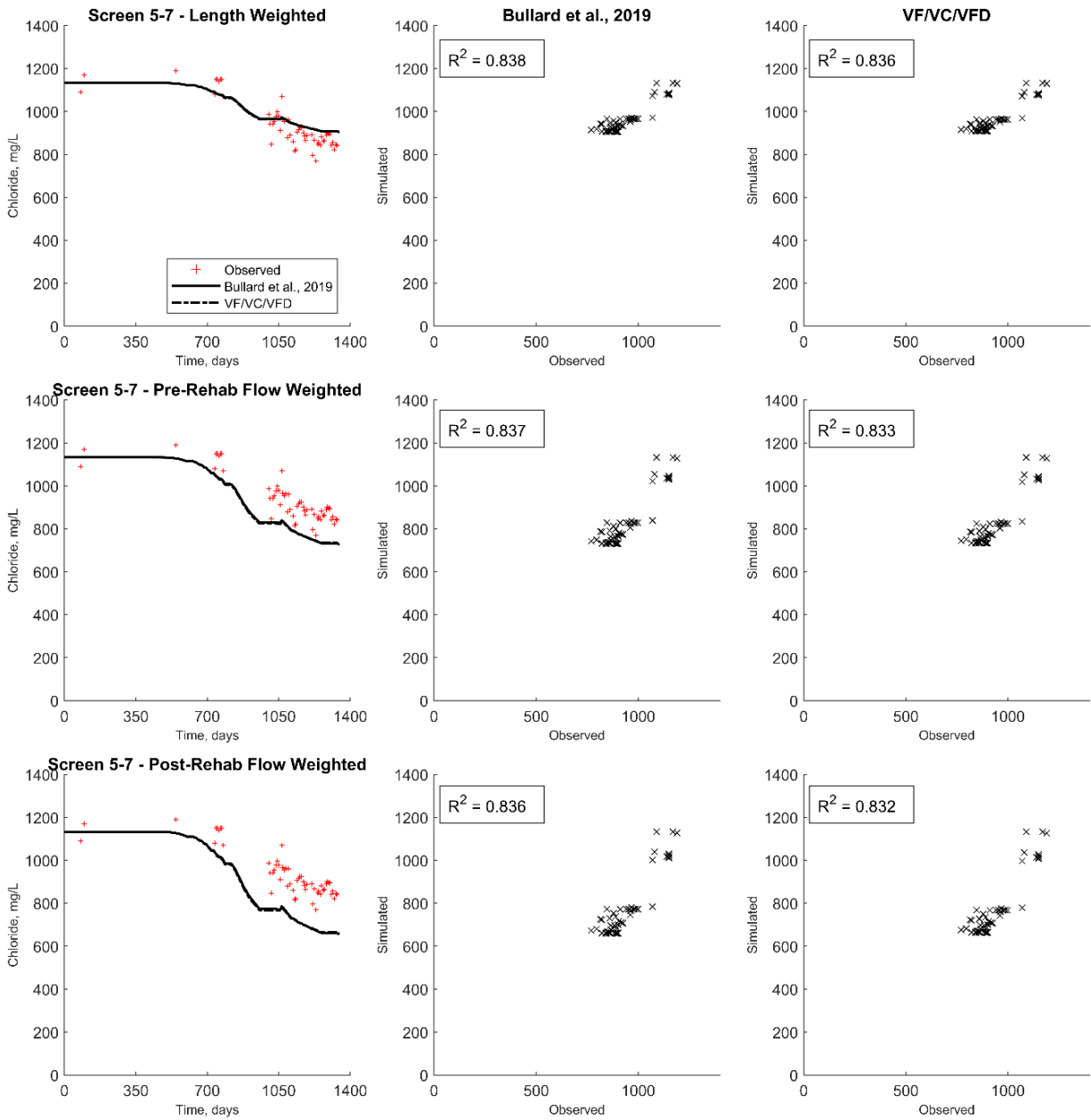


Figure D-31. Flow- and length-weighted models using screens 5-7. Coefficients of determination are shown for the constant concentration model (labeled Bullard et al. 2019) and the variable concentration model (labeled VF/VC/VFD). Both models account for variable flow and variable flow distribution.

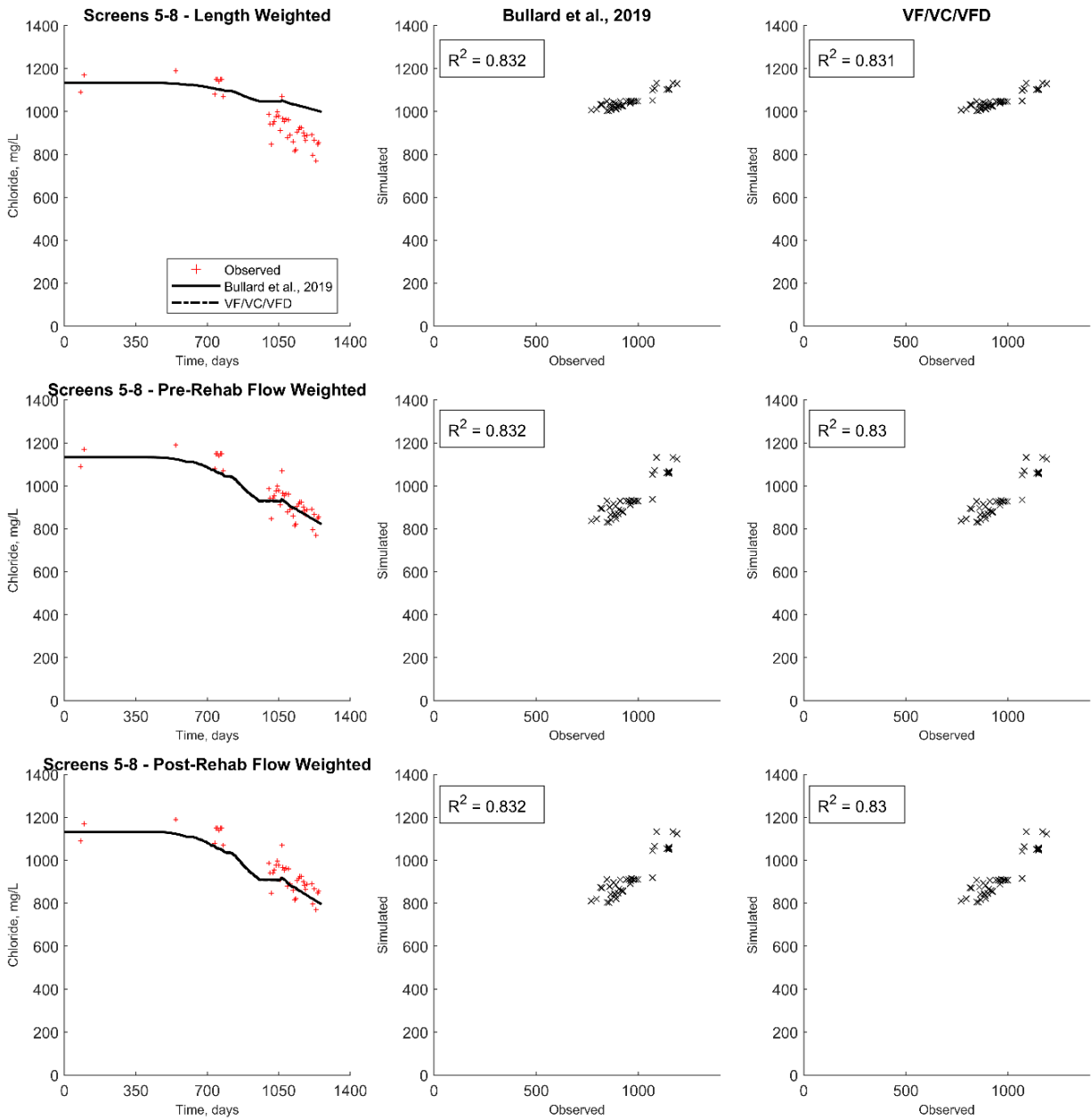


Figure D-32. Flow- and length-weighted models using screens 5-8. Coefficients of determination are shown for the constant concentration model (labeled Bullard et al. 2019) and the variable concentration model (labeled VF/VC/VFD). Both models account for variable flow and variable flow distribution.

Appendix E: Bromide Tracer Supplemental Information

Sampling Schedule

Table E-2. Bromide Tracer initial sampling frequency chart. Frequencies were adjusted over time based on screen-specific responses.

Well ID	Initial Sampling Frequency	Increase Frequency Threshold (mg/L)	Threshold Sampling Frequency	Estimated Time to Sampling Increase (days)	Estimated Time to Breakthrough (days)	Estimated Maximum Concentration (mg/L)	Decrease Frequency Threshold (mg/L)	Decreased Sampling Frequency
MW-SAT Screen 1	4x/day (every 6 hours)	--	--		3.5	186	74	1x/day
MW-SAT Screen 2	4x/day (every 6 hours)	--	--		3.25	173	69	1x/day
MW-SAT Screen 3	4x/day (every 6 hours)	--	--		8.5	36	14	1x/day
MW-SAT Screen 4	4x/day (every 6 hours)	--	--		5.25	39	16	1x/day
MW-SAT Screen 5	4x/day (every 6 hours)	--	--		4.5	105	42	1x/day
MW-SAT Screen 6	2x/day (every 12 hours)	15	4x/day	4	8	21	8	1x/day
MW-SAT Screen 7	2x/day (every 12 hours)	15	4x/day	2	4.25	37	15	1x/day
MW-SAT Screen 8	1x/day	10	2x/day	7	14	20	8	1x/day
MW-SAT Screen 9	4x/day (every 6 hours)	--	--		4.75	82	33	1x/day
MW-SAT Screen 10	1x/day	2	2x/day	38	76	3	2	1x/day
MW-SAT Screen 11	1x/day	1.5	2x/day	60	112	2	1.5	1x/day
MW-UPA	1x/week	8	1x/day	50	65	14	6	1x/week
MW-MPA	1x/week				252	3.12		
MW-LPA	1x/month	--	--		7,500	0.128	--	

Experimental Data

Mass injected was calculated using tote drawdown and the measured concentration from the totes (Table E-3). Cumulative volume for a time period was calculated based on measured flow using a Rosemount 8750W Magnetic Flowmeter System. Instantaneous flow rates were recorded using SWIFT’s supervisory control and data acquisition (SCADA) system, and one-minute increment flows were accessed and averaged over the period of the injection phase.

Table E-3. Calculation of influent concentration using drawdown measured in the totes.

Date	Start Time	End time	% of Time Recharging	Drawdown, cm	Weight injected, mg	Recharge Volume, L	Influent Concentration, mg/L
9/29/2020	09:25	10:25	100%	6.80	33,325,145	154,914	215
9/29/2020	10:25	11:25	100%	6.60	32,344,994	154,196	210
9/29/2020	11:25	13:25	100%	11.70	57,338,852	308,890	186
9/29/2020	13:25	14:25	100%	6.00	29,404,540	154,765	190
9/29/2020	14:25	15:25	100%	6.10	29,894,615	154,079	194
9/29/2020	15:25	16:25	32%	2.70	13,225,917	61,254	216
9/29/2020	16:25	17:25	100%	6.00	29,404,540	155,955	189
9/29/2020	17:25	18:25	100%	6.00	29,404,540	154,502	190
9/29/2020	18:25	19:25	100%	6.00	29,404,540	154,970	190
9/29/2020	19:25	20:25	100%	6.00	29,404,540	154,283	191
9/29/2020	20:25	21:00	100%	0.00	-	89,587	0
9/29/2020	21:00	21:25	100%	5.20	25,483,934	64,516	395
9/29/2020	21:25	22:25	100%	5.00	24,503,783	154,181	159
9/29/2020	22:25	23:25	100%	5.00	24,503,783	153,697	159
9/30/2020	23:25	00:25	100%	5.00	24,503,783	154,402	159
9/30/2020	00:25	01:25	100%	5.00	24,503,783	153,392	160
9/30/2020	01:25	02:25	100%	5.00	24,503,783	153,733	159
9/30/2020	02:25	03:25	100%	5.00	24,503,783	153,539	160
9/30/2020	03:25	04:25	100%	4.50	22,053,405	153,213	144
9/30/2020	04:25	05:25	35%	2.50	12,251,892	95,697	128
9/30/2020	05:25	06:25	100%	3.30	16,172,497	120,739	134
9/30/2020	06:25	07:18	100%	6.67	32,675,795	137,350	238
9/30/2020	07:18	08:45	100%	5.08	24,895,844	224,453	111
9/30/2020	08:45	09:58	100%	6.35	31,119,804	188,410	165
9/30/2020	09:58	10:52	100%	5.40	26,451,834	138,983	190
9/30/2020	10:52	12:52	100%	9.53	46,679,707	308,583	151
9/30/2020	12:52	14:37	100%	4.00	19,603,026	269,506	73
9/30/2020	14:37	16:29	65%	0.00	-	198,762	0

9/30/2020	16:29	17:57	76%	10.80	52,903,668	227,090	233
9/30/2020	17:57	19:58	0%	0.64	3,111,980	19,160	162
9/30/2020	19:58	22:01	97%	12.38	60,683,619	236,511	257
9/30/2020	22:01	23:15	100%	8.00	39,206,053	190,521	206
9/30/2020	23:15	00:15	100%	6.50	31,854,918	154,339	206
10/1/2020	00:15	01:15	100%	6.00	29,404,540	154,149	191
10/1/2020	01:15	02:15	100%	6.00	29,404,540	154,042	191
10/1/2020	02:15	03:15	100%	6.40	31,364,842	153,911	204
10/1/2020	03:15	04:15	100%	7.00	34,305,296	153,843	223
10/1/2020	04:15	05:15	23%	4.00	19,603,026	112,567	174
10/1/2020	05:15	06:15	100%	3.70	18,132,799	87,769	207
10/1/2020	06:15	09:45	100%	19.00	93,114,376	543,666	171
10/1/2020	09:45	12:06	100%	17.78	87,135,452	363,977	239
10/1/2020	12:06	13:28	100%	7.62	37,343,765	210,966	177
10/1/2020	13:28	14:57	90%	8.26	40,455,746	229,520	176
10/1/2020	14:57	16:56	76%	9.53	46,679,707	217,093	215
10/1/2020	16:56	17:25	100%	5.40	26,451,834	75,145	352
10/1/2020	17:25	17:58	100%	2.86	14,003,912	85,227	164
10/1/2020	17:58	19:57	100%	10.48	51,347,677	308,063	167
10/1/2020	19:57	21:01	100%	5.72	28,007,824	165,595	169
10/1/2020	21:01	22:01	100%	5.40	26,451,834	154,977	171
10/1/2020	22:01	23:01	100%	5.72	28,007,824	154,534	181
10/1/2020	23:01	00:01	100%	6.03	29,563,814	155,373	190
10/2/2020	00:01	01:01	100%	6.03	29,563,814	154,343	192
10/2/2020	01:01	02:01	100%	6.03	29,563,814	155,060	191
10/2/2020	02:01	03:01	100%	5.72	28,007,824	154,271	182
10/2/2020	03:01	04:01	100%	6.03	29,563,814	154,709	191
10/2/2020	04:01	05:01	35%	8.26	40,455,746	154,320	262
10/2/2020	05:01	06:01	100%	2.22	10,891,932	65,908	165
10/2/2020	06:01	07:42	100%	9.53	46,679,707	262,113	178
10/2/2020	07:42	08:30	100%	6.67	32,675,795	124,167	263
10/2/2020	08:30	09:49	100%	6.99	34,231,785	204,923	167
10/2/2020	09:49	10:22	100%	2.86	14,003,912	85,162	164
10/2/2020	10:22	12:08	100%	9.53	46,679,707	274,494	170
10/2/2020	12:08	13:45	100%	0.00	-	251,014	0
10/2/2020	13:45	14:54	62%	6.99	34,231,785	178,018	192
10/2/2020	14:54	15:30	64%	2.86	14,003,912	92,443	151
10/2/2020	15:30	19:06	100%	12.70	62,239,609	461,667	135
10/2/2020	19:06	20:01	58%	3.24	15,871,100	142,201	112
10/2/2020	20:01	20:43	0%	3.81	18,671,883	108,404	172

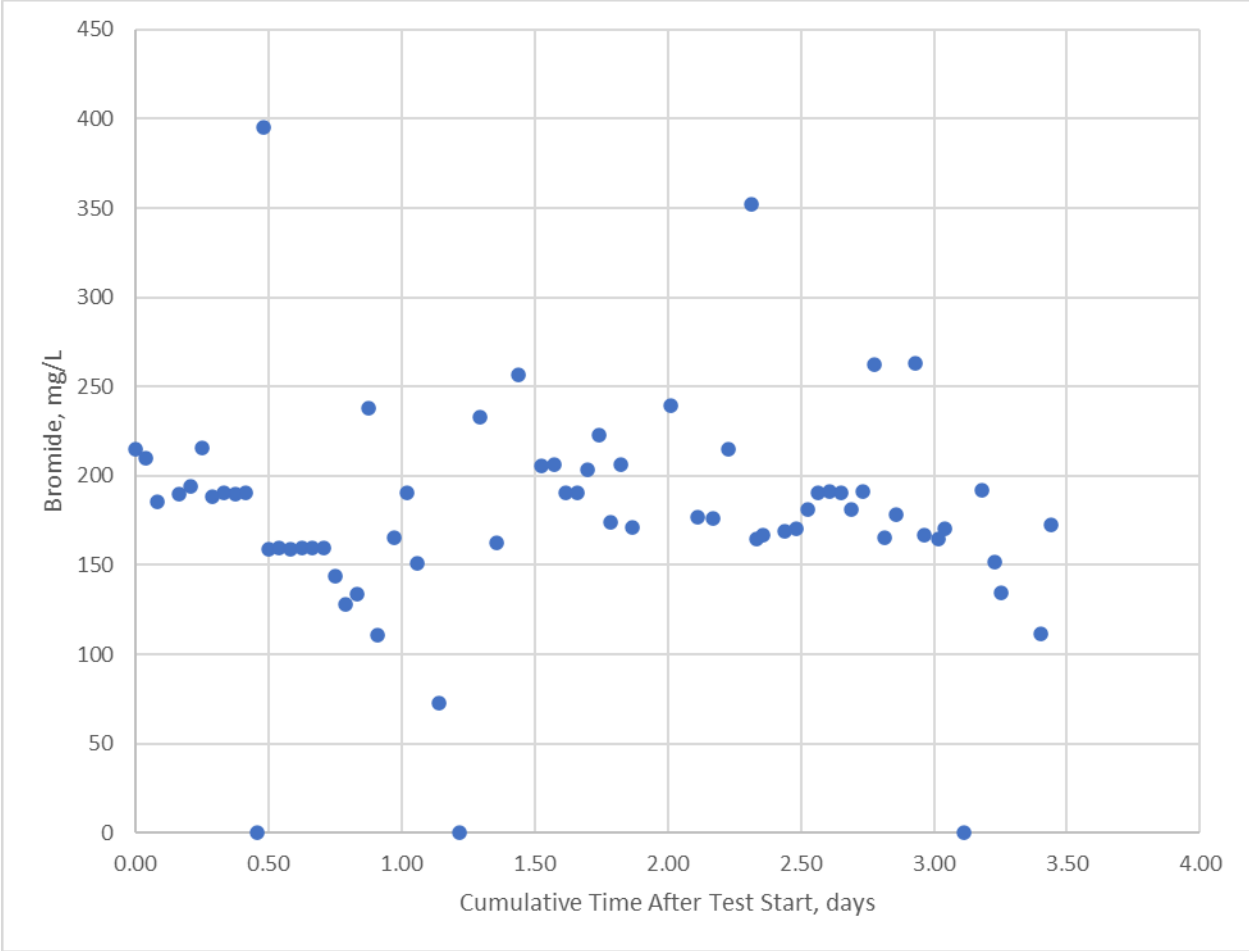


Figure E-33. Bromide concentration (mg/L) during injection period.

Initial Breakthrough Model

The initial model used to predict breakthrough at the wells estimated a constant flow (~680 gallons per minute (gpm)) and accounted for a variable influent concentration. Flow distribution, porosity, and longitudinal dispersivity estimates were developed from this constant flow model. Only the first 100 days were included here because at t = 87 days, the well was shut off for necessary well rehabilitation, and recharge flow stopped at the well.

Table E-4 provides a summary of the results from the initial constant concentration model and compares the estimated flow distribution, porosity, and longitudinal dispersivity to that previously estimated at the site based on the initial breakthrough of SWIFT Water measured in 2018 (Bullard et al. 2019). Flow distribution measured via flowmeter in 2019 is also included (see previous dissertation chapter).

Table E-4. Summary of results from initial constant flow model.

Screen	Flow (%)			Porosity, n		Longitudinal Dispersivity, α	
	Conductivity Initial Model	Flowmeter	Bromide Tracer	Conductivity Initial Model	Bromide Tracer	Conductivity Initial Model	Bromide Tracer
1	18%	19%	6.00%	0.2	0.25	5	5
2	24%	46%	9.00%	0.25	0.25	10	5
3	6%	2%	0.75%	0.27	0.25	10	15
4	9%	7%	4.00%	0.35	0.3	20	10
5	4%	6%	2.00%	0.25	0.27	8	8
6	3.5%	3%	1.25%	0.3	0.3	20	5
7	1.2%	2%	0.85%	0.28	0.29	30	3.3
8	0.8%	2%	1.70%	0.32	0.32	10	1
9	31%	11%	18.50%	0.23	0.29	10	3
10	2%	1%	15.00%	0.25	0.32	10	8
11	0.4%	0.00%	5.00%	0.27	0.3	10	9
SUM	100%	99%	64.05%	0.27	0.29	13	6.57

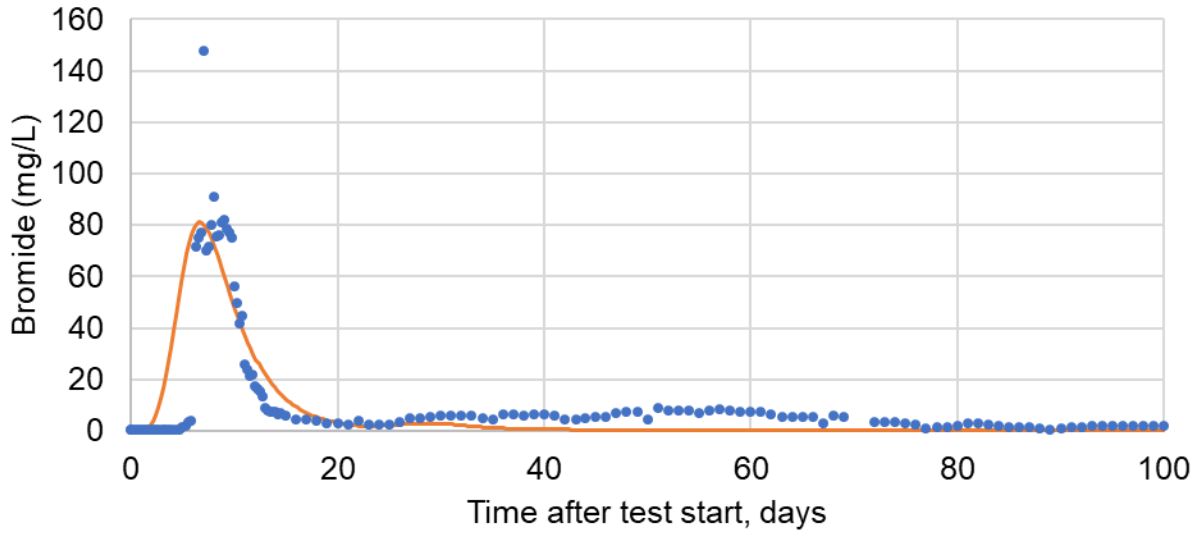


Figure E-34. Screen 1 initial bromide observations and breakthrough model.

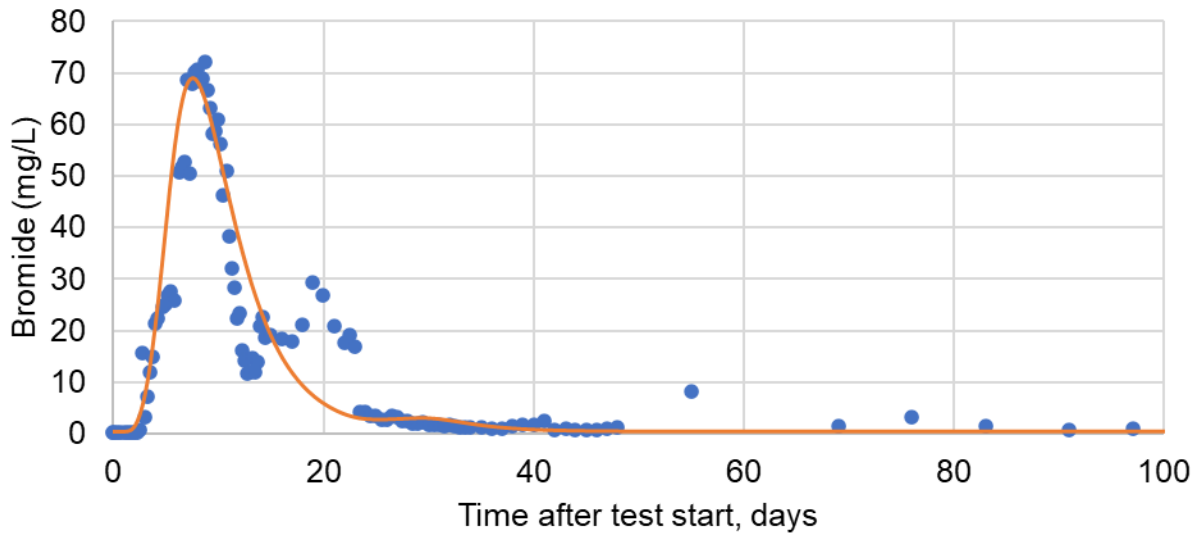


Figure E-35. Screen 2 initial bromide observations and breakthrough model.

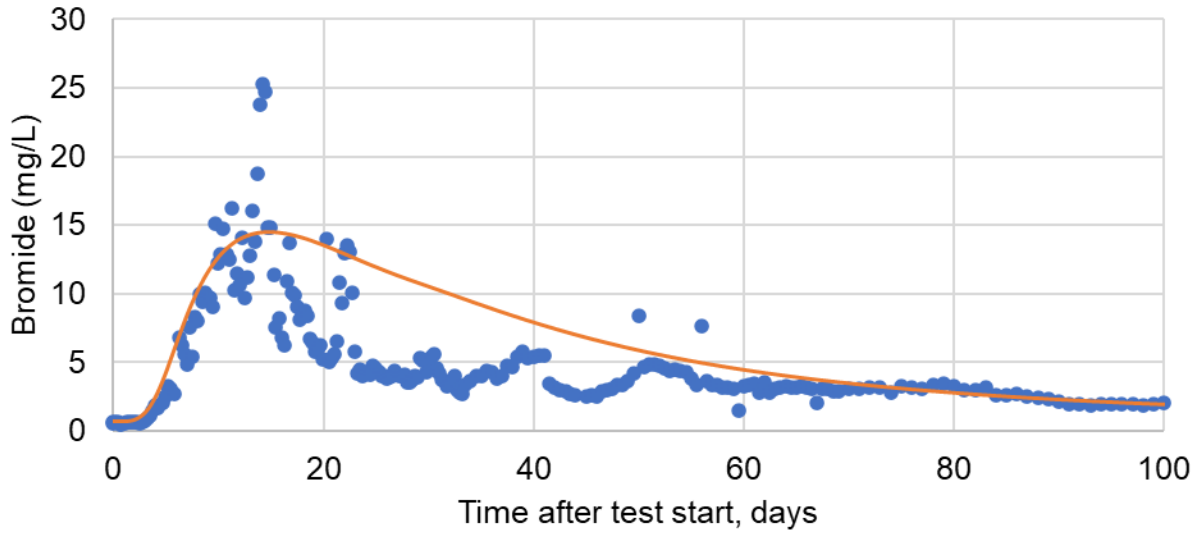


Figure E-36. Screen 3 initial bromide observations and breakthrough model.

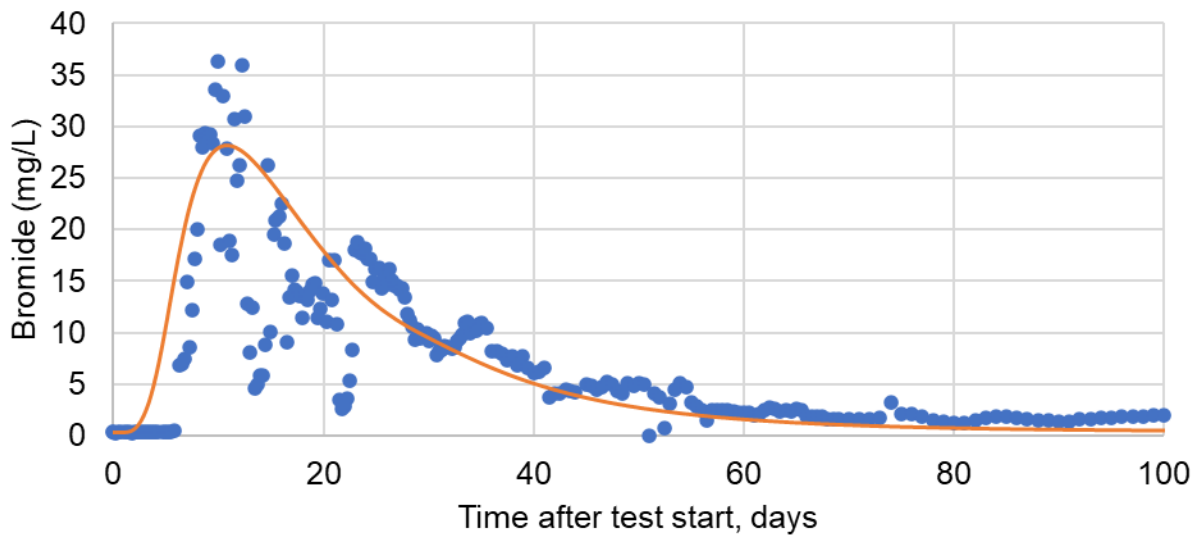


Figure E-37. Screen 4 initial bromide observations and breakthrough model.

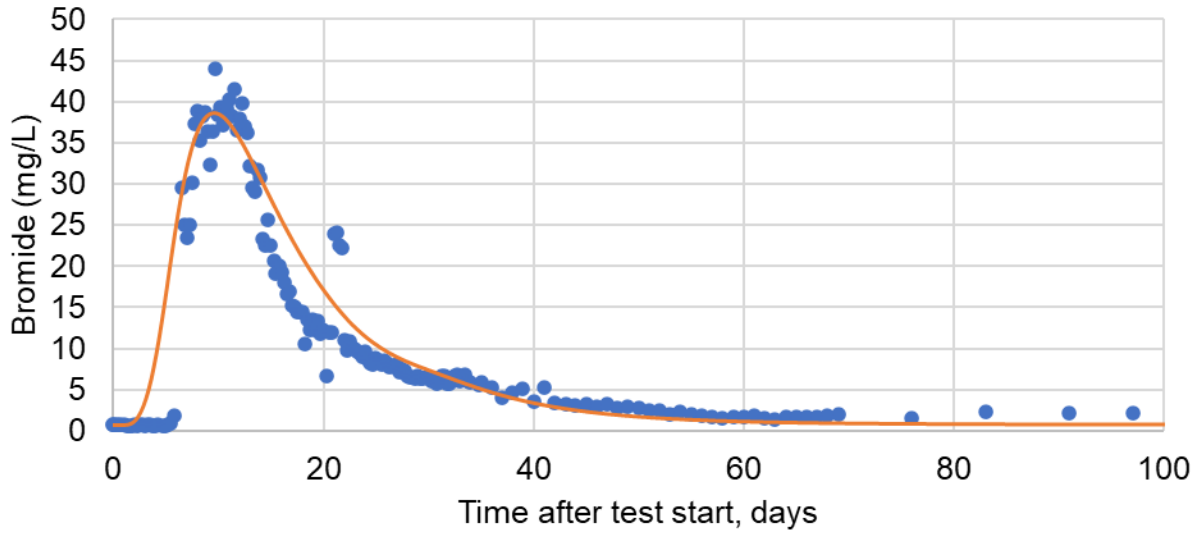


Figure E-38. Screen 5 initial bromide observations and breakthrough model.

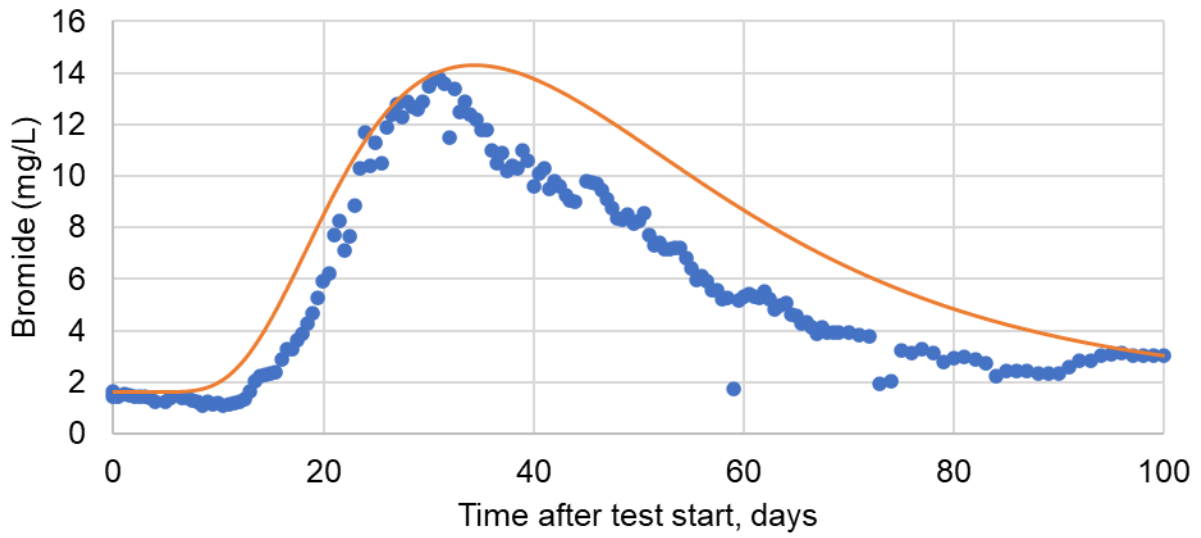


Figure E-39. Screen 6 initial bromide observations and breakthrough model.

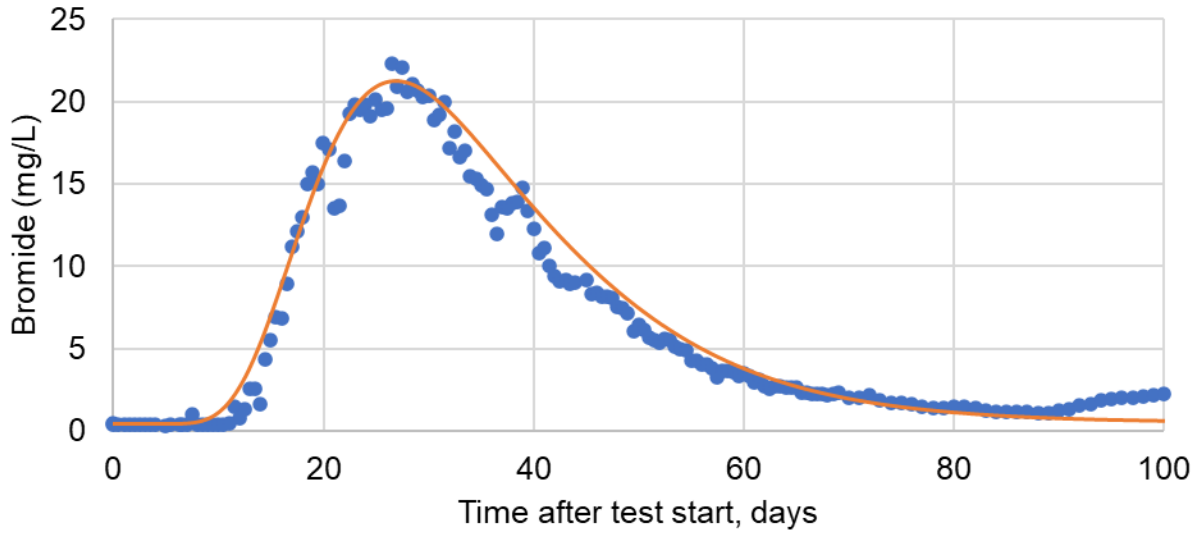


Figure E-40. Screen 7 initial bromide observations and breakthrough model.

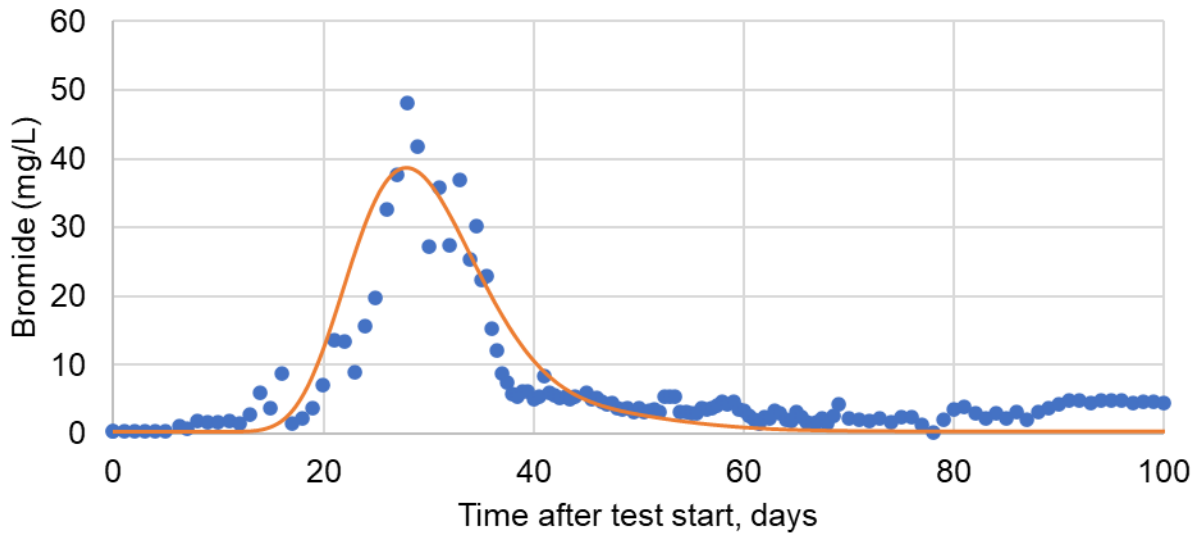


Figure E-41. Screen 8 initial bromide observations and breakthrough model.

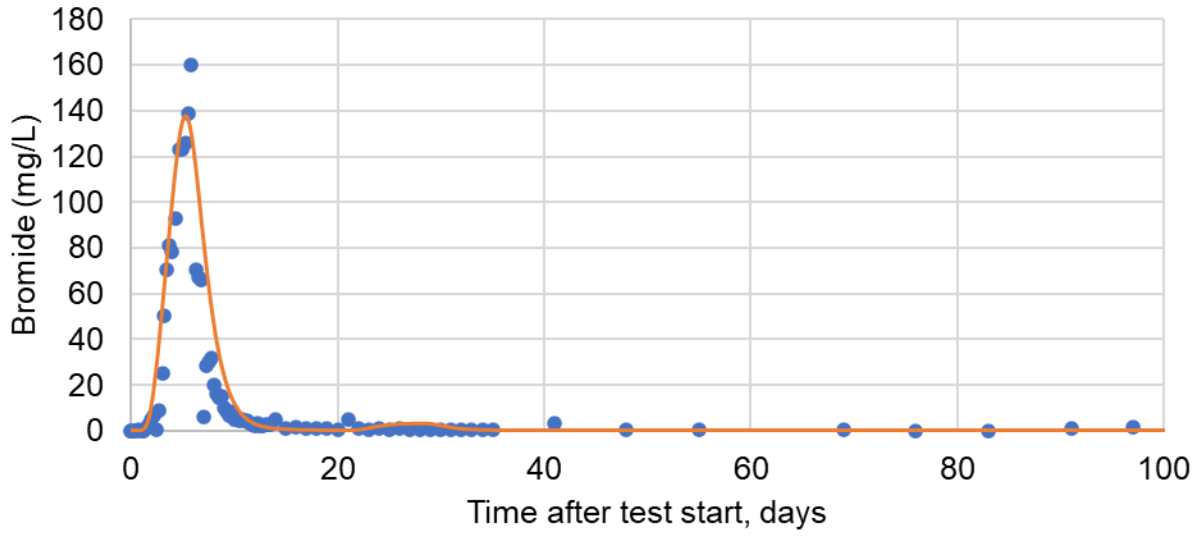


Figure E-42. Screen 9 initial bromide observations and breakthrough model.

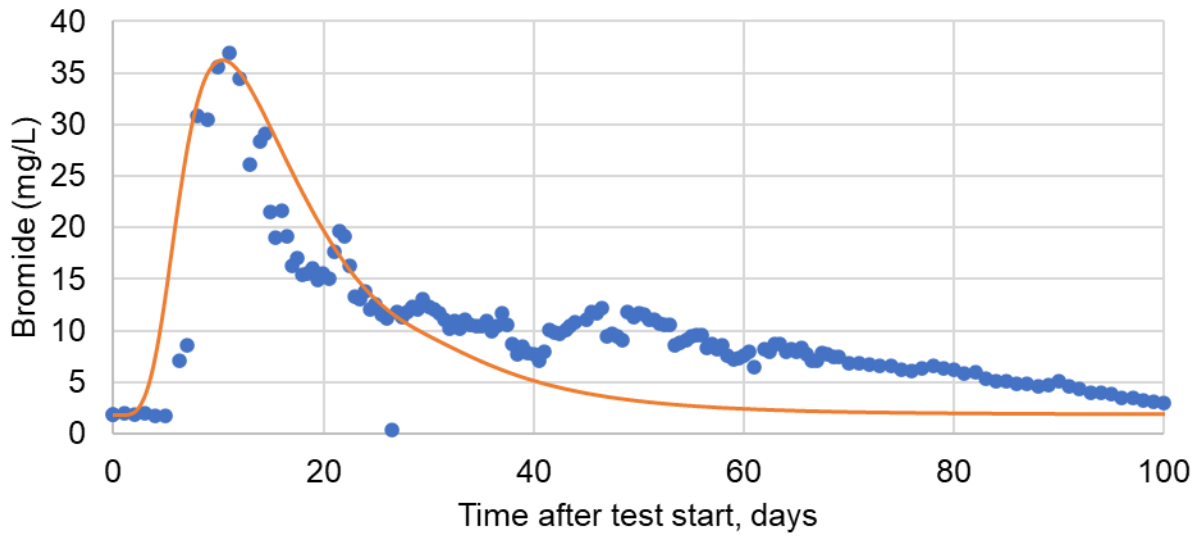


Figure E-43. Screen 10 initial bromide observations and breakthrough model.

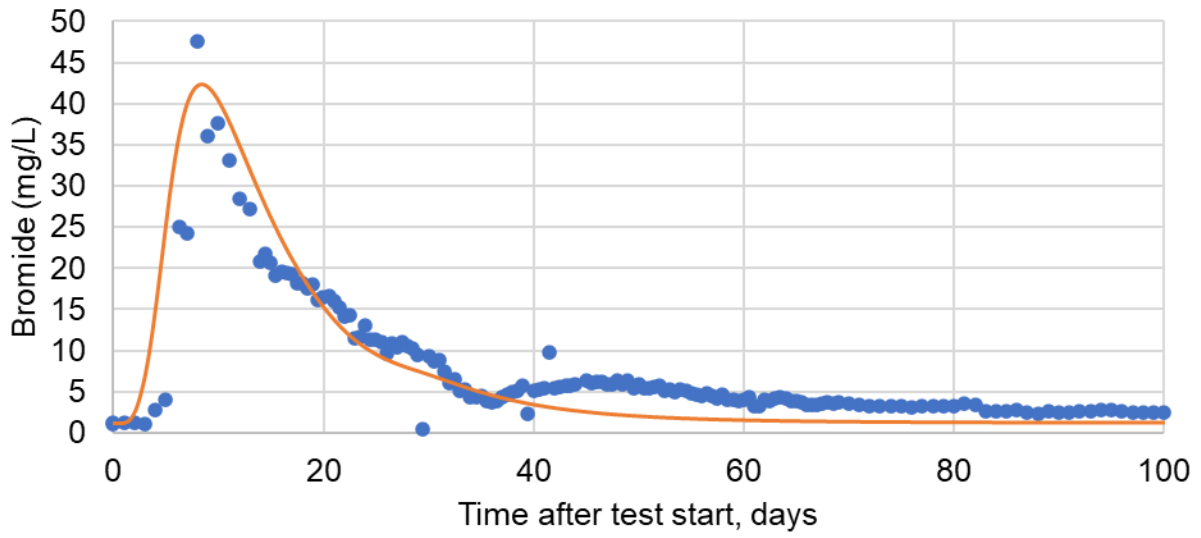


Figure E-44. Screen 11 initial bromide observations and breakthrough model.

Variable Flow Optimization

Single Zone Optimization

The model described in the multi-tracer analysis to account for variable influent concentration and variable flow distribution was implemented in conjunction with MATLAB's optimization tool to estimate the aquifer characteristics. To simplify the model, instead of using separate flow distribution and porosity values, a combined variable that represented both flow distribution and porosity (Q/n) was used. A range of Q/n values is included in Table E-5 to demonstrate the initial boundaries. The results from the constant flow model were used to form the initial estimate for the parameter optimization.

Table E-5. Range of Q/n values.

		Porosity			
		0.2	0.3	0.4	0.5
Flow Distribution	0.05%	0.0025	0.0017	0.0013	0.0010
	1%	0.0500	0.0333	0.0250	0.0200
	2%	0.1000	0.0667	0.0500	0.0400
	5%	0.2500	0.1667	0.1250	0.1000
	10%	0.5000	0.3333	0.2500	0.2000
	15%	0.7500	0.5000	0.3750	0.3000
	20%	1.0000	0.6667	0.5000	0.4000
	25%	1.2500	0.8333	0.6250	0.5000
	30%	1.5000	1.0000	0.7500	0.6000
	35%	1.7500	1.1667	0.8750	0.7000
	40%	2.0000	1.3333	1.0000	0.8000
	45%	2.2500	1.5000	1.1250	0.9000

Table E-6 includes a summary of results from the Single-Zone optimization exercise. Low and high flow estimates were calculated using an assumed range of 0.25-0.43 for the layer porosity.

Table E-6. Optimized Q/n and dispersivity (α) values for the Single-Zone optimization. Ranges of potential flow distribution are included based on estimated porosities.

Screen	Screen Length (ft)	Background Concentration (mg/L)	Dispersivity	Q/n	Low Q	High Q
1	25	0.295	2.78	0.262	6.5%	11.3%
2	45	0.236	6.43	0.400	10.0%	17.2%
3	15	0.647	40.94	0.018	0.5%	0.8%
4	35	0.319	16.81	0.113	2.8%	4.9%
5	15	0.710	9.89	0.084	2.1%	3.6%
6	30	1.614	12.65	0.040	1.0%	1.7%
7	15	0.430	4.83	0.039	1.0%	1.7%
8	25	0.314	1.03	0.077	1.9%	3.3%
9	40	0.212	3.04	0.797	19.9%	34.3%
10	105	1.856	14.53	0.360	9.0%	15.5%
11	30	1.211	14.21	0.152	3.8%	6.5%
Total Flow					58.5%	100.7%

The table of results of the Two-Zone model are included in the manuscript; however, all single screen results are included in the following figures (Figure E-45 to Figure E-66).

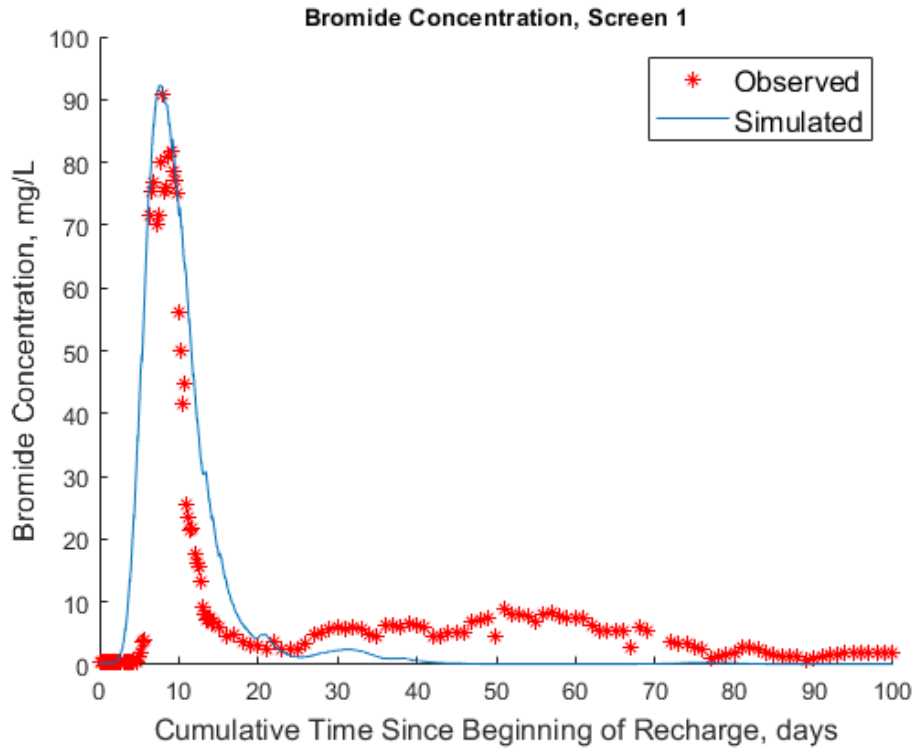


Figure E-45. Single-zone breakthrough at Screen 1.

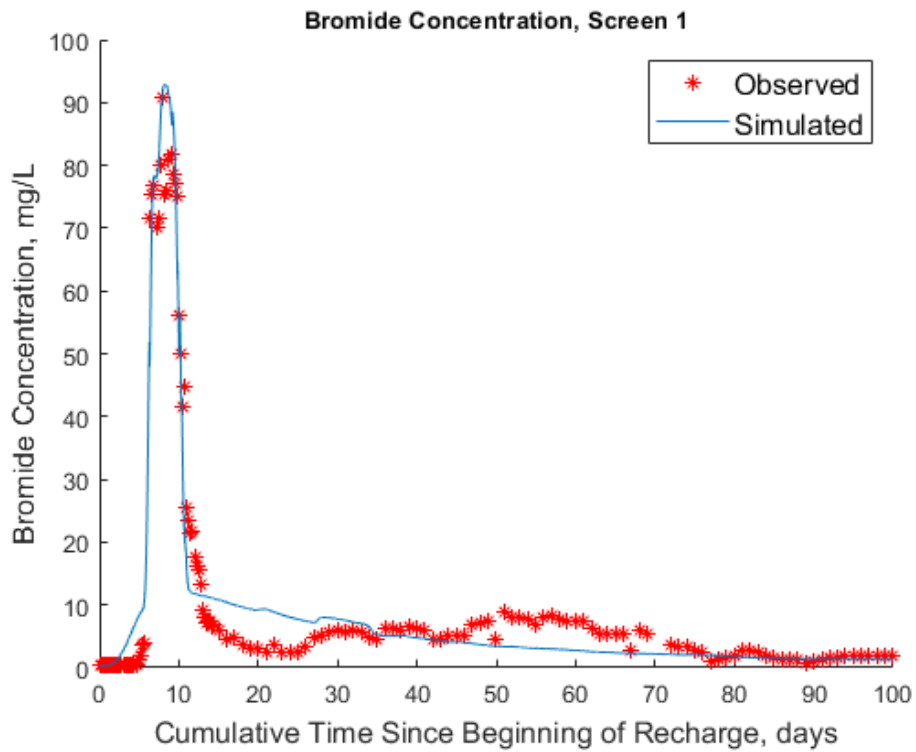


Figure E-46. Two-zone breakthrough at Screen 1.

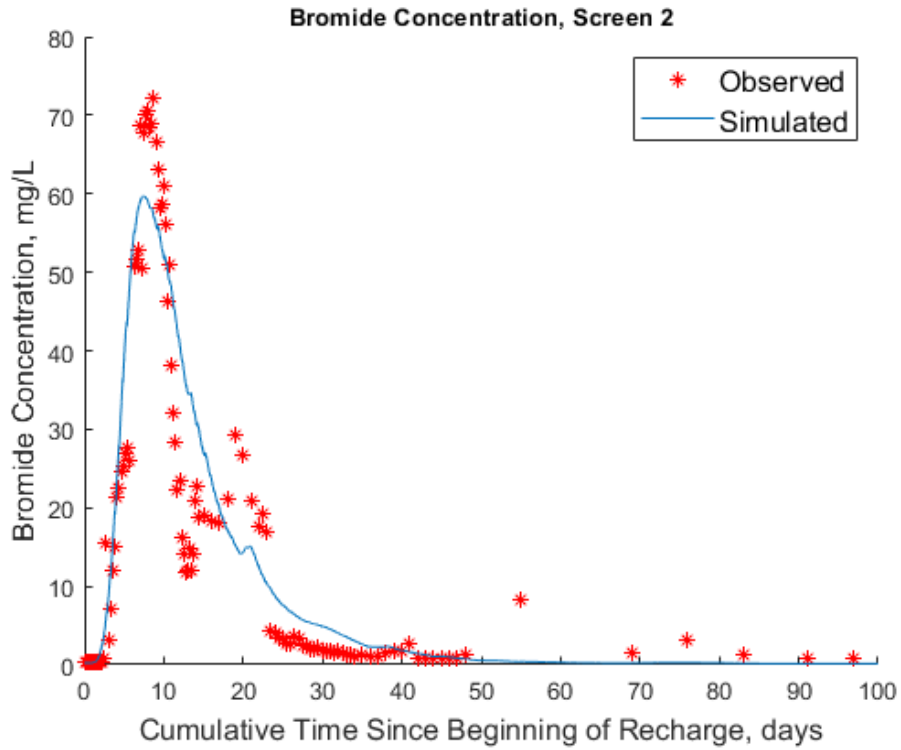


Figure E-47. Single-zone breakthrough at Screen 2.

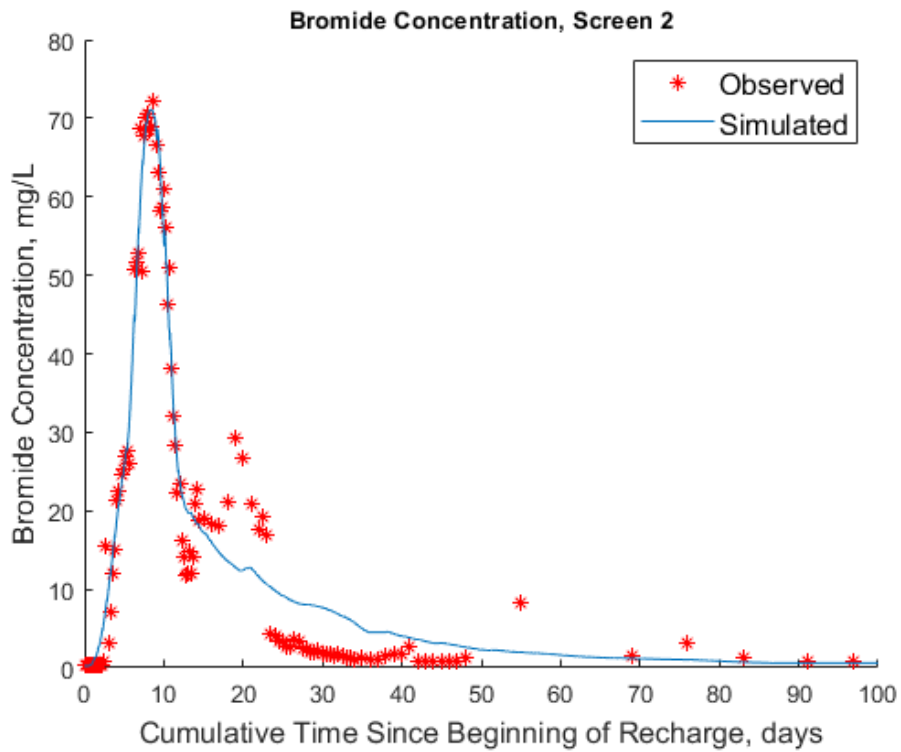


Figure E-48. Two-zone breakthrough at Screen 2.

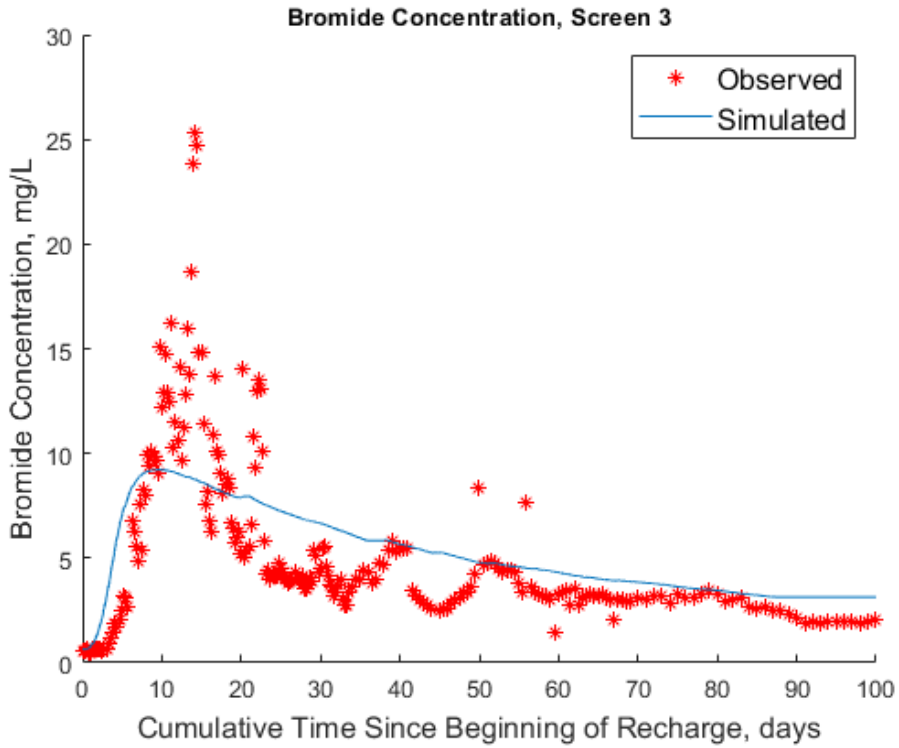


Figure E-49. Single-zone breakthrough at Screen 3.

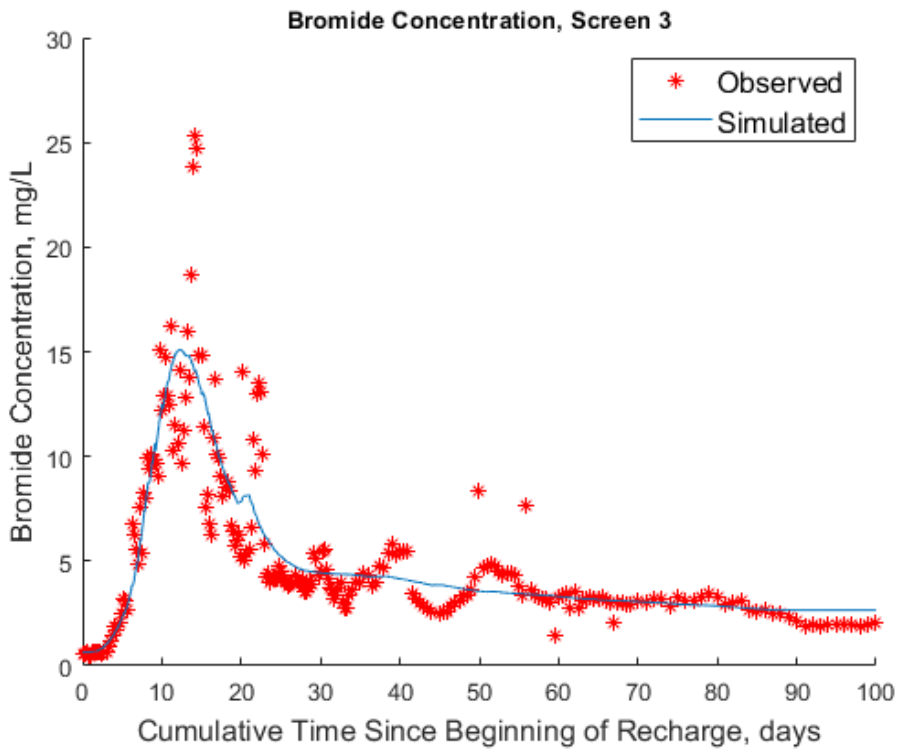


Figure E-50. Two-zone breakthrough at Screen 3.

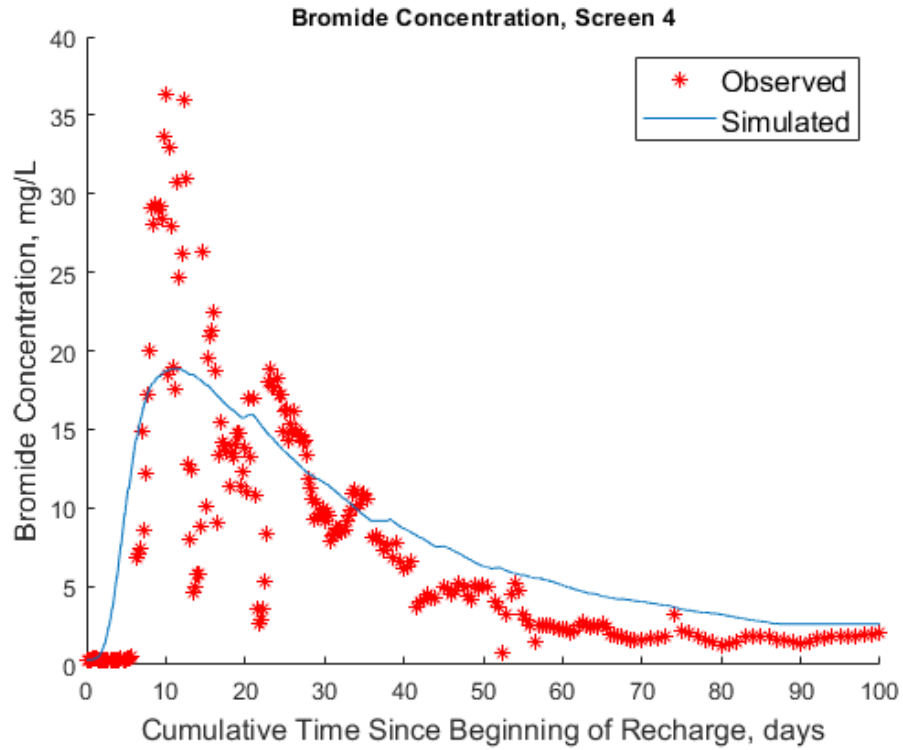


Figure E-51. Single-zone breakthrough at Screen 4.

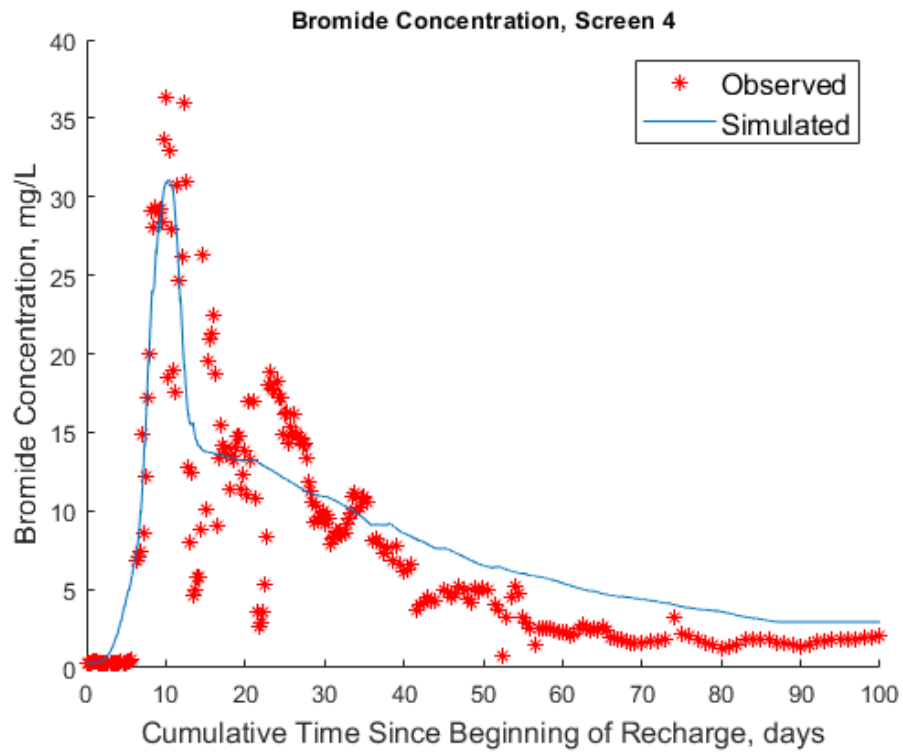


Figure E-52. Two-zone breakthrough at Screen 4.

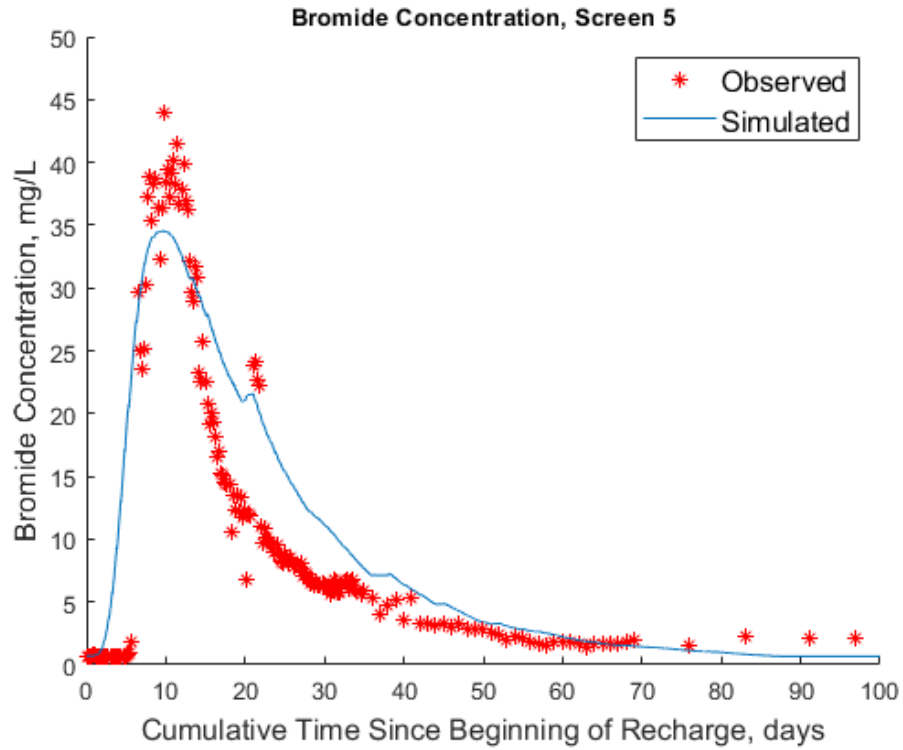


Figure E-53. Single-zone breakthrough at Screen 5.

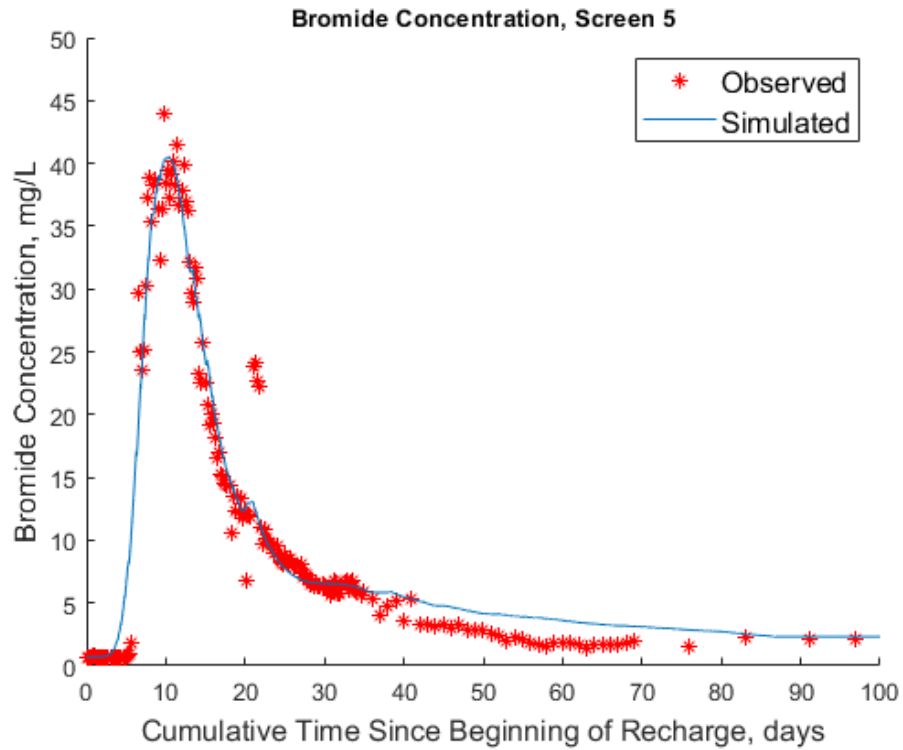


Figure E-54. Two-zone breakthrough at Screen 5.

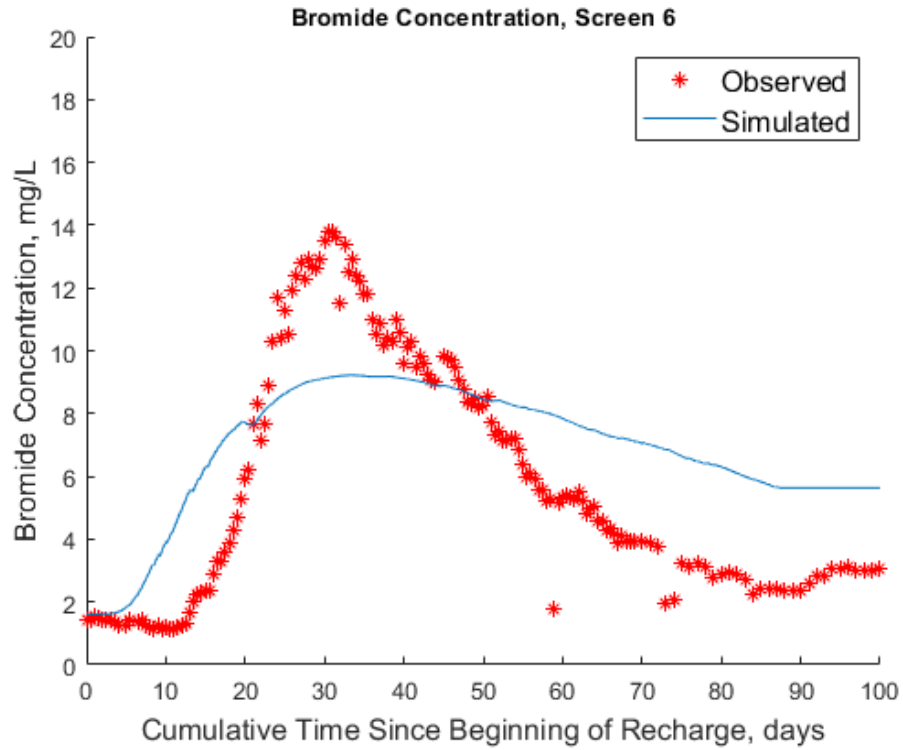


Figure E-55. Single-zone breakthrough at Screen 6.

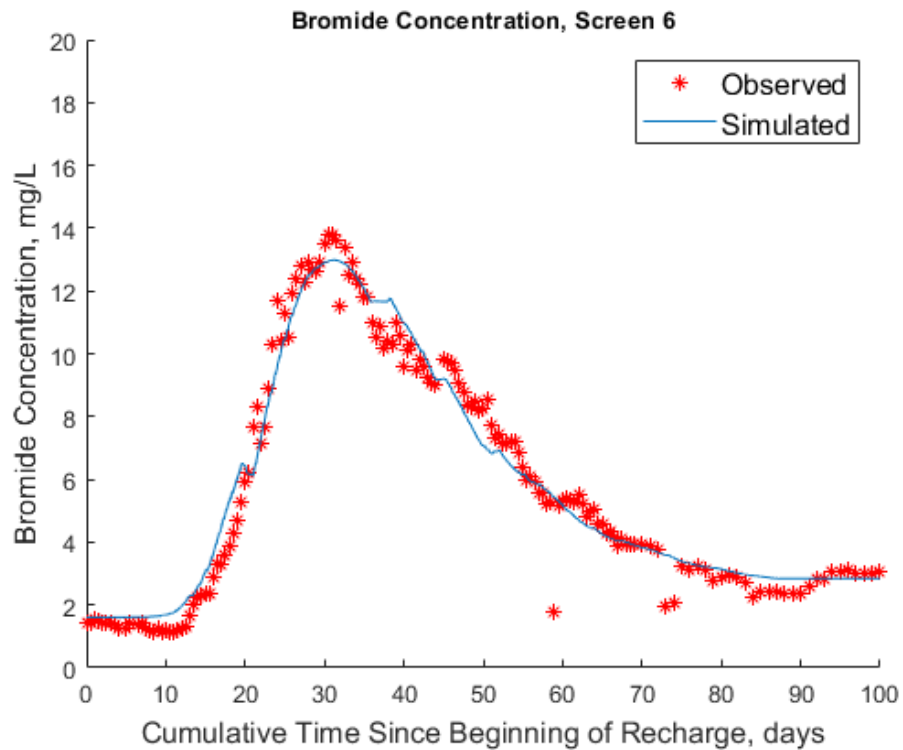


Figure E-56. Two-zone breakthrough at Screen 6.

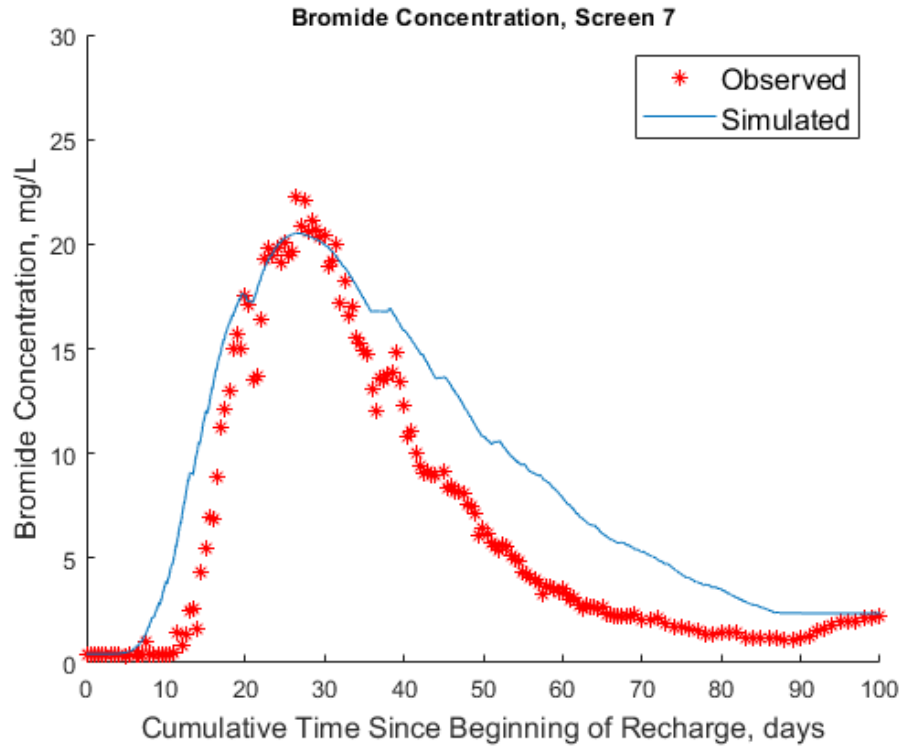


Figure E-57. Single-zone breakthrough at Screen 7.

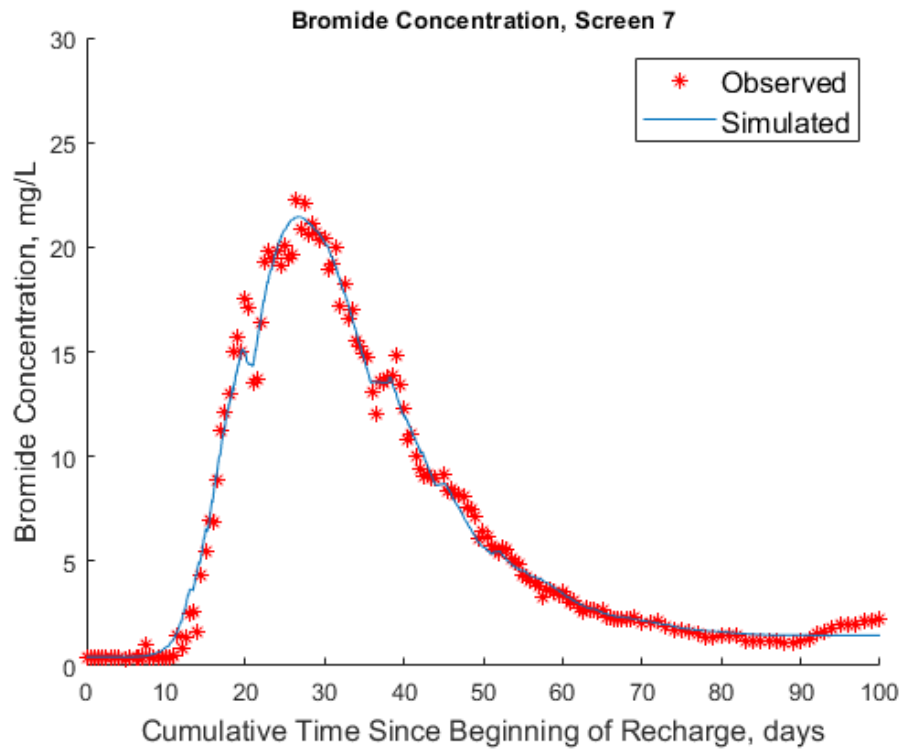


Figure E-58. Two-zone breakthrough at Screen 7.

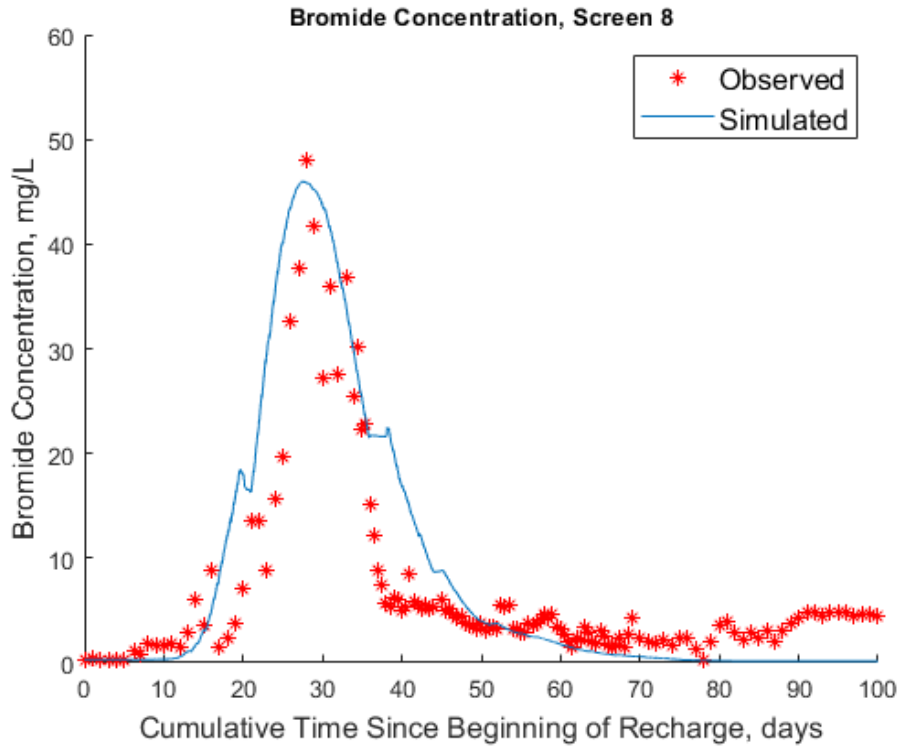


Figure E-59. Single-zone breakthrough at Screen 8.

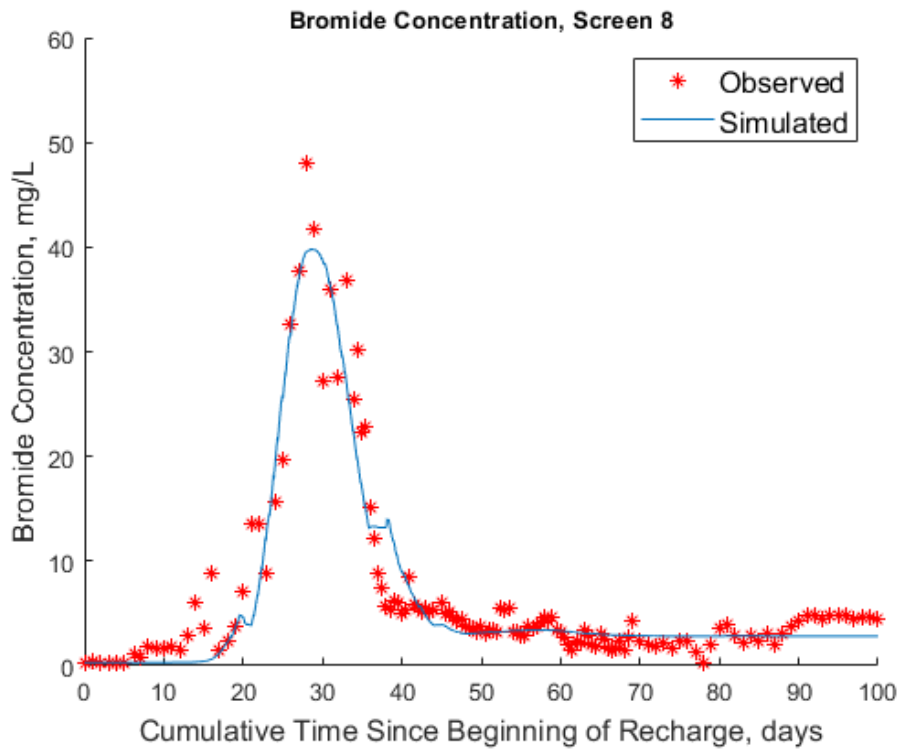


Figure E-60. Two-zone breakthrough at Screen 8.

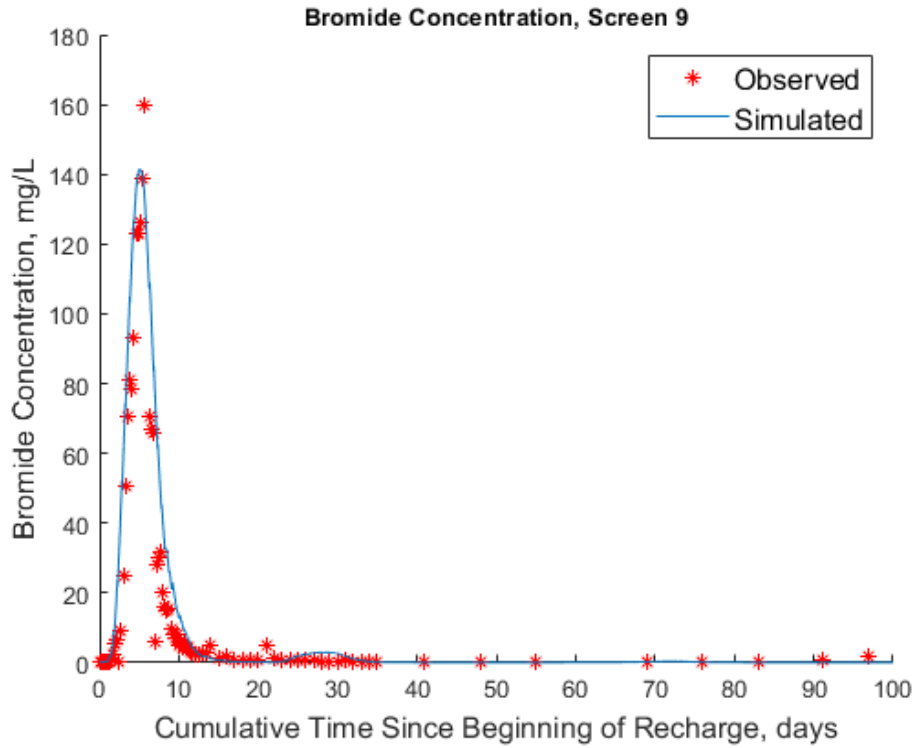


Figure E-61. Single-zone breakthrough at Screen 9.

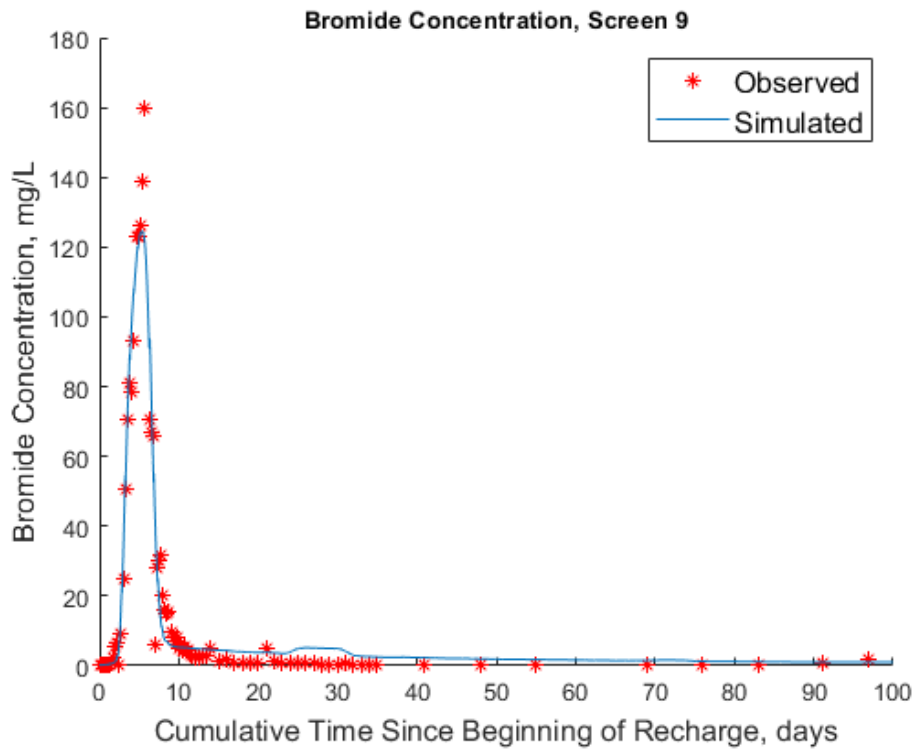


Figure E-62. Two-zone breakthrough at Screen 9.

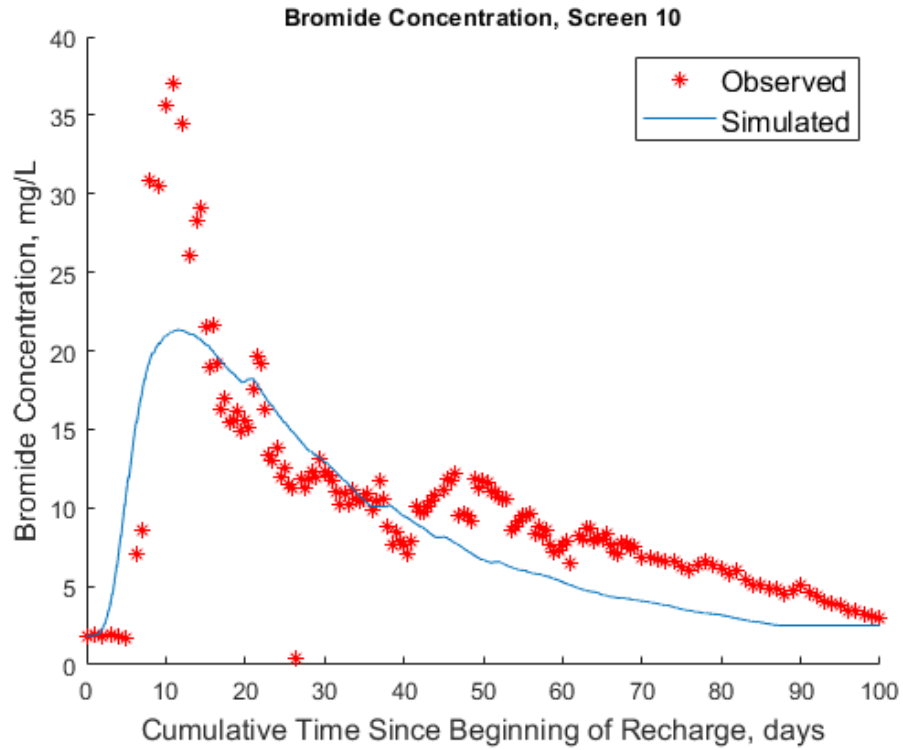


Figure E-63. Single-zone breakthrough at Screen 10.

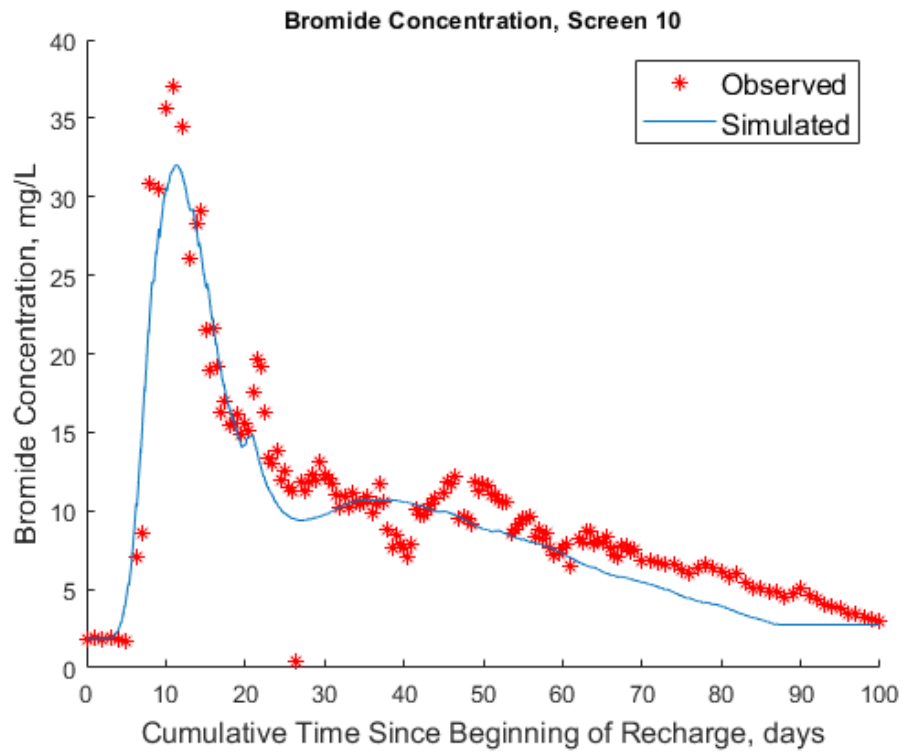


Figure E-64. Two-zone breakthrough at Screen 10.

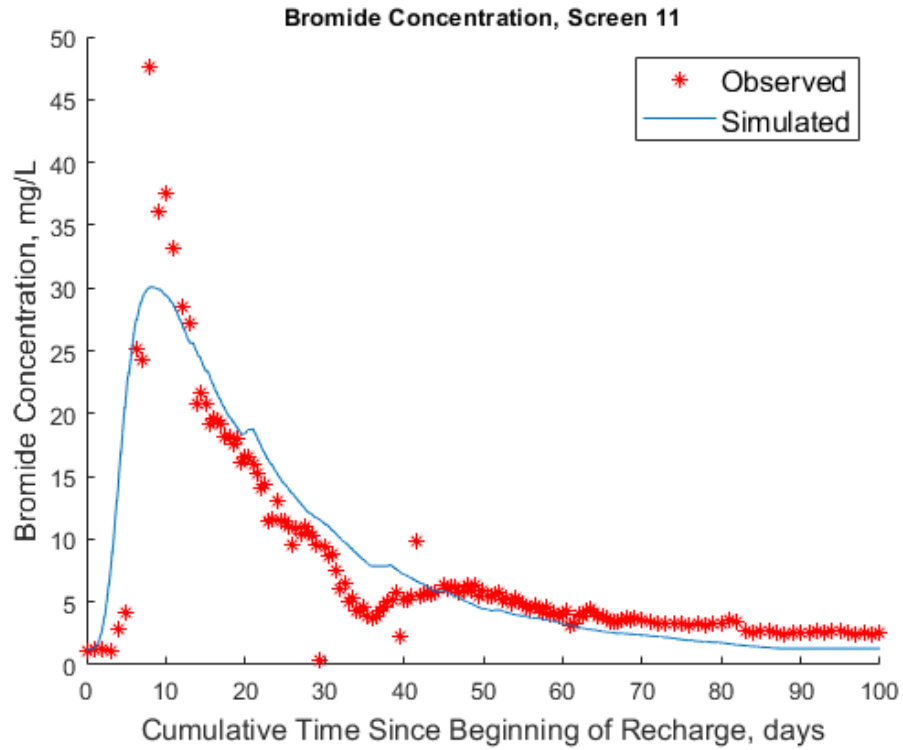


Figure E-65. Single-zone breakthrough at Screen 11.

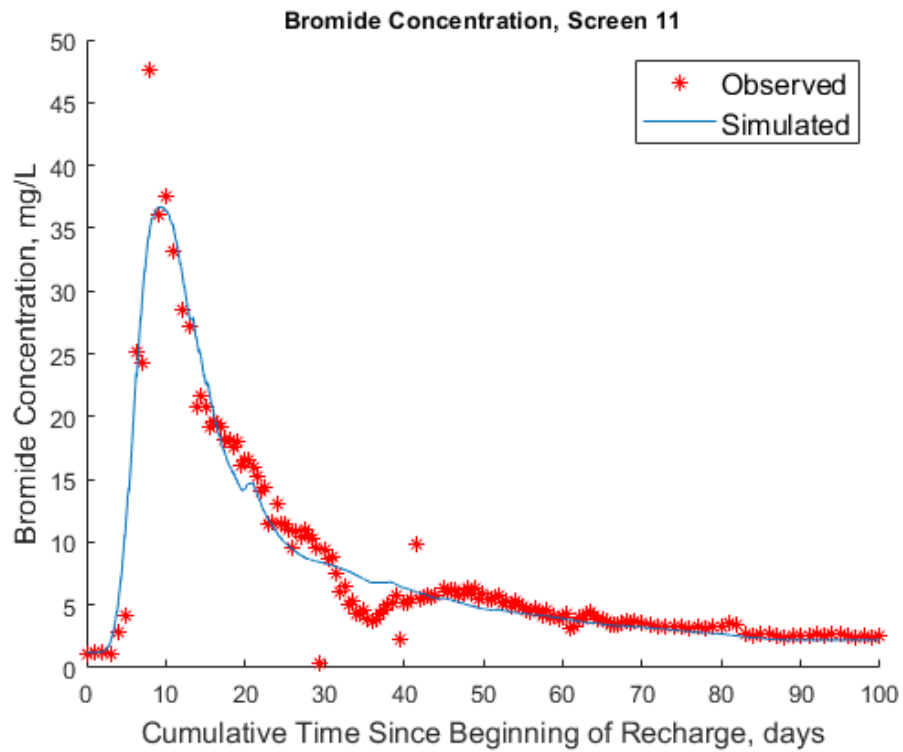


Figure E-66. Two-zone breakthrough at Screen 11.

References

- Bullard, M.G., M. Widdowson, G. Salazar-Benites, J. Heisig-Mitchell, A. Nelson, and C. Bott. 2019. "Managed Aquifer Recharge: Transport and Attenuation in a Coastal Plain Aquifer." In *Proceedings of the EWRI World Environmental and Water Resources Congress 2019: Groundwater, Sustainability, Hydro-Climate/Climate Change, and Environmental Engineering*, 1–14. Pittsburgh: EWRI.
<https://doi.org/https://doi.org/10.1061/9780784482346.011>.